GRIFFITH UNIVERSITY

Decadal-Scale Variability in the Meridional Circulation of Upper Circumpolar Deep Water and its Impact on Primary Production in the Southern Ocean

Author

Johnston, Barbara Mary

Published

2011

Thesis Type

Thesis (PhD Doctorate)

School

Griffith School of Environment

DOI

10.25904/1912/3249

Downloaded from

http://hdl.handle.net/10072/366209

Griffith Research Online

https://research-repository.griffith.edu.au

Decadal-scale variability in the meridional circulation of Upper Circumpolar Deep Water and its impact on primary production in the Southern Ocean

Barbara Mary Johnston
BSc(Hons), Dip Ed (*Tasmania*)

Griffith School of Environment
Science, Environment, Engineering and Technology
Griffith University

Submitted in fulfilment of the requirements of the degree of Doctor of Philosophy

November 2010

Abstract

The Southern Ocean is vitally important in understanding climate change, both regionally and globally. This is due partly to physical factors such as the Antarctic Circumpolar Current (ACC), which facilitates the interchange of heat, nutrients and carbon dioxide between the world oceans. These physical factors also include the seasonal variation in sea-ice around the Antarctic continent and the strong Southern Hemisphere westerly winds, which are responsible for the divergence-driven upwelling of deep water to the surface, south of the Polar Front. The Upper branch of the Circumpolar Deep Water (UCDW) is warm, relative to Antarctic waters, and is high in dissolved inorganic carbon and nutrients, in particular iron. It contributes to carbon dioxide regulation, therefore, through temperature effects on solubility, the out-gassing of carbon dioxide and also via its effect on primary production and the biological pump.

This project examines long-term trends in the meridional circulation of UCDW and in upper-ocean structure, primarily in the Australian region (110-160°E, 40-70°S) of the Southern Ocean. This is achieved by the use of the Simple Ocean Data Assimilation (SODA) 2.0.2/2.0.4 reanalysis of ocean climate variability, which combines output from an ocean global circulation model with observational data, through a sequential data estimation scheme.

Trends are produced for 1958-2007, in five-degree latitudinal bands that approximate the ACC frontal zones, for UCDW and mixed layer hydrodynamic variables and these are related to trends in Southern Hemisphere winds and global climate indices. In addition, similar trends are also produced for the shorter period 1997-2007, for which satellite data are available, and these trends are related to trends in chlorophyll-a, a proxy for phytoplankton biomass, and primary production. As well as these trends, interannual variability in chlorophyll-a in spring and summer, and its controls, are also studied.

Considerable interannual variability, both in the magnitude and phenology of the bloom, is found in chlorophyll-a, as well as differences in its controls, depending on the season and latitudinal zone. In spring near the Antarctic continent, sea-ice concentration and irradiance are major controls. However, in summer, it is wind stress, together with the effect of UCDW via sea-surface

temperature (SST), which is significant. Further north, irradiance is a crucial factor in both spring and summer, while co-varying factors, such as SST, mixed layer depth and stratification are also important.

Negative trends in chlorophyll-a, in 55-60°S in summer, appear to be related to decreases in wind stress and mixing of nutrients, in combination with an increase in SST, which is negatively correlated with chlorophyll-a in that region.

Over the period 1958-2007, mixed layer depth, temperature, density and salinity all show positive trends, with the exception of mixed layer density and salinity near the Antarctic continent and mixed layer temperature in summer, in the Southern ACC Zone and the Antarctic Zone. The mixed layer temperature result holds, not only for the study region, but also in two other sectors studied, one in the Indian Ocean (20-60°E, 40-70°S) and the other in the Pacific Ocean (130-80°W, 40-75°S). It is suggested that this result is related to increasing wind stress that mixes cooler remnant winter water into the mixed layer, counteracting the effect of surface warming.

UCDW vertical velocity is increasing over 1958-2007 in all three sectors in the Polar Frontal Zone, where UCDW upwelling is strongest. However, UCDW temperature trends vary between sectors, with an interesting result that UCDW temperature in the Australian and Pacific sectors is decreasing, where UCDW is deep, north of the Polar Front, in contrast to increasing UCDW temperature in the Indian Ocean. It may be that differences between UCDW in the various sectors are related to the fact that UCDW is composed primarily of old waters that have re-circulated through the Indian and Pacific Oceans, before re-entering the ACC. Unlike the trends in mixed layer variables, however, trends in UCDW seem to operate on centennial rather than decadal time-scales.

Trends in hydrodynamic variables, such as SST and sea-surface salinity, for 1997-2007, are sometimes up to an order of magnitude larger and even of opposite sign to similar trends for 1958-2007. An investigation into this result seems to indicate that these trends are outside the bounds of earlier variability, which may mean that there has been a shift in the state of the Southern Ocean in the last ten to fifteen years.

Statement of Originality

The work in this thesis was carried out at Griffith University, from April, 2007 to October, 2010. This work has not previously been submitted for a degree or diploma in any university. To the best of my knowledge and belief, the thesis contains no material previously published or written by another person, except where due reference is made in the thesis itself.

Barbara M. Johnston

November, 2010

Contents

List of Figures

List of Tables

List of Acronyms

- AABW Antarctic Bottom Water
- AAIW Antarctic Intermediate Water
- AASW Antarctic Surface Water
- ACC Antarctic Circumpolar Current
- AMSR-E Advanced Microwave Scanning Radiometer - Earth Observing System
- ASF Antarctic Slope Front
- AZ Antarctic Zone
- BROKE Baseline Research on Oceanography, Krill and the Environment
- CDW Circumpolar Deep Water
- CLIVAR Climate Variability and Predictability
- CROZEX CROZet natural iron bloom and EXport experiment
- CZCS Coastal Zone Color Scanner
- dFe Dissolved Iron Concentration
- DIC Dissolved Inorganic Carbon
- DOC Dissolved Organic Carbon
- DJF Austral Summer (December, January, February)
- DMSP Defense Meteorological Satellite Program
- ECMWF European Centre for Medium-Range Weather Forecasts
- EisenEx Eisen (iron) Experiment
- ERA-40 ECMWF Re-Analysis
- ENSO El Niño/Southern Oscillation

- GCM Global Circulation Model
- HNLC High-nutrient low-chlorophyll
- IPCC Intergovernmental Panel on Climate Change
- JJA Austral Winter (June, July, August)
- KPP K-Profile Parameterization
- LCDW Lower Circumpolar Deep Water
- LOHAFEX LOHA (iron) Fertilisation EXperiment
- KEOPS KErguelen Ocean and Plateau compared Study
- MAM Austral Autumn (March, April, May)
- ML Mixed Layer
- MLD Mixed Layer Depth
- MOC Meridional Overturning Circulation
- MODIS Moderate Resolution Imaging Spectoradiometer
- NADW North Atlantic Deep Water
- PAR Photosynthetically Active Radiation
- PDO Pacific Decadal Oscillation
- PF Polar Front
- PFZ Polar Frontal Zone
- POP Parallel Ocean Program
- QuikSCAT Quick Scatterometer
- sACCf Southern ACC Front
- sACCZ Southern ACC Zone
- SAF Subantarctic Front
- SAGE SOLAS Atmosphere Gas Exchange Experiment
- SAM Southern Annular Mode
- SAMW Subantarctic Mode Water
- SAF Subantarctic Front

- SAZ Subantarctic Zone
- sBdy Southern Boundary of the ACC
- SeaWiFS Sea-viewing Wide Field-of-view Sensor
- SLW Subtropical Lower Water
- SMMR Scanning Multichannel Microwave Radiometer
- SO Southern Ocean
- SODA Simple Ocean Data Assimilation
- SOFeX Southern Ocean Iron Enrichment Experiment
- SOLAS Surface Ocean Lower Atmosphere Study
- SON Austral Spring (September, October, November)
- SH Southern Hemisphere
- SOIREE Southern Ocean Iron RElease Experiment
- SR3 section (between Tasmania and Antarctica, approximately 140°E)
- SS Sea-Surface
- SSM/I Special Sensor Microwave/Imager
- SSS Sea-Surface Salinity
- SST Sea-Surface Temperature
- Sv Sverdrups (10^6 m^3s^{-1})
- STCZ Subtropical Convergence Zone
- STF Subtropical Front
- SZ Southern Zone
- TAO Tropical Atmosphere Ocean
- TRITON Triangle Trans-Ocean Buoy Network
- UCDW Upper Circumpolar Deep Water
- VGPM Vertically Generalized Production Model
- WOD05 World Ocean Database 2005
- WW Winter Water

Acknowledgements

I would like to pay special tribute to the following people who have been part of my PhD journey:

- My Supervisor Associate Professor Albert Gabric for his guidance and support.
- My Associate Supervisor Dr Anand Tularam for supplying a great deal of information about statistics.
- My husband Peter for his encouragement and belief in me.
- My children Luke, Stuart and Zoë for helping me to see what is important in life.

I would also like to thank Dr Andrew Bowie (University of Tasmania) for supplying unpublished cruise data and Associate Professor Benjamin Giese (Texas A & M University) for providing access to the SODA 5-day datasets.

Financial support from the Australian Postgraduate Award and the Australian Rivers Institute (Griffith University) Top-up Scholarship is gratefully acknowledged. Financial assistance was also provided by the following organisations: Australian Antarctic Division; Australian Meteorological and Oceanographic Society and the Australian Research Council Network for Earth System Science.

Supporting Publications

The following publications have been written based on various parts of this thesis:

Johnston, Barbara M. and Albert J. Gabric (2010), Long-term trends in upper ocean structure and meridional circulation of the Southern Ocean south of Australia derived from the SODA reanalysis, *Tellus Series A - Dynamic Meteorology and Oceanography*, *62A*(5), 719–736.

Johnston, Barbara M. and Albert J. Gabric (2011), Interannual variability in estimated biological productivity in the Australian sector of the Southern Ocean in 1997-2007, *Tellus Series B - Chemical and Physical Meteorology*, DOI: 10.1111/j.1600-0889.2011.00526.x.

Chapter 1

Introduction

The world ocean has been responsible for sequestering around 25-30% of anthropogenic CO_2 emissions, over the last 200 years (*Sabine et al.*, 2004). The Southern Ocean (SO) is of particular importance in this process, given that modelling studies (*Orr et al.*, 2001; *Khatiwala et al.*, 2009) have suggested that it dominates the current air-sea flux of anthropogenic CO_2. Using an observationally based technique, *Khatiwala et al.* (2009) estimated that, in 2008, the oceanic inventory of anthropogenic CO_2 was 140±25 PgC with an annual uptake rate of 2.3±0.6 $PgCyr^{-1}$ and that the SO contributed over 40% of the anthropogenic CO_2 inventory in the ocean.

A number of studies have suggested that the rate of increase of ocean uptake of anthropogenic CO_2 has decreased in the last few decades, including the study by *Khatiwala et al.* (2009), a modelling study by *Lovenduski et al.* (2007) and a study by *Takahashi et al.* (2009), which used repeated surface-ocean CO_2 observations. *Lovenduski et al.* (2007) connected positive phases of the Southern Annular Mode (SAM), which result in the southward shift and strengthening of the Southern Hemisphere (SH) westerly winds, with anomalous out-gassing of natural CO_2. A study by *Le Quere et al.* (2007) also concluded that the SO CO_2 sink has weakened in recent years and, since the authors believe this is connected to an increase in the SH winds, they suggest that this trend will continue in the future in line with increases in the SAM. However, other authors (*Zickfeld et al.*, 2008) believe that the SO sink will increase in efficiency in the 21st century. There is thus considerable interest in detecting any changes in factors that may affect the CO_2 sink in the SO.

The SO has a number of unique oceanographic and physical features that contribute to its role in global and regional climate change. For example, the SO is the only region where a circumpolar current, the Antarctic Circumpolar Current (ACC), circles the globe. The ACC flows unimpeded from west to east around Antarctica along a 20 000 km path, connecting the Indian, Pacific and Atlantic Oceans and allowing vast amounts of heat, moisture, nutrients

and CO_2 to be stored and transported (*Rintoul and Trull*, 2001; *Sarmiento et al.*, 2004). In addition, the SH westerlies are among the strongest winds in the world (*Trenberth and Caron*, 2000). They not only drive the ACC but they also move the surface waters away from the Antarctic continent by Ekman transport. The effect of these winds and the polar easterlies along the Antarctic coast, which steer surface waters southwards, is to bring deep water to the surface south of the Polar Front via divergence-driven upwelling.

This upwelling is part of the meridional circulation, the north-south flow of water, which has been represented in a simplistic fashion as the "great ocean conveyor belt" (*Broecker*, 1991). The depth from which the water is upwelled (2-3km) is another feature that is unique to the SO (*Russell et al.*, 2006). The movement of the upwelled water in the SO is often represented as consisting of upper and lower cells (*Speer et al.*, 2000). The upper cell is formed by upwelled water that is modified by interactions between the ocean, atmosphere and sea-ice and then moves north, eventually sinking at lower latitudes, forming Antarctic Intermediate Water. The other branch of the upwelled water moves towards the Antarctic continent, becomes more dense and sinks, forming Antarctic Bottom Water, and then flows northward at depth, thus "ventilating" the deep ocean (*Speer et al.*, 2000; *Russell et al.*, 2006).

The upper branch of the upwelled water, the Upper Circumpolar Deep Water (UCDW), is rich in nutrients, especially iron (*Hiscock et al.*, 2003). This supply of nutrients is crucial for primary production and ecosystem function (*Hoppema et al.*, 2003; *Hiscock et al.*, 2003) in the SO, since iron has been demonstrated to be the limiting factor for primary production (*Martin et al.*, 1990b,a; *Boyd et al.*, 2000; *Coale et al.*, 2004) in the ACC region of the SO.

Another important feature in the SO is the seasonal variation in sea-ice around the Antarctic continent. Sea-ice acts as a physical, chemical and biological barrier between the atmosphere and the ocean (*Constable et al.*, 2003). It is a source of phytoplankton for the spring bloom and affects stratification during melting and the energy budget due to its high albedo. It also has an impact on the supply of iron during ice melt, as it can act as a storage reservoir over autumn/winter for iron supplied from above by airborne dust or below either from upwelling or from advection from continental margins (*Lannuzel et al.*, 2007; *Sedwick et al.*, 2008).

Insights into decadal-scale changes in the meridional overturning circulation in the SO are important, since such changes have the potential to affect the CO_2 sink through both the solubility pump (the localised sinking of cold, dense winter water enriched with dissolved inorganic carbon (DIC)) and the biological pump (the sinking to depth of carbon fixed during photosynthe-

sis). For example, a strengthening in the meridional overturning circulation might lead to higher primary production in the high latitudes, due to increased upwelling of nutrients and therefore to increased drawdown of CO_2 via the biological pump (*Lovenduski and Gruber*, 2005). At the same time, deep waters such as UCDW, with higher concentrations of DIC (*Iudicone et al.*, 2010), would be upwelled, leading to an out-gassing of natural CO_2 to the atmosphere (*Le Quere et al.*, 2007; *Lovenduski et al.*, 2007).

Changes in the westerly winds which drive the ACC not only potentially affect the position and strength of the ACC, but also the upwelling of UCDW, because of variations in the Ekman transport. Such changes are likely to be related to a number of different climate patterns that represent the natural climate variability on various time-scales. These include the SAM, El Niño/Southern Oscillation (ENSO) and the Pacific Decadal Oscillation (PDO). The SAM is the most important mode of climate variability in the SH middle and high latitudes on intra-seasonal and inter-annual timescales (*Lovenduski and Gruber*, 2005) and is associated with north-south movements of the westerly winds. The SAM index (*Marshall*, 2003; *Visbeck*, 2009) has been moving towards a more positive mode since the 1970s (*Thompson and Solomon*, 2002), indicating a poleward intensification of the SH winds, although it has levelled off in the last decade (*Monaghan et al.*, 2008). However, while the SAM is generally considered to be zonally symmetric, recent studies have found that the wind response is not (*Drost and England*, 2009) and neither is the oceanic response of the fronts (*Sallee et al.*, 2008). Thus, the effect of the SAM differs in the various regions of the SO and potentially so do the effects of the winds on the meridional circulation of UCDW and its effects on primary production.

The present study focuses on the Australian sector of the SO (110-160°E, 40-70°S), although results there are also compared with two other SO sectors, Indian (20-60°E, 40-70°S) and Pacific (130-80°W, 40-75°S). *Sallee et al.* (2008) found that, in the Australian sector, the trend associated with more positive SAM results in an intensification, but no distinct meridional shift, of the ACC fronts. Another factor to take into account is the fact that, when considered on a seasonal scale, the SAM shows significant positive trends only in summer (DJF) and autumn (MAM), over the period 1957-2004 (*Marshall*, 2007). This seasonal variation in the effect of the SAM may be important, given that peak primary production occurs in spring and summer. It is also necessary to study the effect of ENSO which, while it is a tropical coupled system, still has an impact on the winds in the study region (*Holbrook and Bindoff*, 1997; *L'Heureux and Thompson*, 2006). For completeness, the effect of the PDO (*Mantua and Hare*, 2002) will also be considered.

To some extent it is possible to assess mid- to late-twentieth century trends

for hydrodynamic variables in the SO via observations in specific areas at different times (*Gille*, 2002, 2008; *Aoki et al.*, 2003; *Hill et al.*, 2008) or via climatologies (*Levitus et al.*, 2005; *Boyer et al.*, 2005; *Jacobs*, 2006; *Böning et al.*, 2008). Other methods include numerical simulation studies (*Zhang*, 2007; *Trenberth et al.*, 2007; *Henson et al.*, 2010) or model reanalysis datasets, such as the Simple Ocean Data Assimilation (SODA) dataset (*Yang et al.*, 2007a). Since observational data in the SO are temporally and spatially inhomogeneous, this study uses SODA (*Carton et al.*, 2000, 2005; *Carton and Giese*, 2008) model reanalysis data for hydrodynamic variables. Reanalysis data have the advantage, over both the sparse set of observations and numerical simulation, that data are synthesised in such a way that they are consistent with the model physics, that complete temporal and spatial coverage is possible, and that information can be provided on both directly and indirectly observed variables. The SODA 2.0.2/2.0.4 reanalysis covers the 50 year period from 1958 to 2007. This reanalysis of ocean climate variability begins with a state forecast produced by a General Circulation Mode (GCM) based on POP (Parallel Ocean Program) numerics (*Smith et al.*, 1992) and this forecast is continuously updated by available contemporaneous observations, via a multi-variate two-stage sequential updating algorithm.

In addition to changes in the physical oceanography of the SO, it is also important to consider changes in the biological oceanography, since phytoplankton are responsible for almost half of global primary production (*Field et al.*, 1998). In fact, according to *Hoppema et al.* (2000), biological drawdown of CO_2 is more important than physical processes for establishing the CO_2 sink in the southern ACC.

Previous work (*Steinacher et al.*, 2010) has identified a number of physiochemical controls on primary production in the SO. These include sea-ice concentration/extent (near the Antarctic continent), sea-surface temperature (SST), photosynthetically active radiation (PAR), mixed layer depth (MLD), stratification, macro- and micro-nutrient availability and community composition and grazing. The fact that climate variability can affect many of these controls on primary production, particularly on interannual timescales (*Boyce et al.*, 2010), has been established by studies which link climate indices, such as the SAM index, the Multi-variate ENSO Index (MEI) (*Wolter and Timlin*, 1993) and the PDO index, with variability in chlorophyll-*a* and primary production (*Lovenduski and Gruber*, 2005; *Behrenfeld et al.*, 2006; *Arrigo et al.*, 2008; *Martinez et al.*, 2009) through variability in wind stress and its position, SST, MLD and stratification.

Even more so than for hydrodynamic variables, trends are difficult to establish for primary production, due to the sparse nature of the observational data.

The advent of the satellite era, and, in particular Sea-viewing Wide Field-of-view sensor (SeaWiFS) (*McClain et al.*, 2004), has provided an opportunity to consider trends in standing stock (chlorophyll-*a*) or primary production since 1997. A few modelling studies, which use satellite-derived chlorophyll-*a* values to calculate primary production, have examined trends for the SO (*Arrigo et al.*, 2008; *Smith and Comiso*, 2008; *Barbini et al.*, 2005). Using an algorithm calibrated specifically for use in the SO, *Arrigo et al.* (2008) found no trend in 1997-2006 for annual primary production in the whole SO, although statistically significant trends for primary production in the Ross Sea (increasing) and the south Indian Ocean sector (decreasing) were found. In contrast, *Smith and Comiso* (2008) found annual production over the entire SO, calculated using the Vertically Generalised Production Model (VGPM) of *Behrenfeld and Falkowski* (1997), has increased significantly since 1998, and that production has increased particularly in January and February.

Using ocean transparency measurements and *in situ* chlorophyll-*a* observations, *Boyce et al.* (2010) found a decline, since 1899, in global chlorophyll-*a* of -0.006±0.0017 mg $m^{-3}yr^{-1}$, with the one of the largest declines (-0.015±0.0016 mg $m^{-3}yr^{-1}$) being in the SO region south of 60°S. On the other hand, a modelling study (*Steinacher et al.*, 2010) looking at primary production projected over the 21st century, has found that, for parts of the SO, an alleviation of the limitations of light and/or temperature will lead to an increase in primary production, but that absolute change in productivity in the SO (south of 45°S) will vary regionally.

The importance of potential changes in the upwelling of nutrients in UCDW in the ACC is highlighted in a recent modelling study by *Palter et al.* (2010), who found that these nutrients support 33-75% of global production between 30°S and 30°N, via the subduction of these waters in the Subantarctic Mode Water and the subsequent remineralisation of the nutrients. Given the importance of the SO to world climate and UCDW to primary production, the main question to be examined in this study is:

What is the range of interannual and decadal variability in the meridional circulation of UCDW and how does this relate to variability in phytoplankton standing stock and primary production in the SO?

This can be broken down into a number of sub-questions:

- What is the range of interannual and decadal variability in UCDW hydrodynamic properties, as well as in characteristics associated with its meridional circulation?

- What is the range of variability in upper ocean properties and SH winds?
- Is there a correlation between changes in the SH winds and changes in UCDW?
- What is the interannual variability in primary production in the Australian region of the SO?
- What factors influence primary production in this region?
- Is there a connection between variability in these factors, and, in particular the upwelling of UCDW, and variability in phytoplankton biomass and primary production?

The thesis is structured in the following way. The Literature Review (Chapter 2) considers information from previous studies about UCDW, its circulation and importance in primary production in the SO and the effect changes in the SH winds may have on the SO climate sink. Chapter 3 (Methodology) presents information about the SODA reanalysis and the data analysis and statistical techniques used in this study. These chapters precede five chapters which consider the questions posed above. The first of the five Results chapters (Chapter 4) examines SODA's skill at representing hydrodynamic data in the SO and then studies UCDW movement in the Australian sector of the SO, as well as dissolved iron in UCDW. Chapter 5 is a study of UCDW and upper ocean climatological properties, in the Australian region of the SO. Connections are examined between global climate indices (SAM, MEI and PDO) and wind stress and then wind stress and UCDW and mixed layer (ML) properties. Finally, trends in all these variables are derived for 1958-2007. Results for the Australian sector are compared with results for the Indian and Pacific sectors in Chapter 6, in order to consider the robustness of trends. Interannual variability (1997-2007) in chlorophyll-a (a proxy for phytoplankton biomass) and primary productivity, again in the Australian sector, are studied in Chapter 7, as well as factors that affect chlorophyll-a. Chapter 8 is a study of trends in these factors, as well as in chlorophyll-a and primary productivity, over the period 1997-2007. These ten-year hydrodynamic trends are then compared with the 1958-2007 trends. Overall conclusions are given in Chapter 9, as well as a discussion of possible future work. This chapter is followed by an Appendix, which presents tables of 1958-2007 trend results by season, for each of the three ocean sectors. The final chapter in the thesis is the Bibliography.

Chapter 2

Literature Review

2.1 The Southern Ocean

The term "Southern Ocean" is generally used to refer to the ocean around Antarctica, but there is no official definition of the term. Instead, the International Hydrographic Organization (IHO, 1953) considers the area between 146°55'E and 67°16'W to be part of the Pacific Ocean, the area from 20°E to 146°55'E to be part of the Indian Ocean and the remaining area to be part of the Atlantic Ocean, with the limits of those oceans extending south to the Antarctic continent. A more recent (2000) definition of the SO as being south of 60°S has not yet been ratified by the IHO. The approach of *Tomczak and Godfrey* (1994) will be adopted in this work - that is, the SO is the region south of the Subtropical Front, where tropical/temperate dynamics give way to polar ocean dynamics.

2.2 The Antarctic Circumpolar Current

The ACC flows eastward around Antarctica, driven by the prevailing westerly winds. It is a continuous circumpolar current that moves along a 20 000 km path connecting the the Indian, Pacific and Atlantic Oceans, uninterrupted by continental barriers. The ACC has the largest mass transport of all the ocean currents, around 130-140 Sv (million cubic metres per second) (*Whitworth et al.*, 1982), due to its width (up to 2000 km) and the great depths (deeper than 2000 km) to which the current extends (*Tomczak and Godfrey*, 1994).

The position of the ACC lies approximately between 35-38°S and 60-65°S, but depends on the sector, so it is usual to define the ACC as consisting of a number of fronts (where rapid changes in water properties, such as salinity, density and temperature, occur over a short distance), as well as the zones between these fronts (where water mass properties are relatively uniform). This definition for the ACC is used because no continental reference point

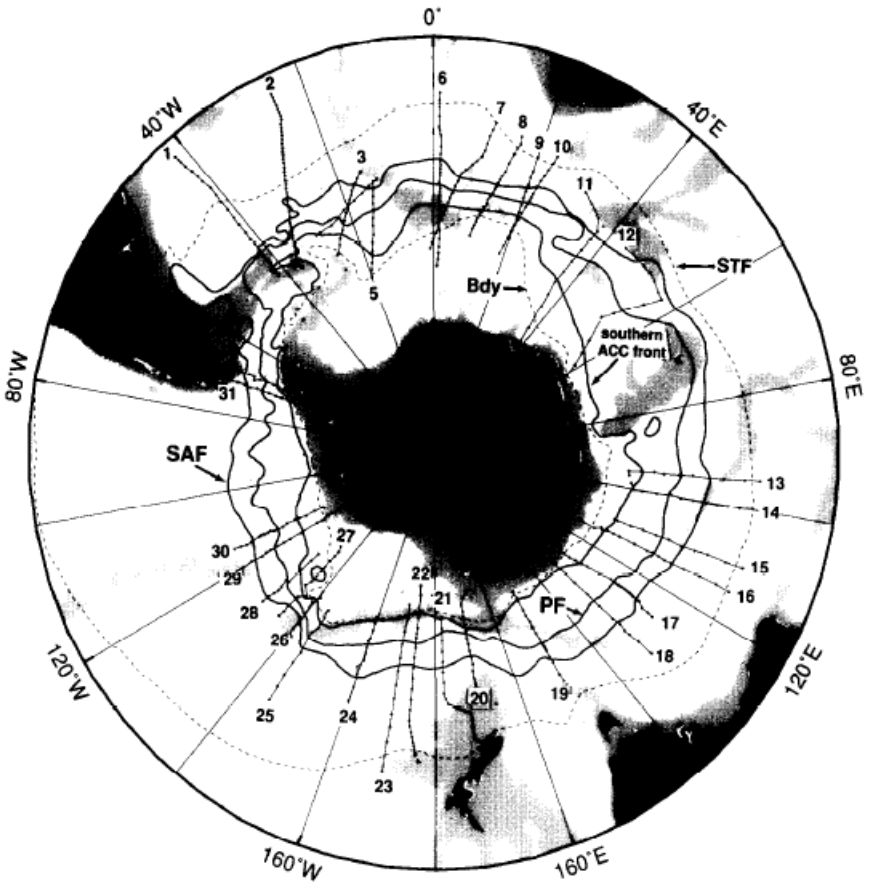

Figure 2.1: The fronts of the Southern Ocean. From north to south they are Subtropical Front (STF), Subantarctic Front (SAF), Polar Front (PF), Southern ACC Front and the Southern Boundary of the ACC (sBdy). Reprinted from *Orsi et al.* (1995) with permission from Elsevier.

exists, other than the fact that, by convention, all flow through Drake Passage (at the tip of South America) is the ACC (*Orsi et al.*, 1995).

The three primary fronts of the ACC, from north to south, are the Subantarctic Front (SAF), Polar Front (PF) and the Southern ACC Front (sACCf) (*Whitworth and Nowlin*, 1987; *Orsi et al.*, 1995). Between these lie the Polar Frontal Zone (PFZ) and the Antarctic Zone (AZ), respectively. In addition, the Subantarctic Zone (SAZ) lies between the northern boundary of the ACC, the Subtropical Front (STF) and the SAF. The Southern Boundary of the ACC (sBdy) is found either south of or sometimes coincident with the sACCf and was defined by *Orsi et al.* (1995) to be the poleward edge of the UCDW signal. The Southern ACC Zone (sACCZ) is found between the sACCf and the sBdy, with the most southerly zone being the Southern Zone (SZ). Figure 2.1 shows the positions of the above fronts as determined by *Orsi et al.* (1995) and Table 2.1 shows the positions of the zones in relation to the fronts.

Work by *Sokolov and Rintoul* (2002), using high resolution hydrographic data collected along the CLIVAR section SR3 (near the 140°E meridian), showed that each of the ACC fronts was consistently split into two or more

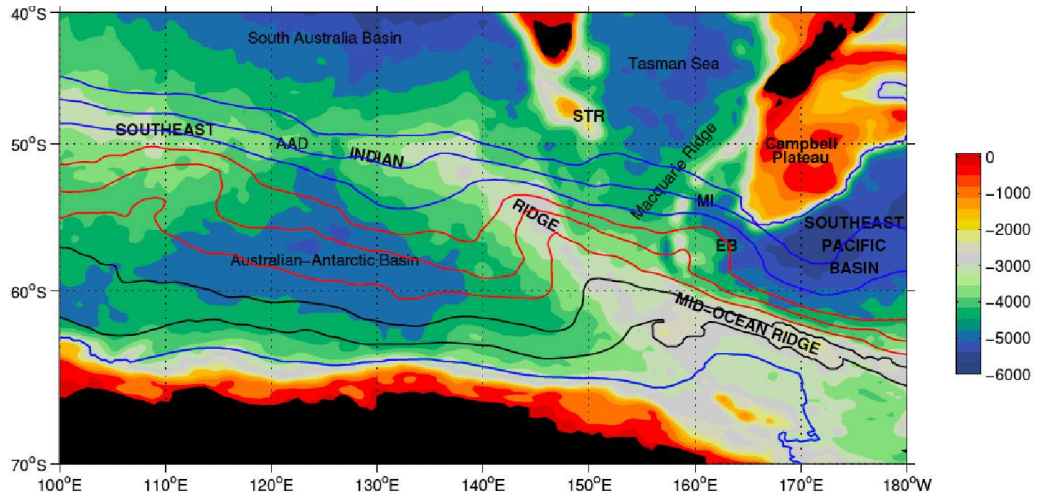

Figure 2.2: The mean positions of fronts of the Southern Ocean south of Australia and New Zealand (*Sokolov and Rintoul*, 2007). The ACC fronts shown from north to south are: SAF (blue), PF (red), sACCf (black) and sBdy (blue).

Table 2.1: Positions of Southern Ocean zones relative to Southern Ocean fronts

Front	Zone
STF	
	SAZ
SAF	
	PFZ
PF	
	AZ
sACCf	
	sACCZ
sBdy	
	SZ
ASF	

branches, and they recently showed (*Sokolov and Rintoul*, 2007) that this result applies to the entire SO.

The mean positions of the various fronts of the ACC, for the region south of Australia and New Zealand, can be seen in Figure 2.2, bearing in mind that the frontal positions vary in time. In this figure, the sBdy can be seen south of sACCf2 at around 65°S. The ACC is strongly steered by major topographic features, such as Drake Passage, Kerguelen Passage (and Island), Campbell Plateau, South-East Indian Ridge and Macquarie Ridge (*Tomczak and Godfrey*, 1994).

The mean positions of the fronts on the section SR3 are given in Table 2.2 (*Sokolov and Rintoul*, 2002), where the final front found on SR3 was the Antarctic Slope Front (ASF), located over the upper continental slope of Antarctica. The ASF separates cold, fresh shelf water from warmer, more saline offshore water.

Table 2.2: Mean Positions of Southern Ocean fronts along SR3 (140°E) (*Sokolov and Rintoul*, 2002)

Front	Latitude
STF	42.5°S
SAF1	50.5°S
SAF2	52°S
PF1	53-54°S
PF2	59-60°S
sACCf1	62°S
sACCf2	64°S
ASF	65°S

Table 2.3: Water Masses along SR3 (140°E) (*Sokolov and Rintoul*, 2002)

Latitude	Depth	Water Mass	Characteristics
North of 45°S	0-200m	Subtropical Lower Water (SLW)	high salinity core
46-50°S	100-500m	Subantarctic Mode Water (SAMW)	uniform temp and salinity
	below 500	Antarctic Intermediate Water (AAIW)	salinity minimum
South of 53°S	surface	Antarctic Surface Water (AASW)	relatively fresh
	100-300m	Winter Water (WW)	temperature minimum
	below 200m	Upper Circumpolar Deep Water (UCDW)	temp, nutrient max, O_2 min
	below UCDW	Lower Circumpolar Deep Water (LCDW)	salinity max, nutrient min
	below LCDW	Antarctic Bottom Water (AABW)	cold, fresh layer

A summary of the major water masses along SR3, their main characteristics and where they can be found is given in Table 2.3. On this section, UCDW is found at depths of 1500-2000 m north of the SAF and it shoals to 400-1000 m, south of the SAF (*Sokolov and Rintoul*, 2002).

2.3 Upper Circumpolar Deep Water

Circumpolar Deep Water, comprised of Upper (UCDW) and Lower (LCDW) Circumpolar Deep Water, is the most extensive water mass in the ACC (*Gordon*, 1967), while UCDW is the only water mass found exclusively in the ACC (*Orsi et al.*, 1995). UCDW is characterised by a nutrient maximum and an oxygen minimum, making it critical for primary production when it reaches the upper ocean. On the other hand, LCDW is oxygen-rich and is characterised by a salinity maximum and a nutrient minimum. UCDW lies above LCDW and below the Antarctic Surface Water (AASW) in the temperature maximum layer, which lies below a temperature minimum layer. This so-called Winter Water (WW) is remnant water, a cold and relatively deep mixed layer

(ML) formed due to winter cooling, which is overlaid by a shallow, warm, ML, created by summer warming (*Sokolov and Rintoul*, 2002) (Table 2.3).

UCDW can be identified (*Sievers and Nowlin*, 1984; *Orsi et al.*, 1995) by $[O_2] < 4.5$ ml l^{-1} (201 μmol l^{-1}) at density values 27.35 kg m^{-3} $< \sigma_0 <$ 27.75 kg m^{-3}, where $[O_2]$ is oxygen concentration and σ_0 is potential density anomaly at 0 dbar. This is is equivalent to the density criterion with temperature, $\theta > 1.5$°C (*Orsi et al.*, 1995; *Sokolov and Rintoul*, 2002), giving a salinity S range of between 34.5 psu and 34.7 psu.

UCDW is supplied mainly from the eastern south Pacific Ocean and the western Indian Ocean (*Callahan*, 1972; *Whitworth and Nowlin*, 1987; *Park et al.*, 1993), whereas North Atlantic Deep Water (NADW) is the source for LCDW (*Patterson and Whitworth*, 1990; *Park et al.*, 1993). The CDW is split into upper and lower parts when the relatively warm, salty, oxygen-rich and nutrient-poor NADW enters the ACC in the southwest Atlantic, just below the oxygen-minimum layer (*Reid et al.*, 1977; *Whitworth and Nowlin*, 1987). UCDW retains the oxygen minimum, whereas oxygen increases in LCDW during ACC flow, due to the high oxygen concentration in the overlying NADW and the underlying Antarctic Bottom Water (AABW) (*Whitworth and Nowlin*, 1987).

UCDW is relatively old water (*Patterson and Whitworth*, 1990; *Park et al.*, 1993) and owes its low oxygen content to southward recirculation of aged NADW/LCDW, which originally entered the Indian and Pacific oceans from the south (*Callahan*, 1972; *Reid*, 1981). While there it aged, its oxygen content decreased and deep upwelling and diapycnal mixing caused a slight decrease in potential density and salinity, which brought the recirculated UCDW above the high-salinity LCDW core (*van Aken*, 2007). Aging of this deep water is indicated by the oxygen, dissolved silicate and radiocarbon distributions. Studies have found (*van Aken*, 2007) that the lowest oxygen concentrations in UCDW in the ACC are found near Australia and South America. Examples of low oxygen, recirculating water are North Indian Deep Water and Pacific Deep Water, which re-enter the SO at subsurface levels, above the LCDW core, where they contribute to the maintenance of the UCDW core (*van Aken*, 2007). Recent observational studies (*Kawabe and Fujio*, 2010) have found that 7 Sv of UCDW is transported to the North Pacific from the ACC. The recirculation of Circumpolar Deep Water (CDW), in the Indian and Pacific Oceans, is shown in the schematic meridional overturning circulation diagram of *Schmitz* (1996) in Figure 2.3.

As UCDW circulates around the Antarctic continent, it is also shoaling upwards to the south and losing its characteristic properties by mixing with the Antarctic Surface Water. It will then move northwards in the Ekman

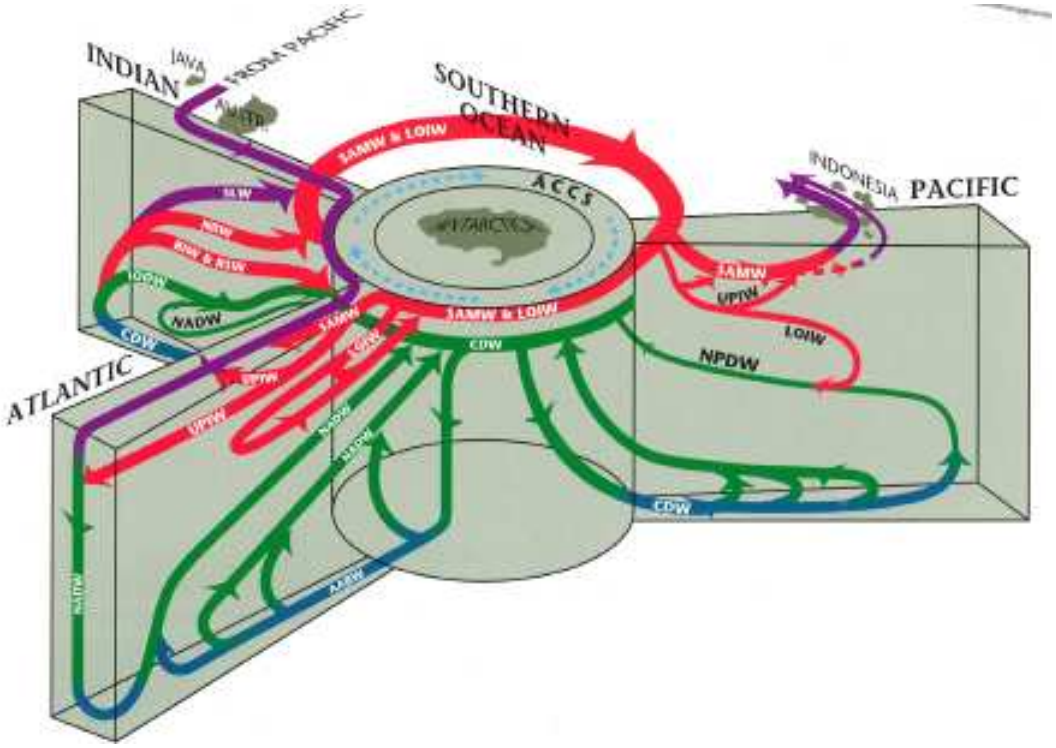

Figure 2.3: Schematic meridional overturning circulation diagram (*Schmitz*, 1996), showing the recirculation in blue/green of Circumpolar Deep Water (CDW) in the Indian and Pacific Oceans. Colours for the various circulations are: surface (red); intermediate and SAMW (purple); deep (green) and near bottom (blue).

layer due to the atmospheric forcing (*Speer et al.*, 2000; *Lumpkin and Speer*, 2007). For example, in data collected along 170°W, by *Hiscock et al.* (2003), as part of the Joint Global Ocean Flux Study in 1997/98, UCDW can be seen to shoal from below 2000 m south of the SAF to around 500 m near the sACCf, with UCDW being found in the upper 200 m just north of the sBdy (Figure 2.4). UCDW was also found to rise to near 200 m on most of the 84 sections examined by *Orsi et al.* (1995) to trace the southern extent of the UCDW signal (ie. the sBdy). South of the sBdy no evidence of UCDW is found and the water column consists almost entirely of LCDW and AABW (*Whitworth and Nowlin*, 1987; *Patterson and Whitworth*, 1990). The sBdy (and the southern-most extent of UCDW) is found approximately at: 65°S in most of the Indian and Pacific Oceans, from 50°E to the dateline; at 60°S, east of the dateline to 140°W; near 70°S by 120°W; at 60°S, east of the Drake Passage and near 55°S at 10°E (Figure 2.1).

The upwelling of nutrients in UCDW, and in particular iron, has been linked by many studies (for example, *DeBaar et al.* (1995); *Löscher* (1999); *Lefevre and Watson* (1999); *Watson et al.* (2000); *Hoppema et al.* (2003); *Meskhidze et al.* (2007)) with primary production south of the PF. In certain areas, where the sBdy is very close to the Antarctic continent (eg.the Western Antarctic Peninsula), intrusions of UCDW onto the continental shelf have been reported

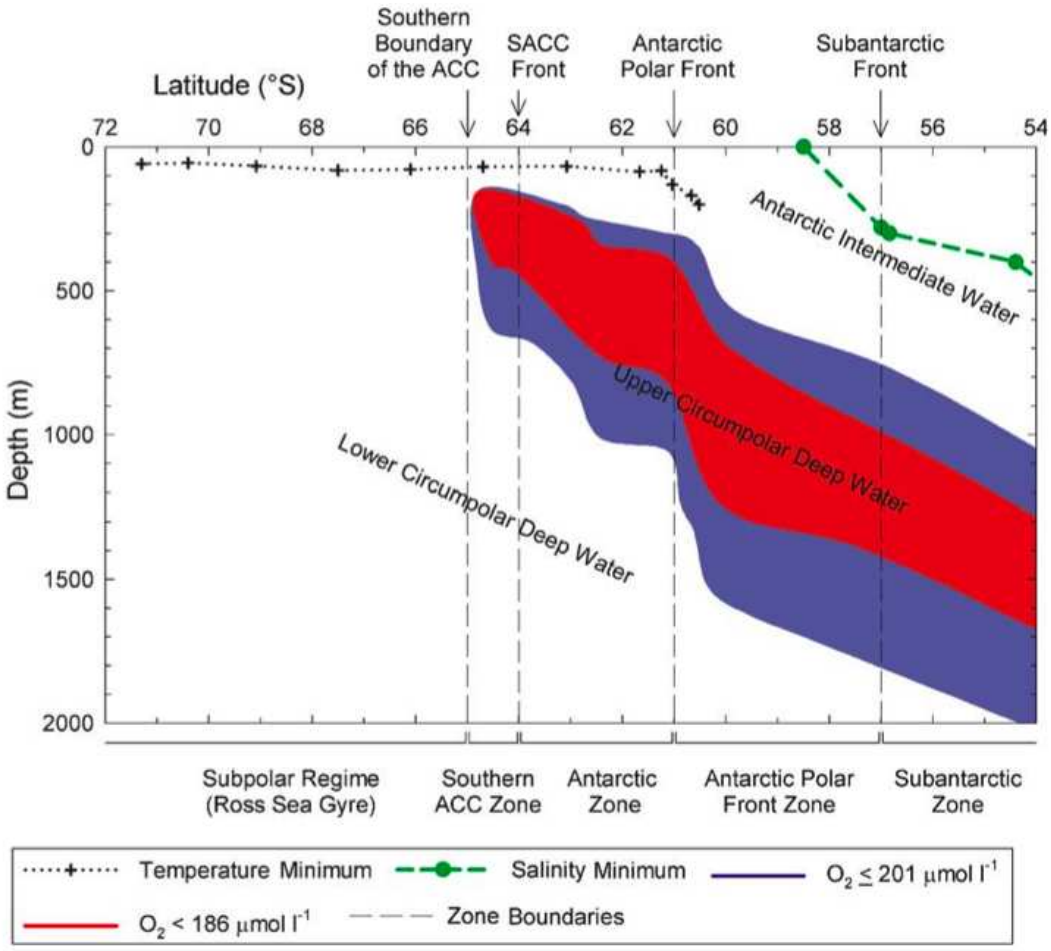

Figure 2.4: UCDW along 170°W during the austral summer of 1997-1998. Reprinted from *Hiscock et al.* (2003) with permission from Elsevier.

(*Pollard et al.*, 1995; *Prezelin et al.*, 2000, 2004; *Martinson et al.*, 2008; *Whitehouse et al.*, 2008b; *Moffat et al.*, 2009; *Reiss et al.*, 2009) and these intrusions have been linked to high biomass blooms, as have Ross Sea blooms (*Peloquin and Smith*, 2007). In addition, the presence of UCDW is thought to be crucial to the life-cycle of Antarctic krill, a foundation species for the SO ecosystem. This is not only due to UCDW supplying nutrients to the phytoplankton which provide the krill food supply, but also because the warmer UCDW water speeds up the development of krill embryos and provides a path for krill larvae from deep water to the continental shelf (*Constable et al.*, 2003). Another recently suggested (*Behrenfeld*, 2010) role for UCDW occurs when UCDW waters mix with the surface layer in winter and help to disperse the grazers that keep phytoplankton in check.

In addition to these effects on primary production and ecosystem function, UCDW is rich in DIC (*Iudicone et al.*, 2010) and thus its upwelling also impacts on CO_2 levels in the atmosphere.

2.4 Meridional Overturning Circulation

The thermohaline circulation (*Rahmstorf*, 2006) is that part of the ocean which is driven by fluxes of heat and freshwater across the sea surface and subsequent interior mixing of heat ("thermo") and salt ("haline"). Key features of the thermohaline circulation are (*Rahmstorf*, 2006):

1. deepwater formation (in the Greenland-Norwegian, Labrador, Weddell and Ross Seas);

2. spreading of deep waters (NADW and AABW), mainly as Deep Western Boundary Currents;

3. upwelling of deep waters (mainly in the ACC, through Ekman divergence caused by a combination of the SO westerly winds and the Coriolis force, where the divergence of surface currents leads to an upwelling of deep waters), and

4. near-surface currents (which close the flow).

This leads to a large-scale deep overturning motion of the oceans, which is represented schematically in Figure 2.5 (*Broecker*, 1991) as the "great ocean conveyor belt". This figure illustrates the north poleward movement of warm water, which cools, becomes denser and sinks at high latitudes, forming NADW, which then flows southward into the other ocean basins and upwells in the SO. The return flow of surface water from the Pacific to the Atlantic then completes the conveyor belt (*Jacobson et al.*, 2000).

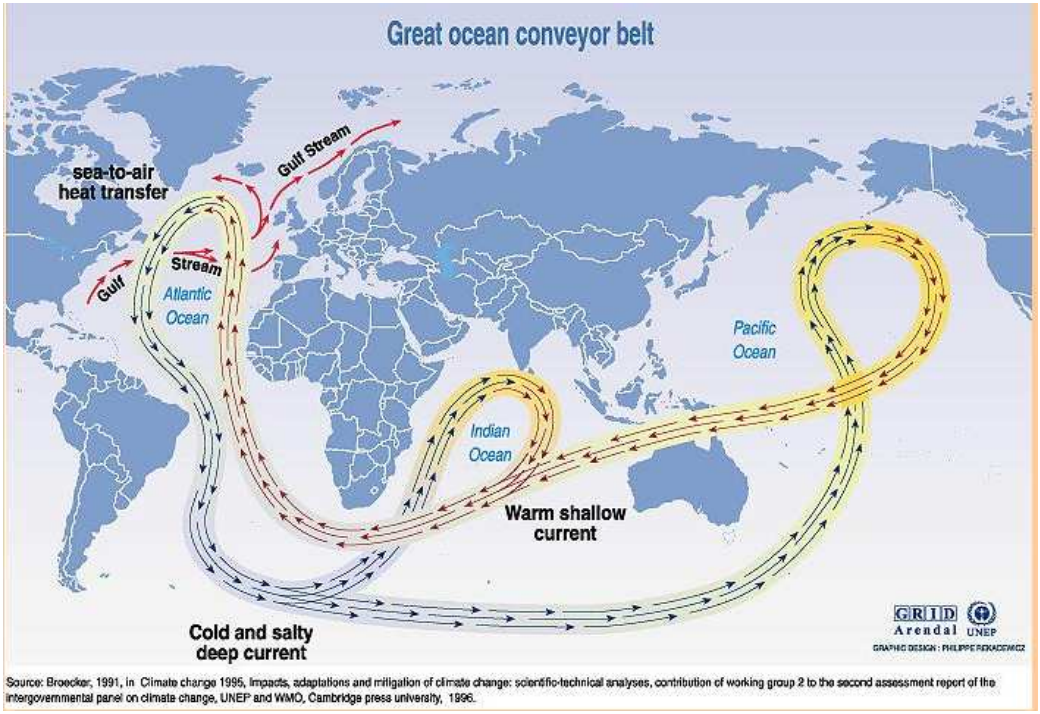

Figure 2.5: The great ocean conveyor belt (*Broecker*, 1991; *Watson et al.*, 1996).

A concept which is related and complementary to the thermohaline circulation is that of the meridional overturning circulation (MOC). This refers to the north-south flow as a function of latitude and depth, often integrated in an east-west direction across an ocean basin or the globe and depicted graphically as a stream function (*Rahmstorf*, 2006). That is, the MOC is the two-dimensional flow field with a transport defined as the zonally integrated meridional flux of mass (*Lozier*, 2010). The terms MOC and thermohaline circulation are often used interchangeably, but this is not strictly accurate as parts of the MOC, such as the near-surface Ekman cells, are clearly wind-driven (*Rahmstorf*, 2006). Even the interior circulation is increasingly seen as driven by turbulent mixing from winds and tides and thus the wind-driven circulation is no longer seen as independent of the MOC (*Toggweiler and Russell*, 2008; *Visbeck*, 2007). A recent study of MOC transport in the North Atlantic (*Biastoch et al.*, 2008) has shed light on the question of whether buoyancy or wind forcing controls the variability of the overturning. It was found that wind forcing dominated on interannual to decadal time-scales, whereas on centennial time-scales buoyancy forcing was dominant (*Lozier*, 2010).

The composition of the water upwelling in the SO, and of the resulting water moving northward and southward, are a matter of great debate in the oceanographic community (*Marinov et al.*, 2006). The conventional view regards the MOC in the SO as consisting of upper and lower cells (*Lumpkin and Speer*, 2007). The upper (Deacon) cell is formed primarily by northward Ekman transport and southward eddy transport in the UCDW layer (*Speer*

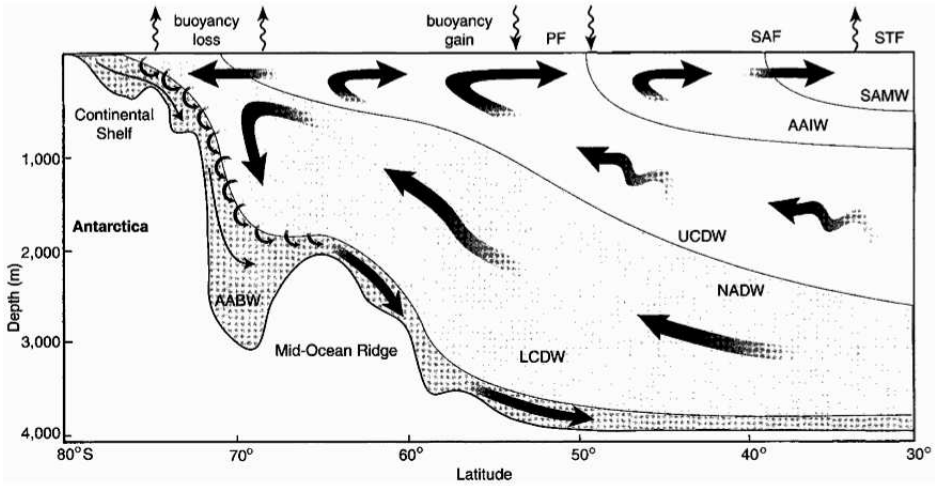

Figure 2.6: The upper and lower cells of the meridional circulation in the Southern Ocean (*Speer et al.* (2000), reprinted with permission from the Journal of Oceanography).

et al., 2000), a dynamical necessity since UCDW is generally at a shallower level than the topographic obstacles in its path, so that deep-water upwelling associated with the Ekman cell must be confined below the crests of these obstacles (*Olbers et al.*, 2004; *Sloyan and Rintoul*, 2001). After water upwells southwards to the near-surface along steeply tilted isopycnals and is entrained in the ACC, it moves northward by surface Ekman transport and then forms SAMW or downwells beneath the warmer SAMW to form AAIW (*Speer et al.*, 2000; *Marinov et al.*, 2006). This northward near-surface flow is driven by the SH westerly winds and the southward flow required by conservation of mass is provided by the NADW flow from the North Atlantic in addition to the inflow of aged waters from the Indian and Pacific Oceans.

This upper cell can be seen in Figure 2.6, as can the lower cell, which is driven primarily by density-driven formation of AABW, near the Antarctic continent. This bottom water then moves slowly northwards to the North Atlantic and North Pacific (*Orsi et al.*, 1995).

Using nine hydrographic sections in an inverse box model of the SO, Sloyan and Rintoul (*Sloyan and Rintoul*, 2001) found a transport of 50 Sv in the deep overturning circulation, which consists of an equatorward flow of LCDW and AABW and a poleward flow of UCDW including Indian Deep Water and Pacific Deep Water. These southward flows shoal and 34 Sv of outcropping UCDW is converted by air-sea fluxes to AASW. This compares with a total eastward ACC transport of around 130-140 Sv (*Whitworth et al.*, 1982), although the figure is higher near Australia, 147 $\pm$ 10 Sv (*Rintoul and Sokolov*, 2001).

An alternative viewpoint suggests that the upper and lower circulations may be connected. A recent study (*Garabato et al.*, 2007) measured rates

of mixing and upwelling in the ACC using a natural tracer (mantle Helium from hydrothermal vents). These mixing processes in the ACC are key to the MOC, because they control the rate at which water, which sinks at high latitudes, returns to the surface in the SO. The study's authors (*Garabato et al.*, 2007) propose a revised circulation, based on the effect of topography on the flow of the ACC. The suggestion is that waters, situated near the boundaries of the two cells, can rapidly flow both along and across isopycnals, creating a "short circuit" in the MOC. Thus, the simplicity of the conveyor-belt model is increasingly being seen as unhelpful (*Lozier*, 2010) since it ignores the complexity of the ocean's overturning, as well as the role of eddies and the ocean's wind field.

2.5 Scales of Variability

When considering climate variability on time-scales of several years or larger, the role of the oceanic circulation is extremely important because of the thermal inertia of the ocean's waters. Since the uppermost few metres of the ocean have the same heat capacity as the entire overlying atmosphere, the oceans act as a key factor for moderating rapid variations in climate. However, on longer time-scales this stored heat can be transported by oceanic circulation, altering the position of the thermal anomaly caused when the heat entered the ocean to where it is finally released (*van Aken*, 2007).

Two different time-scales can be recognised in this regard: decadal versus centennial. The former is associated with the upper ocean [O(1 km)] wind-driven circulation and the latter with the MOC, where the full water column (mean depth 3700 m) is involved (*van Aken*, 2007).

As mentioned in Section 2.3, CDW is a mixture of NADW, AABW and AAIW, as well as relatively old water from the Indian and Pacific Oceans (*Callahan*, 1972). Some direct observations of temperature and salinity variations on decadal scales within UCDW have been reported (*Johnson and Orsi*, 1997; *Gille*, 2002; *Aoki et al.*, 2003, 2005) and a recent modelling study by *Santoso et al.* (2006) has examined the natural $\theta - S$ variability of CDW on longer time-scales. Three modes, which account for 68% and 82% of the total variance in UCDW and LCDW respectively, were identified. The first mode involves inter-basin (North Atlantic and SO) variability via NADW on multi-centennial time scales and is less significant for UCDW than LCDW (37% versus 60% of the total variance respectively). The second mode, on the other hand, is more significant for UCDW than LCDW (21% versus 16%) and involves multi-decadal to centennial timescales, with variability controlled by meridional advection driven by fluctuations in the southward Deep West-

ern Boundary current and the northward Malvinas current. The third mode suggests an AAIW source in the South Pacific, which contributes to UCDW variability, particularly by vertical mixing and zonal advection.

2.6 Southern Hemisphere Winds

Strong SH westerlies drive the eastward motion of the ACC around Antarctica. The wind stresses in the SO (especially in 0-150°E, 40-60°S) are the greatest in the world (*Trenberth et al.*, 1990), primarily during Austral winter, but also in other seasons. The strongest westerly winds tend to be found between 45°S and 50°S (*Toggweiler and Russell*, 2008), whereas the ACC is generally found south of this (Section 2.2). Thus any change in the the mean position or strength of the westerlies is significant in that it will affect the zonal circulation and, because variations in Ekman transport will affect convergences and divergences, including the upwelling of nutrient-rich UCDW, it will then in turn affect the MOC and potentially the pathways of intermediate water ventilation (*Sen Gupta and England*, 2006).

2.7 Global Climate Indices

2.7.1 Southern Annular Mode Index

The SAM or Antarctic Oscillation is the most important mode of climate variability in the SH middle and high latitudes on intra-seasonal to inter-annual timescales (*Lovenduski and Gruber*, 2005). The SAM is characterised by shifts in the atmospheric mass between mid- and high-latitudes and is associated with north-south movements in the westerly winds.

Gridded reanalysis data sets, such as those from the National Center for Environmental Prediction-National Center for Atmospheric Reanalysis (*Thompson et al.*, 2000) and ERA-40 (*Trenberth et al.*, 2005), have been used to derive time series of SAM values. Indices to measure the SAM, prior to the satellite era (1979), have been constructed by *Marshall* (2003) and also *Visbeck* (2009) using SH atmospheric pressure observations from stations situated either near 40°S or 65°S. Positive values of the SAM index indicate lower than normal wind pressures over the polar regions, while negative values mean the opposite (that is, higher than normal pressures over the polar regions). The index constructed by *Marshall* (2003) is used here because both seasonal and annual values are available.

Changes in SAM have been linked to changes in ocean circulation (*Hall and Visbeck*, 2002; *Saenko et al.*, 2005; *Sen Gupta and England*, 2006; *Fyfe and Saenko*, 2006; *Verdy et al.*, 2006; *Fyfe et al.*, 2007), sea-ice (*Lefebvre et al.*,

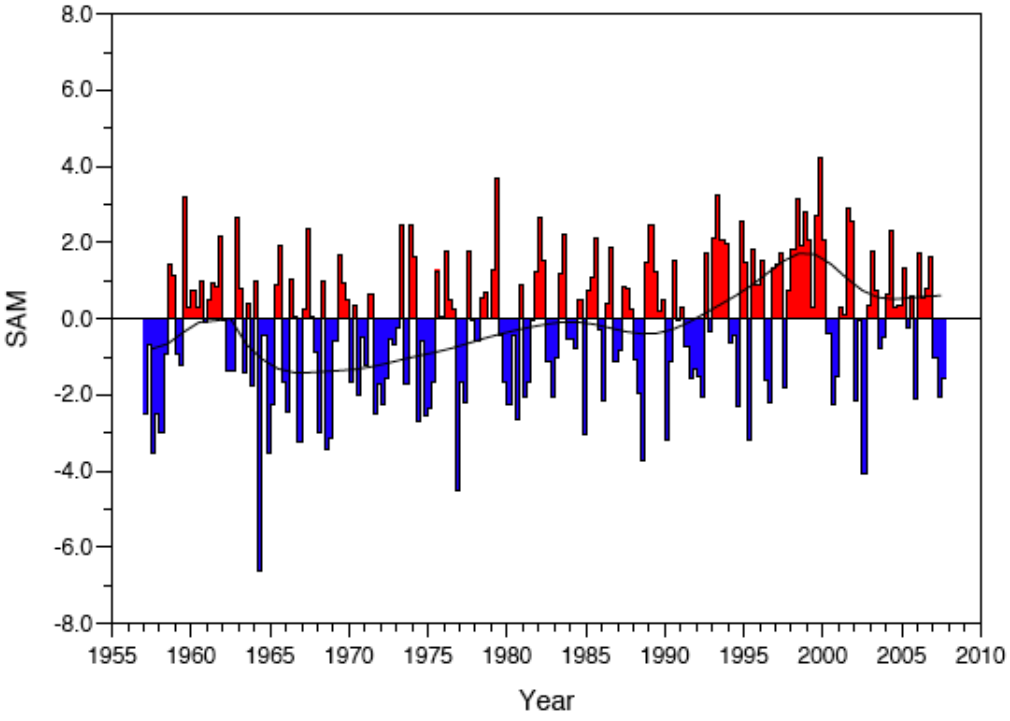

Figure 2.7: The annual Southern Annular Mode (SAM) index (*Marshall*, 2003) for 1957 - 2008 (http://www.nercbas.ac.uk/icd/gjma/sam.html).

2004; *Stammerjohn et al.*, 2008), and CO_2 uptake and biological productivity (*Lovenduski and Gruber*, 2005; *Russell et al.*, 2006; *Lovenduski et al.*, 2007; *Lenton and Matear*, 2007; *Butler et al.*, 2007; *Verdy et al.*, 2007).

When considered on an annual basis the SAM index shows an upward trend since 1970 (Figure 2.7), which has been linked to increases in greenhouse gases and ozone depletion (*Arblaster and Meehl*, 2006; *Yang et al.*, 2007b). However, when considered seasonally, the SAM shows significant positive trends only in summer (DJF) and autumn (MAM), over the period 1957-2004 (*Marshall*, 2007). A useful plot in *Monaghan et al.* (2008), which allows trends in the index to be estimated on a "running" basis, from a starting year up to 2005, also shows positive trends in SAM in DJF and MAM for starting years from the 1950s until the 1980s. The SAM index (*Marshall*, 2003; *Visbeck*, 2009) has been moving towards a more positive mode since the 1970s (*Thompson and Solomon*, 2002), indicating a poleward intensification of the SH winds. However, while the SAM is generally considered to be symmetric, recent studies have found that the wind response is not (*Drost and England*, 2009) and neither is the oceanic response of the fronts (*Sallee et al.*, 2008) and thus its effect differs in the various regions of the SO. This has been confirmed recently by *Sallee et al.* (2010), using Argo float data, who found that winds associated with departures of SAM from global symmetry cause heat flux anomalies that can explain changes in MLD and SST. For example, increasing SAM is associated with the deepening of MLD in the Eastern Indian and Central Pacific

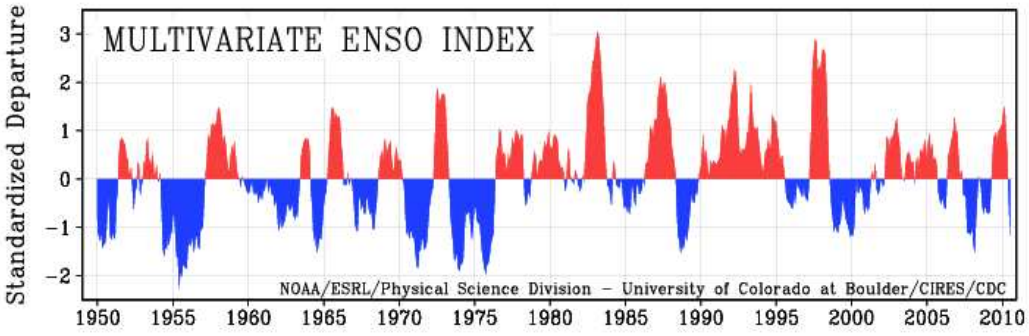

Figure 2.8: The Multivariate El Niño/Southern Oscillation (ENSO) index (*Wolter*, 1987; *Wolter and Timlin*, 1993) for 1950-2010 (http://www.esrl.noaa.gov/psd/people/klaus.wolter/MEI/mei.html).

oceans, but shallowing in the western part of these basins. This is significant because variations in MLD affect the capacity of the ocean to store heat and carbon and also the growth of phytoplankton, due to the availability of light and nutrients (*Sallee et al.*, 2010).

Another possible effect of increasing SAM, independent of fluctuations in the strength of the jet (*Marshall*, 2007), is latitudinal shifts in the jet, generally thought to be south with increasing SAM (*Thompson and Solomon*, 2002). However, it has recently been recognised that there is a non-zonal spatial variability across seasons in SAM (*Marshall*, 2007), due to non-zonally symmetric winds (*Sen Gupta and England*, 2006). This results in a meridional wind shift that is equatorward over large regions of the eastern hemisphere, the eastern Pacific and the Atlantic, and is poleward around New Zealand, South America and Africa (*Drost and England*, 2009). This means that the temporal shift of the SAM towards its positive phase on the zonal mean wind is negated to a certain extent, at various longitudes, due to the spatial shift of the SAM (*Drost and England*, 2009).

2.7.2 The Multi-variate El Niño/Southern Oscillation Index

It is also necessary to consider the effect on the SO winds of ENSO which, while it is a tropical coupled system, still has an impact in the Australian region, due to the effect of the East Australian Current (*Holbrook and Bindoff*, 1997; *L'Heureux and Thompson*, 2006). This work uses the multivariate ENSO Index (MEI) (*Wolter*, 1987; *Wolter and Timlin*, 1993), which monitors ENSO using observations, over the tropical Pacific, of sea-level pressure, zonal and meridional surface wind components, SST and total cloudiness fraction of the sky. Positive values of the MEI represent the warm ENSO phase (El Niño). The MEI for 1950-2010 is shown in Figure 2.8.

2.7.3 Connection between the SAM Index and MEI

Studies have found that ENSO and SAM indices are often anti-correlated (*L'Heureux and Thompson*, 2006; *Morrow et al.*, 2008) and that there is a strong resemblance between the impacts of SAM and ENSO on high-latitude SH climate, during the summer season (*Ciasto and Thompson*, 2008). In fact, *L'Heureux and Thompson* (2006) found that, during the Austral summer, roughly 25% of the temporal variability in the SAM is linearly related to fluctuations in the ENSO cycle (*L'Heureux and Thompson*, 2006).

2.7.4 Pacific Decadal Oscillation Index

The PDO is a pattern of SST anomalies in the subtropical North and South Pacific, that are out of phase with SST anomalies in the tropical Pacific (*Martinez et al.*, 2009). The PDO is defined (*Mantua and Hare*, 2002) as the leading empirical orthogonal function (EOF) of mean November through March SST anomalies for the Pacific Ocean north of 20°N latitude. Positive values indicate months of above normal SSTs along the west coast of North and Central America and on the equator, and below normal SSTs in the central and western north Pacific at about the latitude of Japan. Figure 2.9 shows the PDO Index for 1900-2005.

Recently, *Martinez et al.* (2009) have demonstrated, using about two decades of chlorophyll-a and SST satellite data, that multidecadal changes in global phytoplankton abundances are related to basin-scale oscillations of the physical ocean. Specifically, their work shows that the co-variability of chlorophyll-a and SST, in both the Pacific and Indian Oceans, is related to the PDO, most likely through the uplift or deepening of the pycnocline.

Interestingly, even though *Martinez et al.* (2009) found similarities in the basin-scale patterns of SST/chlorophyll-a and pycnocline/chlorophyll-a, they did not find these same relationships when the MLD rather than the pycnocline was used. They interpret this as showing that the chlorophyll-a/MLD relationship probably bears the imprints of changes which are more regional and intervene at shorter, interannual, scales.

2.7.5 Differences between ENSO and PDO

There are two main differences between ENSO and the PDO: firstly, the duration of these events (in the twentieth century, 6-18 months for la Nina/el Niño and 20-30 years for the PDO warm/cold phases) and secondly, the region where the climate signatures can be seen (the North Pacific/North American sectors, with secondary signatures in the tropics, for the PDO, and the opposite for ENSO).

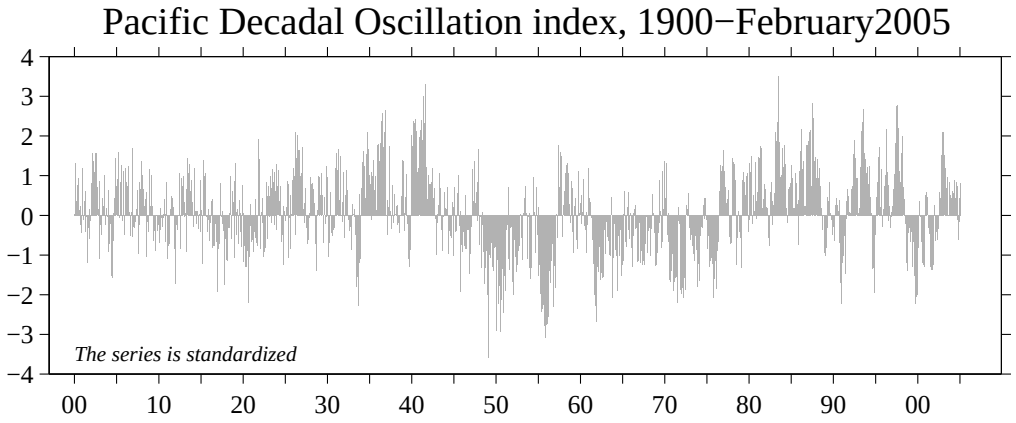

Figure 2.9: The Pacific Decadal Oscillation (PDO) index (*Mantua and Hare*, 2002) for 1900 - February, 2005 (http://jisao.washington.edu/data_sets/pdo/#analysis).

2.8 Chlorophyll-*a* and Primary Production

Primary productivity is the conversion, by phytoplankton, of inorganic materials into new organic compounds by photosynthesis. Gross primary productivity is measured as the rate at which carbon is fixed in new organic material (*Lalli and Parsons*, 1997). Net primary production is defined as gross primary production minus cellular respiration, and is important for carbon sequestration (*Cassar et al.*, 2007). In the work that follows, primary production will refer to net primary production.

Since 1997, satellite ocean colour data (reflectance data in the visible spectrum that can be used to derive chlorophyll concentration data (*O'Reilly et al.*, 1998)), has been provided by SeaWiFS and, since 2002, by the Moderate Resolution Imaging Spectoradiometer (MODIS) on the Aqua satellite. Prior to that time, the Coastal Zone Color Scanner (CZCS) also collected data between 1978 and 1986, although data collection was not uniform in either time or space. Chlorophyll concentration data have also been measured during various cruises in the SO (eg. *Nicol et al.* (2000); *Westwood et al.* (2010)). A few modelling studies, which use satellite-derived chlorophyll-*a* values to calculate primary production, have been conducted for the SO (*Arrigo et al.*, 2008; *Smith and Comiso*, 2008; *Barbini et al.*, 2005).

The pattern of chlorophyll-*a* in the SO is seasonal; values are low (less than 0.15 mg/m^3) during winter (June-August), then begin to rise near Antarctica in September, increasing and extending to the north in October/November and then occupying the AZ, south of the PF, until February (with chlorophyll-*a* concentrations up to 0.4 mg/m^3) (*Sokolov and Rintoul*, 2007). The mean summer chlorophyll-*a* concentration pattern between 100°E and 180°W can be seen in Figure 2.10. The lowest chlorophyll-*a* concentrations are in the SAF, while the overall pattern is consistent with the upwelling of nutrient-rich deep water south of the PF (*Sokolov and Rintoul*, 2007). Previous studies (*Tynan*,

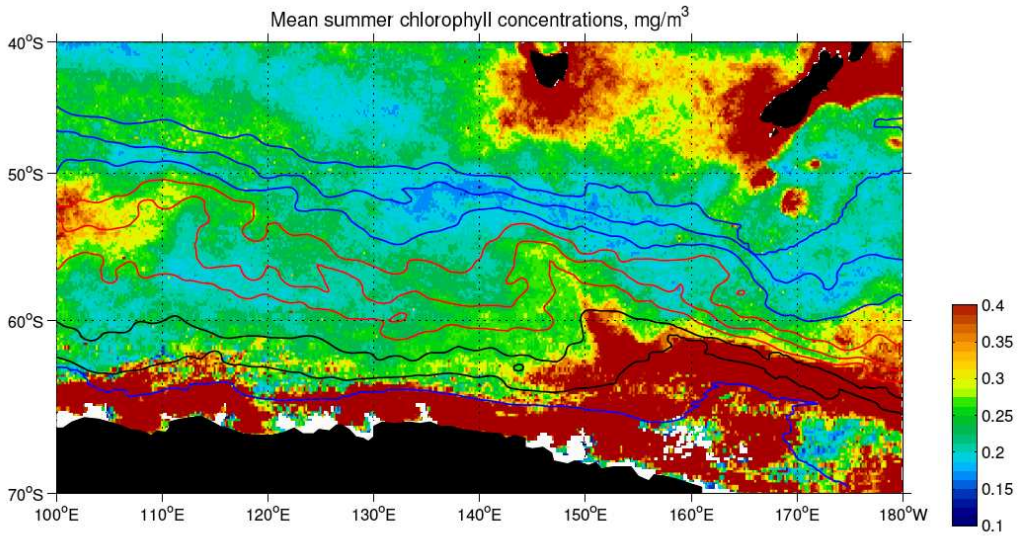

Figure 2.10: Mean summer chlorophyll-*a* concentration in the Southern Ocean south of Australia and New Zealand (*Sokolov and Rintoul*, 2007).

1998) had suggested that the SO fronts were regions of increased productivity but, by averaging surface chlorophyll-*a* measured along streamlines, *Sokolov and Rintoul* (2007) showed that the fronts define the limits of zones with similar concentration and seasonality of chlorophyll.

While the major controls on primary production are (*Schlitzer et al.*, 2003) SST and PAR, various factors can affect primary production either singly, or in combination: temperature, seasonal irradiance, mixing/mixed layer depth, stratification, sea-ice, macro- and micro-nutrient availability and grazing. For example, a recent study (*Rose et al.*, 2009), into the combined effect of iron addition and increased temperature (+4°C) on plankton assemblages in the Ross Sea, has found greatly magnified effects compared with the effect of either of these variables individually. These effects include total phytoplankton abundance, changes in community composition, as well as photosynthetic parameters and nutrient drawdown. Another Ross Sea study (*Feng et al.*, 2010), which examined the various interactive effects of iron, irradiance and CO_2, found that shifts in these variables and their mutual interactions all play a role in controlling present day Ross Sea plankton community structure, with the main influence of high CO_2 being the effect on diatom community structure. It has also recently been found that there is a connection between variability in iron speciation and irradiance/temperature (*Tagliabue et al.*, 2009). This is significant because not all forms in which iron exists in seawater are bioavailable. Using a global ocean biogeochemistry model, *Tagliabue et al.* (2009) found that higher irradiance promotes the conversion of dissolved iron into bioavailable forms, while temperature plays a secondary role with cold MLs increasing bioavailable iron concentrations.

Although the pattern of chlorophyll-a is affected by the seasonal variation in irradiance, this needs to be considered in relation to MLD and, if appropriate, sea-ice as well. MLD in the SO follows a seasonal cycle, with maximum depths in the SAZ between August and October, in the region where SAMW is formed, whereas south of the SAZ, the winter ML shoals southward. Summer MLD is nearly 60m in the SAF, shoaling to less than 40m near the Antarctic continent (*Sokolov*, 2008). Previous studies have shown that there is a good correlation between phytoplankton production and MLD (*Mitchell and Holm-Hansen*, 1991).

Sea-ice retreat near Antarctica is thought to affect summer primary production by seeding the upper ocean with phytoplankton cells growing in or on the ice, providing iron in melt-water (*Constable et al.*, 2003), and by forming a low salinity, stable surface layer (*Smith and Nelson*, 1985). A stable ML is conducive to bloom development, since cells are not mixed away from suitable light levels. However, this can lead to depletion of nutrients and, in practice, wind-induced mixing erodes the stable ML (*Smith et al.*, 2000). In practice, stratification is not only affected by wind and sea-ice melt, but also by temperature. A recent study in the SO south of Australia and New Zealand (*Sokolov*, 2008), looking at these factors, found that there is a strong seasonal signal in chlorophyll-a concentration, caused by sea-ice melt water flux, particularly between the sACCf and the sBdy. The author attributes this to melt-water flux, which forms very shallow MLs, both improving irradiance and also providing iron which triggers the blooms.

2.9 Nutrients

The SO is often referred to as a "high nutrient/low-chlorophyll" (HNLC) region (*Coale et al.*, 2003; *Whitehouse et al.*, 2008a). This terminology reflects the observation that, despite an abundance of the major nutrients nitrate, phosphate and silicate (except north of the PF in summer for silicate (*Cassar et al.*, 2007)), in general, the SO is an area of relatively low primary production (80-300 $\mathrm{mgCm^{-2}day^{-1}}$ compared with coastal values in excess of 1000 $\mathrm{mgCm^{-2}day^{-1}}$) (*Löscher et al.*, 1997).

2.9.1 Macronutrients

Figures 2.11-2.13 show annual concentration levels for the macronutrients nitrate, phosphate and silicate (*Garcia et al.*, 2006), respectively, and it can be seen that in each case in the SO, nutrient concentrations increase to the south. This is due to the fact that the geostrophic balance of the ACC requires isopycnals to slope up to the south and nutrients move to the surface by

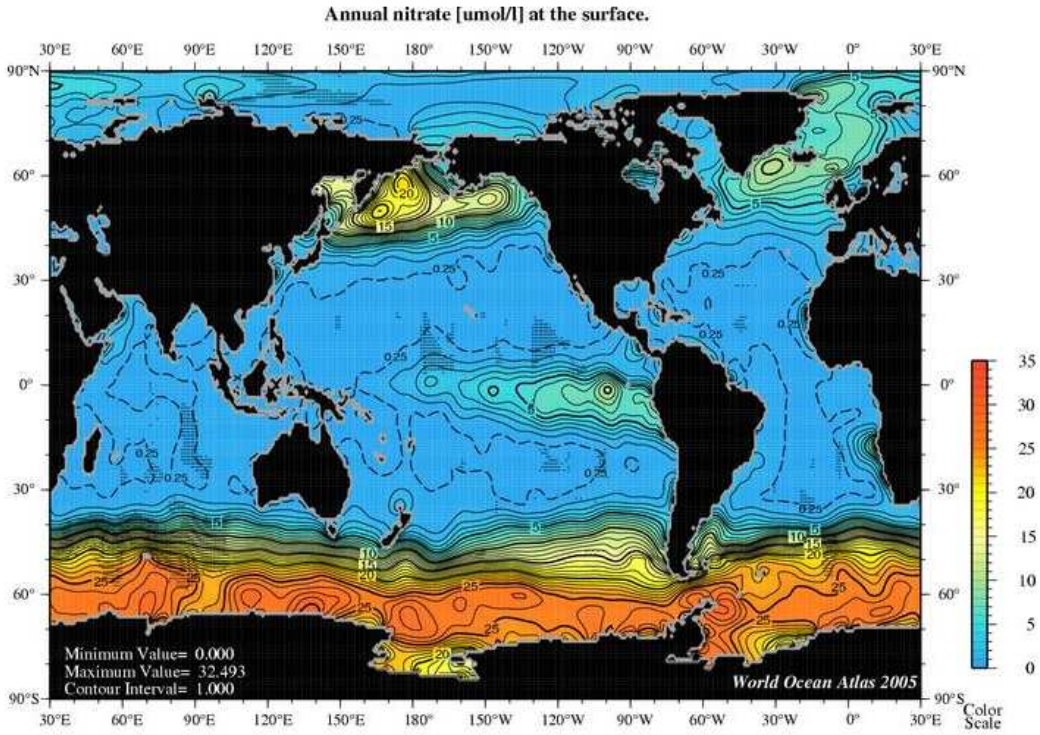

Figure 2.11: Annual concentration of nitrate from the World Ocean Atlas (*Garcia et al.*, 2006) (http://www.nodc.noaa.gov/cgi-bin/OC5/WOA05F/woa05f.pl).

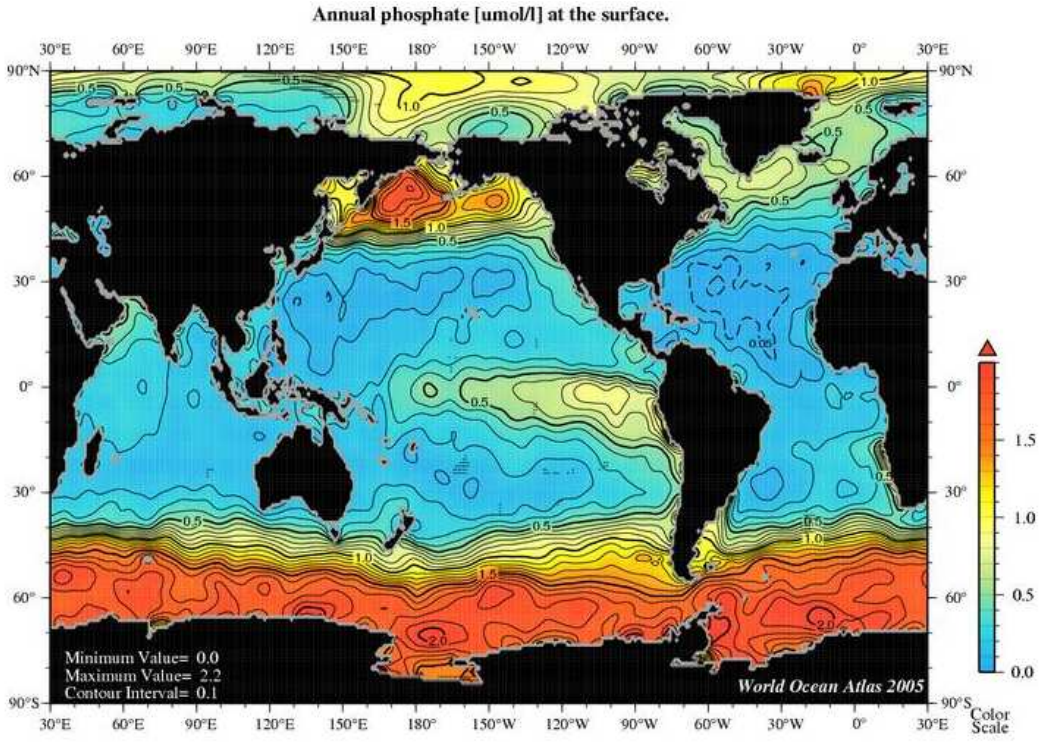

Figure 2.12: Annual concentration of phosphate from the World Ocean Atlas (*Garcia et al.*, 2006) (http://www.nodc.noaa.gov/cgi-bin/OC5/WOA05F/woa05f.pl).

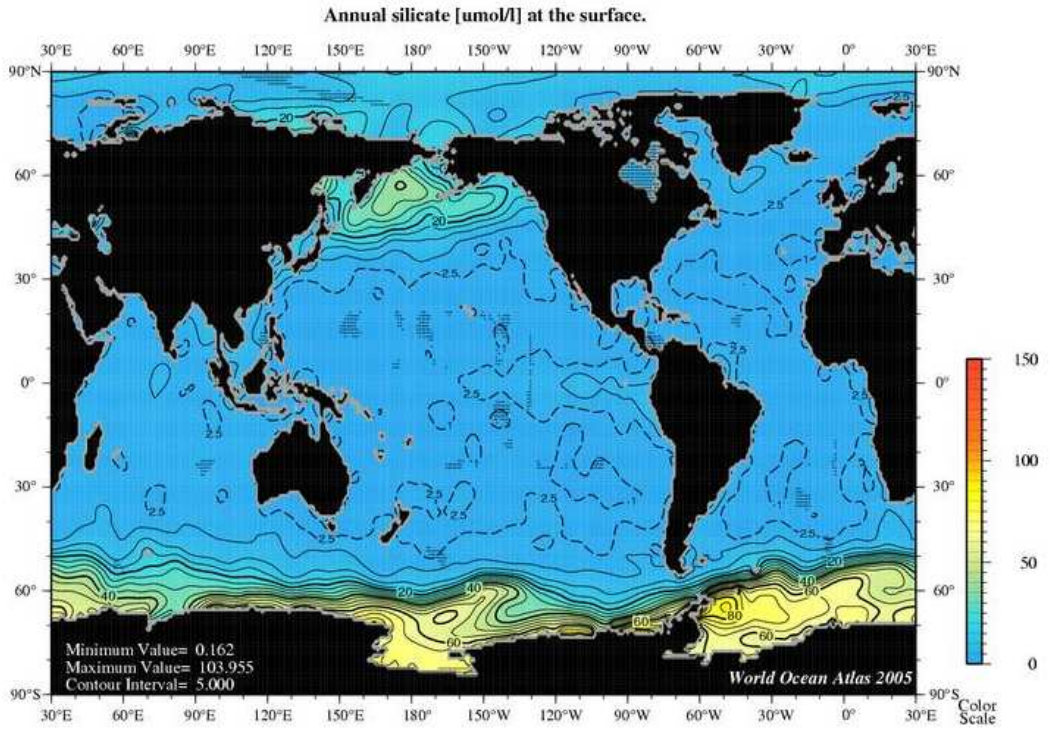

Figure 2.13: Annual concentration of silicate from the World Ocean Atlas (*Garcia et al.*, 2006) (http://www.nodc.noaa.gov/cgi-bin/OC5/WOA05F/woa05f.pl).

both along-isopycnal advection and mixing and by diapycnal (across-isopycnal) mixing (*Pollard et al.*, 2002). Mean nutrient concentrations for the SO on the neutral density surface 27.8 kg m^{-3}, which corresponds to the core of UCDW (*Pollard et al.*, 2002), have been calculated by *Pollard et al.* (2006) to be 72.2 μmol kg^{-1} for silicate and 34.7 μmol kg^{-1} for nitrate. They have also introduced the concept of the surface-influenced depth, below which little variation in nutrient concentrations can be seen on any particular neutral density surface, around the entire SO. This leads them to infer that isopycnic stirring by meso-scale eddies homogenise nutrient distributions faster than they can be modified by diapycnic mixing with adjacent neutral density surfaces. They also note that the surface-influenced depth to which nutrient depletion extends is significantly deeper than the winter MLD.

2.9.2 Micronutrients: Trace elements

One suggestion in relation to the puzzle associated with the persistence of HNLC systems was that the extremely low levels of some trace elements (eg. Fe, Cu, Mn, Ni, Co, Zn, Cd) in some ocean basins may limit phytoplankton growth (*Morel and Price*, 2003). This hypothesis has been tested by a number of experiments in various oceanic waters. For example, the addition of Fe, Mn, Cu and Zn to sub-Arctic surface waters (*Coale*, 1991) found that natural levels of Fe and Cu (but not Mn and Zn) may influence phytoplankton productivity

and trophic structure in open-ocean HNLC systems. Another experiment, combining Fe with any of Mn, Co and Zn in Antarctic waters along 6°W (*Scharek et al.*, 1997) led to the conclusion that Fe is the most important trace metal controlling phytoplankton development and that co-limitation by the other metals did not occur. More recent deckboard enrichment experiments in the Ross Sea and ACC along 170°W, have demonstrated that Zn is not a limiting factor in these regions.

2.9.3 Micronutrients: Iron

In 1990, *Martin* (1990) proposed his "iron hypothesis", which suggested that the solution to the HNLC paradox was that primary production in the SO was limited by bio-available iron. This has been demonstrated by bottle incubation experiments (*Martin et al.*, 1990b,a) and satellite observations (*Comiso et al.*, 1993; *Moore et al.*, 1999; *Moore and Abbott*, 2000). It has also been shown in the SO, for various regions and seasons, by field and in-situ fertilisation experiments, such as SOIREE (*Boyd et al.*, 2000), EisenEx (*Gervais et al.*, 2002), SOFeX (*Coale et al.*, 2004), EIFEX (*Hoffmann et al.*, 2006), SAGE (*Boyd et al.*, 2007) and LOHAFEX (*Breitbarth et al.*, 2009) and, by natural fertilisation experiments, such as KEOPS (*Blain et al.*, 2008) and CROZEX (*Pollard et al.*, 2009). See Table 2.4 for a summary of the various SO iron fertilisation experiments.

However, studies have found that phytoplankton response to iron enrichment is a complex process, which depends on individual taxa and also on the surrounding level of silicate (*Coale et al.*, 2003; *Hiscock et al.*, 2003).

Five sources of iron bio-available to SO surface waters can be identified (*Cassar et al.*, 2007):

1. aeolian deposition (*Cassar et al.*, 2007; *Gabric et al.*, 2002, 2010);
2. sea-ice melt (*Sedwick et al.*, 1997, 2000; *Lannuzel et al.*, 2010b);
3. the release of dissolved iron or the resuspension of shelf sediments (*Prezelin et al.*, 2000);
4. vertical mixing induced by rough bottom topography (*Moore and Abbott*, 2002; *Sokolov and Rintoul*, 2007; *Blain et al.*, 2007) and
5. upwelling (*Hiscock et al.*, 2003; *Meskhidze et al.*, 2007).

Distinguishing between the above factors is difficult because processes may occur simultaneously in time or position and a number of factors may work together; for example, iron may be supplied to the ML by Ekman divergence after topographic upwelling transports iron vertically to shallower depths (*Sokolov*

Table 2.4: Artificial (*) and Natural Iron Fertilisation Experiments in the Southern Ocean

SOIREE* (*Boyd et al.*, 2000)	Southern Ocean IRon Enrichment Experiment	February 1999	141°E, 61°S (AZ)
EisenEx* (*Gervais et al.*, 2002)	Eisen (Iron) Experiment	November 2000	21°E, 48°S (PFZ)
SOFeX-North* SOFeX-South* (*Coale et al.*, 2004)	SO Iron Experiment	Jan/Feb. 2002	170°W, 54°S (SAZ) 172°W, 66°S (SZ)
EIFEX* (*Hoffmann et al.*, 2006)	European Iron Fertilisation Experiment	Feb/Mar 2004	20°E, 50°S (PFZ)
SAGE* (*Boyd et al.*, 2007)	SOLAS Air-Sea Gas Exchange Experiment	Mar/Apr 2004	173°E, 48°S (SAZ)
LOHAFEX* (*Breitbarth et al.*, 2009)	LOHA (Hindi for iron) Fertilisation EXperiment	Jan-Mar 2009	37°W, 50°S (PFZ)
CROZEX (*Pollard et al.*, 2009)	CROZet natural iron bloom and EXport experiment	Summer 2004/5	52°E, 44°S (PFZ)
KEOPS (*Blain et al.*, 2008)	KErguelen Ocean and Plateau compared Study	Jan/Feb. 2005	72°E, 50°S (AZ)

and Rintoul, 2007). Also, since processes such as aeolian deposition and supply of iron via advection from continental margins are episodic, they generally act on short time-scales, although they also affect the overall distribution of iron in the SO (*Sedwick et al.*, 2008).

1. **Aeolian Deposition**

   Aeolian deposition (atmospheric deposition of mineral dust originating from arid regions in South Africa, Australia and South America) is generally thought to play only a minor role in iron supply to the open SO (*Fung et al.*, 2000; *Hoppema et al.*, 2003; *Meskhidze et al.*, 2007; *Wagener et al.*, 2008). A recent paper by *Cassar et al.* (2007), which correlates SO net community production (based on either O_2/Ar samples or the O_2 triple isotope anomaly) with model simulations of aerosol iron deposition, argues to the contrary. One of the authors' main arguments relates to the observed increase in productivity from south to north, which they argue cannot be driven by upwelled iron, because it would rapidly be removed by scavenging and export. However, *Boyd and Mackie* (2008a) dispute this claim and point out that high production can be sustained by recycling iron during northward transport in this region, as evidenced by plumes of length 2000 km, downstream of South Georgia. Also, *Jickells*

et al. (2005) state that dissolved iron has a residence time of decades in the ocean, due to it being predominantly organically complexed, which protects it against rapid scavenging. Other authors agree that aeolian deposition is a significant source of dissolved iron to the upper ocean in the SAZ, but not further south (*Jickells et al.*, 2005; *Sedwick et al.*, 2008).

2. **Sea-ice**
   Seasonal sea-ice covers a large area of the SO and can act as a "dust collector", which, after melting, can release a significant amount of bioavailable iron that can contribute to sea-ice-edge algal blooms. For example, in summer 1995/96, Sedwick and DiTullio (*Sedwick and DiTullio*, 1997) measured surface ML dissolved iron (dFe) concentrations in the Ross Sea, in the presence of sea-ice and, 17 days later, in ice-free conditions. There iron concentrations dropped from 0.72-2.3 nM to 0.16-0.17 nM, while algal biomass doubled. In addition, measurements taken in spring in the Atlantic sector by *Croot et al.* (2004) found dFe concentrations of 0.3-1.5 nM near the ice edge. In contrast, however, dFe measurements along SR3 in spring by *Sedwick et al.* (2008), in both ice-free and ice-melt areas, found that melting sea-ice was not a significant source of dissolved iron to surface waters. The authors suggest that either the sea-ice contained less iron than previously sampled sea-ice (*Lannuzel et al.*, 2007) or that there had been significant biological removal of dissolved iron prior to the measurements. Iron measurements taken in the western Weddell pack ice in 2004/05 led the authors to conclude that pack ice is a storage reservoir over, autumn/winter, for iron supplied from below by upwelling (5) and/or vertical diffusion and lateral advection from the continent (3), which becomes bioavailable in spring.

3. **Resuspension and release of iron near continental shelves**
   Sediment resuspension in McMurdo Sound has been demonstrated by sediment trap collections and underwater observations (*Berkman et al.*, 1981) and sediment resuspension has been demonstrated to be a significant source of iron in the California Current System (*Johnson et al.*, 1999; *Elrod et al.*, 2004). Episodic iron flux has also been shown (*Prezelin et al.*, 2000; *Martinson et al.*, 2008) for the case of the outer Western Antarctic Peninsula continental shelf, where topographically-induced upwelling of UCDW occurred. Iron-rich waters from continental margins are also a source of iron to SO surface waters via advection (*Sedwick et al.*, 2008).

4. **Topographically induced vertical mixing**
   Sokolov and Rintoul (2007) argue that most regions of elevated chloro-

phyll in the SO can be explained by topographically-induced persistent upwelling (vertical mixing) of nutrients, induced by the ACC flowing over rough bottom topography, followed by lateral advection. The mechanism presented involves a non-zero bottom pressure torque, which then implies a vertical velocity at the sea-floor, which is coherent throughout the water column. This leads to upwelling at a number of sites in the SO, such as the Pacific-Antarctic Ridge, East Pacific Rise, Drake Passage, Scotia Sea, mid-Atlantic Ridge and Southeast Indian Ridge, in addition to the two natural fertilisation experiments mentioned above in Table 2.4. *Sokolov and Rintoul* (2007) also note that the sACCf has the highest and most spatially variable chlorophyll concentrations of the three main ACC fronts and that there is a weaker relationship between bathymetry, upwelling and phytoplankton biomass for the sACCf, compared with the PF. They suggest that this may be due to iron from sea-ice melt (see (2)) or from shelf sediments (see (3)), despite noting that the sACCf has the highest levels of "background" upwelling (as discussed in (5) below).

5. **Upwelling**

   The type of upwelling discussed in this section differs from that mentioned in (4) above and refers to the large-scale upwelling south of the PF associated with Ekman divergence. This sets the broad-scale pattern of vertical velocity in this region (*Sokolov and Rintoul*, 2007), associated with the vertical transport of iron-rich deep water (*DeBaar et al.*, 1995; *Löscher*, 1999; *Hoppema et al.*, 2003). Indeed, *Coale et al.* (2005) calculated, from iron measurements in the ACC along 170°S in 1996/97, that upwelling may supply 50% of the export production of iron near the sACCf. Even *Sokolov and Rintoul* (2007) conclude that both Ekman- and topographically-induced upwelling contribute to the strong upwelling of deep water containing higher concentrations of iron, which is likely to be the primary factor associated with the higher productivity observed south of the PF. Also, modelling studies by *Archer and Johnson* (2000) and *Moore et al.* (2002) found that iron from deep water sources is capable of sustaining 70-80% of total new oceanic production. Interestingly, another modelling study by *Sarmiento et al.* (2004) shows that three-quarters of biological production **north** of 30°S is accounted for by the SO nutrient supply, due to northward Ekman transport of nutrients upwelled south of the PF.

2.9.4 Measurements of dissolved iron

There are few direct measurements of iron available for the SO, although a concentrated effort to identify the biogeochemical properties of iron and other trace elements is underway at present, via the GEOTRACES programme (`http://www.geotraces.org`). *Sohrin et al.* (2000) found that iron distributions change markedly across the SO fronts and, in 2001, *Measures and Vink* (2001) summarised data on surface-water iron distributions in the SO, away from continental land masses, to that point in time, as consisting of low values (<0.5 nM) and decreasing towards the south. They also commented on abrupt changes in iron concentrations, spatially (near the PFZ) and temporally (related to biological activity).

More recently, *Sedwick et al.* (2008) showed that ML dissolved iron concentrations, measured along SR3 in the top 300 m of the water column in March 1998 and November/December 2001, generally decreased from north to south, from 0.76 nM in the STF to <0.1 nM south of the PF. They also found nutrient-like vertical dFe profiles at four stations between 60°S and 64°S on the spring 2001 cruise, suggesting that dFe had been biologically depleted prior to sampling. In addition, it was found that, consistent with the uptake of dissolved iron by phytoplankton, the lowest dFe concentrations appear to be associated with elevated levels of chlorophyll-*a* (>0.3 mgm^{-3}), in the region south of the PF (*Sedwick et al.*, 2008).

Even fewer measurements are available for dissolved iron in UCDW. Data collected by *Hiscock et al.* (2003), along 170°W from 54°S to 72°S on four cruises during the growing season of 1997/98, showed that UCDW was present at the surface in both the AZ and in the sACCZ, but absent south of the sBdy and north of the PF. It was found (*Measures and Vink*, 2001) that dissolved iron concentrations in UCDW in that region were around 0.3 nM. Earlier measurements, made along the 6°W meridian in Austral spring 1992, found elevated dissolved iron concentrations in UCDW in the PF region compared with further south *Löscher et al.* (1997). *Hoppema et al.* (2003) estimate that, given a typical dissolved iron concentration of about 0.4-0.5 nM within UCDW (*Löscher et al.*, 1997; *Sedwick et al.*, 2000; *Hiscock et al.*, 2003) and an annual mean estimate for UCDW upwelling of 34 Sv (*Sloyan and Rintoul*, 2001), then the annual iron flux is about 0.5 Gmol Fe yr^{-1}. This translates to 14 mmol m^{-2} yr^{-1}, based on a surface area of $35{\times}10^{12}$ m^2 south of the PF (*Hoppema et al.*, 2003), which is similar to the estimate of 8-16 mmol m^{-2} yr^{-1} by *Watson et al.* (2000).

2.9.5 Utilisation of iron

Hoppema et al. (2003) also suggest that the large-scale dynamics of the ACC are a major reason for the sub-optimal utilisation of this large flux of iron into the surface layer and that at least 25% of upwelled iron is exported northwards within the Ekman layer without being used by phytoplankton. They estimate mean equatorward velocities of 2.4 cm s^{-1} (based on a PF path length of 25 000 km, an Ekman layer depth of 50 m and a volume transport of 30 Sv), which leads to the meridional distance between the sBdy and the PF being covered in one year. They further argue that a substantial part of the upwelled iron enters the surface layer in autumn and winter, when the strongest winds promote turbulent mixing and convection. However, this entrainment of iron into the deepening ML occurs when light levels are low, sea-ice is present and phytoplankton are less able to utilise the iron. The figure of 25% utilisation comes from half the iron moving out of the ACC during the six months, in addition to the ML being twice as deep. The argument also hinges on upwelling occurring over a widespread area south of the PF, for which they present evidence, contrary to the classical view that all upwelling occurs near the Antarctic Divergence (sACCf) (*Hoppema et al.*, 2003).

However, in later work using nutrient concentrations on SO neutral density surfaces and climatological winds, *Pollard et al.* (2006) argue that nutrients, such as nitrate, silicate or iron, are likely to take several years (not one) to advect out of the SO. The reasoning is based on the upwelling of UCDW occurring between 56°S and 67°S, where the mean Ekman flux is less than half of that used by *Hoppema et al.* (2003) in the above calculation. Measurements of winter-time dFe (and nitrate) distributions in the SAZ, west of New Zealand, also suggest that waters from the south that supply iron to the SAZ remain at the surface for approximately three years (*Ellwood et al.*, 2008).

2.10 Southern Ocean Ecosystems

The key herbivores in the SO are thought to be salps, copepods and krill (*Euphausia superba*) (*Constable et al.*, 2003). The SO supports one of the most productive marine ecosystems in the world, with the high biomass of krill fundamental to the distribution of whales, seals and birds. A recent review (*Bost et al.*, 2009) highlights the importance of the SO oceanographic fronts to marine birds and mammals and points out that high mean species richness and diversity for whales and seabirds are consistently associated with the sBdy, SAF and STF. Other studies highlight the importance of the PF. For example, a study (*Nishikawa et al.*, 2010) into euphausiids along SR3 during austral summer in 2001/2002 found that both their total abundance

and biomass were much higher in the south of the southern branch of the PF (60-61°S) than north of there and that the two regions contained distinct communities of euphausiids. A number of authors (eg. *Sokolov and Rintoul* (2007)) have explained the difference in productivity north and south of the PF as being due to the strong upwelling of nutrient-rich UCDW south of the PF. A recent hypothesis (*Alderkamp et al.*, 2010) suggests that, in open areas with deep MLs, it is not low light or low iron that controls phytoplankton growth, but photo-damage that occurs during the high irradiance portion of the mixing cycle.

Tynan (1998) argues that the sBdy of the ACC is crucial to the functioning of the SO ecosystem, since it corresponds to high patches of phytoplankton and krill and circumpolar distributions of baleen whales. In addition, *Tynan* (1998) found that the distribution of UCDW corresponds to spring to mid-summer distributions of blue, fin and humpback whales. However, other authors do not agree; for example, measurements taken in East Antarctica (80-150°E) during the 1996 BROKE (Baseline Research on Oceanography, Krill and the Environment) survey found enhanced biological activity south of the sBdy rather than in association with it (*Nicol et al.*, 2000). It was found that phytoplankton, primary production, krill, whales and seabirds were concentrated in the area where sea-ice extent was greatest, unlike salps which seem to be adapted to open water. These authors propose that both sea-ice conditions and the ocean circulation determine the spatial variation of secondary producers such as salps, copepods and krill. A more recent follow-up survey entitled BROKE-West was conducted in 2006 and this studied the oceanography and marine systems again off East Antarctica, this time to the west (30-80°E) of the BROKE region. In this region, no clear oceanographic boundary was found that influenced the distribution of krill surveyed (*Williams et al.*, 2010), but significant diatom growth in the eastern section of the survey area was linked to the presence of the sACCf (*Westwood et al.*, 2010).

2.11 Carbon Cycling and Climate Change

The marine carbon cycle is a crucial component of the cycling of carbon between the biosphere, atmosphere and ocean, particularly since the amount of CO_2 stored in the ocean is estimated to be around 38000 Gt (3.8×10^{13} t), which is about 50 times the amount of CO_2 in the atmosphere (*Lalli and Parsons*, 1997). A simplified diagram illustrating the basic elements of the carbon cycle in the ocean, is shown in Figure 2.14. It is comprised of various pumps, which are discussed below.

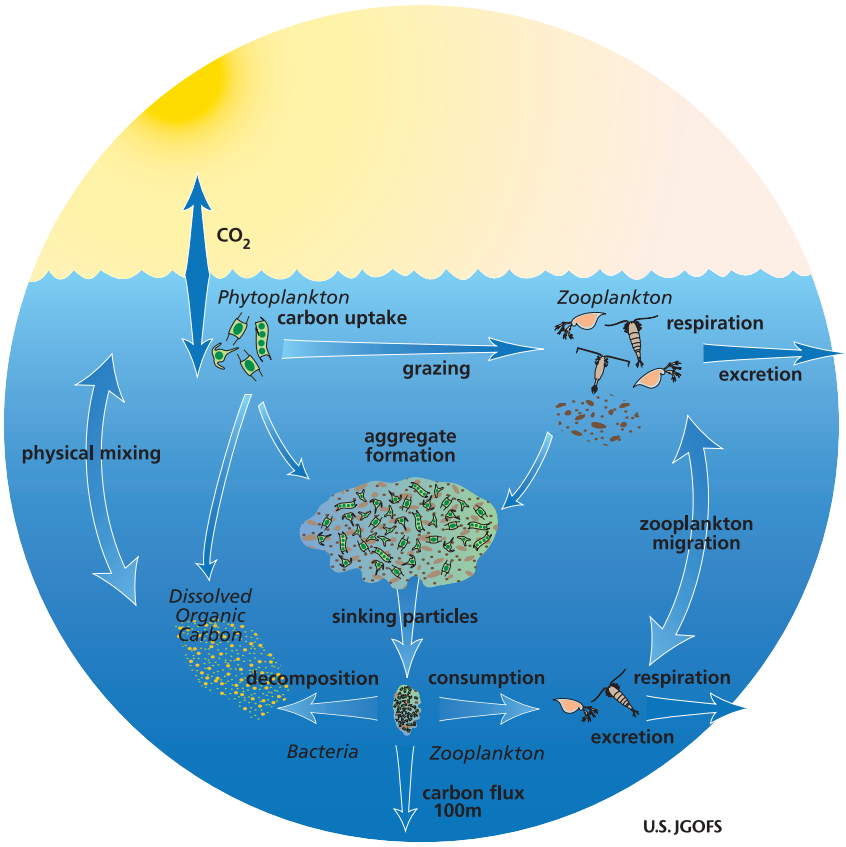

Figure 2.14: A simplified diagram showing the basic elements of the carbon cycle in the ocean (http://www1.whoi.edu/general_info/gallery_modeling/slide4.html)

2.11.1 The "solubility pump"

There is a continuous flux of CO_2 between the air and the ocean, where CO_2 reacts with sea-water to form DIC, comprised of bicarbonate (HCO_3^-) and CO_3^{2-} ions. Localised sinking of cold, winter water, enriched with DIC, associated with the MOC, is known as the "solubility pump", where the sinking is balanced, over time, by upward transport of DIC into warm, surface waters (*Denman et al.*, 2007). The strength of the solubility pump is dependent upon salinity, surface ocean temperature, ice cover and the strength of the MOC (*Denman et al.*, 2007).

2.11.2 The "biological pump"

When phytoplankton fix carbon during photosynthesis, a proportion of the carbon is exported to depth via the "biological pump", when dead organisms and particles (for example, coccolithophores, foraminiferans or pteropods, which form calcium carbonate shells), sink from the surface layer (*Lalli and Parsons*, 1997). In addition, some carbon reaches the deep ocean as dissolved organic carbon (DOC) through downwelling rather than sinking. The sinking of organic particles out of the surface layer is known as the "organic carbon pump", while the release of CO_2 in surface waters during the formation of carbonate

shell material is known as the "$CaCO_3$ counter pump" (*Denman et al.*, 2007).

Most of the carbon in the sinking particle flux is eventually recirculated to the surface as DIC, after being respired due to bacterial action. Of the remainder, a small fraction is either buried or resuspended in the deep ocean sediments (*Denman et al.*, 2007). The efficiency of the biological pump can be affected by changes in the ocean circulation, nutrient supply and the composition and physiology of the plankton community (*Denman et al.*, 2007; *Lalli and Parsons*, 1997). Also, any future changes in the relative contribution of the various phytoplankton types to the total ocean biomass could have a significant impact ocean biogeochemistry and ocean carbon storage, as well as the higher trophic levels that are dependent on them (*Marinov et al.*, 2010).

2.11.3 The SO biogeochemical divide

Modelling studies by *Marinov et al.* (2006) have pointed to the existence of a biogeochemical divide, which separates the Antarctic from the Subantarctic, due to the fact that different regions control atmospheric CO_2 production and global export production. The authors suggest that the biological pump and Antarctic deep-water formation mainly control the air-sea balance of CO_2, while the biological pump and circulation, in the Subantarctic region where AAIW and SAMW are formed, mainly control global export production. This is significant because climate change may affect one of the two without affecting the other, thus affecting the balance between outgassing of natural CO_2 and the uptake and storage of anthropogenic CO_2.

2.11.4 Climate Change

The oceanic uptake of CO_2 is crucial in the context of climate change, bearing in mind that approximately 25-30% of anthropogenic emissions of CO_2 have been taken up by the oceans, over the last 200 years (*Sabine et al.*, 2004). Various physical factors, such as changes in ocean temperatures, stratification and in the strength and latitudinal position of the SO westerly winds, may impact on the efficiency of the carbon sinks, in addition to changes to the biological pump and ecosystems. For example, in high latitudes, climate change leading to a longer growing season and decreased ice cover has been suggested to lead to increased production (*Sarmiento et al.*, 2004; *Steinacher et al.*, 2010). Much recent emphasis has been on understanding the ocean processes that regulate CO_2 uptake and on documenting the impact of climate change trends on air-sea fluxes (*Doney et al.*, 2009).

Global modelling analyses suggest that the SO dominates the present-day air-sea flux of anthropogenic CO_2, with one third to one half of global uptake

occurring south of 30°S (*Orr et al.*, 2001; *Khatiwala et al.*, 2009). Another study using interior ocean observations of DIC and using a suite of 10 ocean general circulation models (GCMs) (*Mikaloff Fletcher et al.*, 2006, 2007) has found out-gassing of natural (pre-industrial) CO_2 between 44 and 59°S, vigorous uptake in the mid-latitudes and strong out-gassing in the tropics.

Recently, *Le Quere et al.* (2007) investigated the SO CO_2 sink for the period 1981 to 2004, using an inverse method based on observed CO_2 concentrations. They concluded that the sink has weakened by 0.08 Gt C per year per decade, relative to the trend expected from the increase in atmospheric CO_2. This compares with estimates for the SO CO_2 sink of between -0.1 and -0.4 Gt C yr^{-1} (*Gruber et al.*, 2009; *Takahashi et al.*, 2002; *McNeil et al.*, 2007), where an updated estimate is found by *Takahashi et al.* (2009) for the ice-free zones from 50-62°S, using a global climatology of surface ocean pCO_2 measurements, to be -0.06 Gt C yr^{-1} (compared with a total global figure of -2.0 Gt C yr^{-1} in 2000). The small size of the sink is related to the near-cancellation of the (winter) outgassing of the natural CO_2 and the (summer) uptake of the anthropogenic CO_2 (*Takahashi et al.*, 2009; *Gruber et al.*, 2009). A comparison (*Gruber et al.*, 2009) of the above pCO_2 method (*Takahashi et al.*, 2009) and the inversion of interior ocean carbon observations, mentioned above (*Mikaloff Fletcher et al.*, 2006, 2007), has found that both methods point to a small contemporary sink in the SO (south of 44°S), but, while the inversion suggests a relatively uniform uptake, the pCO_2 estimate suggests strong uptake in the region between 44 and 58°S and a source in the region south of 58°S.

It is worth bearing in mind that, while the SAM was strongly positive during the 1990s, it shows only a very weak trend between 2000 and 2007 and a study (*Metzl et al.*, 2009) into the surface ocean pCO_2 measurements has found a corresponding drop in the surface ocean pCO_2 trends for 40-62°S, from 2.3μatm yr^{-1} for 1993-1999 to 1.3μatm yr^{-1} for 2000-2007. This led to the suggestion of a link between changes in the SAM and the decadal reduction of the SO carbon sink (*Metzl*, 2009). Other studies have also found that the SAM and CO_2 variability are correlated (*Le Quere et al.*, 2007; *Lenton and Matear*, 2007), where a positive correlation indicates that CO_2 is outgassed from the ocean, compared with its mean state. The weaker trend in the CO_2 sink in high latitudes is attributed (*Le Quere et al.*, 2007) to an increase in the strength of the extra-tropical SH winds, in line with increasing positive SAM, which causes an increase in the MOC, so that deep waters with higher concentrations of DIC are upwelled, leading to outgassing of natural CO_2 to the atmosphere and a reduction in the difference between pCO_2 in the ocean and the atmosphere, hence reducing CO_2 uptake. Conversely, in lower latitudes (north of 40°S), where the carbon-rich waters are transported and the wind

stress is decreasing, the sink is found to increase (*Metzl*, 2009; *Borges et al.*, 2008). These results are consistent with field results (*Metzl et al.*, 2006; *Metzl*, 2009; *Borges et al.*, 2008) and hindcast model studies (*Lovenduski et al.*, 2007, 2008; *Lenton and Matear*, 2007).

A recent study (*Lenton et al.*, 2009) has found that, for coupled-climate-carbon-models to capture the decreasing trend in the SO sink, it is necessary for the model to account for stratospheric ozone depletion. The model then shows a reduced SO uptake of CO_2 of 2.47 PgC from 1987 to 2004 (consistent with atmospheric inversion studies), due to the ventilation of carbon-rich deep water by stronger winds. This then accelerates ocean acidification, despite the reduced CO_2 uptake.

Other authors (*Zickfeld et al.*, 2008) disagree with this conclusion and believe that the SO sink will increase in efficiency in the 21st century. The disagreement is not related to the effect that the winds have on the MOC, but rather related to the balance between the outgassing of natural CO_2 and the uptake of anthropogenic CO_2. *Zickfeld et al.* (2008) believe that the effect of the poleward-intensifying winds will be such that the balance of outgassing of natural CO_2 and uptake of anthropogenic CO_2 will shift towards the latter, due to the increase in the levels of anthropogenic CO_2 in the atmosphere, leading to a more efficient SO sink.

Another viewpoint is given by *Russell et al.* (2006) who use climate modelling to conclude that the poleward intensification of the westerly winds may reduce the effect of the stratification of the global ocean (due to warming), which would allow additional anthropogenic CO_2 and heat to be removed by the ocean. In addition, a recent study (*Tortell et al.*, 2008), into the sensitivity of SO phytoplankton to CO_2 concentrations, concluded that the effect of increasing CO_2 levels and increasing temperatures and stratification may be modulated by CO_2-dependent changes in the region's biological pump.

In contrast to observational estimates, which show that the SO inventory of anthropogenic CO_2 is very low (*Sabine et al.*, 2004), modelling studies suggest that more than 40% of the uptake of anthropogenic CO_2 occurs in the SO (*Orr et al.*, 2001; *Mikaloff Fletcher et al.*, 2006). This discrepancy is explained *Ito et al.* (2010), using a high-resolution ocean circulation and carbon cycle model, by the advection via the SO circulation, of much of the anthropogenic carbon away from the uptake regions. Although this circulation is controlled by the interplay among Ekman flow, ocean eddies and subduction of water masses, *Ito et al.* (2010) found that Ekman transport across the PF is the primary mechanism, with little compensation from eddies. Northward of the ACC, however, the subduction and circulation of thermocline waters becomes increasingly important. A consequence of these results is pointed out

by *Tjiputra et al.* (2010), who used a coupled climate-carbon model to quantify the lateral transport of anthropogenic carbon over the period 1850-2100. They suggest that, because in the high latitude SO (south of 58°S) more than half of the anthropogenic carbon in continuously transported northward, this will allow a continuous increase in future carbon uptake, where the uptake strength could reach 3.5 $gCm^{-2}yr^{-1}$, nearly triple the global mean of 1.3 $gCm^{-2}yr^{-1}$, by the end of the 21st century. This highlights the importance of the SO in controlling long-term future carbon uptake and, in particular, the importance of understanding the upwelling and northward Ekman transport of UCDW.

Chapter 3

Methodology

3.1 Study Regions

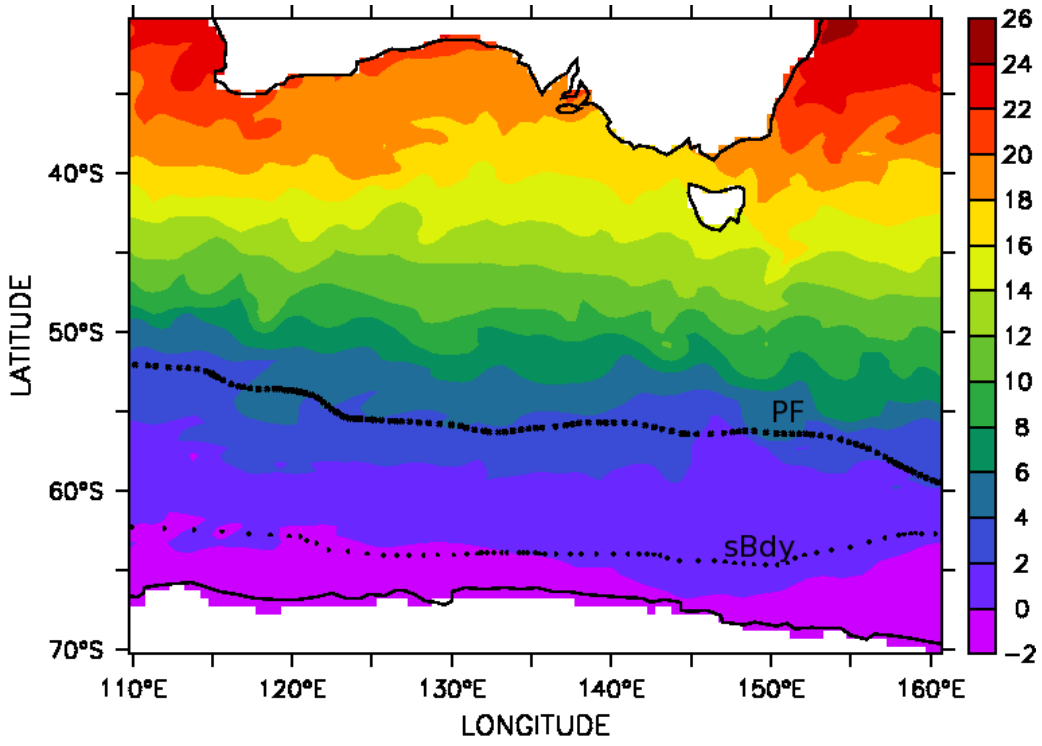

Figure 3.1: A plot from SODA showing sea surface temperature in November 2001 in the study area 110-160°E by 40-70°S, overlaid by the Polar Front (PF) and the Southern Boundary (sBdy) of the ACC (*Orsi and Ryan*, 2001, updated 2006), between which UCDW upwells.

The main region studied in this work is the Australian sector of the Southern Ocean (110-160°E, 40-70°S). This is shown in Figure 3.1, along with a plot of sea-surface temperature (SST) in November 2001 from SODA, overlaid by the Polar Front (PF) and the Southern Boundary (sBdy) of the ACC (*Orsi and Ryan*, 2001, updated 2006). Data for the Australian sector are compared with data from two other Southern Ocean sectors, one in the Indian Ocean (20-60°E, 40-70°S) and one in the Pacific Ocean (130-80°W, 40-75°S). These are

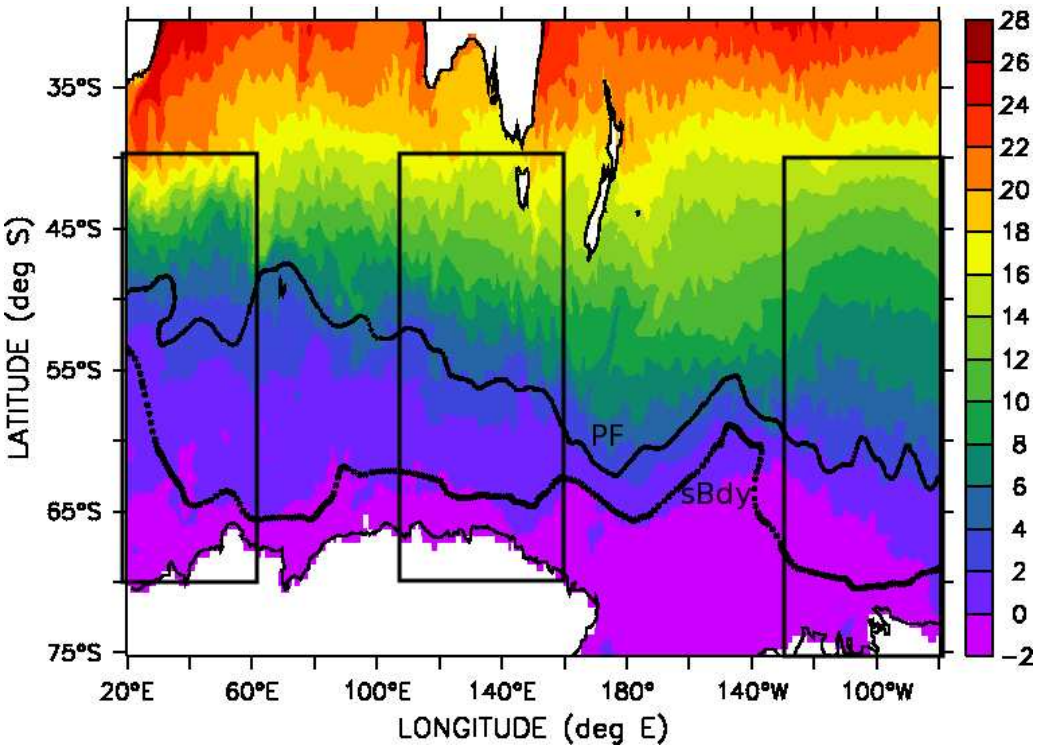

Figure 3.2: A plot of SST in January 2000 from SODA, overlaid by the PF and sBdy (*Orsi and Ryan*, 2001, updated 2006), between which UCDW upwells. Study sectors are Indian (20-60°E, 40-70°S), Australian (110-160°E, 40-70°S) and Pacific (130-80°W, 40-75°S).

chosen to cover approximately the same latitudinal range as the Australian sector, whilst avoiding potential confounding regions such as Kerguelen or South Georgia. The plot of SODA SST data (estimated at 5 m depth), given in Figure 3.2, illustrates the three sectors mentioned above, as well as showing the PF and the sBdy (*Orsi and Ryan*, 2001, updated 2006) in these sectors.

3.2 Data Sources

3.2.1 Satellite data

Chlorophyll-*a* and PAR are derived from SeaWiFS (Version 5.1) (*McClain et al.*, 2004) level 3 monthly data which is gridded at 9km×9km resolution. Monthly sea-ice concentration data (*Comiso*, 1999, updated 2008) are derived using measurements from the Scanning Multichannel Microwave Radiometer (SMMR) on the Nimbus-7 satellite and the Defense Meteorological Satellite Program (DMSP) Special Sensor Microwave Imagers (SSM/I). Data were generated using the Advanced Microwave Scanning Radiometer-Earth Observing System (AMSR-E) Bootstrap algorithm and gridded on a polar stereographic grid at 25km×25km resolution. Chlorophyll-*a* and PAR data were obtained from `http://oceancolor.gsfc.nasa.gov/cgi/l3` and sea-ice concentration

data from `http://nsidc.org/data/docs/daac/nsidc0079_bootstrap_seaice.gd.html`.

3.2.2 Model data (VGPM)

Net Primary Production is computed using the Vertically Generalized Production Model (VGPM) (*Behrenfeld and Falkowski*, 1997), which estimates primary productivity from chlorophyll-*a* using a temperature-dependent description of chlorophyll-specific photosynthetic efficiency. This study uses the VGPM output, with the caveat that this is a standard algorithm and is not calibrated specifically for the Southern Ocean. However, the VGPM is a widely used model (*Carr et al.*, 2006), that has been used previously in the Southern Ocean (*Behrenfeld et al.*, 2006; *Smith and Comiso*, 2008) and most of the other available models are calibrated for specific regions of the Southern Ocean, such as the Ross Sea, but not for the Australian sector (*Barbini et al.*, 2005; *Dierssen et al.*, 2000; *Smith et al.*, 2000). Also, a recent paper (*Saba et al.*, 2010a), comparing ocean colour model estimates of primary productivity in the Southern Ocean, found that the VGPM estimated primary productivity well compared with other models. However, it is also worth noting that the authors also found that most ocean colour models over-estimated primary productivity but under-estimated its variability in the Southern Ocean, which may mean that this work may also under-estimate variability in primary productivity.

SeaWiFS chlorophyll-*a* and PAR data, as well as SST data from the Advanced Very High Resolution Radiometer are inputs to the VGPM (*Behrenfeld and Falkowski*, 1997) model, where

$$\text{Primary productivity} = 0.66125 * P^B_{opt} * \frac{E_0}{(E_0 + 4.1)} * chla * Z_{eu} * D_{irr} \quad (3.1)$$

and primary productivity is in units of mg C m^{-2} d^{-1}, P^B_{opt} is the biomass specific optimal rate of photosynthesis in the water column (mg C (mg chlorophyll-a)$^{-1}h^{-1}$) and is regulated by temperature, E_0 is the daily surface PAR (Einsteins m^{-2} d^{-1}), *chla* is chlorophyll-*a* concentration (mg m^{-3}), Z_{eu} is the depth of the euphotic zone (m) (depth at which 1% of surface light is available) and D_{irr} is the photo period (h). Physiological variability is linked to the P^B_{opt} variable, which is based on daily integrated productivity measurements. A polynomial of the form, $P^B_{opt} = \sum_{i=0}^{7} a_i(\frac{SST}{10})^i$, is fitted to field data (see *Behrenfeld and Falkowski* (1997) for the a_i values). The P^B_{opt} function increases from -1°C to 20°C (photoacclimation to increasing light levels leads to higher photosynthetic efficiency as light increases in parallel with temperature) and then decreases due to nutrient stress on primary productivity that is light- saturated. The euphotic depth Z_{eu} is calculated from *chla* using

the Case-1 (pelagic) model of *Morel and Berthon* (1989). Primary productivity is calculated on a daily basis, then binned to give 8-day or monthly values. VGPM data are available from `http://www.science.oregonstate.edu/ocean.productivity/`. Note: in this work the words chlorophyll-a and primary productivity will be taken to refer to surface chlorophyll-a and estimated primary productivity, respectively, in the interests of brevity.

3.2.3 Model reanalysis data (SODA)

Simple Ocean Data Assimilation (SODA) data (*Carton et al.*, 2000, 2005; *Carton and Giese*, 2008) (available from `http://dsrs.atmos.umd.edu/DATA`) come from a reanalysis of ocean climate variability that begins with a state forecast produced by an ocean GCM based on POP numerics (*Smith et al.*, 1992), with an average resolution $0.25° \times 0.4° \times$ 40-levels (with 10 m resolution in the top 100 m). The prediction is continuously updated by contemporaneous observations, where available, with corrections estimated every 10 days (*Carton and Giese*, 2008). The GCM is forced by ERA-40 winds, from the European Centre for Medium-Range Weather Forecasts 40-year reanalysis (*Uppala et al.*, 2005).

Subsurface temperature and salinity observations come from the World Ocean Database 2005 (WOD05) (*Boyer et al.*, 2006), extended by observations from the National Oceanographic Data Center/National Oceanic and Atmospheric Administration temperature archive (which includes observations from Argo floats and from the Tropical Atmosphere Ocean/Triangle Trans-Ocean Buoy Network (TAO/TRITON) thermistor array). Data are checked for duplicate reports and errors in the recorded position and time of observations, for static stability, for deviation from climatology, including checks on the relationship between temperature and salinity (*Carton et al.*, 2005). These checks eliminate an additional 5% of the profiles and are in addition to the WOD05 quality control. Surface freshwater fluxes since 1979 come from monthly precipitation data from the Global Precipitation Climatology Project (*Adler et al.*, 2003) and evaporation from bulk formulae (*Schott et al.*, 2009). Although the surface heat flux is also found using bulk formulae, this is overwhelmed by the assimilation of SST (*Schott et al.*, 2009). The vertical diffusion of momentum, heat and salt are carried out using K-Profile Parameterization (KPP) (*Large et al.*, 1994) mixing with modifications to address issues such as diurnal heating (*Carton and Giese*, 2008). Vertical velocity is calculated using the continuity equation (*Smith et al.*, 1992) and does not include entrainment. SODA has no sea-ice model but, when SST $<$ -1.88°C, the fluxes are altered to account for presumed ice formation (B. Giese, pers. communication). The version of SODA used here (2.0.2/2.0.4) is an improvement over earlier versions (*Schott*

et al., 2009), such as those described by *Carton and Giese* (2008), because the analysis is no longer performed on $5° \times 5°$ cells, but on individual grid points. In addition, improvements to the ocean model (now POP 2.0.1) involve the inclusion of river run-off and some minor modifications to the horizontal and vertical mixing parameterisations.

The reanalysis has been evaluated by comparisons with independent observations, such as the historical archive of hydrographic profiles, supplemented by ship intake measurements, moored hydrographic observations, remotely sensed SST and sea level. Comparisons of forecasts and observations, using tide gauge level records and satellite altimetry, are also carried out (*Carton et al.*, 2000).

SODA uses a sequential data estimation scheme to change temperature and salinity in the ocean model in order to accommodate hydrographic observations, which are restricted to depths shallower than about 1000 m for assimilation, due to the scarcity of observations below that depth. A set of linear Kalman equations is used to correct the first guess, based on estimates of the errors contained in the model forecast (the difference between the forecast value and true value (see below) of a variable such as temperature at a particular location and time) and in the observations (*Carton and Giese*, 2008).

The sequential analysis begins (*Giese*, 2006; *Carton and Giese*, 2008) at time t_k, with a state forecast ω_k^f, produced by a forecast model, represented by the operator Ω. An observation vector ω_k^o is constructed from all observations (for example, temperature, salinity and sea-level). The true estimate of state is found from an analysis ω_k^a, which combines the forecast with the observations. This analysis is then used as an initial condition for a subsequent forecast $\omega_{k+1}^f = \Omega\omega_k^a$. A bias model $\mathbf{B}$ is constructed from an analysis of $\omega^f - \omega^o$ statistics and this is used to find a bias forecast $\beta_{k+1}^f = \mathbf{B}\beta_k^a$.

The multi-variate two stage sequential updating algorithm for the bias correction is

$$\beta^a = \beta^f - \mathbf{L}\left[\omega^o - \mathbf{H}(\omega^f - \beta^f)\right] \tag{3.2}$$

and for the state correction, where $\tilde{\omega}^f = \omega^f - \beta^a$, is

$$\omega^a = \tilde{\omega}^f + \mathbf{K}\left[\omega^o - \mathbf{H}\tilde{\omega}^f\right] \tag{3.3}$$

$\mathbf{H}$ is the interpolation matrix that maps variables specified at the model locations onto the observation locations and the gain matrices $\mathbf{K}$ and $\mathbf{L}$ (*Chepurin et al.*, 2005) determine the impact of the observations and depend on terms such as the forecast error covariance.

This work uses the SODA 2.0.2 dataset, which covers the period from 1958-2001 and consists of sea surface heights, surface wind stresses, monthly zonal,

meridional and vertical velocity fields, as well as temperature and salinity, which are presented on a $0.5° \times 0.5° \times 40$ depth level (from 5 m to about 5500 m, with 10 m resolution in the top 100 m) global grid. These variables are saved at 5-day intervals and the publicly available dataset is available in netcdf format in monthly files. SODA reanalysis data for the period 2002-2007 (SODA 2.0.4) is also used, but this reanalysis is different from the one for the earlier period in that it is forced by a merged product (*Schott et al.*, 2009) of QuikSCAT and the National Centers for Environmental Prediction/National Center for Atmospheric Research reanalysis (*Milliff et al.*, 2004), rather than ERA-40 winds. This is a potential source of error in this work, although the two have been used together in other studies, for example (*Schott et al.*, 2008, 2009; *Zheng and Giese*, 2009), and examination of the aggregated time series used here does not show any particular biases. While the majority of this work uses the SODA monthly datasets, certain sections also use the SODA 5-day data, either to facilitate Lagrangian tracking of UCDW or to allow a more accurate detection of UCDW in the ML, when the 10-year period 1997-2007 is being considered.

The remainder of the variables used in this study come either from the SODA reanalysis dataset or are derived from variables therein.

3.2.4 Climate indices

Three global climate indices, SAM, MEI and PDO are considered in this work. Indices to measure the SAM, prior to the satellite era (1979), have been constructed by *Marshall* (2003) and also *Visbeck* (2009) using Southern Hemisphere atmospheric pressure observations from stations situated either near 40°S or 65°S. Positive values of the SAM index indicate lower than normal atmospheric pressures over the polar regions, while negative values mean the opposite (that is, higher than normal pressures over the polar regions). The index constructed by *Marshall* (2003), chosen because both seasonal and annual values are available (from `www.nerc-bas.ac.uk/icd/gjma/sam.html`), is shown in Figure 2.7.

The MEI (*Wolter*, 1987; *Wolter and Timlin*, 1993) is based on observations of sea-level pressure, zonal and meridional surface wind components, SST and total cloudiness fraction of the sky, taken over the tropical Pacific and is available at `http://www.esrl.noaa.gov/psd/people/klaus.wolter/MEI/table.htm`. The MEI values are calculated as the first unrotated principal component of all these fields combined, computed for twelve sliding bi-monthly periods (that is, December/January, January/February and so on) and then standardised with respect to each season and to the 1950-1993 reference period. For seasonal correlation purposes, summer is taken to be November/December,

December/January, January/February. Positive values of the MEI represent the warm ENSO phase (El Niño).

The PDO (*Mantua and Hare*, 2002) is a pattern of SST anomalies in the subtropical North and South Pacific, that are out of phase with SST anomalies in the tropical Pacific (*Martinez et al.*, 2009). The PDO is defined (*Mantua and Hare*, 2002) as the leading empirical orthogonal function (EOF) of mean November through March SST anomalies for the Pacific Ocean north of 20°N latitude. For the EOF calculation, the global mean SST anomaly is first removed for each month in order to reduce the influence of the long-term trends in the data. Positive values indicate months of above normal SSTs along the west coast of North and Central America and on the equator, and below normal SSTs in the central and western north Pacific at about the latitude of Japan. PDO data can be accessed at `http://jisao.washington.edu/pdo/PDO.latest`.

3.3 Identifying UCDW in SODA

UCDW is identified (*Sievers and Nowlin*, 1984; *Orsi et al.*, 1995) by $[O_2] < 201$ μmol l^{-1} at density values 27.35 kg m^{-3} $< \sigma_0 <$ 27.75 kg m^{-3}, where $[O_2]$ is oxygen concentration and σ_0 is potential density anomaly at 0 dbar. This is is equivalent to the density criterion with temperature, $\theta > 1.5$°C (*Orsi et al.*, 1995; *Sokolov and Rintoul*, 2002) and gives a salinity range of between 34.5 psu and 34.7 psu. UCDW is identified in SODA using the density and temperature criteria above. An example of this is given in Figure 3.3, which shows UCDW along 140°E in February 1997. A temperature minimum layer (remnant winter water), overlaid by a shallow warm mixed layer created by summer warming, can be seen above UCDW, which is located in the temperature maximum layer (*Sokolov and Rintoul*, 2007).

UCDW properties examined using SODA data include: the southern-most extent of UCDW; the top depth at which UCDW can be identified (UCDW top depth) and the bottom depth at which UCDW can be identified (to give a depth range for UCDW in a particular latitudinal zone). UCDW vertical velocity is reported for UCDW as it upwells and is reported as a positive velocity, even though in SODA it is negative because the positive z direction is downwards.

3.4 Lagrangian Tracking

The path of UCDW in the SO is determined via Lagrangian tracking using the SODA 5-day data. Firstly, a point (x, y, z) at a particular time is identified

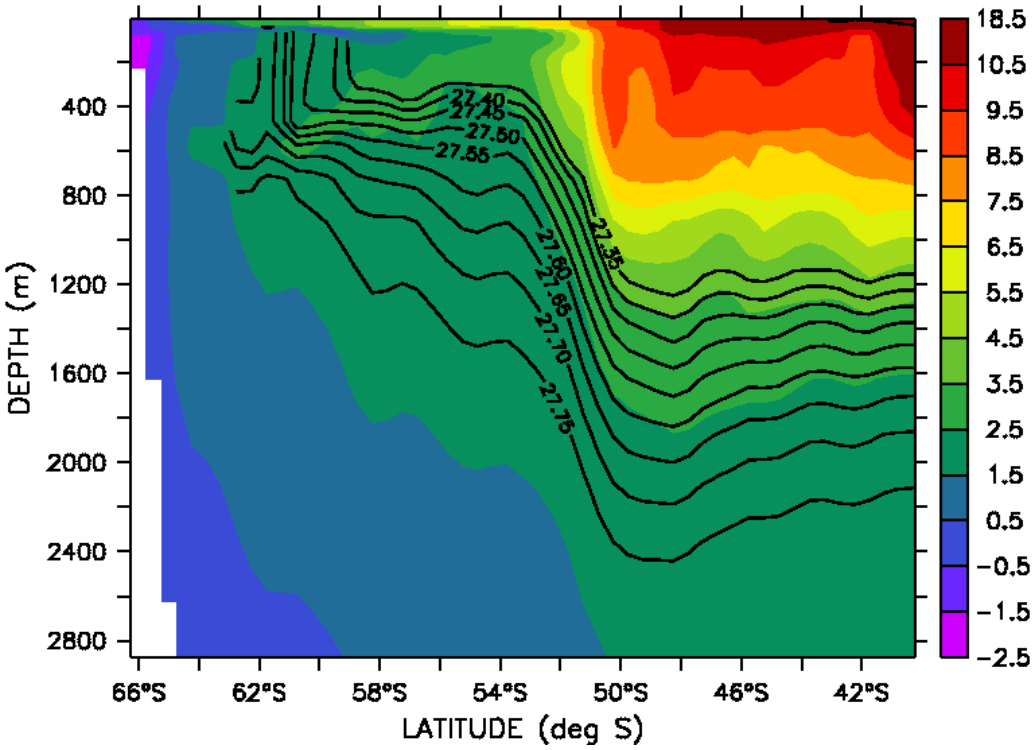

Figure 3.3: .

Isopycnals identifying UCDW overlaid on a temperature plot along 140°E in February 1997. A temperature minimum layer (remnant winter water) can be seen above UCDW and below a shallow warm summer mixed layer.

as likely to be in UCDW by studying a plot such as that in Figure 3.3. Then the velocities (u, v, w) at that point are used to calculate a new position for the point in the next 5-day dataset and so on. The resulting track is then presented as a three-dimensional plot, as well as two-dimensional sections of that plot.

3.5 Time Series Analyses

The Australian sector from 110-160°E to 40-70°S, studied here, is divided latitudinally into 5-degree zones. UCDW variables, such as vertical velocity, temperature, density and salinity are averaged over the depth of UCDW and over the particular latitudinal zone, for example (110-160°E, 50-55°S). Temporal averages are computed at monthly and seasonal (where the year is divided into four sets of three months, December, January, February (DJF) and so on) scales. An example of a full time series of SST for 1958-2007 in the 55-60°S zone is given in Figure 3.4. Examples of the four seasonal time series, which are derived from the full time series shown in Figure 3.4, are found in Figure 3.5. Means by month for these SODA time series (1958-2007) are used to produce monthly climatologies.

Mixed layer depths (MLDs) are calculated in SODA using the criterion of

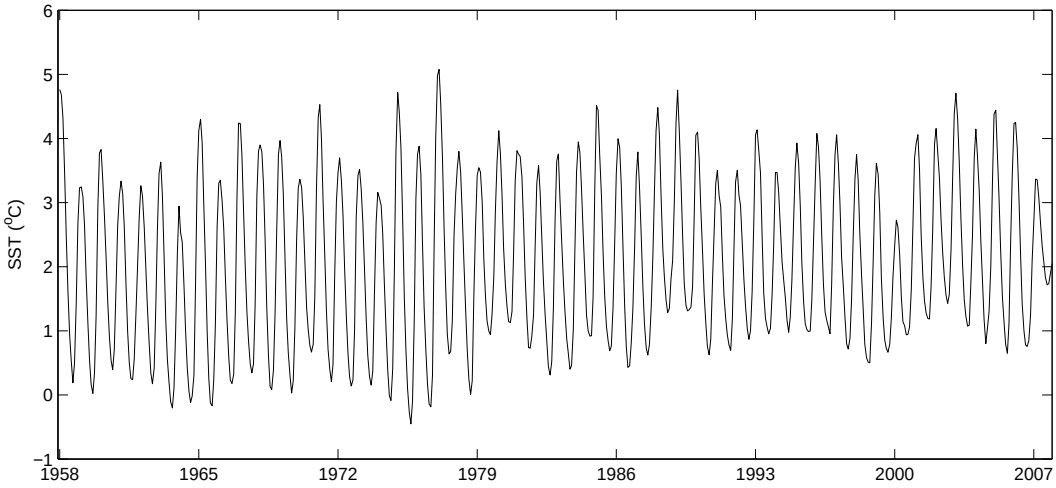

Figure 3.4: Time series for SST in the 55-60°S zone.

an absolute temperature difference of 0.2°C from the surface (*Montegut et al.*, 2004). Temperature, density and salinity in the ML are then calculated as an average over the MLD at each grid point and then averaged over the latitudinal region by month to produce time series. For comparison purposes, MLDs based on the density criterion of a 0.125 kg m^{-3} change in the potential density from the ocean surface (*Monterey and Levitus*, 1997), MLD(σ), are also calculated in SODA. Time series are also calculated for temperature, density and salinity based on MLD(σ) and also for sea-surface variables (estimated at 5 m depth).

Wind stress is calculated as the magnitude of the SODA wind stress vector $\boldsymbol{\tau} = (\tau_x^2 + \tau_y^2)^{\frac{1}{2}}$, from the SODA values for zonal and meridional wind stress, respectively. Maximum wind stress over the whole region, the latitude at which the maximum wind stress occurs and mean wind stress for each latitudinal zone, are also computed.

Other variables considered include stratification at the base of the mixed layer, which is calculated using the Brunt-Vaissala Frequency squared (N^2),

$$N^2 = -\frac{g}{\rho_0}\frac{\partial \sigma_\theta}{\partial z} \tag{3.4}$$

where g is the acceleration due to gravity and ρ_0 is the average density for the zone. In addition the Ekman pumping rate, E, is defined as

$$E = -curl\left(\frac{\boldsymbol{\tau}}{\rho_0 f}\right) \tag{3.5}$$

where f is the Coriolis parameter. Related to the Ekman pumping rate is the northward Ekman transport, Q_E, which can be calculated as

$$Q_E = -\frac{X\tau_x}{\rho_0 f} \tag{3.6}$$

where X is the east-west distance across which the transport is calculated.

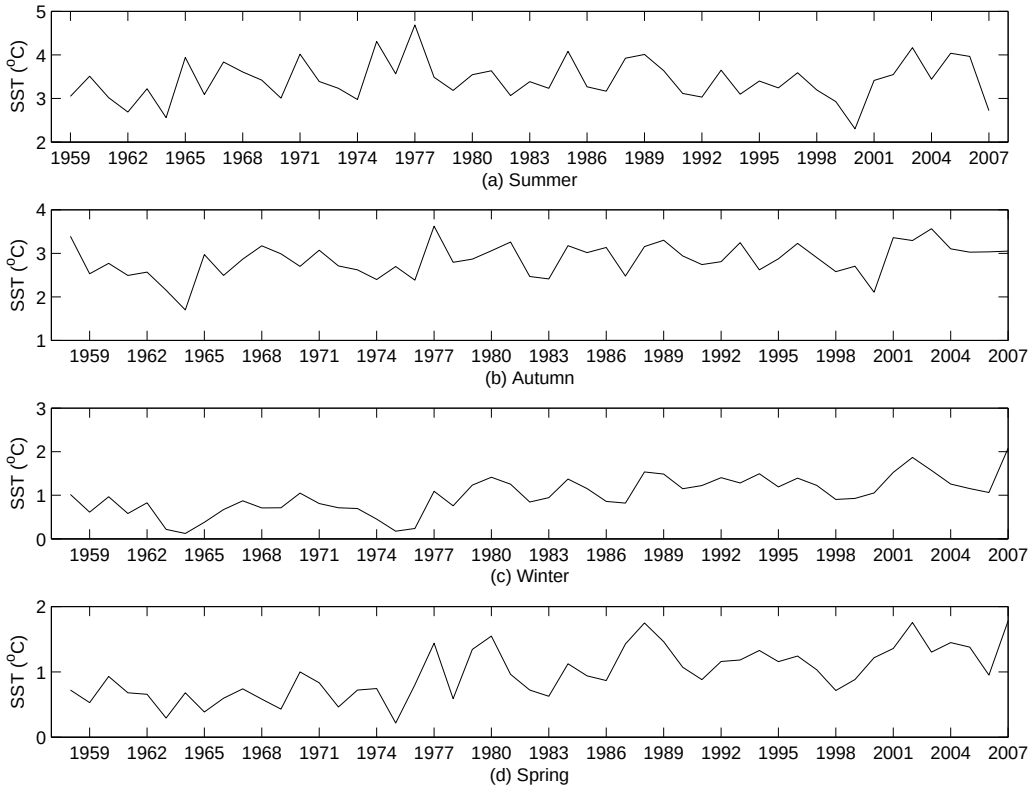

Figure 3.5: The four seasonal mean SST time series in the 55-60°S zone (a) Summer, (b) Autumn, (c) Winter and (d) Spring.

3.6 Statistical Analyses

The Pearson correlation coefficient is used in this work to calculate correlations between time series. Correlations between the three atmospheric indices, the SAM, MEI and PDO, and the wind stress are performed, as well as various other correlations, and in particular, correlations between mean wind stress and other variables. Correlations involving the seasonal time series are calculated using one point per year (that is a seasonal mean), while correlations between full time series use all the points, as do the 1997-2007 seasonal correlations (due to the small number of points involved). Correlations are calculated using either the original time series or detrended time series, depending on the purpose for which the result is intended. In work where the intent is to determine if the wind stress has an effect on trends in other variables, the time series are not detrended. However, in work where the effect of wind stress on interannual variability is being studied, both time series are detrended before the correlation is calculated.

To further investigate correlations between chlorophyll-a and other variables, a multiple linear regression model is fitted between chlorophyll-a and those variables that are not correlated with one another. The R Statistical

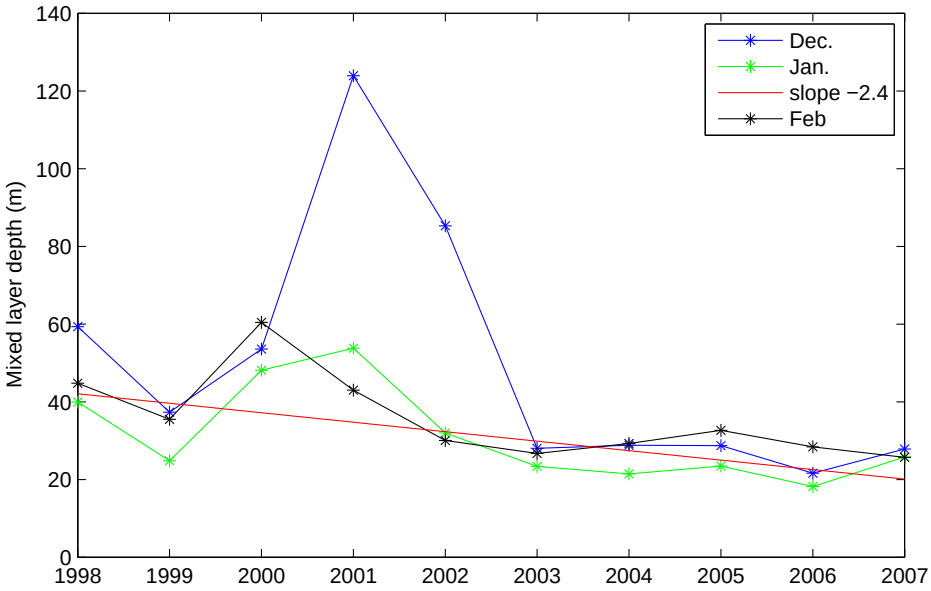

Figure 3.6: Mixed layer depth (1998-2007) time series for the 60-65°S zone, for December, January and February, overlaid by the overall trend line for that season, found using the non-parametric seasonal Sen slope (*Gilbert*, 1987).

and Computing Package (R Foundation for Statistical Computing, Vienna, Austria) is used for this work.

Trends and their significance in full or seasonal (DJF, MAM, JJA and SON) time series are estimated using the non-parametric seasonal Sen slope (*Gilbert*, 1987), a generalisation of Sen's estimator of slope, and the seasonal Kendall test (*Hirsch et al.*, 1982), a generalisation of the Mann-Kendall test, which is not affected by seasonal cycles in the data. The non-parametric estimate of the slope is preferable to linear least squares regression due to its insensitivity to outliers (*Gilbert*, 1987; *Hess et al.*, 2001).

The test involves computing the Mann-Kendall test statistic and its variance separately for each month ("season"), with the data collected over years, and then summing these seasonal statistics to produce a Z statistic (*Gilbert*, 1987). Here the test for the full 1958-2007 time series (50 years of 12 months of data) is applied to each of the 12 months. Alternatively, if the test is used on the seasonal (summer etc) time series (50 years of 3 months of data), it is applied to each each of the 3 months within the particular seasonal time series. The seasonal Sen's slope is then used to estimate a linear trend. Trends at the 95% confidence level are reported here as "significant". An example of the three time series that comprise the summer MLD time series (just for 1998-2007 in this case) in the 60-65°S zone is shown in Figure 3.6. The seasonal trend line, calculated by the above method, is also shown and is clearly insensitive to outliers.

3.7 Trend Analyses

This work uses the SODA ocean reanalysis not only to produce climatological values for the upper ocean and UCDW variables, but also to look at long-term trends in these variables. There are distinct advantages to this approach, but certain caveats must also be borne in mind.

The advantages associated with the use of reanalysis data, rather than traditional climate datasets, include (*Thorne and Vose*, 2010): the fact that in a reanalysis observations are synthesised in such a way that they are consistent with model physics; reanalyses provide complete temporal and spatial coverage (compared with statistical interpolation into regions where there is no data) and reanalyses can provide information on both directly observed and indirect variables (such as vertical velocity).

Atmospheric reanalyses have been available since the mid-1990s and, while having these advantages, because they arise from an observing system that was set up to support weather forecasting, rather than to produce multi-decadal reanalyses, they are affected by changes in the observing system. Thus errors can be introduced into ocean GCMs driven by these winds. Such ocean GCMs are also subject to errors associated with inadequate numerics, unrepresentative parameterisations of ocean physics, internal variability and errors in the initial conditions (*Carton and Giese*, 2008; *Stockdale et al.*, 1998). This means that SODA provides an estimate of state which is an improvement over estimates based solely on either the sparse set of observations or numerical simulation (*Carton and Giese*, 2008).

The idea behind SODA was to correct model errors using direct observations (*Carton and Giese*, 2008), but, again, the ocean observing system was not originally designed for this purpose. Both atmospheric and ocean reanalyses suffer from error terms, which may be considered using the following equation of *Thorne and Vose* (2010), which applies at each time step:

$$R = t + f(O_e, M_e, A_e, B_e) \tag{3.7}$$

where R is the reanalysis output, t is the true (unknown) climate system state and the terms in the function f are error terms, as follows:

1. O_e is the observational error (including the spatio-temporal incompleteness of the observational field and any absolute biases in the observations);

2. M_e is the model error (physical shortcomings of the model being used);

3. A_e is unintentional errors due to the methodological approach, and

4. B_e is the background error, which is the error in the forecast field from the last analysis step.

Estimation of the global ocean state using data assimilation is a rapidly developing field, especially in the past decade since the advent of satellite and in-situ observing systems. Such assimilation methods can broadly be divided into two categories (*Carton and Giese*, 2008): sequential estimation based on stochastic estimation theory (optimal interpolation, three-dimensional variational and Kalman filter/smoother) and variational adjoint methods based on control theory (Lagrange multiplier, four-dimensional variational, *Lee et al.* (2009)).

The SODA reanalysis has been part of an extensive inter-comparison project *Lee et al.* (2009) that compares ocean reanalyses both with one another (*Schott et al.*, 2008; *Carton and Santorelli*, 2008; *Carton et al.*; *Gemmell et al.*, 2008) and also with observations (*Schott et al.*, 2009; *Carton et al.*, 2000, 2005; *Carton and Santorelli*, 2008; *Carton and Giese*, 2008). Although SODA has not previously been applied in the ACC region of the Southern Ocean, it has been used in other areas where the observations are inhomogeneous and it has also been used for other analyses of multi-decadal trends (*Schott et al.*, 2008; *Carton and Santorelli*, 2008), including in the Southern Ocean (*Yang et al.*, 2007a).

Chapter 4

Upper Circumpolar Deep Water and the SODA reanalysis

This chapter examines Upper Circumpolar Deep Water as represented in the SODA reanalysis and then uses that representation to deduce information about the biogeochemical properties of UCDW. Prior to that, SODA's skill at representing hydrographic data in the Southern Ocean is tested by comparing SODA temperature and salinity plots with observational data.

4.1 Comparing SODA with Observations

In order to assess SODA's skill at representing hydrographic data in the Australian (110-160°E, 40-70°S) region of the SO, temperature and salinity plots are produced from SODA and compared with plots produced from hydrographic data. The data were collected along the SR3 track (approximately 140°E) in various months during spring and summer, in January 1995, March 1998, November 2001 and April 2008 and along a less meridional track from P2 (145.9°E, 54°S), ending at P3 (153.2°E, 45.5°S) in February 2007. In the latter case, the track chosen for the SODA plots for Figures 4.4 and 4.9 was along 146°E, so that the plots would be more likely to match near P2. Plots comparing SODA temperature and salinity with the observational data are given in Figures 4.1-4.5 and Figures 4.6-4.10 respectively. These plots (note the different colour maps) show that the SODA data are a very close match for the actual temperature data in each case and are generally a good match for the salinity data. As expected, the plots for 2007 (Figures 4.4 and 4.9) are not as good a match as the other plots, since the section from SODA along 146°E only approximates the non-meridional section from P2 to P3.

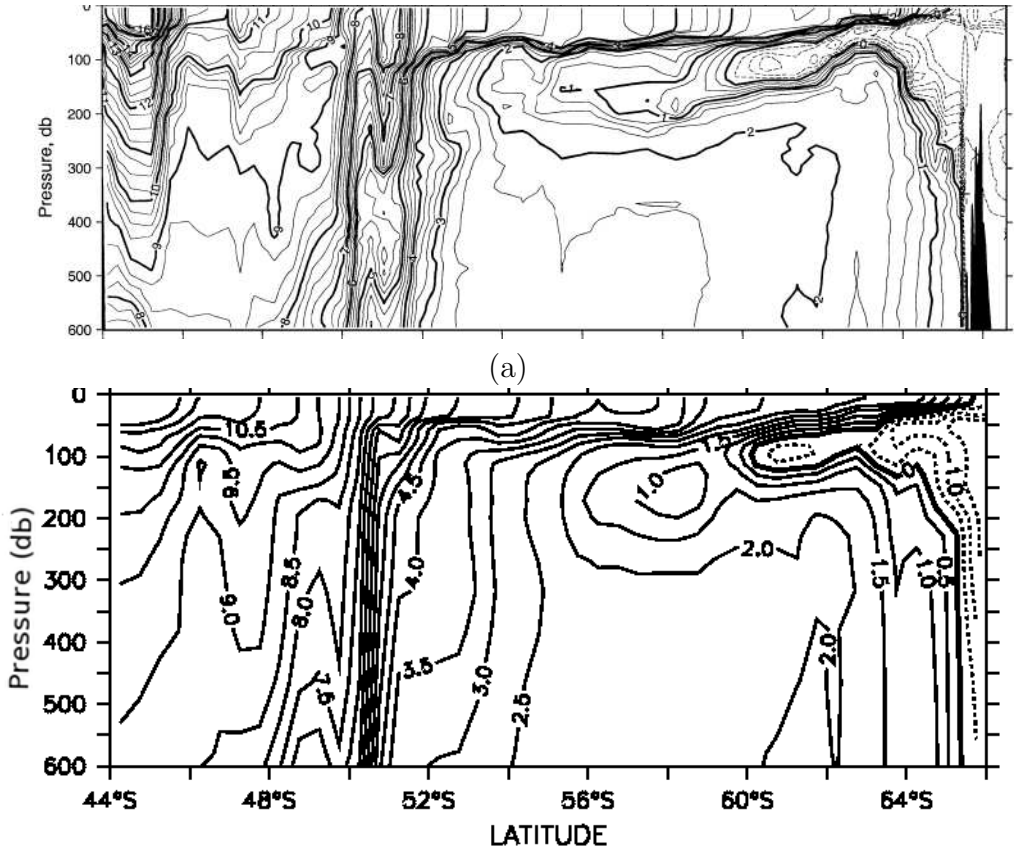

Figure 4.1: Temperature distributions in January 1995 along 140°E, from (a) *Sokolov and Rintoul* (2002), reprinted with permission from Elsevier and (b) SODA.

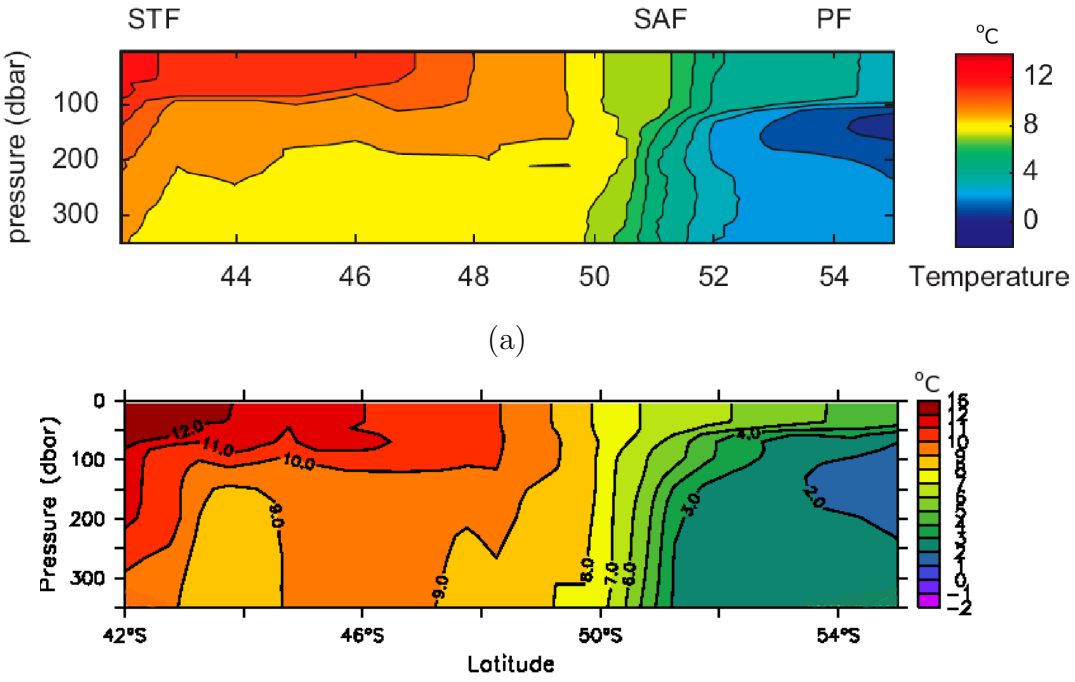

Figure 4.2: Temperature distributions in March 1998 along 140°E from (a) *Sedwick et al.* (2008), reprinted with permission from Elsevier and (b) SODA. Note that the colour scales are different.

It should be noted, however, that the comparison of SODA with the observational data may not really illustrate SODA's skill, since SODA is reproducing data that have most probably already been assimilated into the model in the cases of the 1995, 1998, 2001 and 2007 data. However, to the best knowledge of the data-keeper for the 2008 cruise (AU0806) (Mark Rosenberg, personal communication) the 2008 data have not been assimilated into SODA. This then provides an independent dataset which illustrates SODA's ability (which is very good, Figures 4.5 and 4.10) at reproducing hydrographic data in the SO.

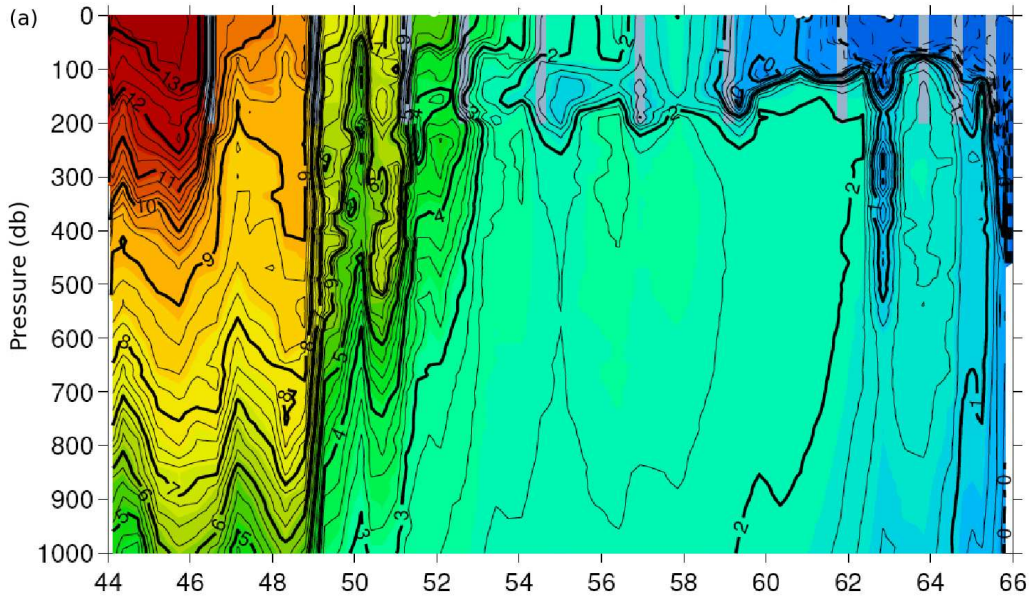

(a)

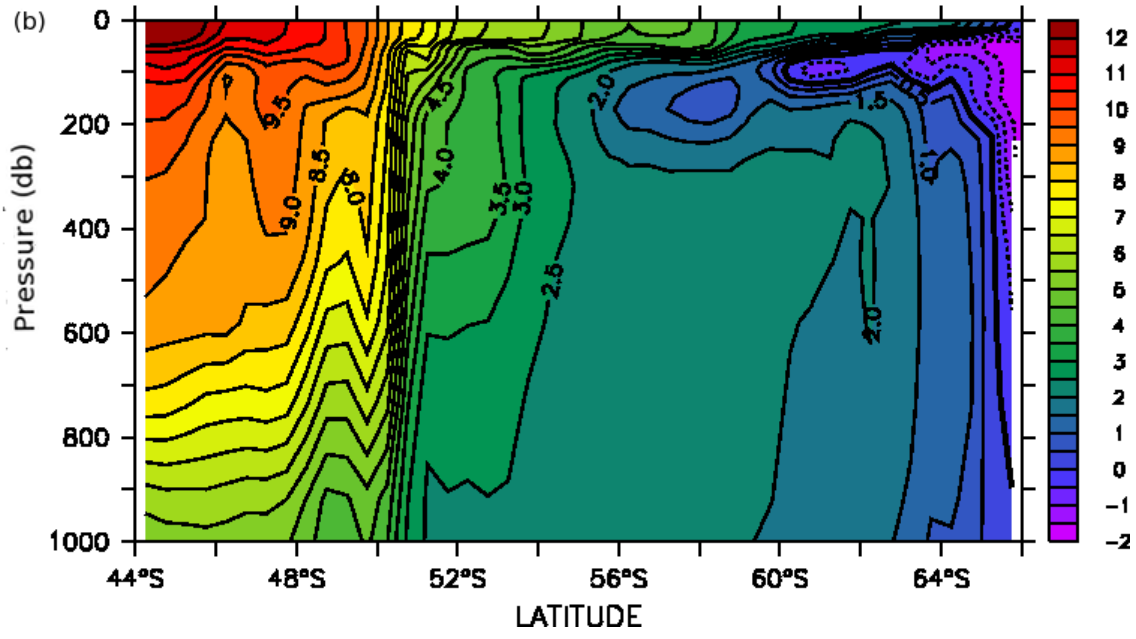

(b)

Figure 4.3: Temperature distributions in November 2001 along 140°E, from (a) *Sokolov and Rintoul* (2007), reprinted with permission from Elsevier and (b) SODA. Note that the colour scales are different.

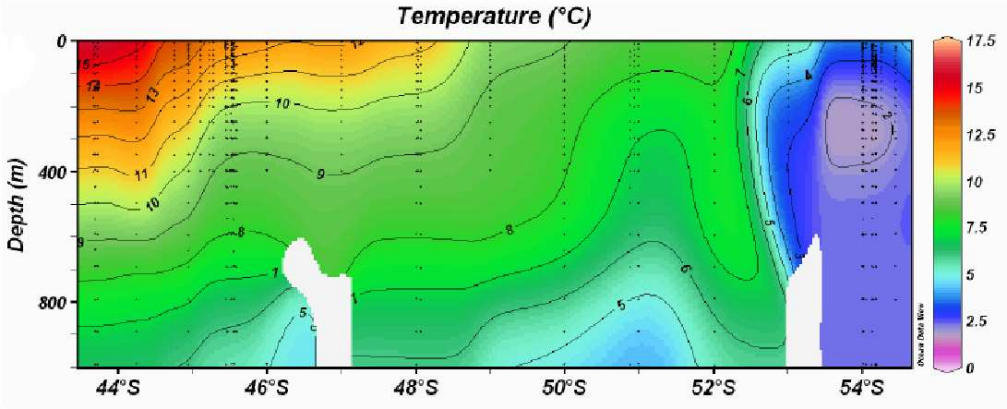

(a)

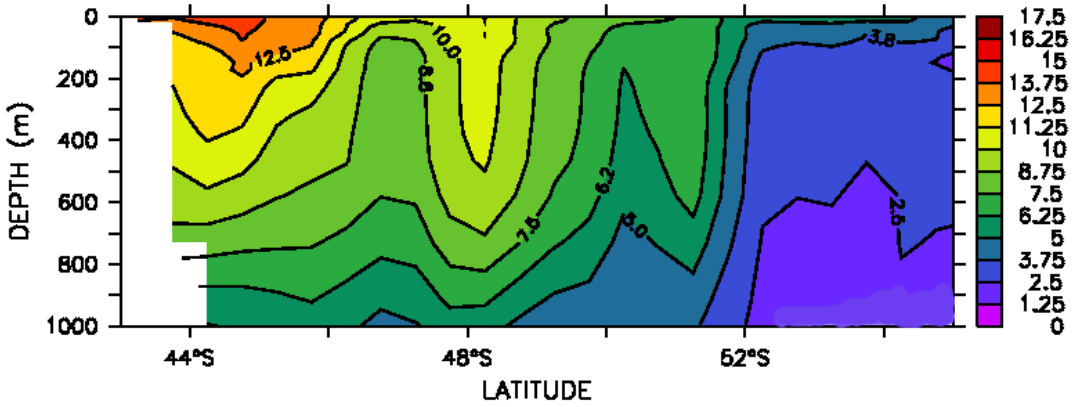

(b)

Figure 4.4: Temperature distributions in February 2007 (a) from (145.9°E, 54°S) to (153.2°E, 45.5°S) (*Bowie et al.*, 2009) and (b) along 146°E in SODA. Note that the colour scales are different.

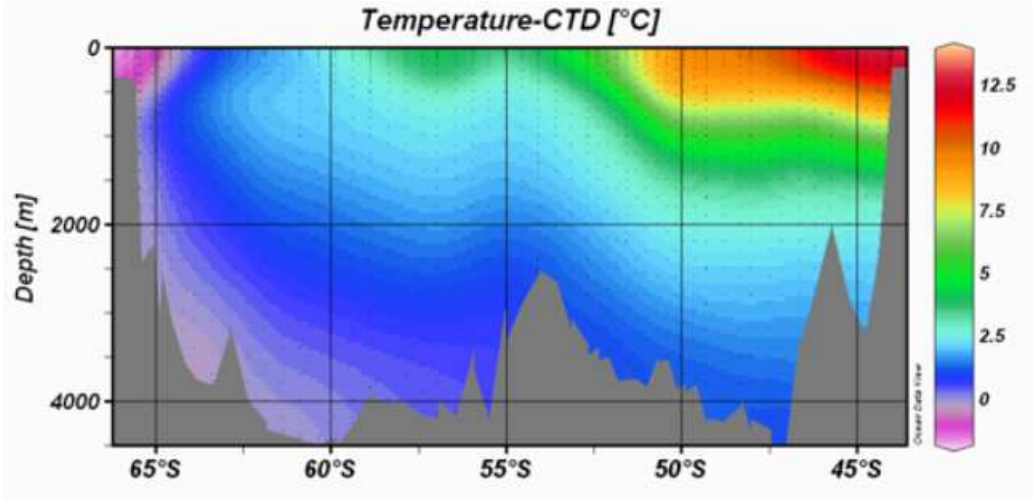

(a)

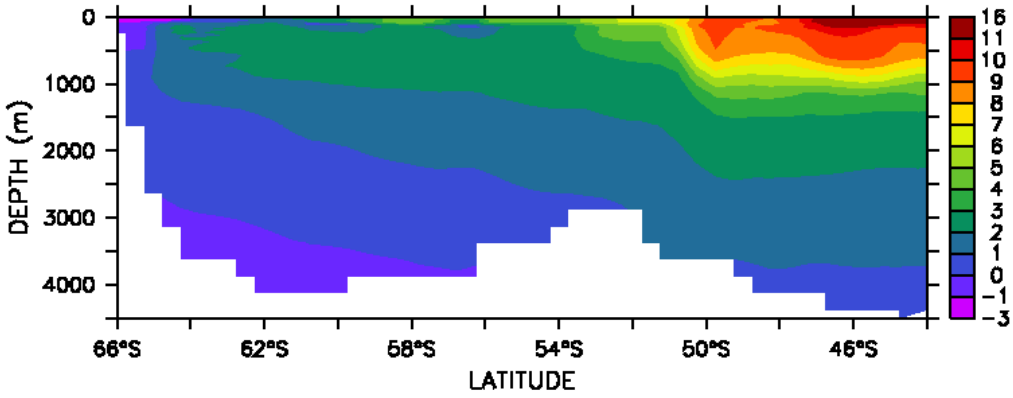

(b)

Figure 4.5: Temperature distributions in April 2008 along 140°E from (a) Andrew Bowie, ACE CRC (unpublished data) and (b) SODA. Note that the colour scales are different.

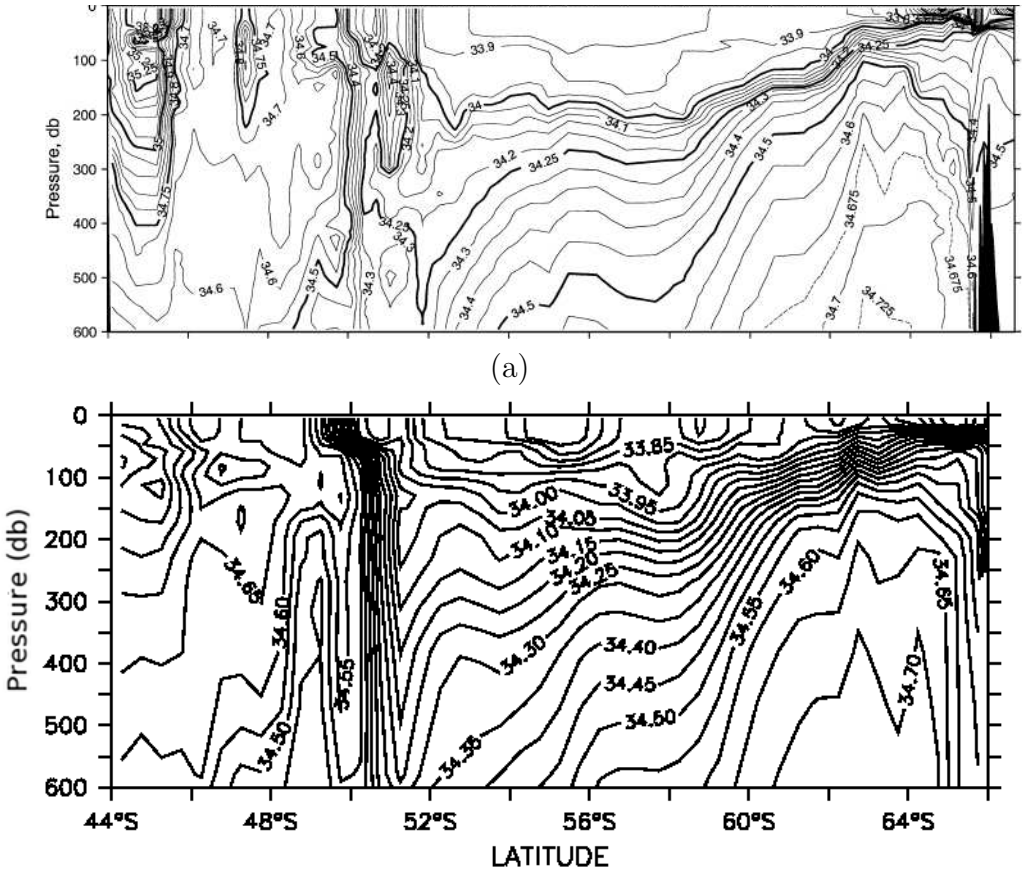

(a)

(b)

Figure 4.6: Salinity distributions in January 1995 along 140°E, from (a) *Sokolov and Rintoul* (2002), reprinted with permission from Elsevier and (b) SODA.

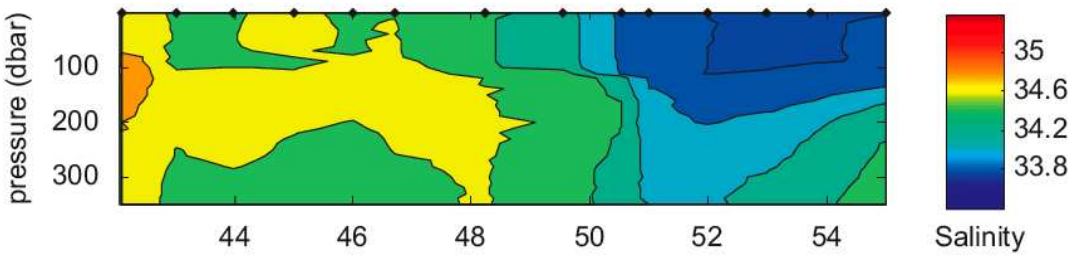

(a)

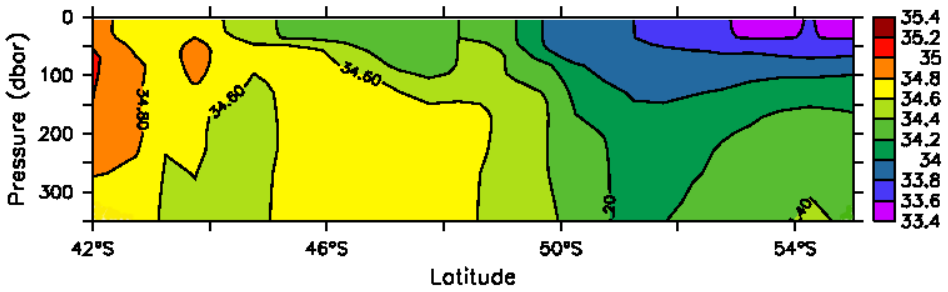

(b)

Figure 4.7: Salinity distributions in March 1998 along 140°E from (a) *Sedwick et al.* (2008), reprinted with permission from Elsevier and (b) SODA. Note that the colour scales are different.

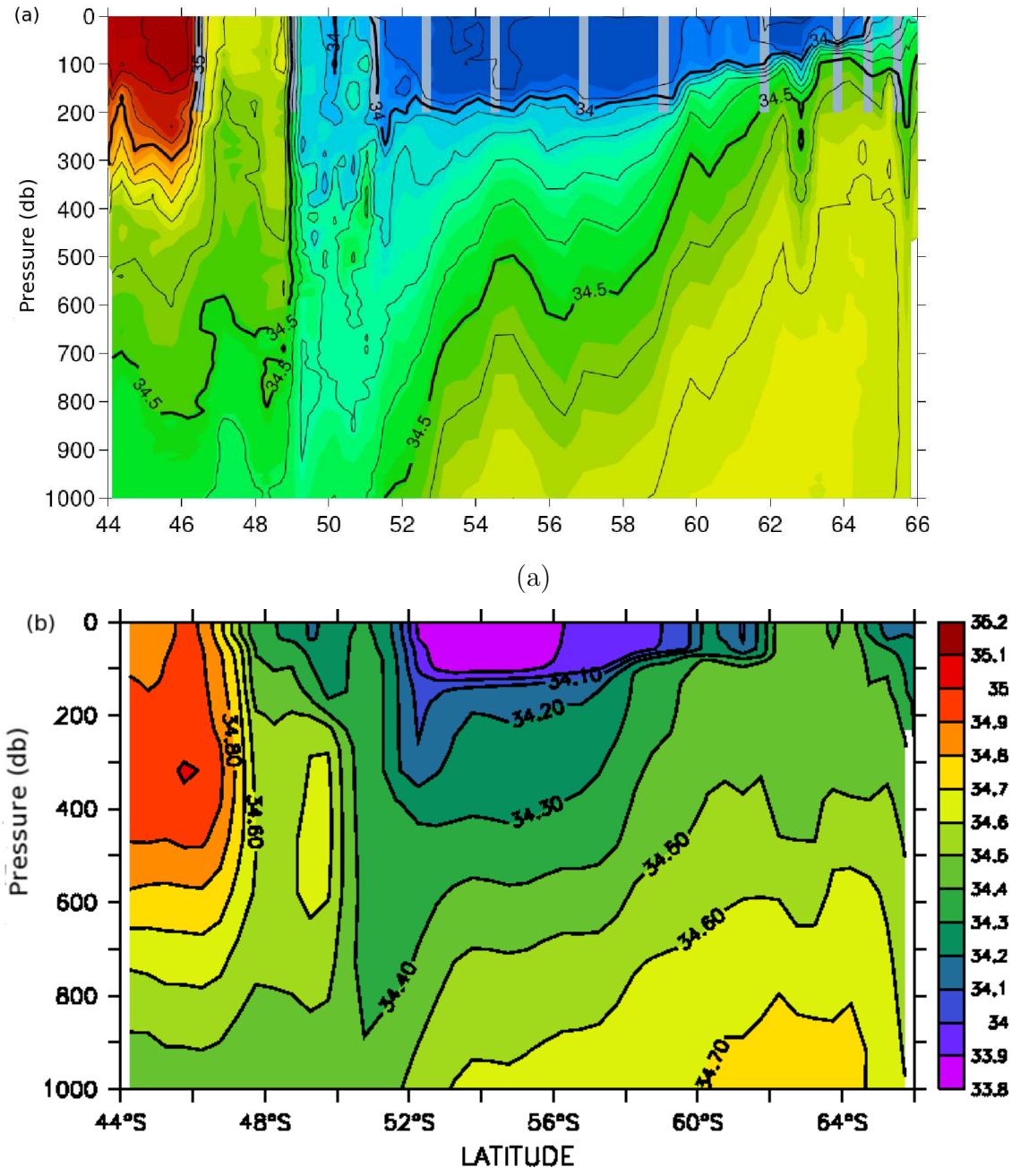

(a)

(b)

Figure 4.8: Salinity distributions in November 2001 along 140°E from (a) *Sokolov and Rintoul* (2007), reprinted with permission from Elsevier and (b) SODA. Note that the colour scales are different.

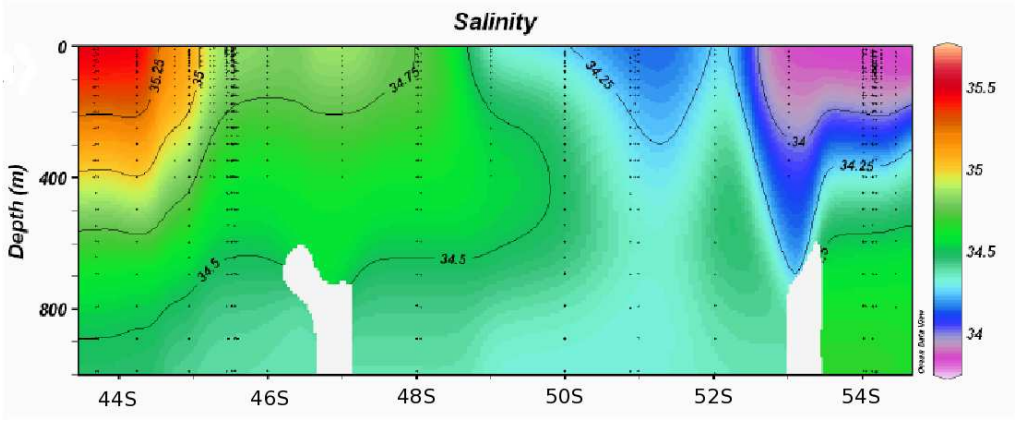

(a)

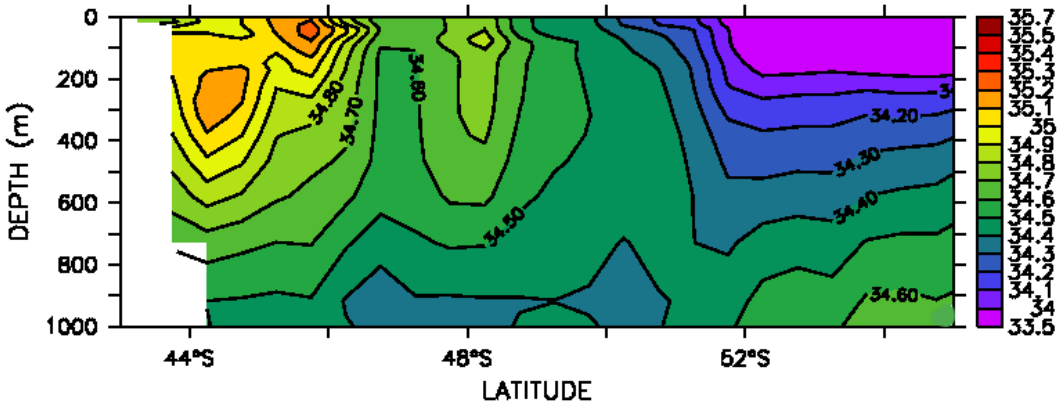

(b)

Figure 4.9: Salinity distributions in February 2007 (a) from (145.9°E, 52°S) to (153.2°E, 45.5°S) (*Bowie et al.*, 2009) and (b) along 146°E in SODA. Note that the colour scales are different.

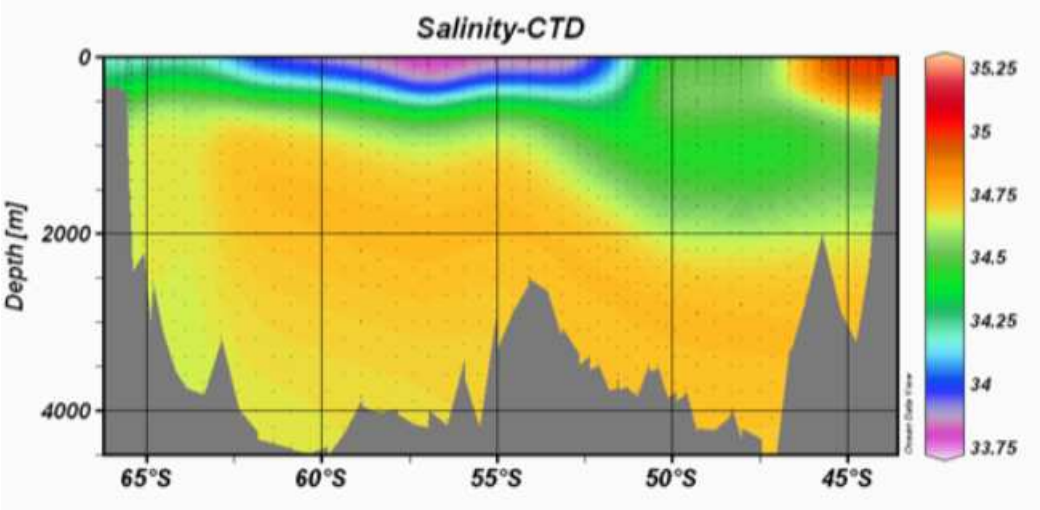

(a)

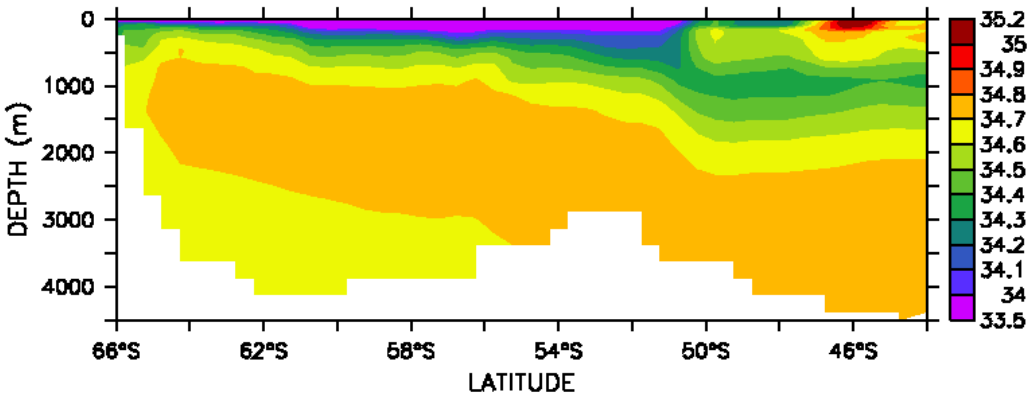

(b)

Figure 4.10: Salinity distributions in April 2008 along 140°E from (a) A. Bowie, ACE CRC (unpublished data) and (b) SODA. Note that the colour scales are different.

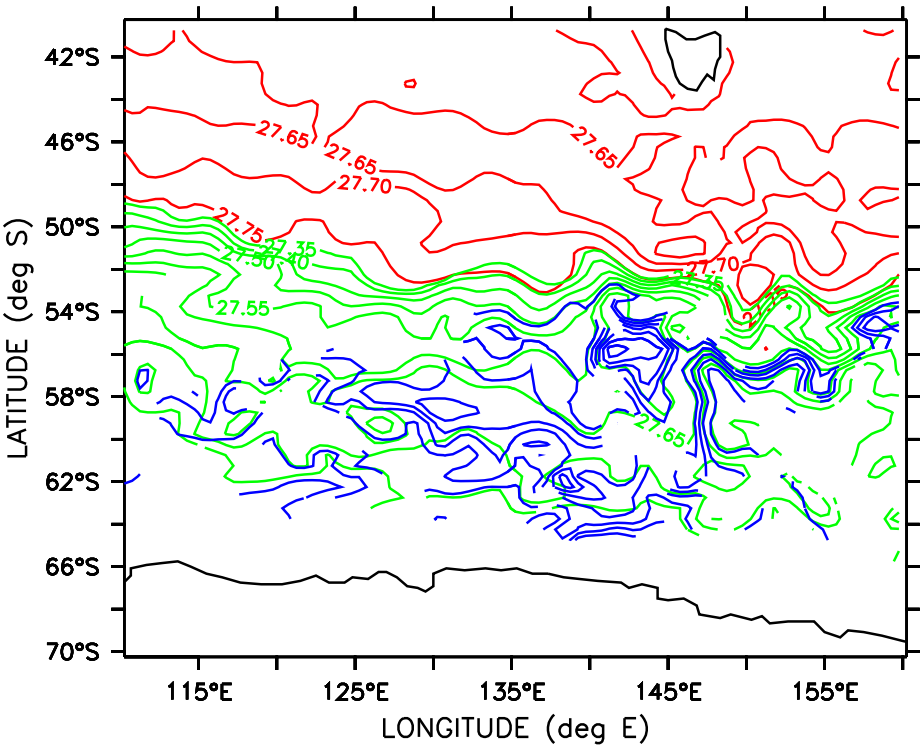

Figure 4.11: Contours showing the position of UCDW in April 1998 at depths 1875 m (red), 579 m (green) and 197 m (blue), as it shoals to the south.

4.2 The Structure of UCDW

UCDW can be identified in SODA using the criteria of *Orsi et al.* (1995) given in Chapter 3 and then its structure can be examined on meridional sections, such as the one along 140°E in Figure 3.3. That figure shows UCDW rising from depths of around 2500 m to about 100 m as it nears the Antarctic continent, with the steepest isopycnals south of the Polar Front (approximately 52°S). The figure is similar to the one constructed from observations along 170°W by *Hiscock et al.* (2003), shown in Figure 2.4. Another way of representing UCDW is given in Figure 4.11. This figure shows UCDW in the study region in April 1998, where UCDW is identified by three sets of contours, which are associated with its position at certain depths. In the figure, red contours show the latitudinal zones occupied by UCDW when it is at a depth of 1875 m. Then UCDW is found further south corresponding to a depth of 918 m (green contours) and finally, blue contours show UCDW at a depth of 197 m. So UCDW can be seen to move closer to the surface as it moves south and possibly then move northwards again under Ekman flow, since the blue and green contours overlap.

Another way of examining UCDW and its movement within the study region is via Lagrangian tracking, where the position of a water parcel within

UCDW is tracked over a number of years. Such a plot is given in Figure 4.12(a), which shows the upward, eastward and southward movement of UCDW over a period of about 4 years from January 2002 beginning at (140°E, 50°S, 2000 m) and ending approximately at (175°E, 64°S, 600 m). Parts (b), (c) and (d) of the figure show longitude-latitude, latitude-depth and longitude-depth plots, respectively, for the same track.

A similar set of plots is given in Figure 4.13, which again begin at (140°E, 50°S), although this time in January 1988. However, in this case three starting parcels are tracked from depths of 1500, 1200 and 1000 m. Again, UCDW is advected upwards, eastwards and southwards, with the three parcels following very similar, almost parallel, tracks. The final set of tracking plots in Figure 4.14 begins at (140°E, 55°S) in January 2002 with a parcel in the ML at a depth of 30 m. The parcel first moves northward to 50°S, then southward as far as 63°S and then northward again. It remains in the ML for the length of its path from the Australian sector, past New Zealand and into the Pacific Ocean. It is difficult to be certain that this water parcel is definitely UCDW, since once UCDW reaches the near-surface it mixes with the Antarctic Surface Water and loses its distinctive characteristics. However, since a study by *Hoppema et al.* (2000) using data collected along the prime meridian between the sACCf and the Weddell front found that around 90% of AASW in that region is UCDW, it is likely that UCDW is being tracked. In any case, it is useful to examine the northward movement of water in the ML due to Ekman transport and this plot is of particular interest because it shows movement in the ACC past New Zealand and then into the Pacific Ocean.

The results from the Lagrangian tracking presented here in Figures 4.12-4.14 are consistent with the upward movement of UCDW to the near-surface, as it is advected southwards and eastwards in the ACC, and its subsequent movement northward in the Ekman layer, as presented in the upper layer of the Deacon cell model of the SO MOC (*Speer et al.*, 2000) and shown in Figure 2.6.

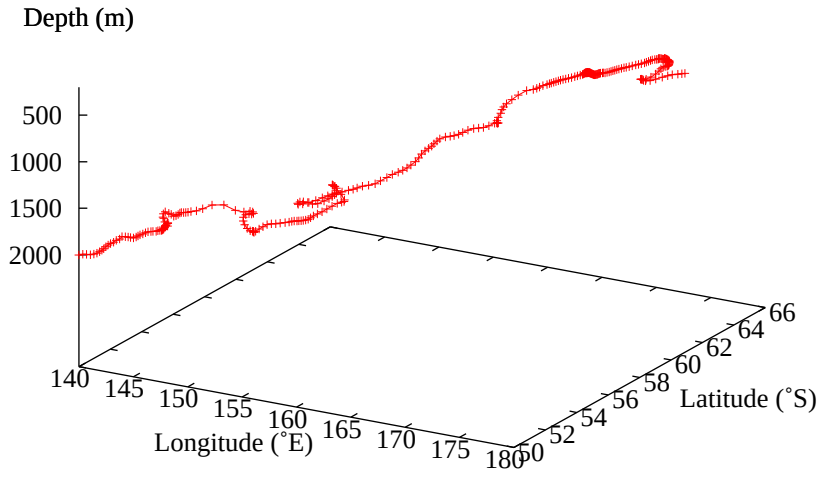

(a)

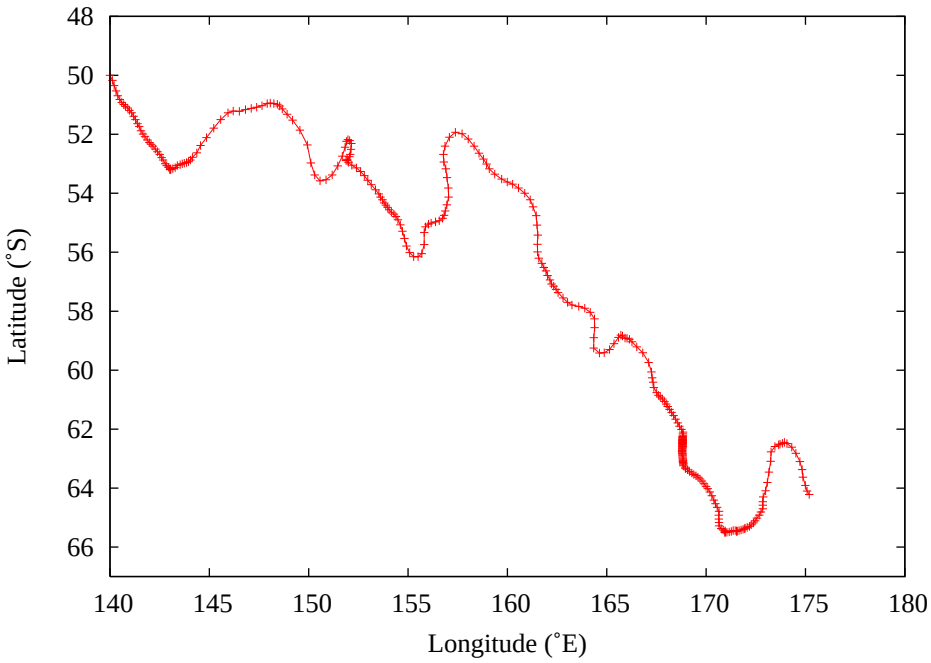

(b)

Figure 4.12

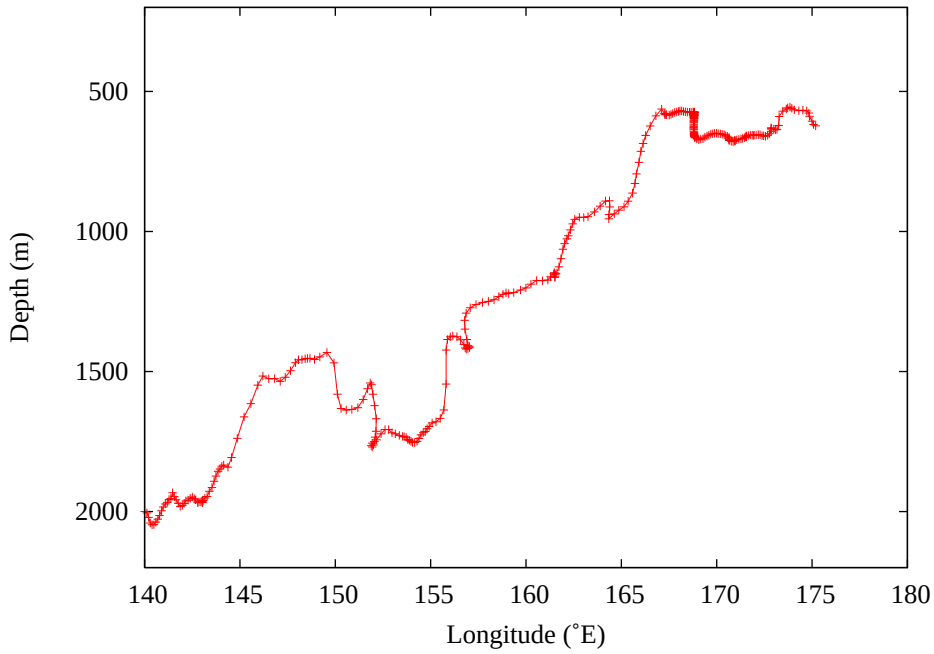

(c)

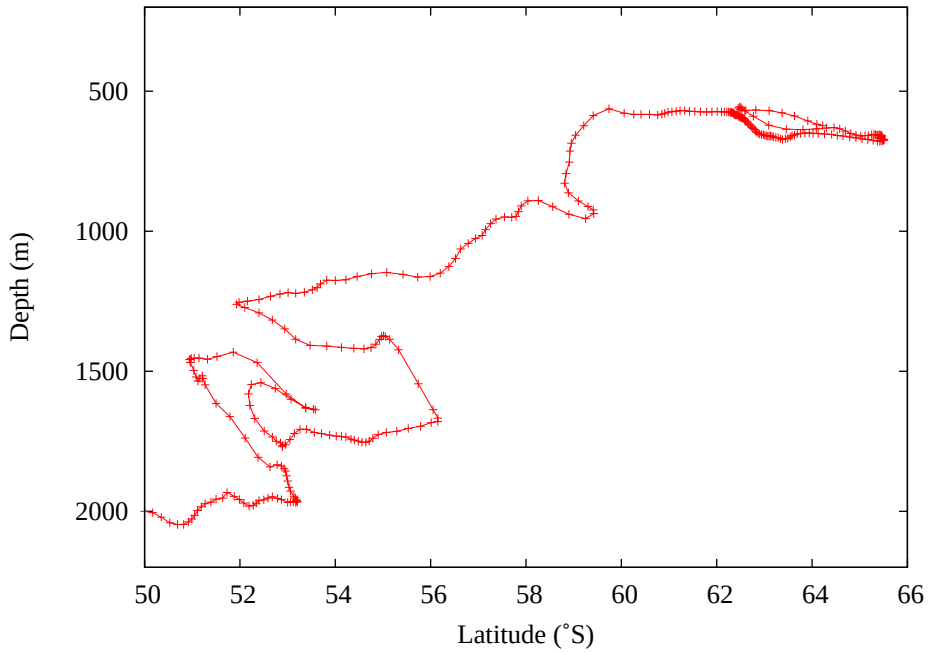

(d)

Figure 4.12: Lagrangian tracking of a parcel of UCDW beginning at (140°E, 50°S, 2000 m) in January 2002 and showing its movement towards the surface as it is advected eastwards and southwards. Part (a) is a three-dimensional plot and parts (b), (c) and (d) show two–dimensional sections of that plot.

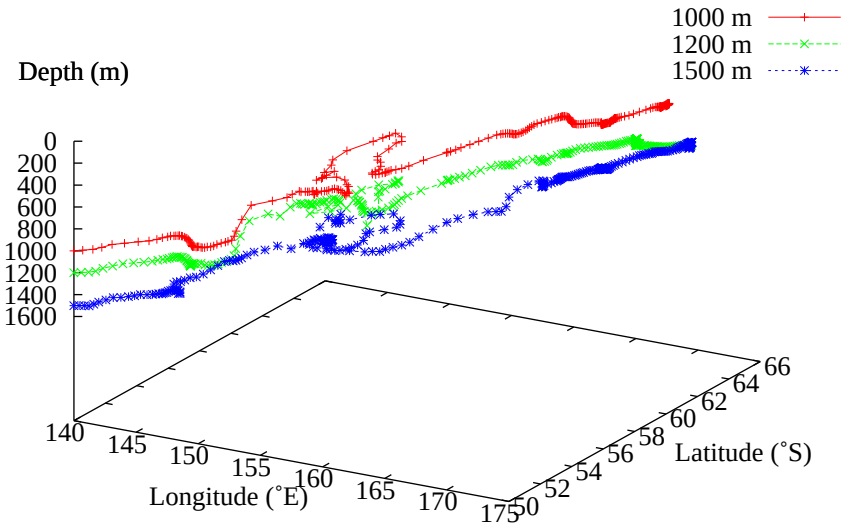

(a)

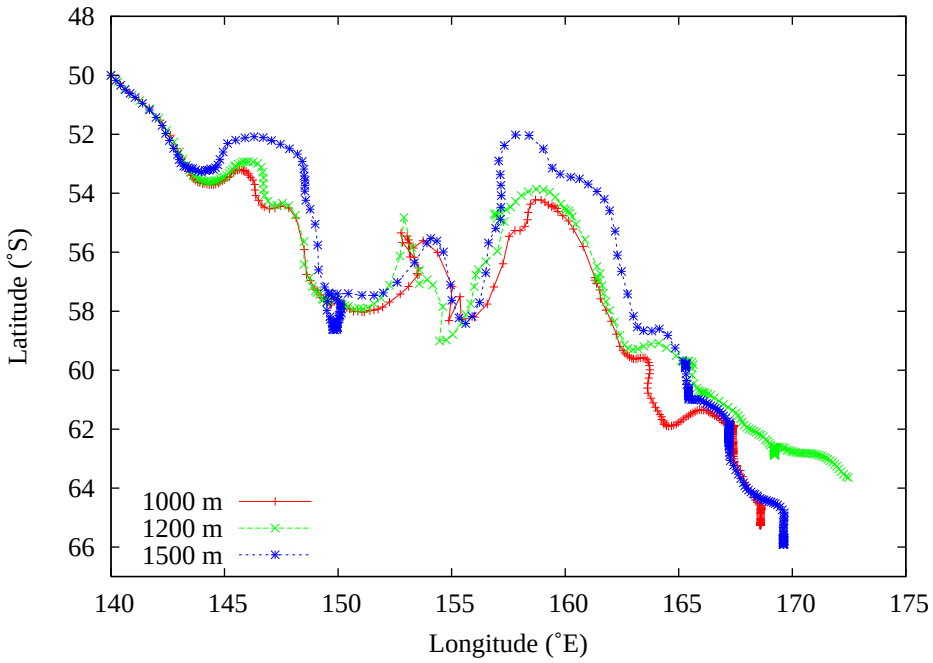

(b)

Figure 4.13

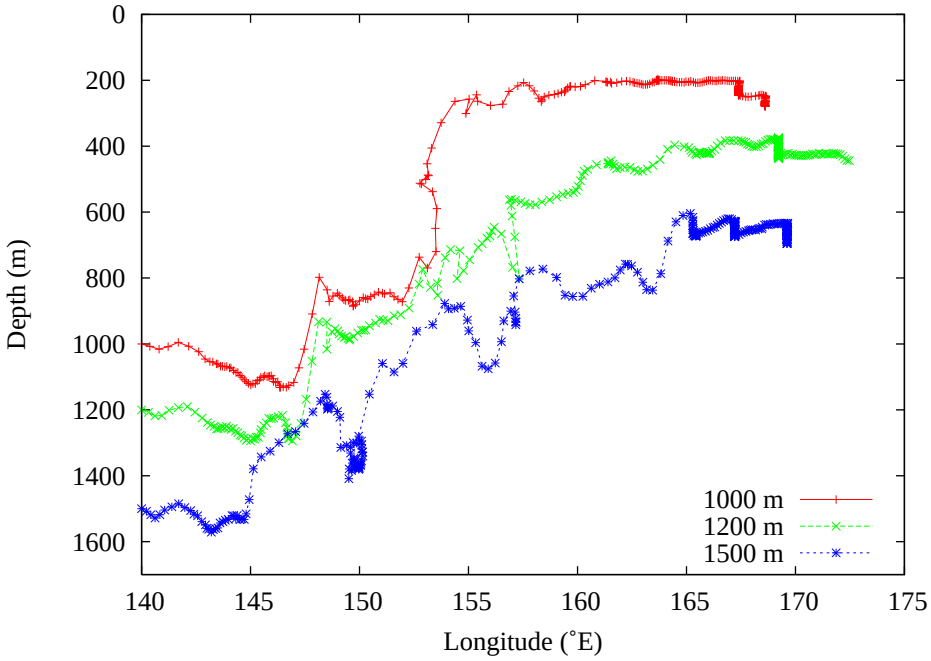

(c)

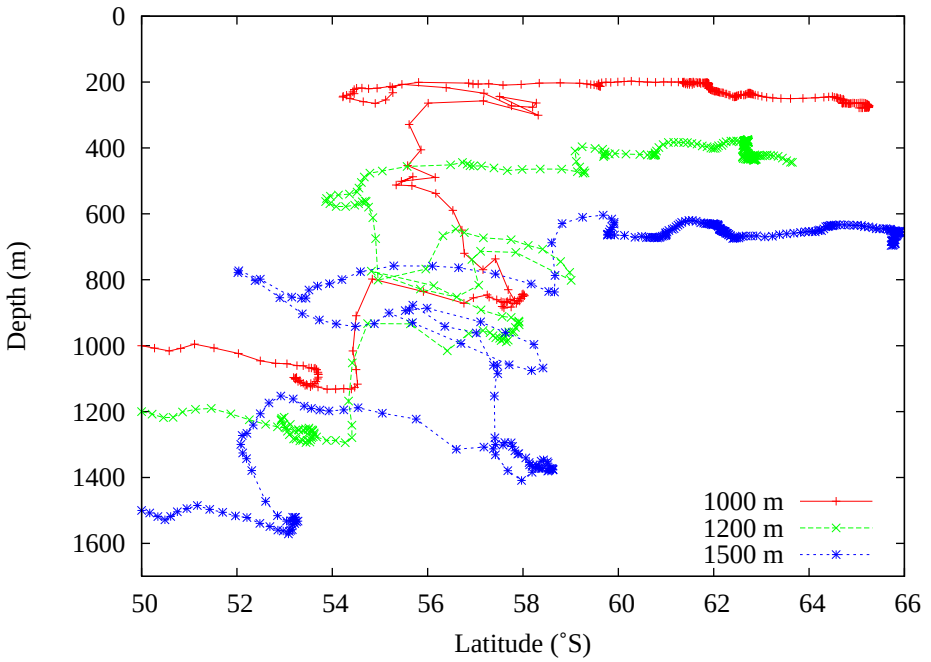

(d)

Figure 4.13: Lagrangian tracking of 3 parcels of UCDW beginning at (140°E, 50°S) and depths of 1500, 1200 and 1000 m in January 1988. UCDW is advected upwards, eastwards and southwards. Part (a) is a three-dimensional plot and parts (b), (c) and (d) show two–dimensional sections of that plot.

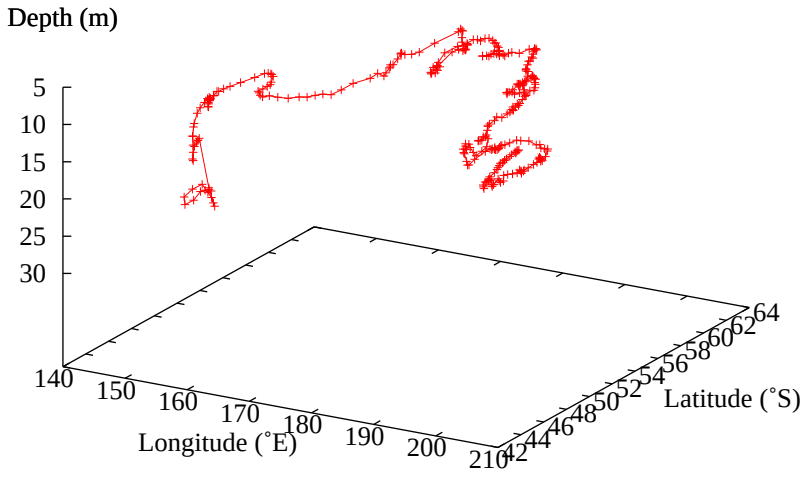

(a)

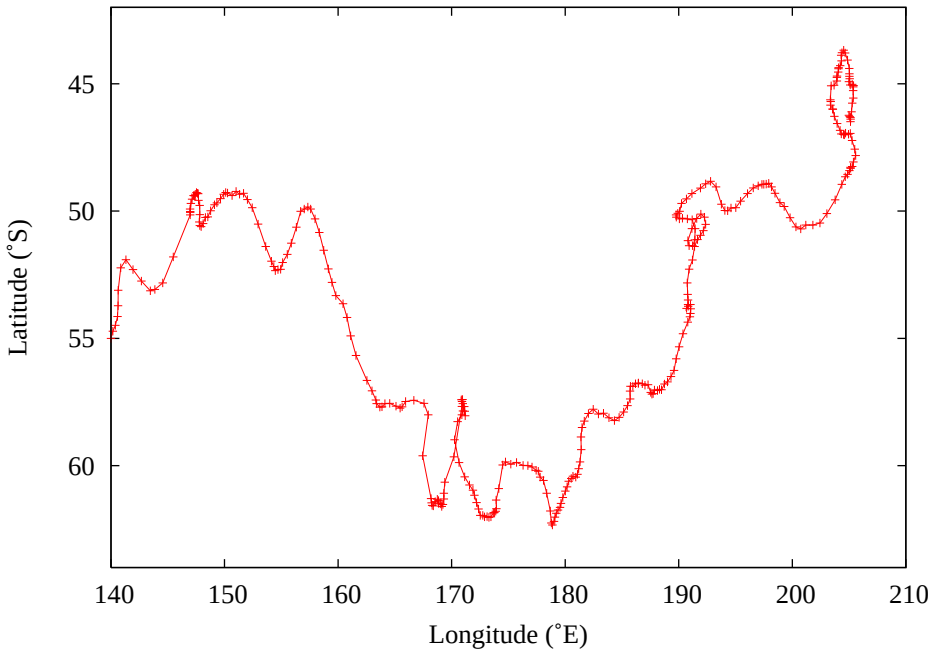

(b)

Figure 4.14

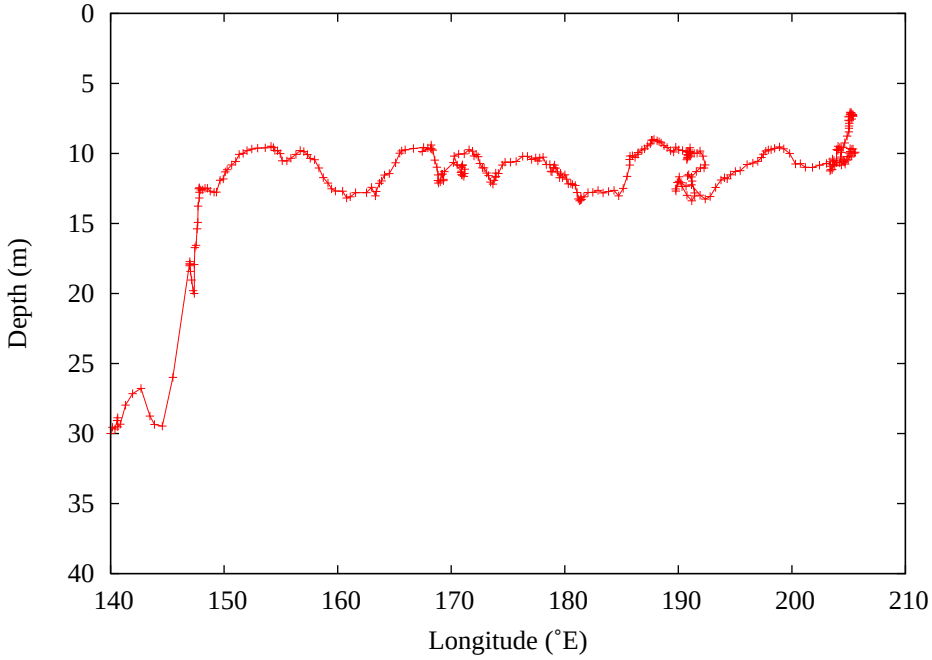

(c)

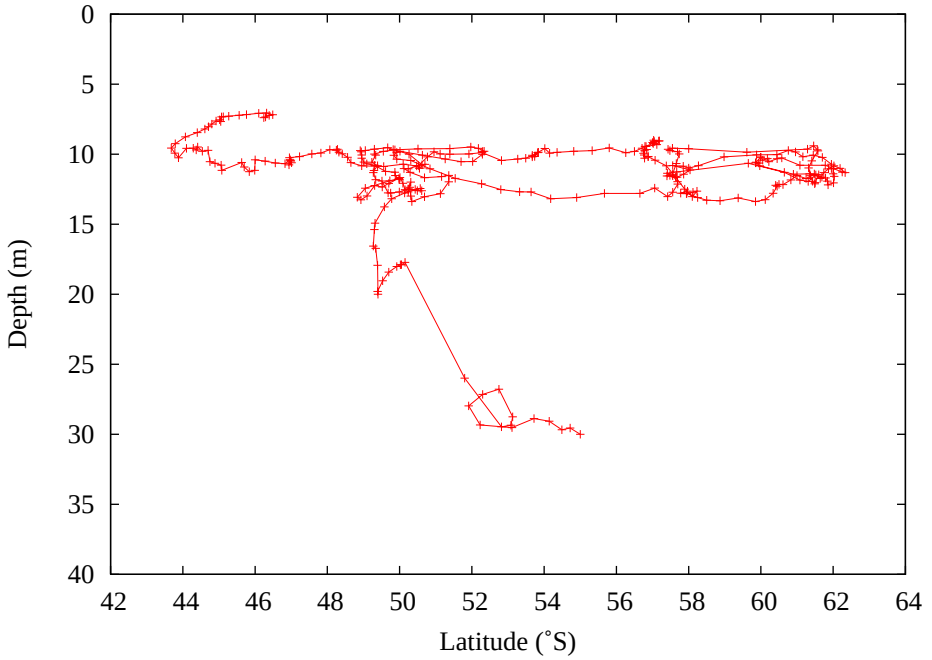

(d)

Figure 4.14: Lagrangian tracking of a parcel of UCDW beginning at (140°E, 55°S) at a depth of 30 m in January 2002. The parcel remains in the mixed layer, while travelling south and then north into the Pacific Ocean. Part (a) is a three-dimensional plot and parts (b), (c) and (d) show two–dimensional sections of that plot.

4.3 Iron in UCDW

The purpose of this section is to compare plots of observations of dissolved iron concentration (dFe) with plots from SODA that identify UCDW in the same region, with the object of examining dFe values in UCDW.

Figures 4.15(a), 4.16(a) and 4.18(a) present dFe data, measured along the SR3 section (approximately 140°E) to various depths, in a number of different years and seasons. The transect for Figure 4.17 was less meridional than the other three, starting at P2 (145.9°E, 54°S) and ending at P3 (153.2°E, 45.5°S) and was conducted as part of SAZ-Sense (Sensitivity of the SAZ to environmental change, *Bowie et al.* (2009)). SODA plots showing isopycnals which identify UCDW, overlaid on temperature plots, have been produced to match each of these dFe plots, where the track chosen for the SODA plots for Figure 4.17(b) was along 146°E, so that the plots would be more likely to match near P2, which is the region of interest in relation to UCDW upwelling. The February 2007 dFe (Figure 4.17) plot is used with the caveat that depth profiles for depths greater than 400 m were only obtained at the P2 and P3 process stations, making it difficult to interpolate on a section below those depths (A. Bowie, personal communication).

Figures 4.15 and 4.16 both go down to only 350 m and so in the first case UCDW is seen only at the very end of the transect near the Polar Front, where it upwells to within about 150 m of the surface. In the second case, the transect goes as far as 66°S and UCDW comes up to within 100 m of the surface between 56 and 62°S. Matching the dFe and UCDW plots puts dFe in UCDW in the upper 350 m at around 0.2-0.25 nM. Figures 4.17 and 4.18 are useful for estimating dFe in UCDW at greater depth, leading to values in the range 0.3-0.37 nM in the first case and similar deep values in the second case, with dFe decreasing towards the surface. An extra plot has been included in 4.18(c), which shows Oxygen concentration on the same transect, since a characteristic of UCDW is its low values of oxygen concentration (<201 μmol/l) (*Sievers and Nowlin*, 1984; *Orsi et al.*, 1995).

The above results, found in February 2007 for dFe by comparing UCDW isopycnals and dFe plots in Figure 4.17, confirm the conclusions of *Lannuzel et al.* (2010a), who comment that the sharp increase in nutrient concentration at depths greater than 200 m reflects a supply of macro-nutrients and iron from below, which is characteristic of Ekman-driven upwelling.

Overall, from Figures 4.15-4.18, it can be concluded that dFe in UCDW in the study region is approximately in the range 0.2-0.4 nM, with the higher values in the deeper waters. This is consistent with values found in the Pacific sector of 0.3 nM (*Hiscock et al.*, 2003; *Measures and Vink*, 2001).

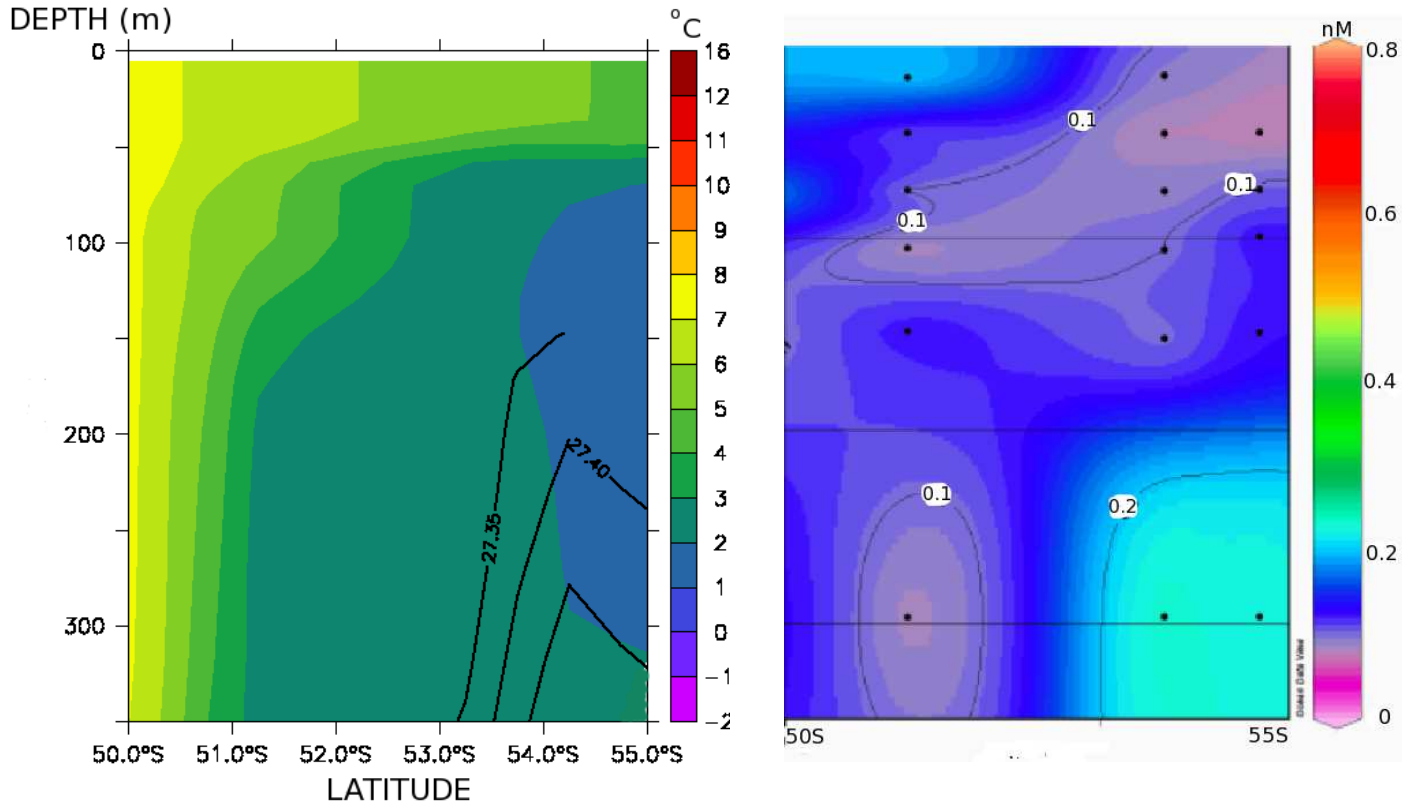

(a) (b)

Figure 4.15: (a) Temperature distribution in March 1998 along 140°E from SODA, overlaid with isopycnals identifying UCDW. Part (b) shows dissolved iron concentrations measured at the same time as the temperatures shown in part (a) (*Sedwick et al.* (2008), reprinted with permission from Elsevier). The isopycnals identifying UCDW coincide with higher values of dissolved iron.

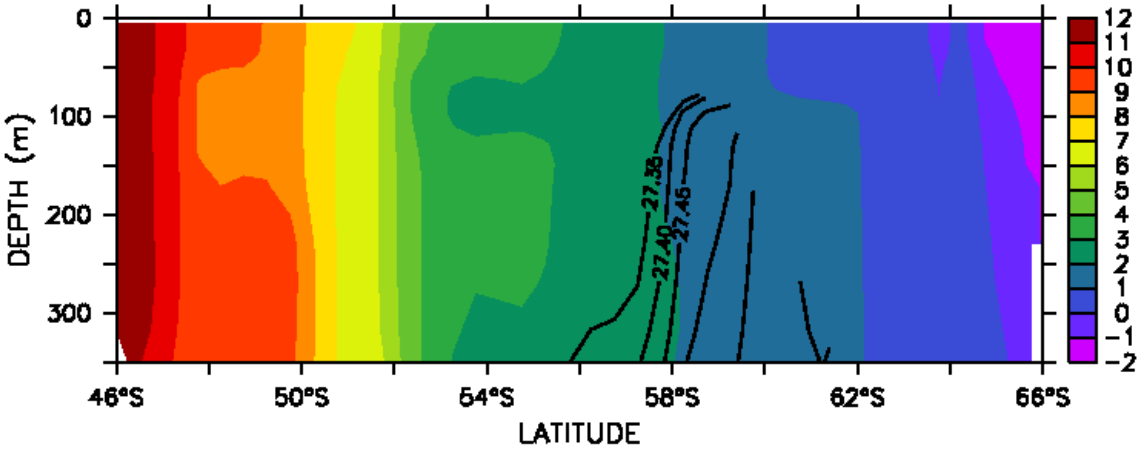

(a)

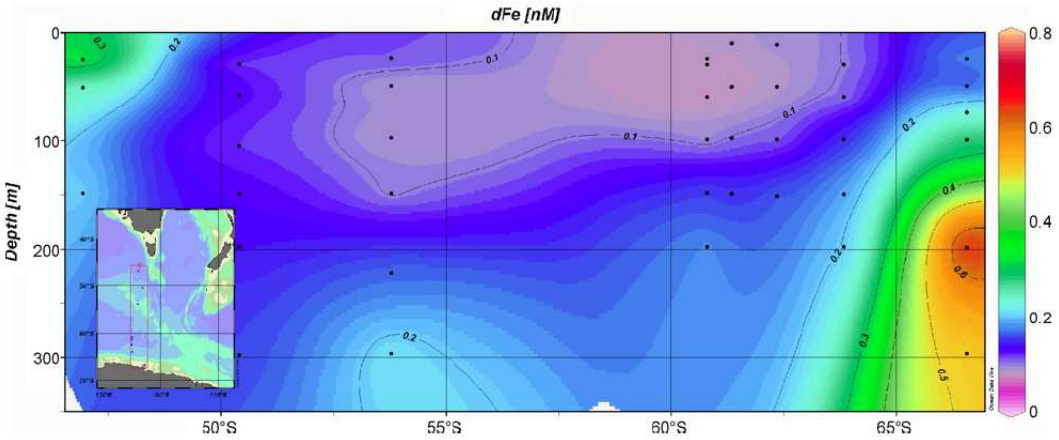

(b)

Figure 4.16: Plots along 140°E in November 2001 showing (a) SODA isopycnals identifying UCDW and (b) Dissolved Iron (*Sedwick et al.*, 2008).

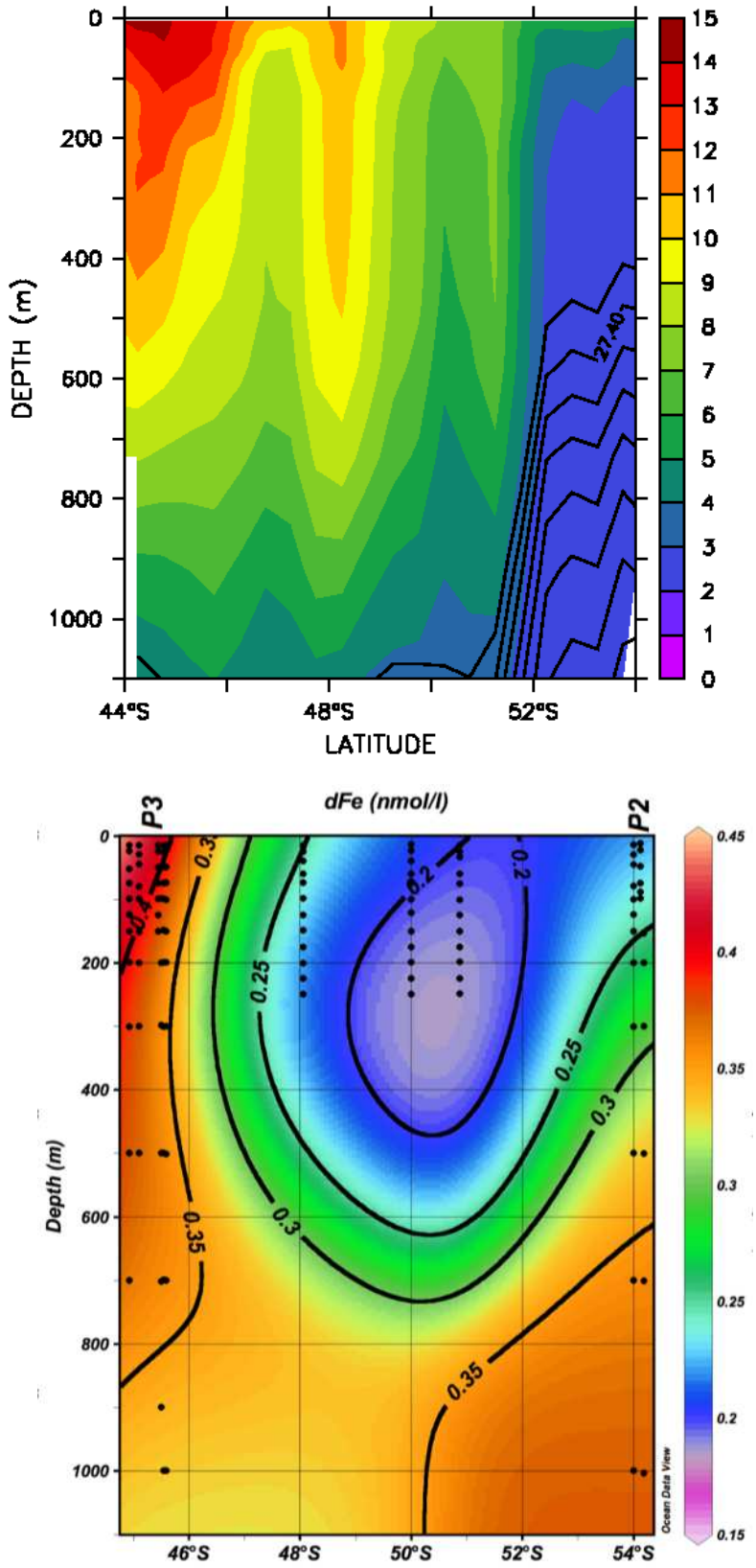

(b)

Figure 4.17: Plots in February 2007 (a) along 146°E in SODA showing isopycnals identifying UCDW and (b) Dissolved Iron (*Lannuzel et al.*, 2010a) along the track from P2 (145.9°E, 54°S) to P3 (153.2°E, 45.5°S).

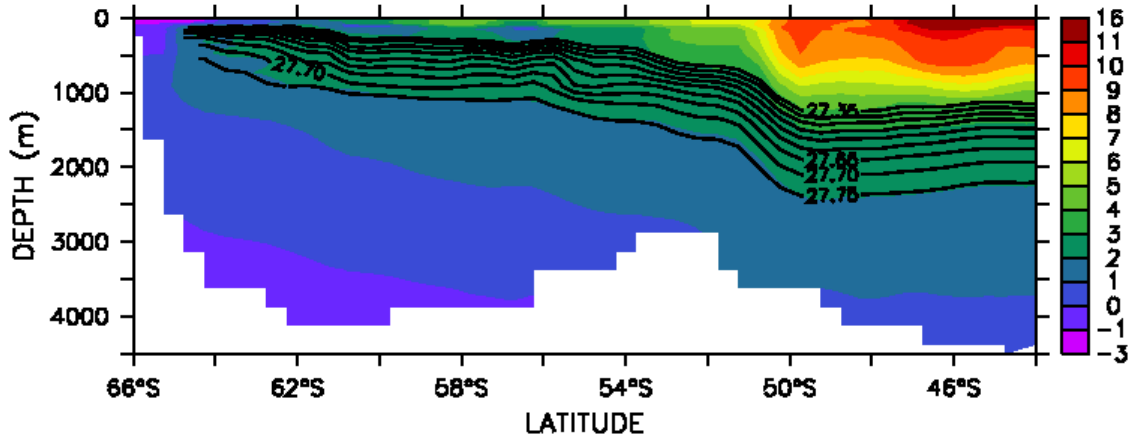

(a)

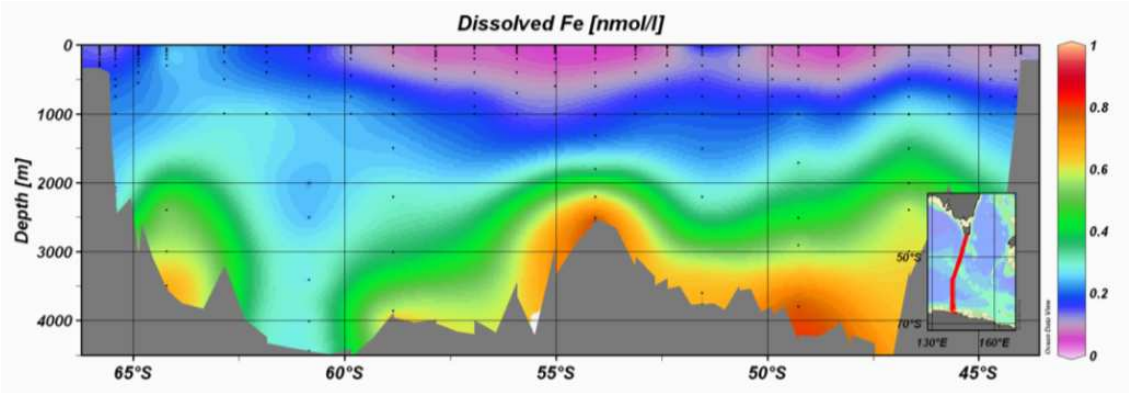

(b)

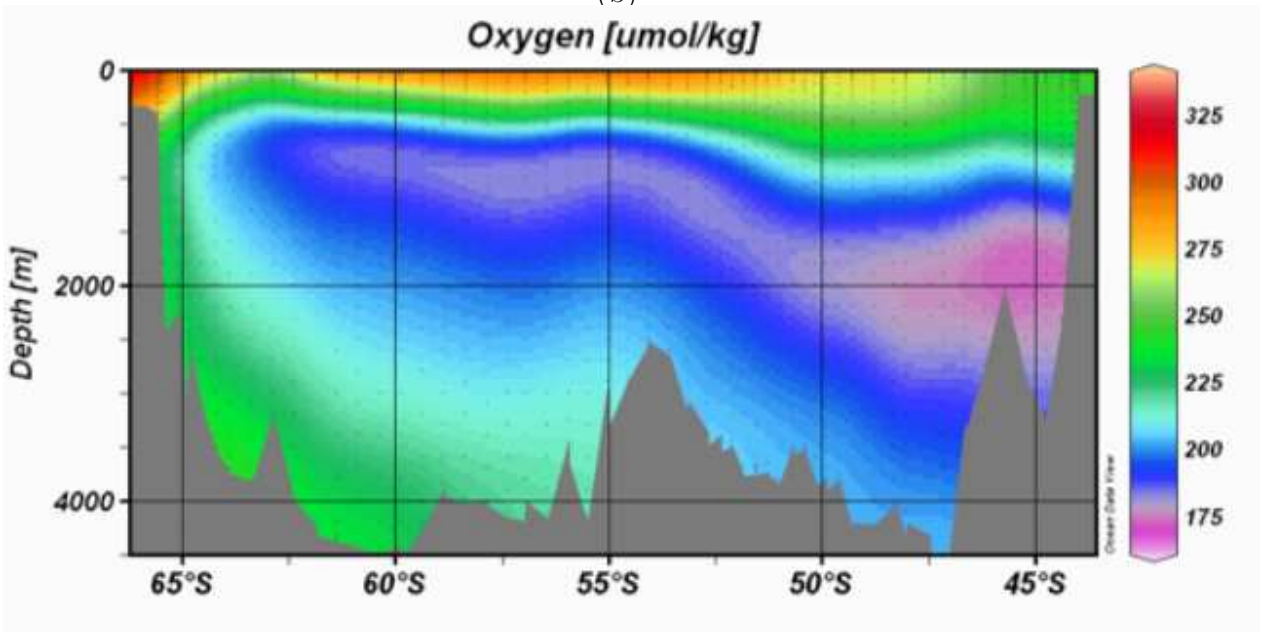

(c)

Figure 4.18: Plots along 140°E in April 2008 showing (a) SODA temperature data overlaid with isopycnals identifying UCDW, and AU0806 cruise data (A. Bowie, ACE CRC, unpublished data) for (b) Dissolved Iron and (c) Oxygen concentration.

Chapter 5

Upper ocean structure and the meridional circulation of the Southern Ocean south of Australia in 1958-2007

Monthly climatologies and seasonal trends in the meridional circulation of UCDW and in upper ocean properties, in the Australian sector of the SO, are examined in this chapter. These trends are over the period 1958-2007, and are in ML variables, such as depth, temperature, density and salinity, as well as in similar UCDW variables. In addition, trends in the location of the maximum wind stress, stratification, Ekman pumping, Ekman transport, UCDW upwelling depth and the southern-most extent of UCDW are examined. Finally, connections between wind stress and these variables are discussed.

5.1 Climatological UCDW, ML and Wind Data

5.1.1 Climatological UCDW

UCDW shoals to the south, as has been demonstrated in Figures 4.11-4.13. In addition, the plot given in Figure 5.1 shows UCDW top depth shoaling from around 1100 m at 45°S to less than 100 m, further south. The isopycnals begin to rise steeply near the Subantarctic Front (around 50°S) and continue to rise, outcropping south of the Polar Front (between 55 and 65°S here). UCDW is found as far south as the Southern Boundary of the ACC (around 64-65°S in the study region, Figure 3.1), but no further south, since the Southern Boundary is defined (*Orsi et al.*, 1995) as the poleward edge of the UCDW signal. The position of the Southern Boundary is consistent with the southern-most location of UCDW identified in SODA (Figure 5.2) at around 65°S, moving

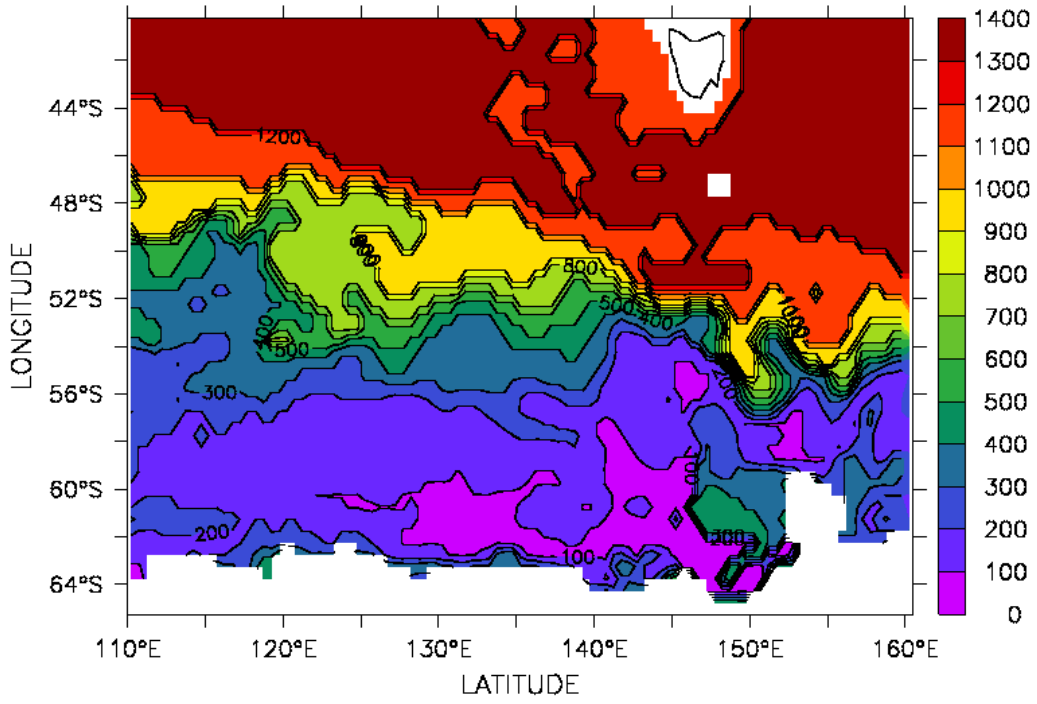

Figure 5.1: SODA plot of the top depth of UCDW for January 2004.

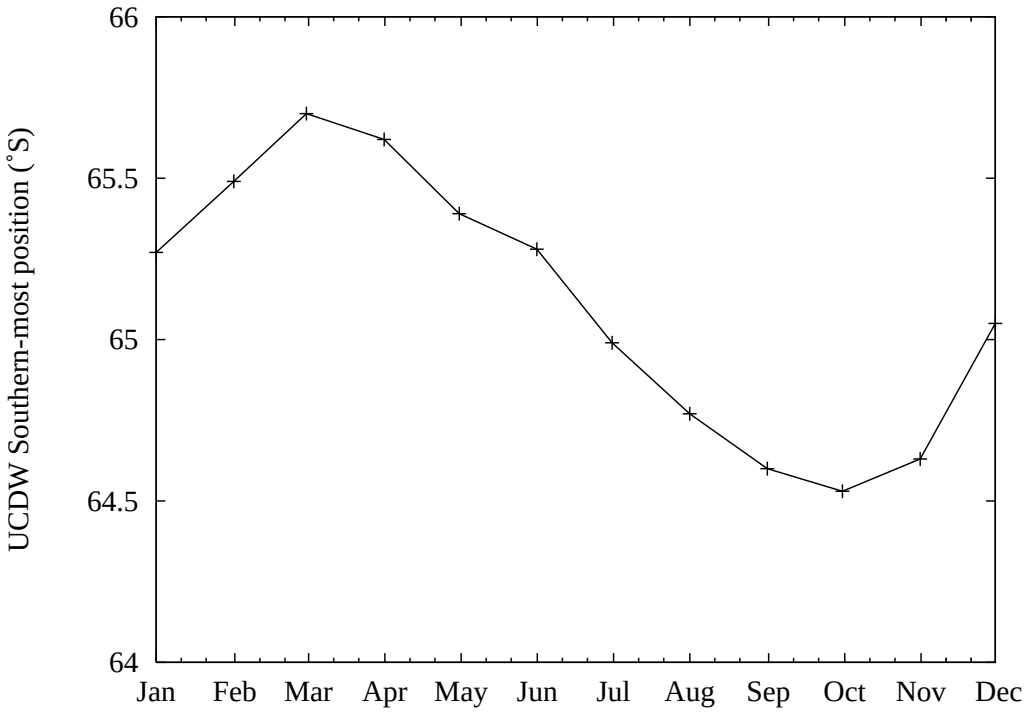

Figure 5.2: Climatology of the southern-most position of UCDW.

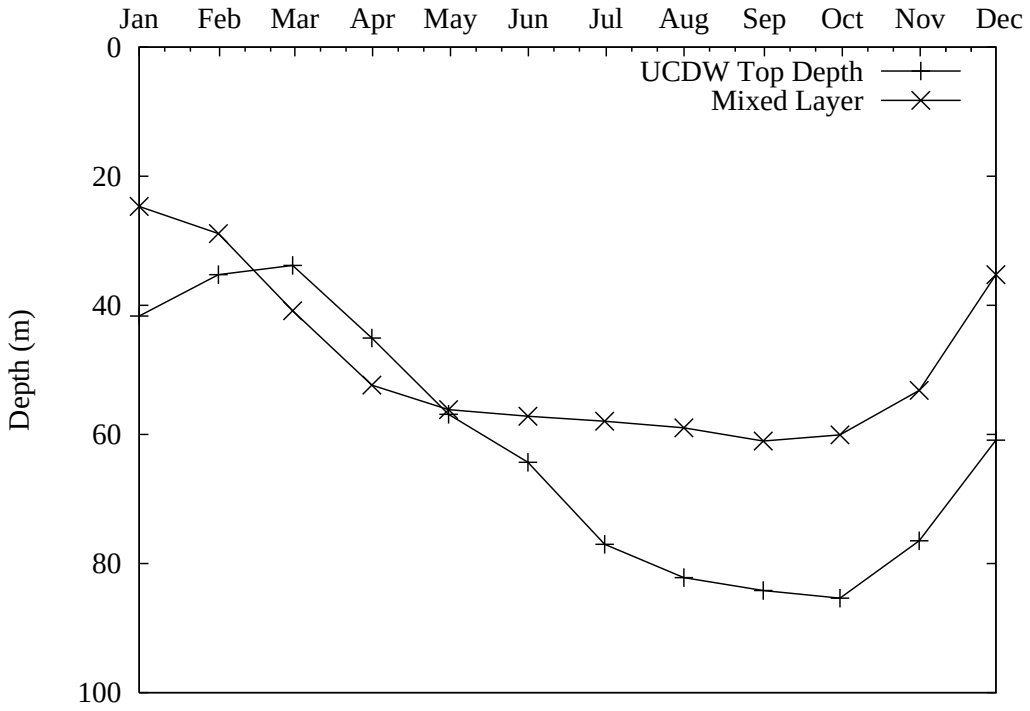

Figure 5.3: Climatologies of mixed layer depths and UCDW top depth for 60-65°S. Note that these are climatologies of mean depths over a latitudinal zone and thus it cannot be concluded that UCDW is always at a lower depth than the mixed layer depth in any particular month.

Table 5.1: Annual means of climatological values for UCDW variables.

Zone 110-160°E by (°S)	Mean Vertical Velocity (ms^{-1})	Mean Temperature (°C)	Mean Density (kgm^{-3})	Mean Salinity	Mean Depth Range (m)
60-65	0.29×10^{-5}	1.9	27.70	34.63	60-800
55-60	1.8×10^{-5}	2.1	27.64	34.58	75-1700
50-55	2.3×10^{-5}	2.4	27.60	34.57	120-2400
45-50	0.91×10^{-5}	2.6	27.59	34.58	470-2400
40-45	0.32×10^{-5}	2.7	27.60	34.59	1100-2400

as far south as 65.7°S in March, when the area is ice free. Vertical velocities in UCDW, presented in Table 5.1 as depth- averaged annual values by latitudinal zone, peak in the 50-55°S zone and then decrease as UCDW shoals upwards. UCDW is then entrained in the surface Ekman layer, which moves back towards the north, forming AAIW, when it downwells beneath the warmer SAMW (*Speer et al.*, 2000). Climatological plots of UCDW top depth (Figure 5.3) indicate that there is a seasonal variation in this depth in the more southerly zones, with UCDW advected closest to the surface in February and March.

Plots from SODA showing UCDW temperature and salinity averaged over depth are presented in Figure 5.4 for January 2001. These plots show UCDW

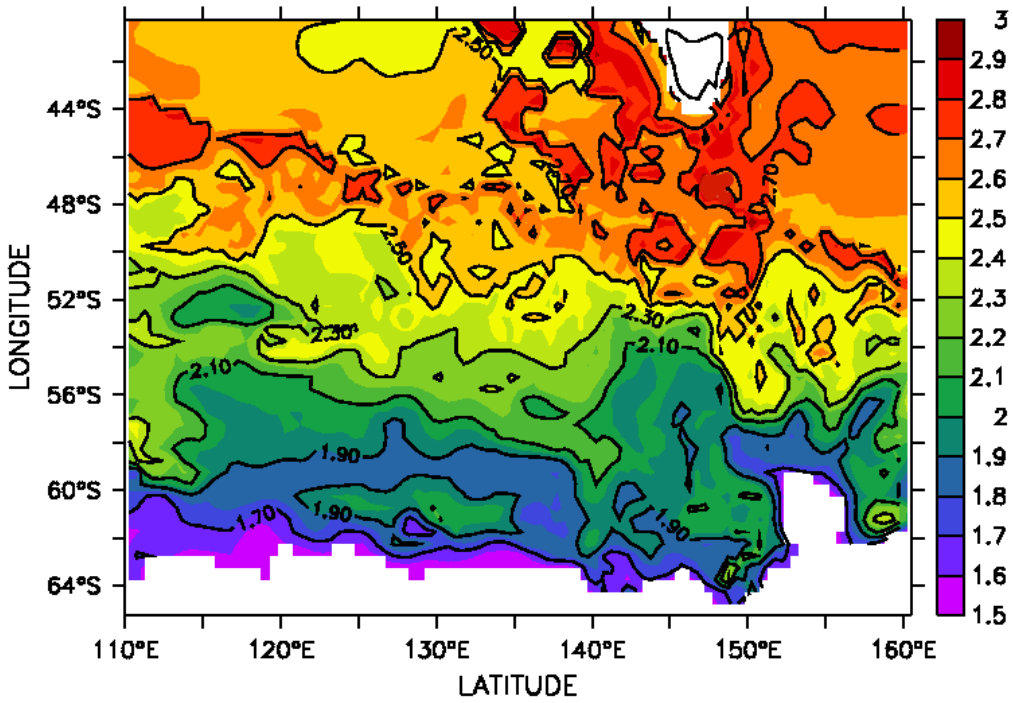

(a)

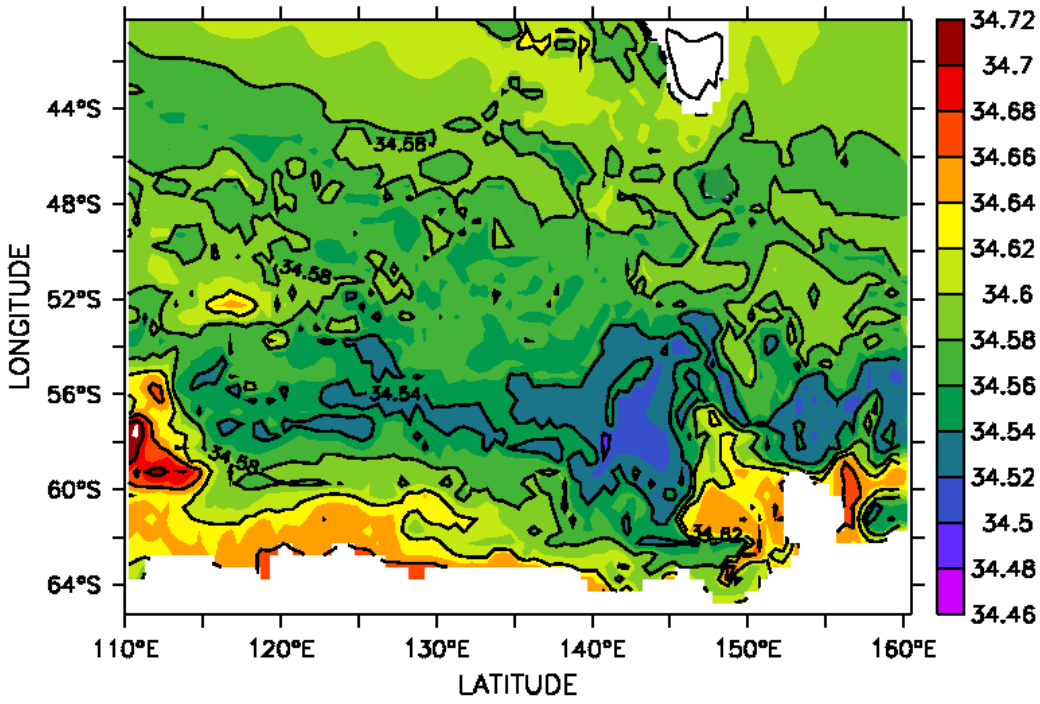

(b)

Figure 5.4: SODA plots of UCDW properties averaged over depth for January 2004, showing (a) temperature and (b) salinity.

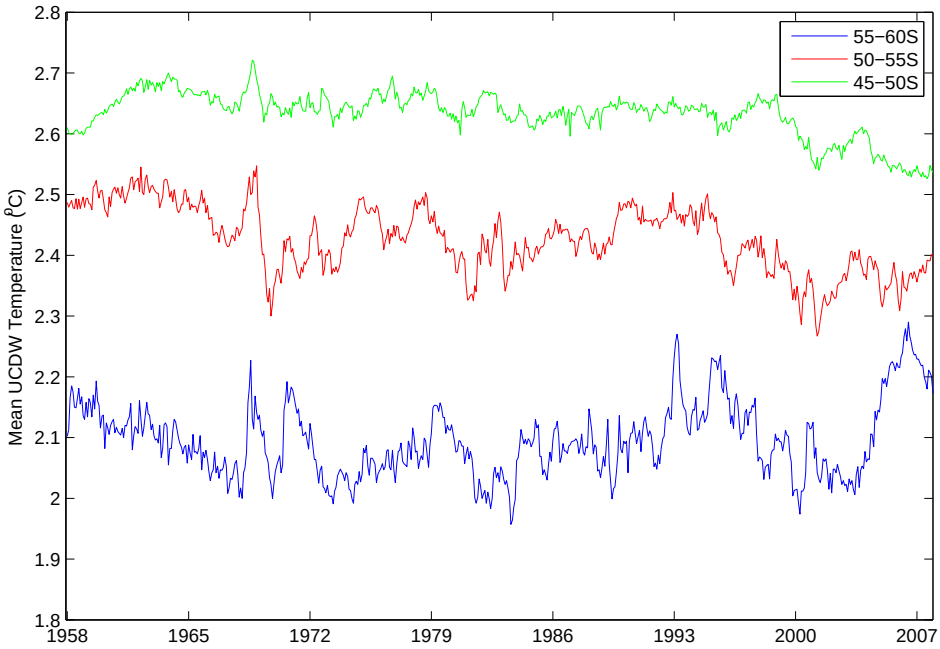

Figure 5.5: Depth-averaged UCDW temperature time series for the 45-50°S, 50-55°S and 55-60°S zones.

temperature decreasing as it shoals southwards, which is consistent with the UCDW temperature time series for three latitudinal zones that are shown in Figure 5.5. Minimum UCDW salinity values occur between about 55°S and 60°S, before salinity increases again towards the Antarctic continent. Climatological information about UCDW is summarised in Table 5.1 which gives annual values for UCDW variables for the various five-degree latitudinal bands, since neither UCDW temperature, salinity nor density varies throughout the year. No values are given for the 65-70°S sector since the sBdy is found very close to 65°S (Figure 3.1) and thus UCDW can be detected only occasionally in the 65-70°S zone. The density (around 27.6 kg m^{-3}), salinity (around 34.6) and temperature values (which are all above 1.5°C) are all consistent with the definition of UCDW water mass characteristics (*Orsi et al.*, 1995). UCDW temperature decreases from 2.7°C for UCDW lying at depths of up to 2400 m in the 40-45°S zone to 1.9°C in the 60-65°S zone, presumably because UCDW is rising towards the surface and coming into contact with cooler water masses.

5.1.2 Climatological wind stress

Summer and winter climatological values, by latitudinal zone, are presented in Table 5.2 for mean wind stress, stratification, Ekman pumping rate and northward Ekman transport.

From Figure 5.6, it can be seen that the location of maximum wind stress,

Table 5.2: Means of climatological values for wind stress, stratification and Ekman variables (n/a = not applicable).

	65-70°S	60-65°S	55-60°S	50-55°S	45-50°S	40-45°S
Mean Wind Stress (Nm^{-2})						
Summer	0.07	0.05	0.11	0.16	0.14	0.08
Winter	0.13	0.10	0.16	0.17	0.16	0.13
Stratification (s^{-2})						
Summer	3.3×10^{-5}	5.9×10^{-5}	5.8×10^{-5}	5.9×10^{-5}	7.1×10^{-5}	8.3×10^{-5}
Winter	2.8×10^{-5}	5.2×10^{-5}	5.5×10^{-5}	3.8×10^{-5}	3.3×10^{-5}	4.2×10^{-5}
Ekman Transport (Sv)						
Summer	n/a	0.9	2.5	4.3	4.7	3.3
Winter	n/a	1.6	3.3	4.4	4.9	4.8
Ekman Pump Rate (ms^{-1})						
Summer	n/a	1.6×10^{-6}	1.1×10^{-6}	n/a	n/a	n/a
Winter	n/a	2.7×10^{-6}	0.7×10^{-6}	n/a	n/a	n/a

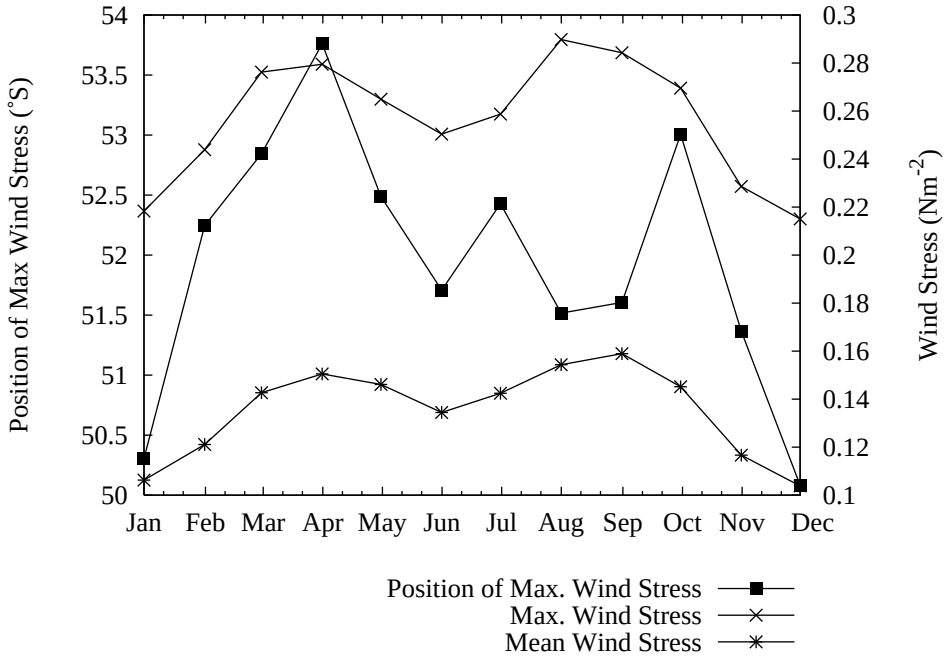

Figure 5.6: Climatology of maximum and mean wind stress, as well as location of maximum wind stress.

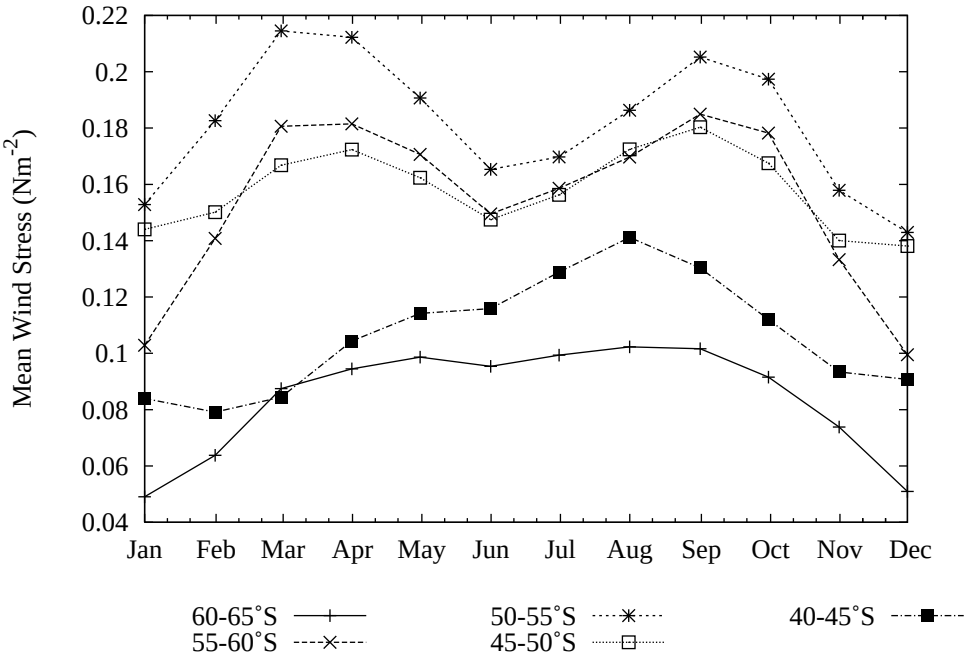

Figure 5.7: Climatology of mean wind stress by latitudinal zone.

as well as the values of regional mean and maximum wind stress, vary seasonally with the semi-annual oscillation of atmospheric pressure, which occurs in the SH due to differing cycles of temperature in the mid-latitude ocean and the Antarctic (*van Loon*, 1967; *Simmonds and Jones*, 1998). Peak wind stress occurs around March/April and August/September and March/April also corresponds to the most southerly locations of the maximum wind stress. The maximum wind stress varies from 0.21 Nm^{-2} in December/January to 0.29 Nm^{-2} in April and September, dropping to 0.25 Nm^{-2} in June. The regional mean wind stress follows a similar pattern, with values in the range 0.10-0.16 Nm^{-2}. The location of the maximum wind stress moves from 50°S in December/January to 54.8°S in April/May. A similar climatological plot for mean wind stress by latitudinal zone in Figure 5.7 shows low values of wind stress in the 60-65°S zone, which is close to the latitudes where the westerly winds give way to the Easterlies near the Antarctic continent. The mean wind stress increases to the north reaching a maximum between 50 and 55°S, as discussed above, and then decreases again.

5.1.3 Climatological stratification and Ekman variables

The monthly climatology for stratification at the base of the ML given by the Brunt-Vaissala Frequency Squared in Equation (3.4) and presented in Figure 5.8, shows seasonal variation in stratification, with maximum stratification in February/March and minimum stratification in September-November. Stratification in the more southerly zones commences later in summer, due to ice

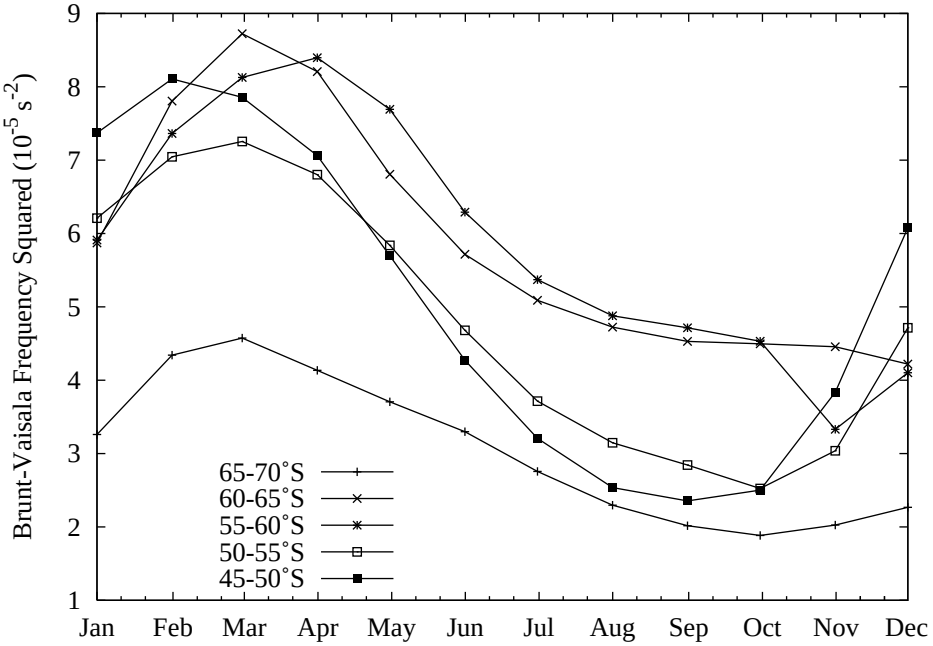

Figure 5.8: Climatology of density stratification (found at the base of the mixed layer) given by the Brunt-Vaissala Frequency squared.

melt and formation. The strongest stratification is found in the 60-65°S zone and the weakest is in the 65-70°S zone. Excluding the latter zone, stratification generally decreases to the north, with the exception being in DJF, where the strongest stratification is found in the 40-45°S zone.

The climatology for the Ekman pumping rate (Equation (3.5)) in Figure 5.9 shows a decrease from positive values (upwelling) of around 2×10^{-6} ms^{-1} in 60-65°S, through zero where curl($\boldsymbol{\tau}$) is equal to 0 (between 53.5°S in summer and 55.3°S in winter) and moves to maximum negative values (downwelling) of around -1×10^{-6} ms^{-1} in 40-45°S. The minimum pumping rate occurs in winter and generally peaks in April and September like the wind stress. However, only the southern-most zone follows the wind stress pattern in Figure 5.6, with a large decrease in summer values.

Peak climatological northward Ekman transport (Equation (3.6)) values for each latitudinal zone, shown in Figure 5.10, occur around March and October, with minimum values in December, similar to the wind stress (Figure 5.6). Values vary from around 1 Sv (10^6 m^3s^{-1}) in 60-65°S to 5 Sv in 45-50°S.

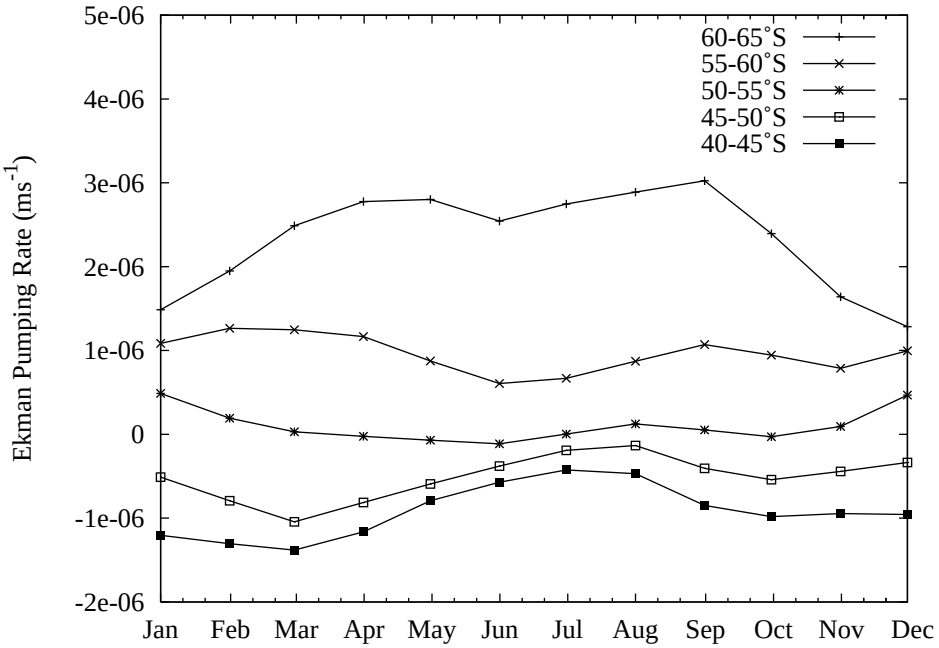

Figure 5.9: Climatology of Ekman pumping by latitudinal zone.

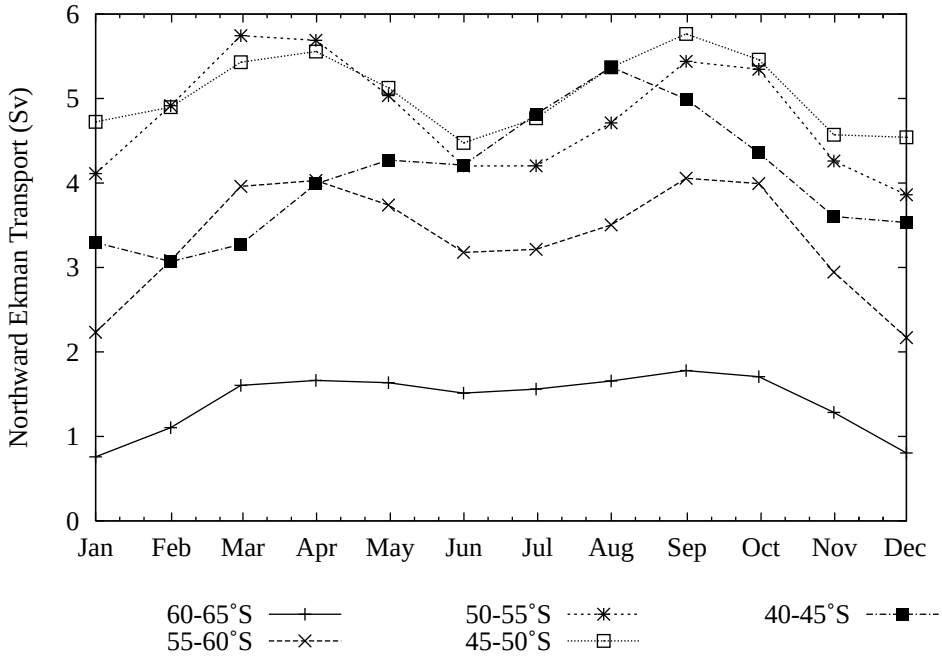

Figure 5.10: Climatology of northward Ekman transport by latitudinal zone.

5.1.4 Climatological mixed layer and sea-surface variables

SODA summer and winter climatological values for ML and sea-surface variables are given in Table 5.3. Examples of MLDs in summer (January) and winter (June) in 2002 are given in Figure 5.11(a) and (b), respectively, while a plot of mean MLD by zone is given in Figure 5.12(a). MLD in the Southern Ocean follows a seasonal cycle (Figure 5.12(a)) with climatological maximum depths averaging around 150 m (with large interannual variations) in the 45-50°S (Subantarctic zone) between August and October, whereas south of this, the winter mixed layer shoals southward. Summer (DJF) MLD is nearly 50 m in the Subantarctic zone, shoaling to less than 30 m in the 60-65°S zone.

An investigation into MLD calculated using the less stringent density criterion, MLD(σ) (Section 2.4), found that MLD $<$ MLD(σ) for climatological values, in almost all zones, as shown in Figure 5.12. For example, in 60-65°S, summer MLD is 29.6 m compared with 48.4 m for MLD(σ). In addition, the seasonal variation in MLD(σ) is very similar to that in MLD, except for the 65-70°S zone, apart from the fact that the MLD(σ) values are larger. The MLDs found here are similar to those found by *Sokolov* (2008) using the ML climatology of *Montegut et al.* (2004). For comparison purposes a table of climatological values, for ML variables based on MLD(σ), is presented in Table 5.4. Although the mixed layer depths are larger in the case of MLD(σ) the values for the other ML variables are almost the same. MLD rather than MLD(σ) will be used in this work, unless otherwise stated.

The climatological ML values given in Table 5.3 indicate that ML density increases to the south, while salinity (both ML salinity and SSS) decreases to the south and then rises again slightly near to the continent. Climatological ML salinity and SSS values are very similar. ML and sea surface temperatures decrease to the south, with SSTs generally higher than ML temperatures (by up to 0.2°C), except in regions of ice formation.

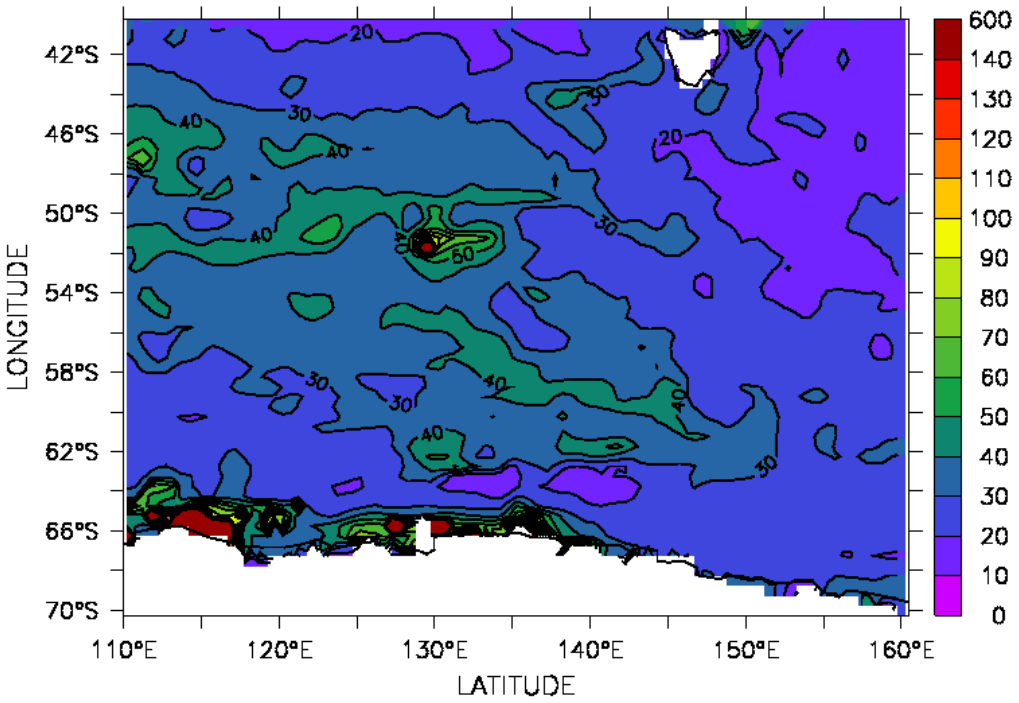

(a)

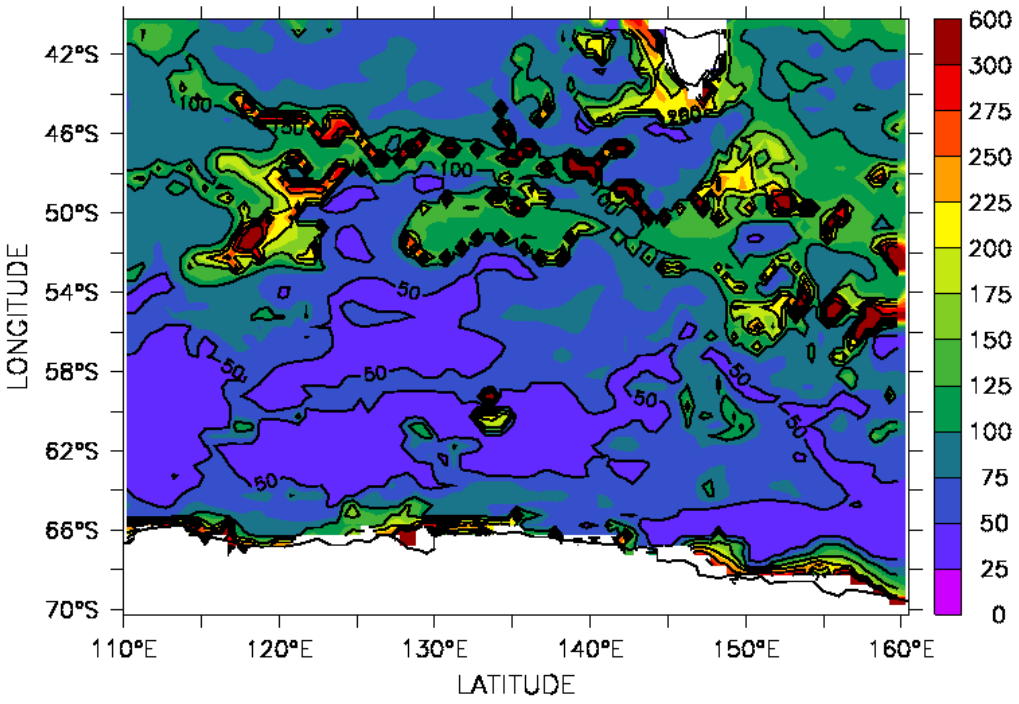

(b)

Figure 5.11: Mixed layer depths from SODA for (a) January and (b) June 2002. Note the different scales.

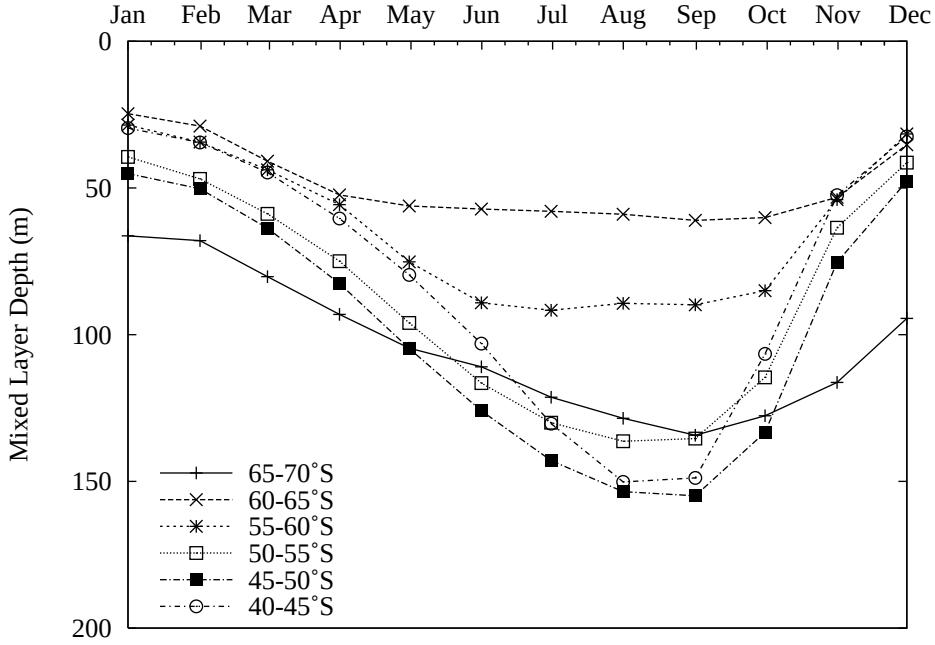

(a)

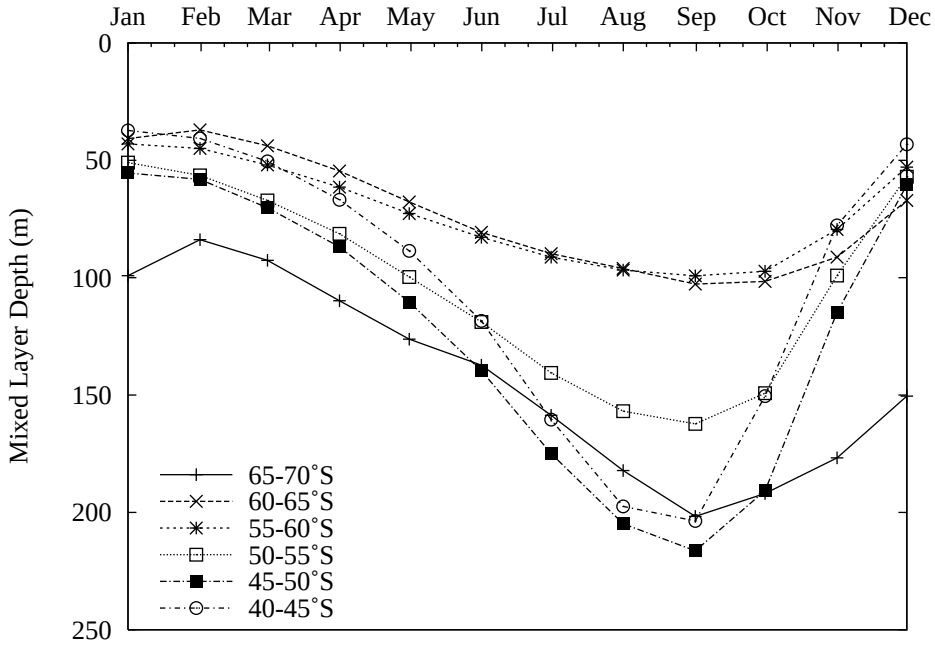

(b)

Figure 5.12: Climatology of mixed layer depth by latitudinal zones, calculated using (a) the temperature criterion and (b) the density criterion.

Table 5.3: Means of climatological values for summer and winter sea-surface variables and mixed layer variables (calculated using the temperature criterion).

Zone 110-160°E by	65-70°S	60-65°S	55-60°S	50-55°S	45-50°S	40-45°S
ML Depth (m)						
Summer	76.5	29.6	31.6	42.9	48.5	32.1
Winter	120.3	58.0	90.0	127.6	140.8	127.9
ML Temperature (°C)						
Summer	-0.9	1.1	3.3	6.1	10.1	13.6
Winter	-1.2	-0.8	1.1	4.3	8.4	11.5
ML Salinity						
Summer	34.1	33.9	33.7	33.8	34.1	34.6
Winter	34.2	34.0	33.8	33.8	34.2	34.7
ML Density (kgm^{-3})						
Summer	27.4	27.2	26.9	26.5	26.2	26.0
Winter	27.5	27.4	27.1	26.8	26.5	26.4
SST (°C)						
Summer	-0.8	1.3	3.4	6.2	10.0	13.8
Winter	-1.3	-0.9	1.0	4.3	8.4	11.5
SSS						
Summer	34.0	33.9	33.7	33.8	34.1	34.6
Winter	34.1	34.0	33.8	33.8	34.1	34.6

Table 5.4: Means of climatological values for mixed layer variables (calculated using the density criterion).

Zone 110-160°E by	65-70°S	60-65°S	55-60°S	50-55°S	45-50°S	40-45°S
ML Depth (m)						
Summer	111.6	48.4	47.4	55.7	59.6	40.5
Winter	159.4	88.8	90.3	138.8	173.1	158.8
ML Temperature (°C)						
Summer	-0.9	1.0	3.1	6.0	10.0	13.5
Winter	-1.2	-0.7	1.1	4.3	8.4	11.4
ML Salinity						
Summer	34.1	34.0	33.8	33.8	34.1	34.6
Winter	34.1	34.1	33.8	33.8	34.2	34.7
ML Density (kgm^{-3})						
Summer	27.4	27.2	26.9	26.6	26.2	26.0
Winter	27.5	27.4	27.1	26.8	26.6	26.4

Table 5.5: Significant correlations between mean wind stress and the SAM, MEI or PDO indices (n/s=no significant correlation found).

	65-70°S	60-65°S	55-60°S	50-55°S	45-50°S	40-45°S
SAM						
DJF	n/s	0.60	0.78	0.49	n/s	n/s
MAM	-0.31	0.44	0.68	0.52	n/s	n/s
JJA	n/s	0.41	0.54	0.54	0.52	n/s
SON	n/s	0.54	0.59	0.41	n/s	-0.40
MEI						
DJF	0.28	n/s	n/s	n/s	0.37	0.42
MAM	n/s	n/s	n/s	n/s	0.37	0.35
JJA	n/s	n/s	n/s	0.43	0.58	0.38
SON	n/s	n/s	n/s	0.35	0.38	n/s
PDO						
DJF	0.34	n/s	n/s	n/s	n/s	0.38
MAM	n/s	n/s	n/s	n/s	0.42	0.39
JJA	n/s	n/s	n/s	n/s	0.36	0.31
SON	0.29	n/s	n/s	n/s	0.30	n/s

5.2 The Connection Between the Southern Hemisphere winds and Changes in UCDW and the Mixed Layer

The time series are not detrended in this work, before the correlations are performed, as the intent is to investigate the effect of the winds on trends in the other variables. A further study (not presented), where the time series are both detrended before correlations are calculated, finds very similar results to the work here.

5.2.1 Correlations between SAM/MEI/PDO and mean wind stress

The aim of this section is to examine the effect of two of the major Southern Hemisphere atmospheric indices, SAM and MEI, on the winds in the region under consideration. In addition, the effect of the PDO will also be investigated. Correlations between the three indices and the mean wind stress are given in Table 5.5, for each latitudinal zone and season. Strong positive correlations between SAM and mean wind stress can be seen in all seasons and zones between 50 and 65°S, with negative correlations in 65-70°S and 40-45°S. Correlations between MEI and mean wind stress are also positive, but generally occur in the more northerly zones, as is also the case for the PDO.

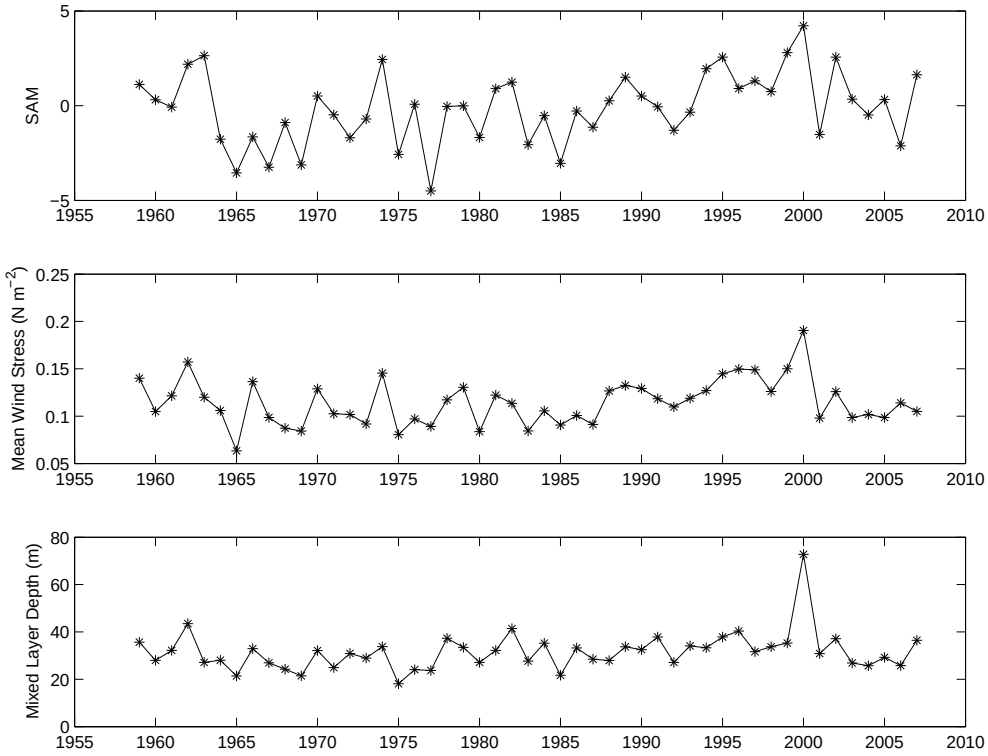

Figure 5.13: Time series for SAM, mean wind stress and mixed layer depth, for the region 110-160°E by 55-60°S during summer (DJF).

5.2.2 Correlations between mean wind stress and other variables

An example of a positive correlation (0.79), between mean wind stress and MLD in the 55-60°S zone in DJF, can be seen in Figure 5.13, where there is also a significant correlation between SAM and mean wind stress (0.78).

The relationship between the wind stress and other variables is summarised in Table 5.6, which presents significant correlations (and when they occur) between mean wind stress and various other variables. Ekman transport is not considered, as it is calculated using $\boldsymbol{\tau}$. There are few significant correlations between mean wind stress and UCDW variables, compared with the number that are associated with the ML and, excluding UCDW temperature in 45-50°S, the correlations are generally only for one season. Correlations between mean wind stress and ML variables are all positive for ML depth, density and salinity, but negative for temperature (with the exception of the 65-70°S zone). Some interesting observations from Table 5.6 include the fact that correlations with ML variables generally occur in more than one season and that the results, for the pairs SST and ML temperature and SSS and ML

Table 5.6: Significant correlations (and when they occur) between the mean wind stress and the variables presented (n/s=no significant correlation found, n/s=not applicable).

Zone 110-160°E by	65-70°S	60-65°S	55-60°S	50-55°S	45-50°S	40-45°S
UCDW Vertical Velocity	n/a	n/s	MAM(0.37) SON(0.29)	n/s	n/s	n/s
UCDW Temperature	n/a	SON(-0.33)	n/s	SON(0.29)	SON(0.32)	n/s
UCDW Density	n/a	n/s	SON(0.31)	SON(-0.40)	SON(-0.31)	MAM(0.29)
UCDW Salinity	n/a	MAM(0.30)	n/s	n/s	n/s	SON(0.28)
UCDW Top Depth	n/a	n/s	DJF(-0.43)	JJA(-0.36)	n/s	n/s
ML Depth	 MAM(0.45) JJA(0.65) SON(0.70)	DJF(0.50) MAM(0.29)	DJF(0.79) MAM(0.41)	DJF(0.62)	DJF(0.43)	DJF(0.81) MAM(0.45) SON(0.28)
ML Temperature	DJF(0.38) SON(0.30)	DJF(-0.38)	DJF(-0.41) SON(-0.44)	 JJA(-0.30) SON(-0.42)	n/s	DJF(-0.31) MAM(-0.32)
ML Density	 MAM(0.37) JJA(0.62) SON(0.54)	DJF(0.58) MAM(0.44) JJA(0.51) SON(0.46)	DJF(0.46) MAM(0.38) JJA(0.41)	n/s	n/s	n/s
ML Salinity	 MAM(0.39) JJA(0.65) SON(0.56)	DJF(0.52) MAM(0.41) JJA(0.51) SON(0.43)	DJF(0.32) JJA(0.31)	 SON(-0.34)	n/s	n/s
SST	DJF(0.29)	DJF(-0.46)	DJF(-0.52) MAM(-0.31) SON(-0.49)	DJF(-0.33) SON(-0.42)	DJF(-0.24)	DJF(-0.42) MAM(-0.36)
SSS	DJF(0.40) MAM(0.33) JJA(0.50) SON(0.56)	DJF(0.56) MAM(0.43) JJA(0.48) SON(0.42)	DJF(0.38)	n/s SON(-0.34)	n/s	n/s
Stratification	JJA(-0.31)	n/s	DJF(-0.39)	DJF(-0.34)	n/s	n/s
Upward Ekman Pumping Rate	n/a	DJF(0.61) MAM(0.81) JJA(0.78) SON(0.74)	MAM(0.29)	n/a	n/a	n/a

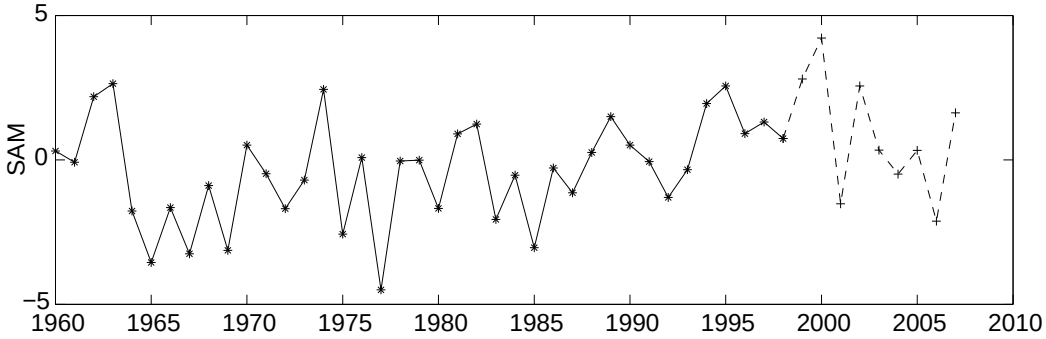

Figure 5.14: Summer time series for SAM (*Marshall*, 2003), showing a positive trend from the 1970s to the mid-1990s and a (non-significant) negative trend for the period 1998-2007.

salinity, are very similar both in magnitude and also in the season when they occur. Few correlations are found between mean wind stress and stratification, while positive correlations are found with Ekman pumping rate in all seasons in 60-65°S.

5.3 Trend Analyses

Before analysing trends for 1958-2007, it is worth noting that even though the SAM index has been moving towards a more positive polarity since the 1970s (*Thompson and Solomon*, 2002; *Marshall*, 2003), this is not true for all seasons (*Marshall*, 2007). Using the data produced by *Marshall* (2003) applied to the study period (1958-2007) it is found that the index shows a positive trend for DJF and MAM only, in agreement with *Marshall* (2007), who analysed the period 1957-2004. The SAM index for summer for 1958-2007 is shown in Figure 5.14 and includes the period 1998-2007, which will be the focus of later work here related to changes in primary production, since widespread satellite remote sensing of chlorophyll-a is available from 1997 onwards. When a similar analysis to the above is conducted for 1958-2007 for the MEI, it is found that the index shows a significant positive trend in MAM and JJA only, meaning that the index is moving to a more "El Niño-like" state. The PDO is also moving to a more positive ("warm") state in all seasons except SON. These results are summarised in Appendix A Table A.1.

Summary tables for the significant linear trends in UCDW variables, stratification, wind stress and Ekman variables, and ML and sea-surface variables, are presented in Tables 5.7-5.9, respectively. Since trends are obtained for a large number of time series (viz., seasonal time series for each variable and latitudinal zone), the data are summarised by presenting the maximum significant trend (over the four seasons), the seasons where there is a significant trend, and marking with an asterisk the time period to which the maximum trend applies. For example, ALL(MAM*) means that there are significant trends in

Table 5.7: Significant maximum trends (per year) for UCDW variables (n/s=no significant trend, * indicates season in which maximum trend occurs). Positive values for UCDW top depth and UCDW southern-most position mean UCDW is found closer to the surface and further south, respectively.

UCDW	Vertical Velocity ($ms^{-1}yr^{-1}$)	Temperature ($°Cyr^{-1}$)	Density ($kgm^{-3}yr^{-1}$)	Salinity (yr^{-1})	Top Depth (myr^{-1})
60-65°S	1.7×10^{-8} DJF,JJA*	3.6×10^{-3} ALL(MAM*)	-4.3×10^{-4} ALL(SON*)	-3.4×10^{-4} SON*	0.68 JJA,SON*
55-60°S	-7.0×10^{-8} SON*	n/s	-2.8×10^{-4} DJF*	n/s	0.7 ALL(DJF*)
50-55°S	9.4×10^{-8} ALL(DJF*)	-2.7×10^{-3} ALL(DJF*)	n/s	n/s	n/s
45-50°S	8.8×10^{-8} ALL(MAM*)	-1.7×10^{-3} ALL(SON*)	n/s	n/s	n/s
40-45°S	3.5×10^{-8} ALL(DJF*)	-8.3×10^{-4} ALL(JJA*)	n/s	n/s	n/s
UCDW Southern-most Position (°S)	1.8×10^{-2} MAM,JJA*				

all four seasons and that the maximum trend presented applies to the MAM time period. Expanded versions of these tables, giving trends for all seasons and zones, as well as 95% confidence intervals for these trends, can be found in Appendix A Tables A.2-A.4.

5.3.1 Linear trends in UCDW variables

The 95% confidence intervals in Table A.2, associated with the trends in UCDW, indicate that trends for UCDW top depth in particular should be viewed with considerable caution. On the other hand, trends for UCDW vertical velocity and UCDW temperature can be used with confidence.

The trends in Table 5.7 show that UCDW vertical velocity is increasing in all seasons in the three most northerly zones (where UCDW is deep) and in DJF and JJA in the most southerly zone (where UCDW upwells). In the two most southerly zones 55-60°S and 60-65°S, UCDW is found to upwell closer to the surface in most seasons, but not in DJF and MAM in 60-65°S. Decreases in UCDW density are found for the 60-65°S zone. In addition, UCDW is found to upwell further to the south over time in MAM and JJA.

UCDW temperature is increasing for all seasons in the 60-65°S zone, but interestingly no significant trends are found in the 55-60°S zone. Another noteworthy result is the decreasing trend in UCDW temperature found in the three northerly zones in all seasons (45-50°S and 50-55°S in Figure 5.5). It might be expected that UCDW would show increasing temperature in accordance with

previous findings of increases in Southern Ocean temperatures (*Aoki et al.*, 2003; *Gille*, 2002) and the trends in 60-65°S agree with this. However, this is not the case for the other zones and, since UCDW, north of 50°S, lies at depths of up to 2400 m (Table 5.1), the cooling trends found in its temperature may well be unrelated to warming in the upper ocean; they may, in fact, be indicative of trends in deep water further in the past, since it is believed that the time taken for NADW to move from the Northern Hemisphere and upwell as UCDW is of the order of centuries (*Santoso et al.*, 2006). This hypothesis is consistent with the lack of significant trends in 55-60°S, where the cooling trend in the deeper water is counteracted by mixing with warming upper ocean water, during upwelling.

The hypothesis that trends in UCDW are not related to surface trends is also supported by the lack of correlations between the mean wind stress and UCDW variables in Table 5.6 (with the exception of correlations with UCDW temperature in 45-50°S), in addition to the relatively low values of the correlation coefficients. For example, there are only two single season correlations between UCDW top depth and mean wind stress (and there are no lagged ones up to a 10 year lag - not presented).

5.3.2 Linear trends in wind stress, stratification and Ekman variables

A full set of trends and confidence intervals for wind stress, stratification and Ekman variables is given in Table A.3. The results indicate that, apart from northward Ekman transport in the two most northerly zones and mean wind stress in 40-45°S, the trends can be used with good confidence. Positive trends for maximum wind stress are found for DJF, consistent with increasing trends in SAM in that season (bottom of Table 5.8), as well as decreasing trends in SON. No significant trends are found for the location of maximum wind stress. Trends in mean wind stress by latitudinal zone (presented in Table 5.8) are positive in DJF and negative in SON. Finally, no trends are found in the location where curl($\boldsymbol{\tau}$) is equal to zero.

Given that there are strong positive correlations between SAM and mean wind stress in all seasons in 50-65°S (Table 5.5) and that SAM shows an increasing trend in DJF and MAM (Section 3.2), it is somewhat surprising that the mean wind stress, unlike the maximum wind stress, shows a significant increasing trend in DJF only in 60-70°S and not in 50-60°S. This is possibly due to a confounding effect from ENSO, since the MEI exhibits a positive trend in MAM (Table A.1).

Increasing SAM may also mean winds moving south (*Thompson and Solomon*, 2002), but recent work has found that the effect of SAM depends on the re-

Table 5.8: Significant maximum trends (per year) for stratification, wind stress and Ekman variables (n/s=no significant trend, n/a=not applicable, * indicates season in which maximum trend occurs).

	Stratification ($s^{-2}yr^{-1}$)	Wind Stress ($Nm^{-2}yr^{-1}$)	Upward Ekman Pumping Rate ($ms^{-1}yr^{-1}$)	Northward Ekman Transport ($Svyr^{-1}$)
65-70°S	-1.0×10^{-7} DJF*,SON	8.9×10^{-4} DJF*	n/a	n/a
60-65°S	n/s	$3.2/-4.2\times10^{-4}$ DJF*/JJA,SON*	$1.2/-1.3\times10^{-8}$ DJF*/SON*	-1.0×10^{-2} SON*
55-60°S	-2.2×10^{-7} DJF,MAM*	-1.1×10^{-3} SON*	8.5×10^{-9} DJF*	-2.4×10^{-2} SON*
50-55°S	-4.6×10^{-7} DJF,MAM* JJA	-7.8×10^{-4} SON*	n/a	-2.2×10^{-2} SON*
45-50°S	-5.8×10^{-7} DJF,MAM* JJA	n/s	n/a	1.7×10^{-2} JJA*
40-45°S	$1.7/-2.0\times10^{-7}$ MAM*/SON*	4.0×10^{-4} MAM*,JJA	n/a	1.6×10^{-2} JJA*
Maximum Wind Stress	7.6×10^{-4} DJF,MAM*	-5.9×10^{-4} SON*	Location of Maximum Wind Stress	n/s

gion (*Sallee et al.*, 2008; *Drost and England*, 2009) and that, in 110-150°E (contained within the study region) the winds will move north (*Drost and England*, 2009). This study does not find a northerly trend, but does find that there is no significant trend in the position of the maximum wind stress.

Data showing significant trends in stratification, upward Ekman pumping rate and northwards Ekman transport are also given in Table 5.8. No trends are given for upward Ekman pumping rate in 50-55°S since in that region pumping varies interannually from upwelling to downwelling, nor north of 50°S, since it is not is applicable there. Trends in Table 5.8 show that the mean upward Ekman pumping rate is increasing in DJF in 55-65°S, but is decreasing in 60-65°S in SON. The other Ekman variable considered in Table 5.8 is the mean northward Ekman transport, which is decreasing in 50-65°S in SON and increasing in JJA in the more northerly zones.

Stratification is decreasing over time, particularly in DJF, except in 60-65°S. An alternative measure for stratification (not presented here, but which is simply the density difference at 200 m and 5 m depth), shows a greater number of seasons where stratification is decreasing. The fact that there are so few correlations between stratification and mean wind stress in Table 5.6 seems to indicate that stratification is affected by factors other than wind stress, such as ML temperature and timing and extent of sea-ice melt (in the

southern-most latitudes only).

5.3.3 Linear trends in mixed layer and sea-surface variables

A summary of trends in ML and sea-surface variables is given in Table 5.9 and the full set of trends can be found in Table A.4, including the 95% confidence interval for the trends. Study of these confidence intervals shows that, excluding some density and salinity trends in the 60-70°S zones, the ML and sea-surface results can be used with a good degree of confidence. Trends for SST and ML temperature, and SSS and ML salinity, in Table 5.9, are very similar in magnitude between the ML and sea-surface variables, with the sea-surface trends often a little larger than the ML trends. With only two exceptions, they also occur in exactly the same seasons. Trends in ML depth found using the two criteria, MLD and MLD(σ) (not presented), are similar in the sense that they are in the same direction and occur in virtually all the same seasons. However, the magnitude of the trends is larger in the case of MLD(σ).

With a few exceptions, all significant trends for ML and sea-surface variables presented in Table 5.9 are positive, indicating increasing SST and SSS and ML depth, temperature, density and salinity in all seasons, except in the most northerly and most southerly zones. In 65-70°S, ML salinity is decreasing in JJA and ML density is decreasing in all seasons but DJF. In addition, in the 60-65°S zone, SST and ML temperature are increasing, but only in JJA and SON, SSS and ML salinity are increasing, but only in DJF, and there are no significant trends in ML density. The final exceptions are the decreasing trends in ML density in 40-45°S in MAM and JJA.

These results appear partly to be related to trends in wind stress, particularly in the more southerly zones, based on the strong correlations in Table 5.6 between mean wind stress and ML variables. In DJF, increasing wind stress contributes to a deepening in the ML, an increase in evaporation and a subsequent increase in salinity and density, as well as mixing of water of greater density into the ML. The negative correlation between ML temperature and mean wind stress in DJF and MAM is explained, in all but 55-60°S and 60-65°S, by the mixing of colder, deeper water into the ML (Tables 5.1 and 5.3 for UCDW and ML temperatures). However, this effect is outweighed by surface heating, leading to positive trends in ML temperatures.

In 60-65°S a different situation arises in DJF and MAM, and in 55-60°S in DJF, where there are no significant positive trends in SST and ML temperature, unlike all other zones and seasons. An explanation for this in DJF in 55-60°S and 60-65°S could be related to the presence in January-March of colder remnant water between the ML and UCDW (Figure 3.3). Increasing

Table 5.9: Significant maximum trends (per year) for mixed layer and sea-surface variables (n/s=no significant trend, * indicates season in which maximum trend occurs).

	ML Depth (myr^{-1})	ML Density ($kgm^{-3}yr^{-1}$)	ML Salinity (yr^{-1})	ML Temperature ($^{\circ}Cyr^{-1}$)	SST ($^{\circ}Cyr^{-1}$)	SSS
65-70°S	n/s	$4.3/-7.7\times10^{-4}$ DJF*/MAM, JJA*,SON	$7.5/-5.7\times10^{-4}$ DJF*/JJA*	6.2×10^{-3} ALL(JJA*)	8.0×10^{-3} ALL(JJA*)	1.3×10^{-3} DJF*
60-65°S	1.7×10^{-1} ALL(JJA*)	n/s	1.0×10^{-3} DJF*	1.2×10^{-2} JJA*,SON	1.4×10^{-2} JJA*,SON	1.1×10^{-3} DJF*
55-60°S	6.3×10^{-1} ALL(JJA*)	2.4×10^{-3} ALL(DJF*)	3.3×10^{-3} ALL(DJF*)	1.7×10^{-2} MAM,JJA, SON*	1.9×10^{-2} MAM,JJA*, SON	3.3×10^{-3} ALL(DJF*)
50-55°S	7.9×10^{-1} ALL(JJA*)	2.9×10^{-3} ALL(DJF*)	5.6×10^{-3} ALL(DJF*)	2.6×10^{-2} ALL(SON*)	2.7×10^{-2} ALL(SON*)	5.7×10^{-3} ALL(DJF*)
45-50°S	1.0 ALL(SON*)	4.6×10^{-3} DJF*,MAM, SON	7.6×10^{-3} ALL(DJF*)	2.6×10^{-2} ALL(SON*)	2.5×10^{-2} ALL(SON*)	7.6×10^{-3} ALL(DJF*)
40-45°S	4.8×10^{-1} SON*	-2.2×10^{-3} MAM*,JJA	2.9×10^{-3} DJF*,SON	1.6×10^{-2} ALL(MAM*)	1.5×10^{-2} ALL(MAM*)	3.0×10^{-3} DJF,JJA, SON*

Table 5.10: Significant maximum trends per year, calculated as a percentage of the median value (n/s=no significant trend, n/a=not applicable, * indicates season in which maximum trend occurs.)

Zone 110-160°E by	65-70°S	60-65°S	55-60°S	50-55°S	45-50°S	40-45°S
UCDW Vertical Velocity	n/a	0.58 DJF,JJA*	-0.38 SON*	0.42 ALL(DJF*)	0.95 ALL(MAM*)	1.13 ALL(DJF*)
UCDW Top Depth	n/a	0.87 JJA*,SON	1.2 ALL(DJF*),	n/s	n/s	n/s
Mixed Layer Depth	n/s	0.48 ALL(DJF*)	0.72 ALL(JJA*)	0.74 ALL(DJF*)	0.94 ALL(SON*)	0.46 SON*
Stratification	-0.52 DJF,SON*	n/s	-0.33 DJF*,MAM	-0.72 DJF,MAM* JJA	-0.86 DJF,MAM*, JJA	0.22/-0.59 MAM*/SON*
Mean Wind Stress	1.34 DJF*	0.60/-0.48 DJF*/ JJA,SON*	-0.63 SON*	-0.42 SON*	n/s	0.41 MAM*,JJA
Upward Ekman Pumping Rate	n/a	0.77/-0.59 DJF*/SON*	0.78 DJF*	n/a	n/a	n/a
Northward Ekman Transport	n/a	-0.65 SON*	-0.65 SON*	-0.45 SON*	0.37 JJA*	0.35 JJA*
Maximum Wind Stress	0.21/-0.29 DJF*/SON*					

winds (Table 5.8) mix this colder water into the ML, where it counteracts the surface warming. The situation in MAM in 60-65°S is different from DJF in that there is no negative correlation between mean wind stress and temperature there (Table 5.6) and there is still a weakly significant (90% confidence level) positive trend in ML temperature.

Maximum significant trends are also presented, as a percentage of (the absolute value of) the median value, in Table 5.10, for those variables where it is meaningful to do so. The values for percentage trend, given in Table 5.10, are greatest for UCDW top depth and some vertical velocity, mean wind stress and ML depth values.

5.3.4 Intrusion of UCDW into the mixed layer

The frequency with which UCDW upwells into the mixed layer is important for the entrainment of nutrients (in particular, iron), which is thought to be critical for primary production (*Martin et al.*, 1990b; *Hoppema et al.*, 2003). The intrusion of UCDW into the ML is studied in SODA by comparing the MLD and the top position of UCDW at each grid-point in a particular zone. If UCDW is detected closer to the surface than the MLD, this is recorded as UCDW having been detected in the ML. Data are presented in Figure 5.15 for the 65-70°S, 60-65°S, 55-60°S and 50-55°S zones and these are broken down by decade and season, where the 2000-2007 data are scaled to 10 years. It is important to note that, although Figure 5.3 presents the seasonal cycles in both MLD and top UCDW, these data are climatological mean depths for the zone only and are misleading in the sense that they imply that UCDW is at a lower depth than the MLD over the whole latitudinal zone, which may not in fact be the case.

Data are presented for the 65-70°S zone for completeness, although UCDW is detected very infrequently in that zone. Figure 5.15 shows noticeable differences between the four zones in the seasons where the majority of detections of UCDW in the ML occur. In 65-70°S and 60-65°S this happens in DJF and MAM, in 55-60°S in MAM, JJA and SON and in 50-55°S in JJA and SON. These results do not appear to be related to the seasonal southward movement in the position of UCDW upwelling, since Figure 5.2 shows that the climatological values of the southern-most position of UCDW vary only between about 64.5°S and 65.7°S and not into the 55-60°S zone. The data in Figure 5.15 suggest that UCDW upwells south of the PF (around 55°S, Figure 3.1), as well as entering the 55-60°S and 50-55°S zones from the south by Ekman transport. The seasonal difference may then be attributed to the time taken for UCDW to move northwards from the 60-65°S into the other two zones. For example, the time to move from 60-65°S to the 55-60°S zone is of the order of several

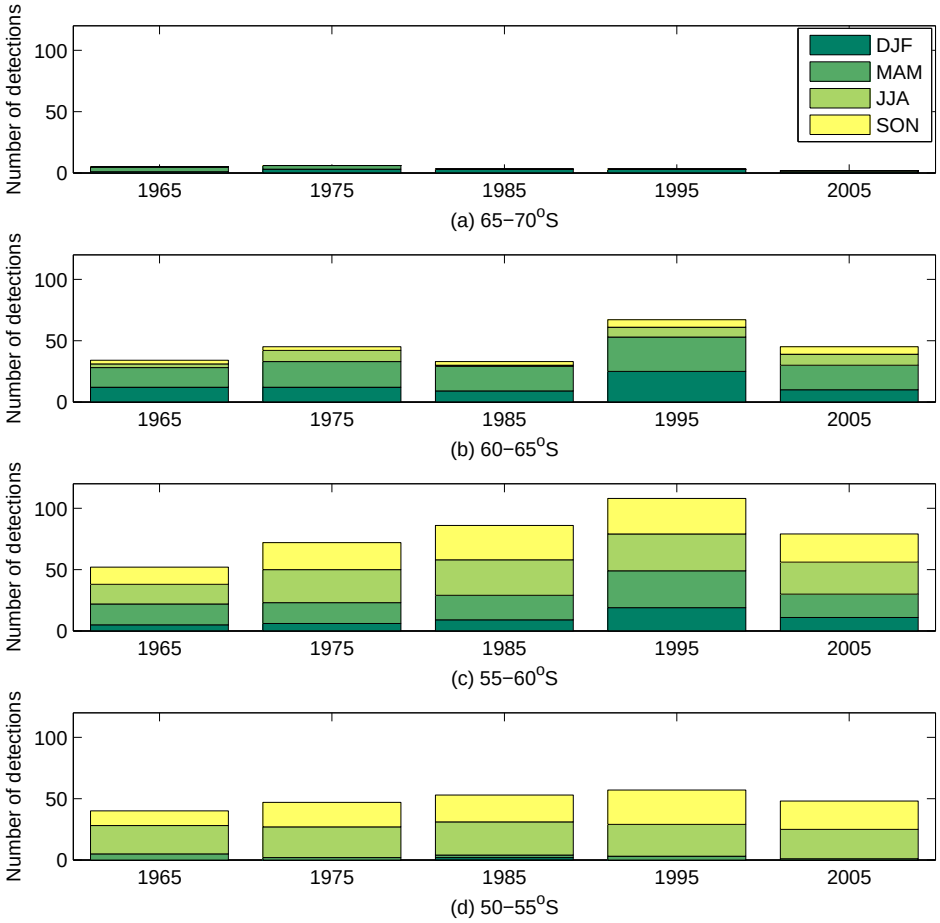

Figure 5.15: Number of times UCDW is detected in the mixed layer by decade and season in (a) 65-70°S, (b) 60-65°S, (c) 55-60°S and (d) 50-55°S. Data from 2000-2007 are scaled to 10 years.

months, based on moving 10° north at the northward Ekman velocity of 0.015 ms^{-1} (*Yang et al.*, 2007a) for the 60-65°S zone and this is consistent with the changes from Figure 5.15(b) to (c).

Even though the overall number of times UCDW is detected in the ML is greater in JJA than in any other season (overall totals for 50-65°S are: DJF (120), MAM (221), JJA (283) and SON (242)), it would seem that UCDW is primarily entrained in the ML in summer/autumn (in 55-65°S), rather than in autumn/winter, as has previously been reported in the Atlantic (*Hoppema et al.*, 2003; *Gordon and Huber*, 1990) and in the Pacific (*Hiscock et al.*, 2003). The usual explanation involves the seasonal deepening of the ML in autumn/winter, but this does not seem to be the case, as both the MLD and the UCDW upwelling depth follow a similar seasonal cycle (Figure 5.3), which means that the deepening of the ML in winter is accompanied by a concomitant deepening of the UCDW upwelling depth.

Figure 5.15 also shows that the total number of times UCDW is detected

Table 5.11: Trends (per year) in top UCDW and ML depth, with 95% confidence interval limits, for the shorter period 1958-2000 in the Australian sector (n/s=no significant trend found. A positive trend in UCDW top depth means that UCDW is found closer to the surface.

	60-65°S	55-60°S	50-55°S
MLD (myr^{-1})			
DJF	0.16±0.11	0.18±0.10	0.39±0.16
MAM	0.21±0.11	0.21±0.10	0.34±0.18
JJA	0.22±0.14	0.58±0.18	0.48±0.26
SON	0.18±0.12	0.51±0.18	0.61±0.26
UCDW Top Depth (myr^{-1})			
DJF	0.52±0.52	1.26±0.51	0.42±0.42
MAM	0.38±0.38	0.70±0.70	n/s
JJA	0.93±0.46	0.75±0.75	n/s
SON	1.02±0.52	0.93±0.49	n/s

in the ML has increased from the 1960s to the 1990s, but not into the 2000s. Trends for 1958-2000, from Table 5.9, show increasing MLD, but it is not entirely clear whether trends for UCDW top depth in Table 5.7 indicate that UCDW is found increasingly near to the surface, given the large range of the 95% confidence intervals in Table A.2. In order to reconcile this with trends in Figure 5.15, trends are re-calculated for these two variables for the shorter time period 1958-2000. These results, given in Table 5.11, show that for 1958-2000, the ML is deepening and UCDW top depth is also increasing (that is, moving closer to the surface), both in the 60-65°S and 55-60°S zones. These trends are consistent with the increase found in the number of times that UCDW is detected in the ML over the period from 1958 to 2000. Of note also in Figure 5.15 is the large number of detections in the 55-60°S zone (particularly in the 1990s, where UCDW is detected in the ML in 108 out of 120 possible months), the result of UCDW entering the ML from below as well as its movement northwards from the 60-65°S zone.

5.4 The Connection with Primary Production in the Southern-most Zones

UCDW upwells in the latitudinal zones 55-65°S and entrains nutrients that are essential for phytoplankton growth into the ML. This work has found that in autumn and winter there is a weak trend southwards in the southern-most latitude where UCDW can be detected. This may be important for regional phytoplankton growth and biomass, due to the fact that, during the BROKE (Baseline Research on Oceanography Krill and the Environment) survey, a

connection was found between circulation patterns (and surface water temperatures) and the structure of the food web, namely the abundance of krill compared with salps (*Nicol et al.*, 2000).

The strongest trend associated with UCDW is in UCDW top depth, which is moving closer to the surface, and, combined with the deepening trend in the MLD, leads to an increase in the number of times UCDW is detected in the ML, again with implications for primary production. In addition, although an increasing trend in the upward Ekman pumping rate is found in summer, this is not accompanied by an increase in the northward Ekman transport. This has the effect of increasing the residence time of the nutrients available for primary production. On the other hand, decreasing transport is found in spring in 50-65°S, as well as decreasing pumping in 60-65°S, resulting in a decreased supply of nutrients. Other significant summer trends in the 55-65°S zone are increasing wind stress (in 60-70°S), increasing ML salinity and density (in 55-60°S). However, the overall impact of the various trends on primary production is difficult to quantify and other factors, such as changes in irradiance levels, also need to be taken into account.

5.5 Comparison with Previous Studies

Significant surface and subsurface warming in some sectors of the Southern Ocean has been found both in a small number of regional observational studies (see below), as well as in the ensemble of coupled climate simulations, which were run as part of the IPCC Fourth Assessment Report (*Trenberth et al.*, 2007). For example, *Levitus et al.* (2005) plotted vertical sections of the upper 1500 m in each of the Pacific, Indian and Atlantic oceans, showing trends in temperature from 1955-2003. These indicated increasing ML temperatures for most of the southern Pacific Ocean, excluding south of 70°S. Global maps of SST trends from 1979-2005 (*Trenberth et al.*, 2007) and some modelling studies (*Zhang*, 2007), indicate warming in the northern parts of the study region and possible cooling near the Antarctic continent, particularly in DJF, although sparse data coverage makes calculation of trends, in some southern parts of the region, problematic. Results from the present study show an increase in ML temperature in the range 1-2$\times 10^{-2}$ °C/yr (Tables 5.9 and A.4), except in DJF and MAM in 60-65°S and DJF in 55-60°S, consistent with the above.

Data in the study region has been collected at Maria Island (42.6°S, 148.23°E) from 1944-2005, and recent work (*Hill et al.*, 2008) has found a strong positive trend and quasi-decadal variability in both temperature and salinity (2.2$\times 10^{-2}$ °C/yr and 3$\times 10^{-3}$/year, respectively). These are consistent in sign and order of magnitude with the ML results found here in that latitudinal region.

Similar vertical sections to those mentioned above for temperature have also been constructed for salinity (*Boyer et al.*, 2005) and these show very different trends for salinity, depending on which ocean is being studied. For example, near-surface salinity increases are found over almost all of the Indian Ocean, whereas in the Pacific Ocean patches of decreasing trends are found, with the largest decreases south of 70°S. This led to the IPCC conclusion (*Trenberth et al.*, 2007) that in the polar region of the Pacific Ocean south of 50°S there is a relatively weak freshening signal. Decreasing salinity has been found at a few Southern Ocean sites near to Antarctica, possibly associated with increased precipitation, sea-ice extent, sea-ice melt or changes in CDW upwelling (*Jacobs*, 2006). This study finds increased ML salinity in most zones in the study region, including the zones near the Antarctic continent in summer but not in the other seasons, and this is consistent with trends of decreased precipitation north of 50°S and the Maria Island results, mentioned above. It is unclear whether the ML trends found here for salinity south of 50°S in summer are inconsistent with previous work, due to uncertainties introduced by the uneven spatial and temporal distribution of observations in this region (*Jacobs*, 2006; *Boyer et al.*, 2005).

The few observational studies available in the SO have reported both surface and sub-surface warming. For example, temperature data (*Gille*, 2002) from the 1950s and 1990s over the SO between 35 and 65°S, in the 700-1100 m depth range, shows an increase of around 4×10^{-3} °C/yr, with warming concentrated within the ACC (*Gille*, 2008). This trend is similar to one found in the Indian sector of the SO (*Aoki et al.*, 2003), close to the sACCf, taken as an average over 200-900 m for 1966-1998. Such results are similar to those found here for UCDW in the 60-65°S zone (3.6×10^{-3} °C/yr), although there are no significant trends in the 55-60°S zone.

A recent study by *Böning et al.* (2008) has used both Argo float and historical data combined into a high resolution (0.5°) gridded climatology to examine temperature and salinity trends over the hemispheric SO. This data set does not resolve the seasonal cycle well and so no inferences are possible for the upper 200 m. The study found temporal changes (1960-2006) across the ACC (SAF and PF), averaged over 300-1000 m, which showed temperature increases of 6×10^{-3} °C/yr and salinity decreases of -4×10^{-4}/year. The UCDW results of this study in 60-65°S for temperature are in agreement with the other studies cited above (*Aoki et al.*, 2003; *Gille*, 2002) and the above results in 60-65°S, where UCDW lies in the depth range of the above results. The present study also finds an increasing trend in UCDW temperature only in 60-65°S and no significant trend in 50-55°S, with decreasing UCDW temperature north of 55°S. The temperature results are, however, consistent with trends found

from measurements taken in the Pacific along 170°W between 40 and 20°S from 1968/69 to 1990 (*Santoso et al.*, 2006; *Johnson and Orsi*, 1997), which show temperature trends of -3×10^{-3} °C/yr (and decreases in salinity) along deep density surfaces corresponding to UCDW. *Böning et al.* (2008) and *Aoki et al.* (2005) also studied UCDW on isopycnal surfaces, which are not directly comparable with this work, as the present results are obtained by averaging over the full UCDW density range (27.35 kg m^{-3} < σ_θ < 27.75 kg m^{-3}) for $\theta > 1.5$°C.

A recent study by *Yang et al.* (2007a) used an earlier reanalysis (1.4.2) of the SODA data to calculate trends associated with the meridional circulation, but in their case the trends are found for the whole SO. The authors found a strengthening of the Deacon cell, from 1980-2000, including an increase in the Ekman pumping rate and the northward Ekman velocity (which also showed a poleward shift), induced by changes in the SAM. However, recently (*Böning et al.*, 2008) have concluded that the SO overturning circulation is insensitive to decadal changes in wind stress, due to stronger westerly winds inducing an increase in eddy activity, which counteracts increases in northward Ekman transport. The present study, which focuses on the region south of Australia and considers a longer time period (1958-2007) than the previous SODA study, finds a complex response to wind forcing, which involves both SAM and ENSO, and, while it does find an increase in Ekman pumping in summer, south of 55°S, does not find that this translates into an increase in northward Ekman transport in the Australian region.

This work is based on the SODA 2.0.2/2.0.4 reanalysis, which constrains POP model output using a wide selection of SO observational data. There are, however, limitations associated with this approach in the data-sparse SO, particularly in earlier time periods and in the deep ocean. This means that trends calculated for hydrographic variables in the deep ocean (for example, UCDW in low latitudes, but not UCDW where it is shoaling) need to be viewed with some caution. Hence, discrepancies between trends found here and those of other studies may possibly be related to the SODA data or they may be due to the fact that the Australian region has its own idiosyncrasies associated with the effect of the SAM there. For example, the response of the oceanic fronts to the SAM varies in different regions of the SO, which the authors (*Sallee et al.*, 2008) identify as the Indian, Central Pacific and Indo-Pacific basins. Thus comparison of trends, found using data from different regions, may not be valid. In addition, in the Australian region, the positive trend in the SAM is not accompanied by a southward shifting of the winds (consistent with no significant trend in the position of the maximum wind stress), unlike some other regions, such as the Indian basin (*Drost and England*, 2009).

It is worth noting here that recent work by *Hosoda et al.* (2009) and *Roemmich and Gilson* (2009), based on Argo float data, which shows decreasing surface layer salinity and temperature in some parts of the Australian sector, cannot be meaningfully compared with the present work, due to the time periods being considered. The trends presented here are over the time period 1958-2007, whereas the other studies compare mean values for 2003-2007 or 2004-2008, respectively, with climatological values from the World Ocean Database (1960-1989) or the World Ocean Atlas, respectively.

5.6 Conclusions

This chapter focuses on the Australian region of the Southern Ocean (110-160°E, 40-70°S) and uses data from the SODA 2.0.2/2.0.4 reanalysis to investigate the climatological physical environment, as well as trends in the time series (1958-2007) of various physical parameters. Results are analysed by season and by five-degree latitudinal zone. Trends, quoted below, represent the range in seasonal values for the southern-most zones 55-70°S.

Significant strong increases are found in ML depth (0.11-0.63 m/year) and ML temperature (0.5-1.7$\times10^{-2}$°C/yr), with the notable exception of ML temperature in DJF and MAM in 60-65°S and DJF in 55-60°S, where no significant trends are found. Density stratification, found at the base of the ML, shows a decreasing trend over time, in some seasons, but not in 60-65°S. Smaller increases are found in ML density in 55-60°S (0.8-2.4$\times10^{-3}$ kg m^{-3}/year) and in salinity (2.2-3.3$\times10^{-3}$/year). It should be noted that these trends are for the period 1958-2007 and cannot be compared with recent results, which show decreases in sea-surface temperature (*Roemmich and Gilson*, 2009) and salinity (*Roemmich and Gilson*, 2009; *Hosoda et al.*, 2009), in some parts of the study region. This is due to the fact that these studies compare more recent Argo data with World Ocean Atlas climatological means, which results in a later and shorter time period being compared.

The above trends can be attributed, at least in part, to changes in the winds in the region, which show increasing strength in DJF, in line with positive trends in the SAM, with the strongest percentage increases in mean wind stress occurring in DJF in 60-70°S. Strong positive correlations, found between mean wind stress and ML depth (in all zones) and with ML density and salinity (south of 55°S), particularly in DJF/MAM, are consistent with increasing ML depth, as well as increasing ML density and salinity, due to increased wind mixing and evaporation. The seemingly anomalous result of no significant temperature trend in 60-65°S in DJF, as opposed to increasing ML temperature in all other zones and seasons, could also be related to wind mixing, where the

increasing wind mixes cooler remnant winter water into the ML, counteracting the effect of surface warming.

Ekman pumping is found to increase in DJF in the southerly zones, but this does not lead to an increase in northward Ekman transport, nor does it seem to be connected to the depth to which UCDW upwells (at least on a decadal time-scale). The upwelling of UCDW to the ML is studied, as it is thought to be crucial in the supply of nutrients in the zones where it upwells (approximately 55-65°S). An increasing trend is found in the number of occasions where UCDW is found in the ML, over the period from the 1960s to 2000; contrary to previous studies in other SO regions (*Hiscock et al.*, 2003; *Hoppema et al.*, 2003; *Gordon and Huber*, 1990), it appears that the main entrainment of UCDW into the ML in the Australian region occurs in summer/autumn, rather than autumn/winter. This is due to UCDW upwelling into the ML in 60-65°S, predominantly in summer and autumn, and then moving northward over a period of months, where it can be detected in the ML more often in winter and spring.

Other significant UCDW trends include an increase in upwelling velocity (but predominantly in the more northerly zones, where UCDW is found at depths up to 2400 m) and a decrease in UCDW temperature there, contrary to general upper ocean warming. An increase in UCDW temperature and a decrease in UCDW density are also found in the most southerly 60-65°S zone where UCDW is found. In addition, a small but significant increase (southerly movement) in the latitude of the southernmost location of UCDW is also found, but only in autumn and winter. It would seem that trends in UCDW, except perhaps in the zones where it upwells and mixes with other water masses, occur on a different, and presumably much longer, timescale than changes in the ML.

In terms of the way the various physical features and trends are related to primary production in the 55-65°S zones in the Australian region studied, it is noted that, summer brings very shallow mixed layers and higher temperatures, very low wind stress, quite high stratification and very low northward Ekman transport, which means that nutrients, injected into the ML by UCDW upwelling, will be advected northwards only slowly. The combination of these factors leads to favourable conditions for primary production, as does the increasing trend in the number of times UCDW can be detected in the ML. However, other trends documented here, such as increased ML depth with no increase in ML temperature or stratification in DJF, in addition to the southward trend in the position of UCDW upwelling, may counteract these effects.

Chapter 6

A comparison of upper ocean structure and the circulation of Upper Circumpolar Deep Water in three Southern Ocean sectors in 1958-2007

In this chapter the robustness of the Australian sector results in Chapter 5 is examined by comparison with SODA data for the Indian and Pacific sectors. Since UCDW consists mainly of water that has recirculated from the Pacific and Indian Oceans (*Callahan*, 1972; *Reid*, 1981) and the time taken for NADW to move from the Northern to the Southern Hemisphere and upwell as UCDW is of the order of centuries (*Santoso et al.*, 2006), it is of interest to see if any decadal-scale trends can be detected in UCDW. The purpose of this chapter is to document UCDW upwelling in each of the sectors, that is, its characteristics, how far south it is found and the top depth to which it upwells, as well as trends in UCDW and ML hydrographic variables. In addition, any possible connections with changes in the westerly winds are also investigated. In order to simplify comparisons between the three ocean sectors, full 600 point (50 years times 12 months) time series are used, rather than seasonal ones.

6.1 Climatological UCDW, ML and Wind Data

6.1.1 Climatological UCDW

UCDW is entrained in the ACC as it shoals meridionally upwards towards the Antarctic continent along steeply tilted isopycnals. This upwelling occurs south of the PF and north of the sBdy of the ACC (*Orsi et al.*, 1995; *Sokolov*

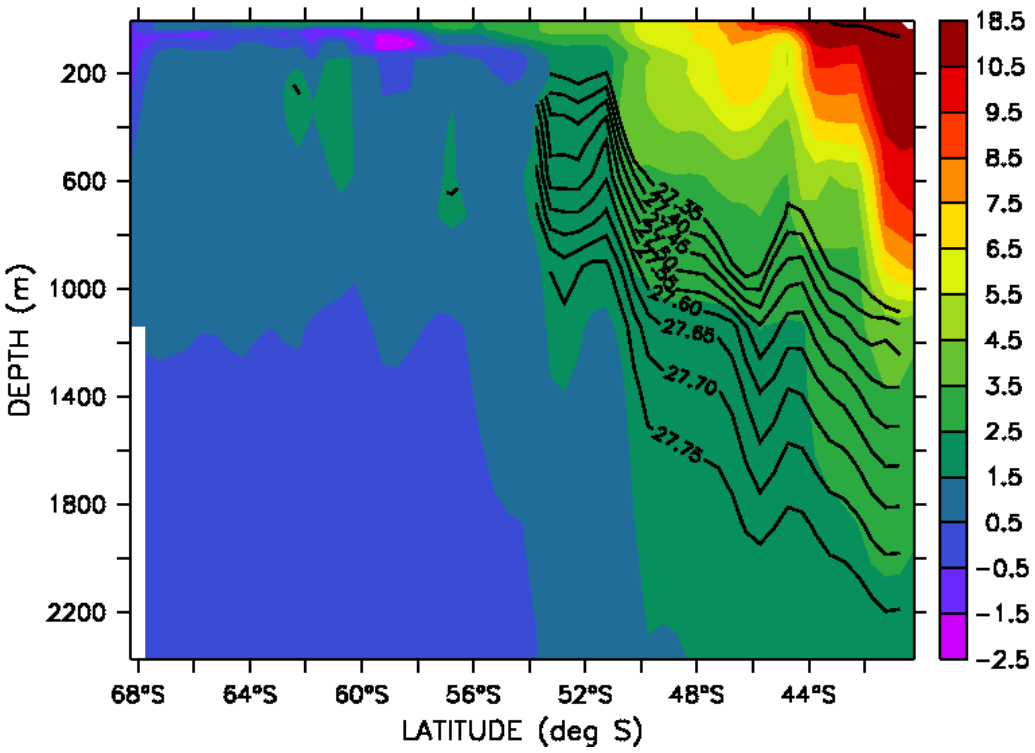

(a)

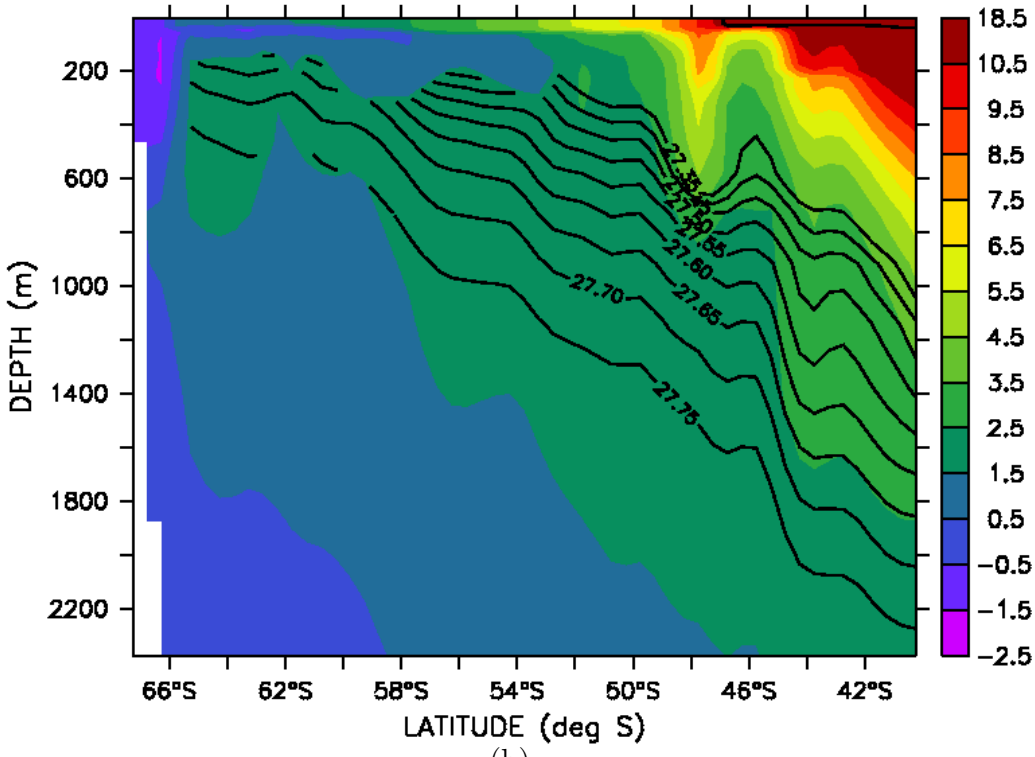

(b)

Figure 6.1: Isopycnals in SODA identifying UCDW are overlaid on a temperature plot along (a) 34°E and (b) 60°E in the Indian sector, in February 1997.

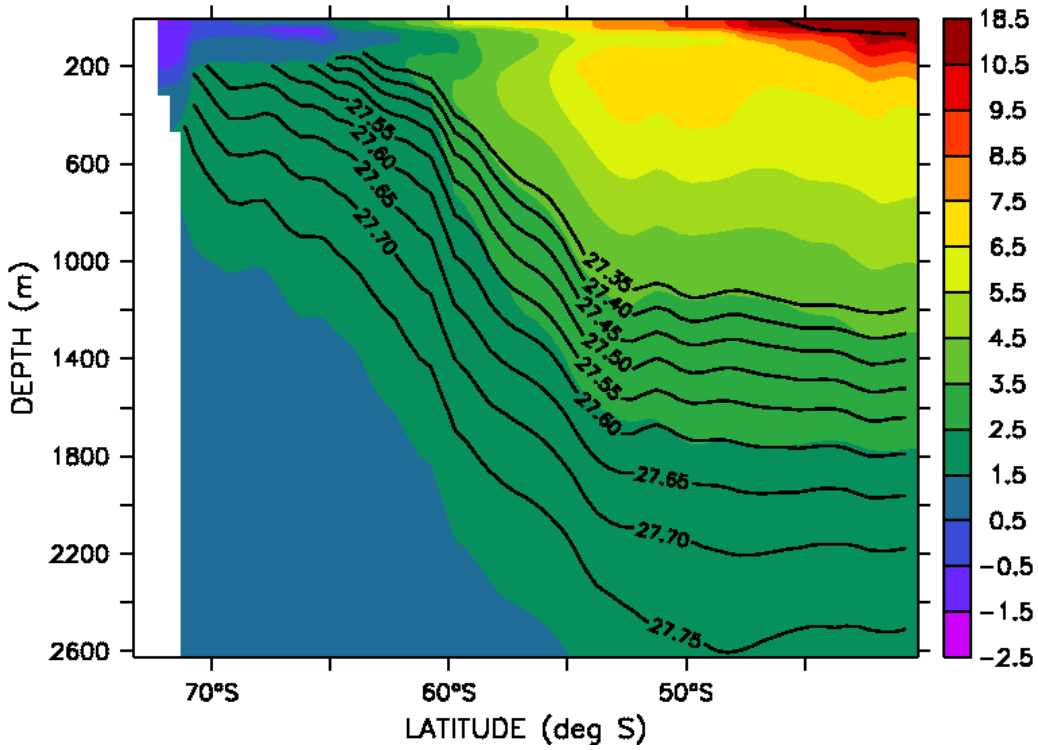

Figure 6.2: Isopycnals in SODA identifying UCDW are overlaid on a temperature plot along 100°W in the Pacific sector, in February 1997.

and Rintoul, 2002; *Hiscock et al.*, 2003) and because of the different latitudinal positions of the PF and the sBdy (Figure 3.2) UCDW is found near the surface further north, in the Indian Ocean sector, and further south, in the Pacific sector, than in the Australian sector. This is illustrated in Figures 6.1 and 6.2, for the Indian and Pacific sectors, respectively, compared with Figure 3.3, for the Australian sector. These show isopycnals identifying UCDW (overlaid on a temperature plot), along (a) 34°E and (b) 60°E in the Indian sector, and in Figure 6.2, along 100°W in the Pacific sector, in February 1997. Note the difference between the Indian Ocean plots along 34°E and 60°E, the former of which is in the part of the Indian ocean sector where the sBdy is very far north compared with further east in the sector (Figure 3.2).

Climatological annual means for the southern-most position of UCDW, viz. Indian (64.5°S), Australian (65.1°S) and Pacific (72.7°S), are consistent with the position of the sBdy as shown in Figure 3.2 and also with the positions of the ACC fronts, shown in Figure 6.3 (*Orsi and Ryan*, 2001, updated 2006). Based on the positions of the PF and sBdy shown in these figures, it can be estimated that UCDW upwells near to the surface in the following latitudinal zones: Indian (50-65°S), Australian (55-65°S) and Pacific (60-70°S). It should be noted that the larger range for the Indian sector occurs because of the large latitudinal range in the sACCf and the sBdy in that particular sector (20-60°E).

In order to compare UCDW in the three sectors, where there is such a

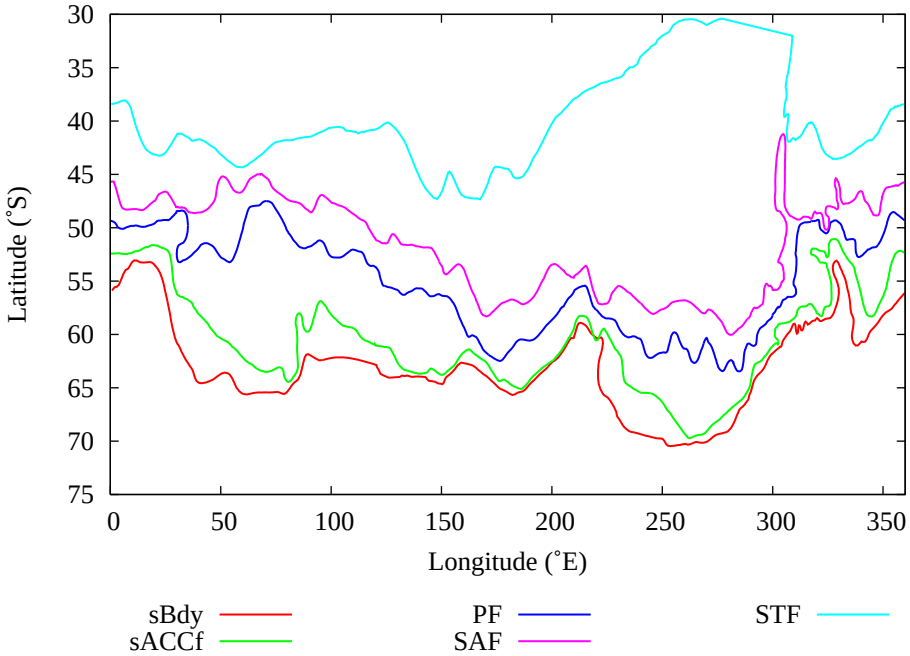

Figure 6.3: Positions of the various fronts of the ACC (*Orsi and Ryan*, 2001, updated 2006). Study sectors are Indian (20-60°E, 40-70°S), Australian (110-160°E, 70-65°S) and Pacific (130-80°W, 40-75°S).

Table 6.1: Latitudinal zones and their relationship to the ACC frontal zones in the three Southern Ocean sectors, as used for sector comparisons in this work.

Frontal Zone	Australian sector	Indian sector	Pacific sector
STCZ	40-45°S	40-45°S	45-50°S
SAZ	45-50°S	45-50°S	50-55°S
PFZ	50-55°S	50-55°S	55-60°S
AZ	55-60°S	55-60°S	60-65°S
sACCZ	60-65°S	60-65°S	65-70°S
SZ	65-70°S	65-70°S	70-75°S

Table 6.2: Annual means of climatological values for UCDW variables

UCDW	sACCZ	AZ	PFZ	SAZ	STCZ
Vertical Velocity (ms^{-1})					
Australian	0.29×10^{-5}	1.8×10^{-5}	2.3×10^{-5}	0.91×10^{-5}	0.32×10^{-5}
Indian	0.16×10^{-5}	0.31×10^{-5}	0.84×10^{-5}	1.1×10^{-5}	1.7×10^{-5}
Pacific	0.21×10^{-5}	0.71×10^{-5}	1.2×10^{-5}	0.46×10^{-5}	0.22×10^{-5}
Temperature (°C)					
Australian	1.9	2.1	2.4	2.6	2.7
Indian	1.7	1.8	2.0	2.3	2.7
Pacific	1.8	2.1	2.4	2.5	2.4
Depth Range (m)					
Australian	60-800	75-1700	120-2400	470-2400	1100-2400
Indian	140-500	130-900	130-1400	180-1900	400-2300
Pacific	150-900	140-1600	180-2200	770-2600	1000-2600

variation in the position of the fronts and therefore in its upwelling position, the comparisons are presented by ACC frontal rather than latitudinal zones. The calculations are still made by latitudinal zone. This means that instead of giving values for ML temperature, for example, for 65-70°S in the Pacific sector (which is in the sACCZ) and in 60-65°S in the other two sectors (also in the sACCZ), the results will be presented in the sACCZ. The zones used (from north to south) will be SAZ, PFZ, AZ, sACCZ and SZ (Table 2.1 gives the relationship between the fronts and the zones). An additional zone, the Subtropical Convergence Zone (STCZ, *Tomczak and Godfrey* (1994)), north of the SAZ, will also be used in this work. The SZ (south of the sBdy) is not relevant for work involving UCDW, but is defined here for later use with ML and other variables. The relationship between the frontal and the various five-degree latitudinal zones is delineated in Table 6.1. The allocation of the various five-degree latitudinal sectors to the various frontal zones, based on the positions of the fronts in Figure 6.3, is only approximate, and that is particularly the case for the Indian sector where the sACCf covers such a wide latitudinal range However, this method does allow useful comparisons to be made between UCDW in the three sectors.

Before comparing UCDW climatological means in the three sectors, it is useful to look at an example for a particular month (January 2004) of UCDW depth-averaged temperature and UCDW top depth in the Indian (Figure 6.4) and Pacific sectors (Figure 6.5). These plots are comparable to those for the Australian sector in Figures 5.4(a) and 5.1. These plots illustrate the extent of UCDW as well as features detected for the Australian sector such as the fact that UCDW temperature decreases as it shoals southwards.

Annual means for various UCDW variables (averaged over UCDW depth in each zone) are given in Table 6.2. UCDW annual density (27.6 kg m^{-3}) and salinity (34.6 psu), which lie in the range over which UCDW is defined, do not vary by frontal zone and are therefore not included in Table 6.2.

In each sector, an increase in UCDW vertical velocity can be seen in the zones where UCDW upwells along steeply tilted isopycnals, followed by a de-

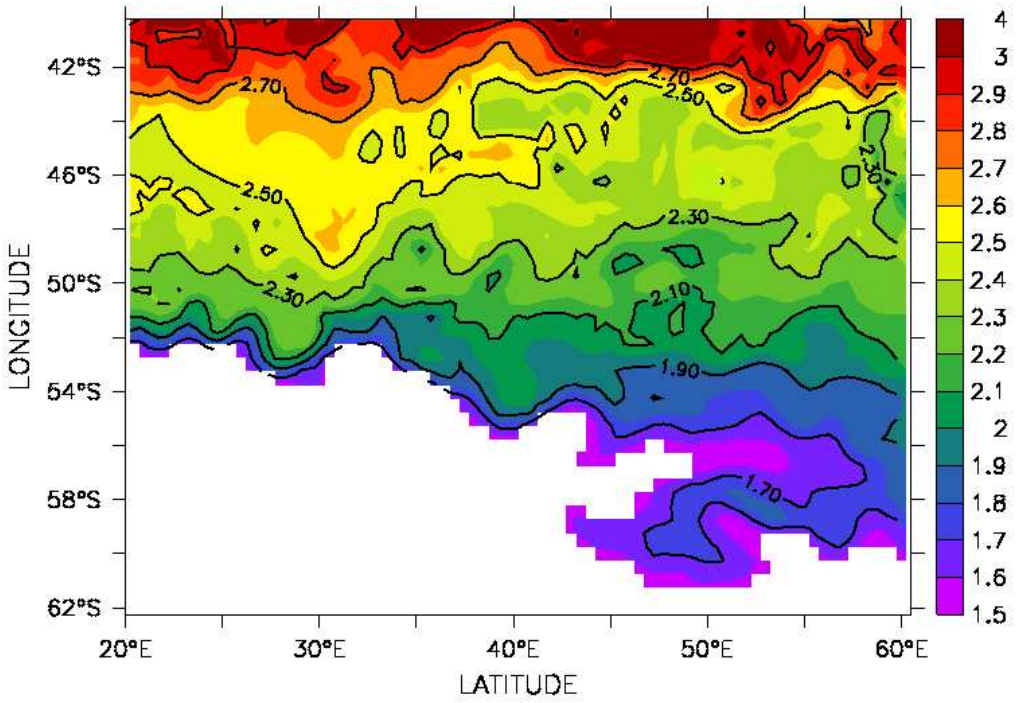

(a)

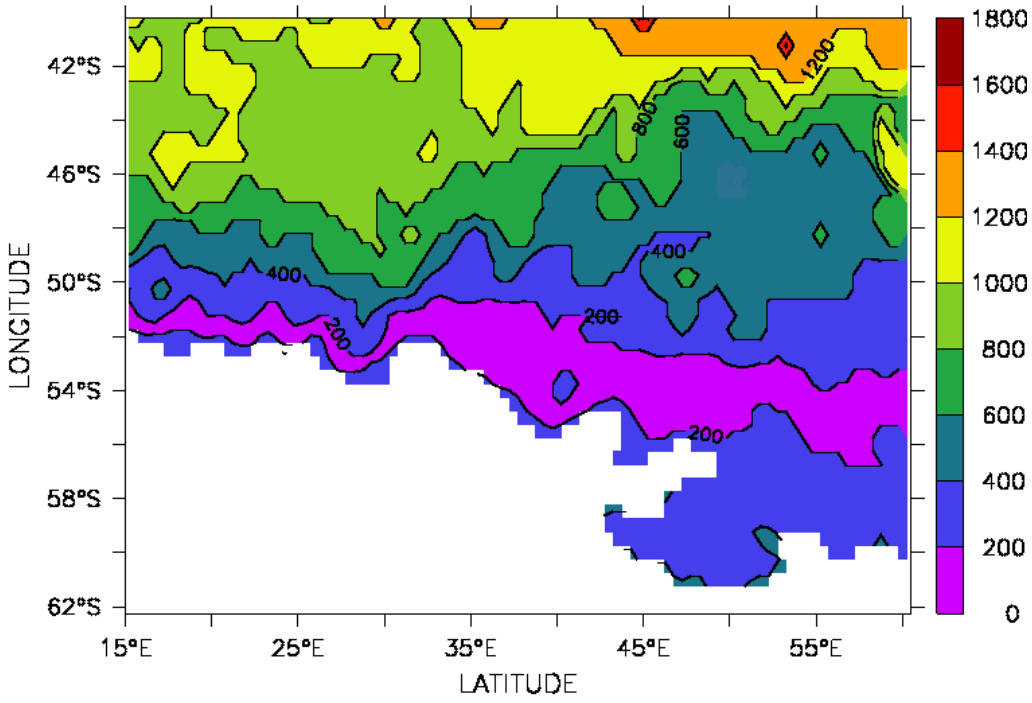

(b)

Figure 6.4: Plots of (a) depth averaged UCDW temperature and (b) UCDW top depth in the Indian sector in January 2004.

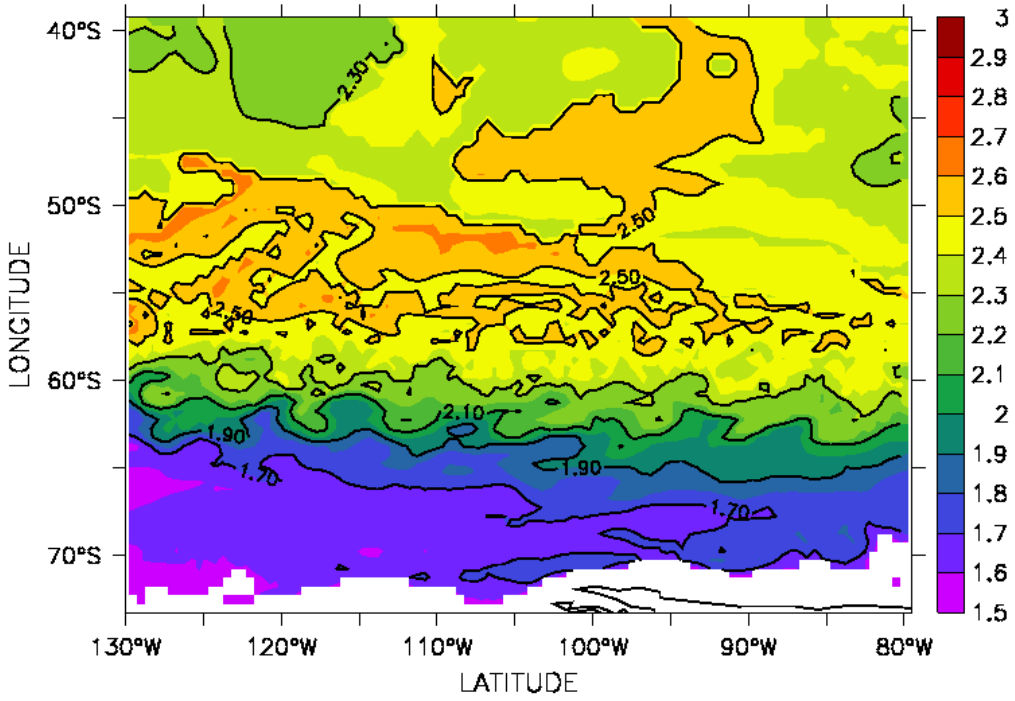

(a)

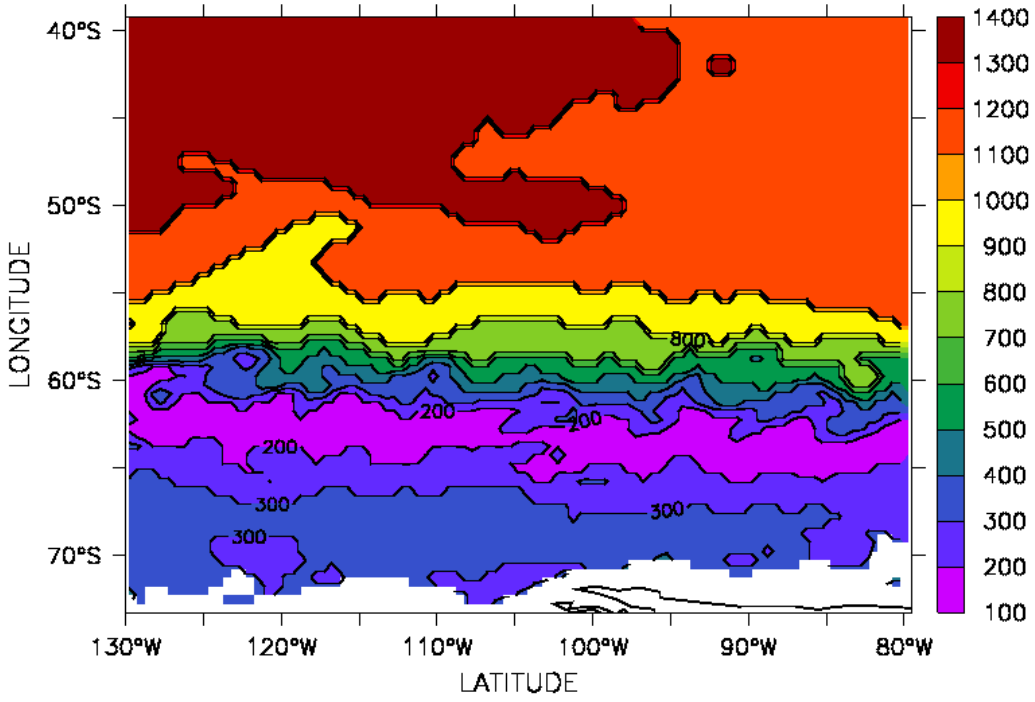

(b)

Figure 6.5: Plots of (a) depth averaged UCDW temperature and (b) UCDW top depth in the Pacific sector in January 2004.

crease in vertical velocity as UCDW nears the surface (for example, Figure 6.2). UCDW temperature also decreases as UCDW shoals from around 2500 m to annual mean top depths which vary from 140 m (Pacific), 130 (Indian) to 60 m (Australian). UCDW temperatures are generally lower in the Indian sector than in the other two sectors and this may be related to the fact that UCDW is not found as deep in the Indian sector as in the other two sectors (Depth Range in Table 6.2).

In both the Indian and Pacific sectors, UCDW upwells higher in the AZ than in the sACCZ (Table 6.2). In the case of the Indian sector this may be due to the fact that UCDW upwells into the 60-65°S (sACCZ) zone only in the eastern part of the 20-60°E sector (Figure 3.2). The explanation for the Pacific sector is possibly related to UCDW upwelling onto the Antarctic shelf in that region.

6.1.2 Climatological wind stress

Yearly climatologies, for each of the sectors, of maximum wind stress over the full zone and its position, are presented in Figure 6.6. Mean wind stress by zone (not presented) varies from low in the most southerly latitudes, peaks in 50-55°S and then decreases again. In all but the most northerly zones, the minimum wind stress occurs in December/January. However, this zonal mean wind stress is more regional in nature and does not necessarily exhibit the same behaviour as the maximum wind stress. Figure 6.6 shows that the maximum wind stress has a very similar pattern in the Australian and Pacific sectors, peaking twice a year in March/April and September/October, with the semi-annual oscillation of atmospheric pressure (*van Loon*, 1967; *Simmonds and Jones*, 1998). Minimum values occur mid-year and in December, although the December minimum is more marked in the Australian sector than in the Pacific. In addition, the magnitude of the maximum wind stress is greater in the Australian sector than in the Pacific sector. Maximum wind stress is greatest in the Indian sector and follows a completely different pattern, increasing monotonically from a January minimum to an August peak and then decreasing monotonically again.

However, when studying the location of the maximum wind stress in Figure 6.6(b) it can be seen that, in this case, similarities exist between the Australian and Indian (not Pacific) sectors, where the winds move south in March/April and August/September and are at their most northerly position in December/January. In contrast, the Pacific winds move (much further) south around July-October.

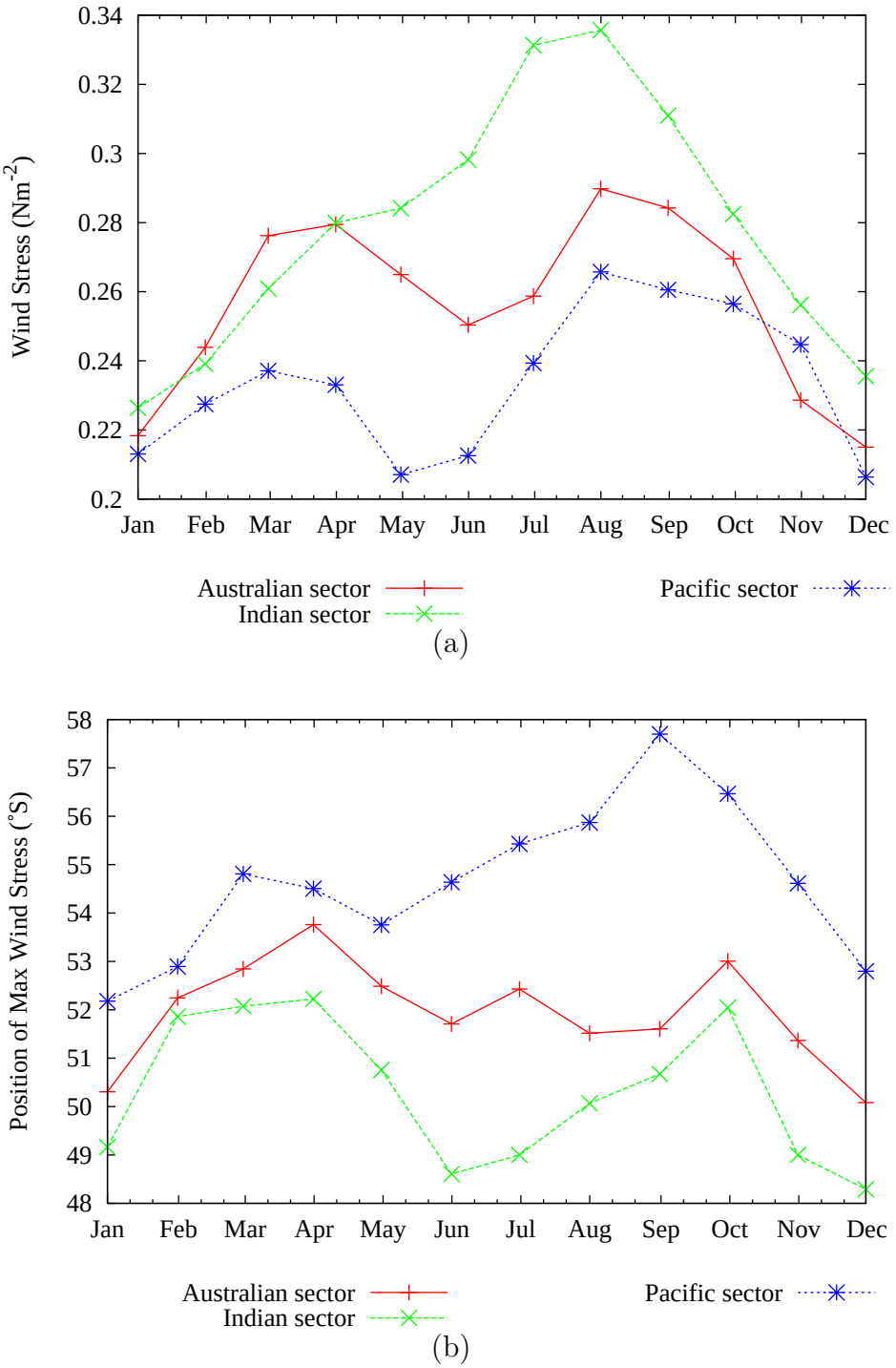

Figure 6.6: Climatology of (a) maximum wind stress and (b) its position.

Table 6.3: Mixed layer and sea-surface annual climatological means

		SZ	sACCZ	AZ	PFZ	SAZ	STCZ
ML Density (kgm^{-3})	Australian	27.4	27.3	27.0	26.7	26.4	26.2
	Indian	27.4	27.2	27.1	27.0	26.7	26.1
	Pacific	27.3	27.1	27.1	26.9	26.6	26.3
ML Salinity	Australian	34.1	34.0	33.8	33.8	34.1	34.6
	Indian	34.1	33.9	33.8	33.8	33.8	34.3
	Pacific	33.9	33.8	33.9	33.9	34.0	33.9
ML Depth (m)	Australian	103.8	48.9	64.0	88.0	98.7	81.1
	Indian	89.1	44.8	57.2	90.4	89.4	68.3
	Pacific	59.8	49.3	70.5	99.8	103.8	77.9
ML Temp (°C)	Australian	-1.1	0.0	2.0	5.1	9.1	12.4
	Indian	-0.8	-0.3	0.5	2.0	5.0	11.1
	Pacific	-1.0	-0.5	1.7	4.4	6.9	8.9
SST (°C)	Australian	-1.2	0.1	2.1	5.2	9.1	12.6
	Indian	-1.0	-0.3	0.5	2.0	5.1	11.4
	Pacific	-1.1	-0.5	1.7	4.5	6.9	9.0
SSS	Australian	34.0	34.0	33.8	33.8	34.1	34.6
	Indian	33.9	33.9	33.8	33.8	33.8	34.2
	Pacific	33.8	33.7	33.8	33.9	33.9	33.9

6.1.3 Climatological mixed layer and sea-surface variables

Climatological means for ML depth, temperature, density and salinity and SST and SSS are given in Table 6.3 for each frontal zone, in each of the three sectors. In each sector, annual ML density decreases and ML temperature increases northwards, whereas a minimum in ML salinity occurs in the middle latitudes. Annual ML depth has near maximum values in the SZ, then minimum values in the sACCZ, after which it increases northwards from the sACCZ to the SAZ, followed by a decrease in the STCZ.

6.2 The Connection between the SH winds and Changes in UCDW and the ML

Correlations in this section are performed between the original (and not detrended) time series, so that the effect of wind stress on trends in other variables can be investigated. However, other work (not presented) indicates that detrending makes little difference to the results.

6.2.1 Correlations between SAM/MEI and mean wind stress

Here the connection between the global climate indices SAM, MEI and PDO and the mean wind stress is investigated in the various zones of the three ocean sectors. Values of significant correlations are given in Table 6.4 and,

Table 6.4: Correlations between mean wind stress and global climate indices (n/s=not significant).

		SZ	sACCZ	AZ	PFZ	SAZ	STCZ
SAM	Australian	-0.12	0.33	0.48	0.38	0.10	-0.16
	Indian	-0.10	0.21	0.41	0.32	n/s	-0.17
	Pacific	n/s	0.16	0.26	0.25	0.15	n/s
MEI	Australian	0.10	n/s	n/s	0.18	0.26	0.17
	Indian	n/s	n/s	n/s	n/s	0.11	n/s
	Pacific	-0.09	0.16	n/s	-0.17	-0.30	-0.36
PDO	Australian	0.17	n/s	n/s	0.13	0.19	0.16
	Indian	n/s	0.08	0.10	0.09	0.08	n/s
	Pacific	n/s	0.11	n/s	n/s	-0.12	-0.15

overall, it can be seen that the stronger correlations between mean wind stress and SAM are in the more southerly zones (excluding SZ), while the stronger correlations with MEI are in the more northerly zones. Also notable are how few correlations there are with MEI in the Indian sector. There are positive correlations between mean wind stress and SAM in most zones, although they are negative in SZ and STCZ. On the other hand, correlations with MEI are negative in the more northerly zones in the Pacific sector. These results are consistent with SAM as the dominant mode of climate variability in the middle and high latitudes of the SH (*Lovenduski and Gruber*, 2005). The opposite signs in the correlations between SAM and mean wind stress, and MEI and wind stress are consistent with studies that have found that ENSO and SAM indices are often anti-correlated (*L'Heureux and Thompson*, 2006). Although ENSO is primarily a tropical Pacific phenomenon, correlations are still seen between the MEI and mean wind stress in the northern Australian sector, in addition to the Pacific sector. They are, however, of opposite sign, perhaps due to the effect of ENSO in the Australian zone being felt through the East Australian Current (*Holbrook and Bindoff*, 1997). Generally, correlations with the PDO are not strong and are positive in the Australian and Indian sectors and negative in the more northern Pacific zones. The results for similar SAM, MEI and PDO correlations, by season for the Australian sector, found in Table 5.5, are consistent with these results, but show stronger correlations for the seasonal time series than for the full time series.

6.2.2 Correlations between mean wind stress and UCDW variables

Table 6.5 presents correlations between mean wind stress and UCDW variables for the three sectors and, in general, most correlations are not strong. The fact that there are correlations for the zones where UCDW is deeper is interesting, but it is unclear if they indicate a true connection between wind

Table 6.5: Correlations between mean wind stress and UCDW variables (n/s=no significant trend).

UCDW		sACCZ	AZ	PFZ	SAZ	STCZ
Vertical Velocity	Australian	n/s	0.13	n/s	n/s	n/s
	Indian	n/s	n/s	-0.10	-0.10	n/s
	Pacific	n/s	n/s	-0.10	-0.16	n/s
Temperature	Australian	n/s	n/s	0.10	0.09	n/s
	Indian	-0.11	n/s	n/s	-0.13	n/s
	Pacific	0.11	0.08	n/s	-0.27	n/s
Density	Australian	0.09	n/s	-0.14	-0.13	0.18
	Indian	-0.13	-0.09	-0.14	n/s	n/s
	Pacific	n/s	0.11	n/s	0.29	-0.14
Salinity	Australian	0.10	n/s	n/s	n/s	0.24
	Indian	-0.13	-0.10	-0.21	n/s	n/s
	Pacific	n/s	0.17	n/s	0.18	-0.19
Top Depth	Australian	0.11	n/s	-0.14	n/s	n/s
	Indian	-0.09	n/s	n/s	n/s	n/s
	Pacific	n/s	n/s	n/s	-0.10	-0.13

stress and UCDW properties, especially due to the mixture of negative and positive correlations. Another consideration is the fact that these are direct correlations and there may be a lag between the winds and changes in UCDW. When this is investigated, using a lag of up to 10 years, no consistent pattern emerges, nor did the strength of the correlations increase greatly. Also, the sign of the correlations often changes, so it would seem that, either there is no correlation between the mean wind stress and changes in UCDW properties, or else it operates over a longer time period than can be investigated with the data available here.

6.2.3 Correlations between mean wind stress and ML and SS variables and stratification

There are strong correlations between mean wind stress and both SS and ML variables and these are given in Table 6.6, along with correlations with stratification. The sign of the ML (and SS) correlations is the same in all three sectors; that is, positive with ML depth, density, salinity and SSS, and negative for both ML temperature and SST (as was also found for the Australian sector seasonal time series presented in Table 5.6). Again the correlations for ML and SS variables are very similar. Mean wind stress and stratification correlations are positive in the southern zones and negative in the northern zones.

Table 6.6: Correlations between mean wind stress and mixed layer and sea-surface variables and stratification (n/s=not significant).

		SZ	sACCZ	AZ	PFZ	SAZ	STCZ
ML Depth	Australian	0.42	0.52	0.38	0.14	0.20	0.52
	Indian	0.51	0.53	0.55	0.57	0.53	0.56
	Pacific	0.46	0.58	0.51	0.21	n/s	n/s
ML Density	Australian	0.15	0.45	0.28	n/s	0.13	0.42
	Indian	0.33	0.36	0.33	0.29	0.42	0.49
	Pacific	0.37	0.53	0.46	0.21	n/s	n/s
ML Salinity	Australian	0.15	0.39	0.19	n/s	n/s	n/s
	Indian	0.36	0.37	0.24	0.11	0.23	n/s
	Pacific	0.38	0.54	0.35	0.12	n/s	0.08
ML Temperature	Australian	n/s	-0.41	-0.27	-0.11	-0.14	-0.42
	Indian	n/s	-0.28	-0.32	-0.31	-0.39	-0.52
	Pacific	n/s	-0.38	-0.44	-0.22	n/s	n/s
SST	Australian	-0.17	-0.45	-0.29	-0.13	-0.15	-0.44
	Indian	-0.13	-0.31	-0.35	-0.37	-0.39	-0.54
	Pacific	-0.11	-0.44	-0.46	-0.24	n/s	n/s
SSS	Australian	0.10	0.38	0.19	n/s	n/s	n/s
	Indian	0.35	0.32	0.26	n/s	0.13	-0.11
	Pacific	0.40	0.52	0.36	0.15	n/s	0.11
Stratification	Australian	n/s	n/s	0.17	n/s	-0.08	-0.35
	Indian	n/s	0.32	0.33	n/s	-0.24	-0.35
	Pacific	0.17	n/s	-0.29	-0.22	n/s	-0.09

6.3 Trend Analyses

6.3.1 Linear trends in UCDW variables

A comparison by sector of significant annual linear trends for UCDW variables over the period 1958-2007 is given in Table 6.7, along with 95% confidence interval limits. The results in this table correspond to those in Tables A.2, A.5 and A.8, but are for the full time series, rather than the four seasonal time series. The trends match fairly well between the two sets of tables, although often the trend for the full time series is smaller than for some of the seasonal time series and sometimes the trend for the full time series is not significant, even though the trends are, for some of its constituent seasonal time series.

In the sACCZ and AZ, where UCDW comes near to the surface, UCDW density is decreasing and UCDW is upwelling closer to the surface, in the Australian and Indian sectors, but no significant trends are found in the Pacific sector. Trends for vertical velocity in the sACCZ vary between sectors: positive for Indian, negative for the Pacific and not significant for the Australian sector.

UCDW vertical velocity is increasing in the Australian and Indian sectors in the PFZ, SAZ and STCZ. This means that there is a positive trend in UCDW vertical velocity in all zones in the Indian sector and in all zones north of the PF in the Australian sector. This is not the case, however, in the Pacific sector

Table 6.7: Trends (per year, with 95% confidence interval limits) for 1958-2007 in UCDW variables (n/s=not significant). Positive trends for UCDW Top Depth indicate that UCDW is moving nearer to the surface. Additional trends are UCDW Salinity -4.3±1.2yr^{-1} in AZ Indian sector. No trends are found for the Southernmost Position of UCDW.

UCDW		sACCZ	AZ	PFZ	SAZ	STCZ
Vertical Velocity						
(ms^{-1}yr^{-1}) × 10^{-8}	Australian	n/s	n/s	7.2±2.1	6.4±1.3	3.4±0.4
	Indian	0.8±0.6	2.4±0.6	3.3±1.2	6.3±1.3	8.8±2.4
	Pacific	-1.0±0.4	n/s	2.2±1.1	n/s	-0.5±0.3
Temperature						
(°Cyr^{-1}) × 10^{-3}	Australian	3.3±0.5	0.4±0.4	-2.4±0.3	-1.5±0.2	-0.7±0.1
	Indian	1.9±0.8	2.6±0.5	3.2±0.3	0.9±0.2	n/s
	Pacific	0.8±0.4	1.4±0.4	n/s	-0.2±0.1	-0.2±0.2
Density						
(kgm^{-3}yr^{-1}) × 10^{-4}	Australian	-4.3±0.8	n/s	n/s	n/s	n/s
	Indian	-2.7±2.7	-5.9±0.9	-4.7±0.5	n/s	n/s
	Pacific	n/s	n/s	n/s	n/s	n/s
Top Depth						
(myr^{-1})	Australian	0.4±0.4	0.5±0.3	n/s	n/s	n/s
	Indian	0.9±0.9	1.0±0.3	n/s	n/s	n/s
	Pacific	n/s	n/s	n/s	n/s	n/s

Table 6.8: Trends (per year, with 95% confidence interval limits) for 1958-2007 for global climate indices.

SAM	**MEI**	**PDO**
(1.8±1.1)×10^{-2}	(1.1±0.5)×10^{-2}	(2.0±0.6)×10^{-2}

where there is a mixture of positive and negative trends, although UCDW vertical velocity is increasing in the PFZ in all three sectors.

Increasing UCDW temperature can be seen in all three sectors in the sACCZ and the AZ. In addition, UCDW temperature trends north and south of the PF are very interesting as, unlike the Indian sector, where temperature in increasing in all zones, in the Australian sector, UCDW temperature is increasing south of the PF and decreasing north of it. Similar results also hold for the Pacific sector, excluding the PFZ itself.

6.3.2 Linear trends in global climate indices, wind stress, stratification and Ekman variables

Annual linear trends for 1958-2007 for the three global climate indices, presented in Table 6.8, are all positive. This indicates that: for SAM, lower than normal air pressure is found over the polar regions; the MEI is moving to a more "El Niño-like" state' and the PDO is moving to a "warmer" state (Section 2.7).

The few significant trends that are found for mean wind stress and the Ekman variables are presented in Table 6.9, along with trends in stratification for the various zones of all three ocean sectors. These results are consistent

Table 6.9: Trends (per year, with 95% confidence interval limits) for 1958-2007 in wind stress, Ekman variables and stratification (n/a=not applicable, n/s=not significant). No significant trends were found for maximum wind stress or its position, except in the latter case in the Pacific where the trend is (-2.4±2.4)×10^{-2}.

	SZ	sACCZ	AZ	PFZ	SAZ	STCZ
Stratification						
($s^{-2}yr^{-1}$) × 10^{-7}						
Australian	n/s	-0.7±0.7	-1.3±0.7	n/s	n/s	n/s
Indian	n/s	n/s	-1.9±1.0	-2.4±0.7	n/s	1.3±0.9
Pacific	-1.3±0.4	0.7±0.6	n/s	n/s	n/s	-1.8±0.8
Mean Wind Stress						
($Nm^{-2}yr^{-1}$) × 10^{-4}						
Australian	n/s	n/s	n/s	n/s	n/s	n/s
Indian	n/s	n/s	n/s	n/s	-6.8±2.3	n/s
Pacific	n/s	n/s	n/s	n/s	n/s	n/s
Ekman Transport						
($ms^{-1}yr^{-1}$) × 10^{-2}						
Australian	n/a	n/s	n/s	n/s	n/s	1.1±0.8
Indian	n/a	n/s	n/s	n/s	n/s	n/s
Pacific	n/a	n/s	n/s	n/s	n/s	n/s
Ekman Pump Rate						
($Svyr^{-1}$) × 10^{-9}						
Australian	n/a	n/s	4.0±3.1	n/a	n/a	n/a
Indian	n/a	n/s	-3.7±3.3	n/a	n/a	n/a
Pacific	n/a	n/s	n/s	n/a	n/a	n/a

with the seasonal trends presented in Tables A.3, A.6 and A.9, in the sense that, either the trends are apparent for one season only and therefore do not hold for the full time series, or the oppositely signed trends in different seasons mitigate against an annual trend. No trends are found for maximum wind stress in any of the three sectors, nor in the position of maximum wind stress, except in the Pacific sector. In the Indian and Pacific sectors, stratification shows both positive and negative trends, depending on the frontal zone, while the Australian sector exhibits decreasing stratification in the sACCZ and AZ.

6.3.3 Linear trends in mixed layer and sea-surface variables

Annual ML and SS linear trends, with 95% confidence interval limits, are given in Table 6.10. Similar seasonal trends are presented in Tables A.7 and A.10 for the Indian and Pacific sectors, along with Table A.4, already presented for the Australian sector. The trends for ML and SS salinity, and ML and SS temperature, are identical in sign and similar in magnitude, except for a couple of occasions where there is a trend in one case but not the other. So the subsequent discussion will just focus on ML trends.

There are positive trends for both ML density and salinity in the Australian and Indian sectors, whereas, in the Pacific sector, trends in these variables are negative. Interestingly, in all three sectors, there are no significant trends in

Table 6.10: Trends (per year, with 95% confidence interval limits) for 1958-2007 in mixed layer and sea-surface variables.

	SZ	sACCZ	AZ	PFZ	SAZ	STCZ
ML Depth (myr^{-1})						
Australian	n/s	0.14±0.04	0.26±0.07	0.49±0.09	0.57±0.10	n/s
Indian	-0.23±0.09	0.11±0.04	0.32±0.06	n/s	-0.13±0.07	n/s
Pacific	n/s	n/s	n/s	n/s	0.29±0.09	0.14±0.05
ML Density ($kgm^{-3}yr^{-1}$) $\times 10^{-3}$						
Australian	n/s	n/s	1.3±0.4	1.5±0.3	2.1±0.6	n/s
Indian	n/s	n/s	1.9±0.2	n/s	n/s	n/s
Pacific	n/s	n/s	n/s	n/s	n/s	-0.6±0.6
ML Salinity (yr^{-1}) $\times 10^{-3}$						
Australian	n/s	n/s	2.6±0.4	4.7±0.3	6.3±0.8	1.7±0.8
Indian	n/s	n/s	2.9±0.4	1.4±0.4	1.7±0.3	4.1±0.8
Pacific	n/s	n/s	-1.4±0.4	-0.8±0.5	-1.6±0.5	-1.7±0.4
ML Temperature ($°Cyr^{-1}$) $\times 10^{-2}$						
Australian	0.6±0.1	n/s	n/s	n/s	n/s	1.1±0.2
Indian	0.6±0.1	n/s	n/s	1.8±0.2	2.6±0.2	3.6±0.3
Pacific	0.4±0.1	n/s	n/s	n/s	n/s	-0.4±0.2
SST ($°Cyr^{-1}$) $\times 10^{-2}$						
Australian	0.7±0.1	n/s	n/s	n/s	n/s	1.1±0.2
Indian	0.4±0.1	n/s	n/s	n/s	2.7±0.2	3.6±0.3
Pacific	0.4±0.1	n/s	n/s	n/s	n/s	-0.5±0.2
SSS (yr^{-1}) $\times 10^{-3}$						
Australian	0.3±0.3	0.8±0.5	2.9±0.4	5.1±0.5	6.7±0.9	2.2±0.8
Indian	n/s	n/s	3.3±0.2	2.1±0.4	2.1±0.4	4.3±0.8
Pacific	n/s	n/s	-1.1±0.4	-0.8±0.6	-1.4±0.7	-1.5±0.5

these variables in either the SZ or the sACCZ. MLD is generally increasing, except in the SZ and SAZ in the Indian sector and in the southern part of the Pacific sector.

Finally, ML temperature (and SST) is increasing only in the most southern (SZ) and northern (STCZ) zones in all three sectors, in addition to the PFZ and the SAZ in the Indian sector. This is a somewhat unexpected result, especially in view of the results for ML temperature, given in Table A.4 for the Australian sector, where ML temperature is increasing in all seasons and in all zones, except for DJF and MAM in 60-65°S (sACCZ) and DJF in 55-60°S (AZ). From this, one might expect that, at least, the annual ML temperature trend in the Australian sector in the 50-55°S (PFZ) and 45-50°S (SAZ), would be positive. In fact, all the annual ML temperature trends for all the Australian zones, calculated using the Seasonal Kendall test (Section 3.6), are positive, but only those for the SZ and STCZ are valid. This is because the test checks (*Gilbert*, 1987) to see if the trends for all the "seasons" (in this case, months) are homogeneous in direction and, if that is not the case, then the overall trend is not valid, as is the case here. Despite this being the case for the full time series, the trends within a season (say, MAM) are homogeneous, as shown in the results found in Table A.4.

To examine this further, seasonal ML and SS trends for the Indian and Pacific sectors are presented in Tables A.7 and A.10. These results indicate

that ML temperature and SST are increasing in all seasons in the SZ, PFZ, SAZ and STCZ in the Indian sector, but not in every season in the sACCZ and the AZ. The situation in the Pacific sector is less clear-cut, with the SZ the only zone where the trend (positive) applies to all seasons. In the Pacific sector, positive temperature trends are found for all seasons except DJF (and sometimes in MAM), whereas trends for DJF (and sometimes MAM) are either not significant or negative, north of the SZ. In summary, even though ML temperature and SST are generally increasing, they are not increasing in DJF and MAM in the sACCZ or in DJF in the AZ and this holds for all three ocean sectors. In DJF, these trends match trends of increasing wind stress (Tables A.3, A.6 and A.9), leading to the possibility that increased mixing of cooler remnant winter water (Figures 3.3, 6.1 and 6.2) into the ML, counteracts the surface warming effect.

6.3.4 Intrusion of UCDW into the mixed layer

The intrusion of UCDW into the ML, is defined to occur if, for a given month, at a particular grid point in SODA, UCDW is detected at a depth above the MLD. Data for 1960-2010, where the 2000-2007 data are scaled to 10 years, are presented in two different ways here: firstly by decade (Figure 6.7) and secondly, by frontal zone (Table 6.11). In the latter case, the data are further broken down by season to allow a comparison to be made between the upwelling in the various sectors. Note that the data in Table 6.11 show UCDW in the SZ, contrary to the definition of the sBdy as the poleward edge of the UCDW signal (*Orsi et al.*, 1995). However, the data indicate that UCDW can occasionally be found in the 65-70°S zone (for the Australian and Indian sectors). The apparent anomaly arises because the definition of 65-70°S here as the SZ does not take into account the slight movement of the sBdy with time (see Figure 5.2 for the climatology of the southern-most position of UCDW in the Australian sector).

As can be seen in Figure 6.7 and Table 6.11, there are considerably fewer occasions when UCDW can be detected in the ML in the Pacific sector, compared with the other two sectors. Figure 6.7 also shows that the number of detections by decade seems to be decreasing recently in the Indian sector, is increasing since the 1970s in the Pacific sector and is increasing gradually in the Australian sector up until the 1990s.

Table 6.11 allows the number of times UCDW can be detected in the ML to be examined both by frontal zone and season. For the Indian sector, for example, the total number of detections by frontal zone suggests that, after UCDW upwells south of the PF (*Hiscock et al.*, 2003), it then moves northward into the PFZ, AZ and STCZ. This is indicated not only by the total number of

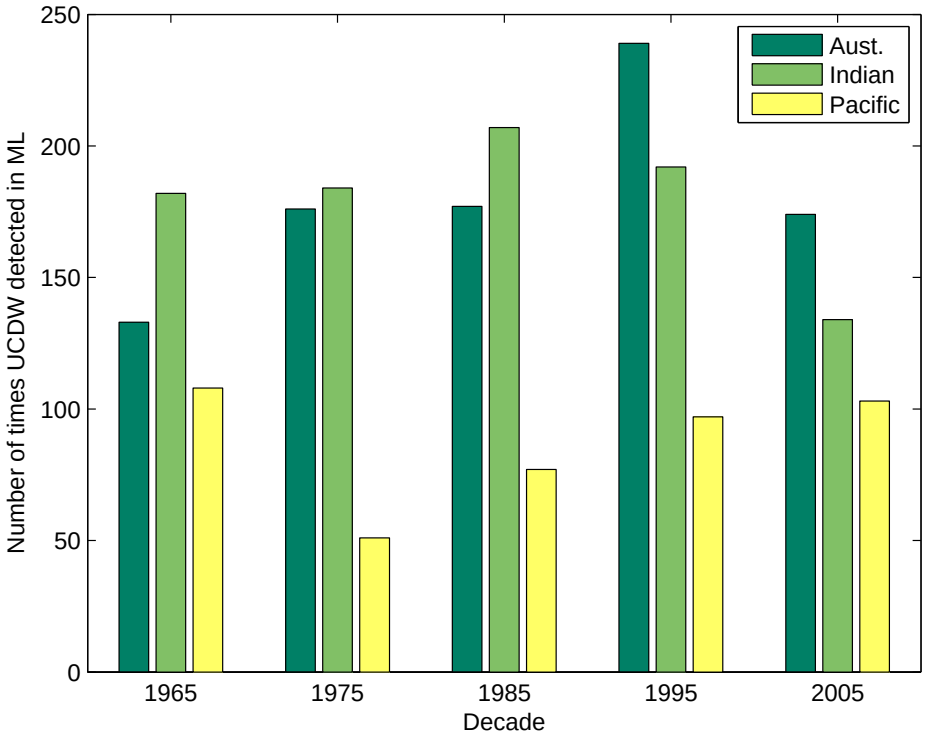

Figure 6.7: Number of times UCDW can be detected in the mixed layer by decade (Aust.=Australian). Data for the decade centred on 2005 are scaled to 10 years.

Table 6.11: Number of times UCDW can be detected in the mixed layer, by season and frontal zone (Aust.=Australian).

	SZ	sACCZ	AZ	PFZ	SAZ	STCZ	Total
Australian							
DJF	11	68	50	2	1	0	132
MAM	7	105	103	13	0	0	228
JJA	1	30	128	125	8	0	292
SON	0	21	116	105	5	0	247
Aust. Total	19	224	397	245	14	0	899
Indian							
DJF	6	17	22	65	11	0	121
MAM	7	27	60	92	24	0	210
JJA	3	4	29	144	124	3	307
SON	0	0	3	132	124	2	261
Indian Total	16	48	114	433	283	5	899
Pacific							
DJF	1	2	11	11	0	0	25
MAM	0	19	57	34	0	0	110
JJA	0	15	95	78	3	0	191
SON	0	9	58	41	2	0	110
Pacific Total	1	45	221	164	5	0	436

detections, but also by the numbers by season. For example, in the sACCZ, the majority of detections occur in DJF/MAM, in the AZ in MAM/JJA and in the PFZ and SAZ in JJA/SON. This shows the northward movement of UCDW in the ML from south to north of the PF, in addition to some upwelling in DJF in the sACCZ and AZ. Similar arguments also apply to the Australian sector and Pacific sectors, except that, in the Pacific sector, the majority of detections in the sACCZ are in MAM/JJA, moving to MAM/JJA/SON in the AZ and PFZ. This is interesting because it has previously been reported in the Pacific sector (*Hoppema et al.*, 2003; *Gordon and Huber*, 1990) that the entrainment of nutrients into the ML occurs predominantly in autumn(MAM)/winter(JJA). The data here are in agreement with this for the Pacific sector, but suggest that the situation is different in the other two sectors.

It is not clear why there are fewer detections in the Pacific sector than in the other two sectors, since the mean MLD is similar in all three (Table 6.3) and UCDW upwells higher on average in the Australian sector than the other two (Table 6.2). This would imply that there would be more detections in the Australian sector, which is not the case, perhaps because using mean rather than actual values changes the result. It would seem, then, that fewer detections in the Pacific sector may be related to the lack of movement north of UCDW in the ML rather than the upwelling of UCDW. This is supported by the figures in Table 6.11, which show substantial numbers of detections in the Pacific sector in two zones only, unlike the other sectors.

6.4 Comparison with Previous Studies

6.4.1 Winds

Given that there are many significant correlations between mean wind stress and both the ML and SS variables, as well as stratification (Table 6.6), and that there are sometimes quite strong correlations between SAM or MEI and mean wind stress (Table 6.4), it is worth looking closely at trends in SAM, MEI or PDO and their effects.

As indicated in Table 6.4, there is a significant effect on the winds in each sector, not only from SAM, but in some zones, from ENSO or the PDO. These effects vary between zones, leading to different trends in wind stress. The present study finds almost no significant trends in annual mean wind stress and no trends in annual maximum wind stress, in any of the sectors, possibly due to the effect of seasonal wind stress trends in opposite directions or trends existing in one season only (for example, Table A.3).

Results from the study of *Drost and England* (2009), over a similar time period to this study, indicate that a positive trend for SAM results in a wind

shift that is: poleward in 20-50°E and equatorward in the remainder of the Indian sector 50-60°E; equatorward for almost all but the last 10° of the 110-160°E Australian sector and equatorward for part (130-100°W) of the 130-80°W Pacific sector. The results of the present study, which indicate a possible southward movement of the maximum wind stress for the Pacific sector, but no significant trend for the Australian and Indian sectors, are not inconsistent with the above results, bearing in mind that the Australian and Pacific winds are often affected, not just by SAM, but also by ENSO, as is evident in Table 6.4.

6.4.2 Meridional circulation

Two alternative points of view have been suggested by previous studies with regard to changes in the meridional circulation. *Yang et al.* (2007a), using an earlier (1.4.2) and less sophisticated version of the SODA reanalysis used here (*Schott et al.*, 2009), which considers the shorter time period 1980-2000, found that, over the full SH, the meridional circulation is strengthening and the Ekman pumping rate and northward Ekman velocity (which also shows a poleward shift) are increasing. A more recent study (*Böning et al.*, 2008) using a high resolution gridded climatology based on Argo float and historical data has concluded that the meridional circulation is insensitive to decadal wind changes, since stronger winds lead to increased eddy activity, which counteracts increased northward Ekman transport. The present study has found increased Ekman pumping in the AZ in the Australian sector, but decreased pumping in the AZ in the Indian sector (Table 6.9) and no trends in northward Ekman transport.

6.4.3 UCDW

Observational data, which would allow conclusions to be drawn about long-term trends in UCDW in a particular ocean, is quite sparse. The available observations generally show sub-surface warming. For example, sections of temperature trends for 1955-2003, between 50-1450 m, in each of the Indian and Pacific Oceans by *Levitus et al.* (2005), show sub-surface warming in the Indian Ocean and the Pacific Ocean, except south of 70°S, where there is cooling. A comparison of 1950s and 1990s SO temperature data from 35-65°S in the 700-1100 m depth range by *Gille* (2002) has found increases of around 4×10^{-3} °C/year, concentrated in the ACC (*Gille*, 2008). This is of similar magnitude to increases found by *Aoki et al.* (2003) in the Indian ocean, near the sACCf, averaged over 200-900 m for 1966-1998. The study by *Böning et al.* (2008), which considers trends over the whole SH, has also found a warming

trend for 1960-2006 across the ACC (SAF to PF), averaged over 300-1000 m, of 6×10^{-3} °C/year, as well as decreasing salinity (-4×10^{-3} psu/year).

The UCDW temperature trends found in the present study are of the same sign and approximate magnitude as the above (Table 6.7) in the sACCZ and AZ, in addition to the PFZ in the Indian sector. This is consistent with the above results because UCDW lies at the depths considered in the above studies only in the zones mentioned above (Table 6.2). The single salinity trend found in the present study (Table 6.7) is for the AZ in the Indian sector only and again it is of the same sign (negative) and magnitude as found by *Böning et al.* (2008). There is an intriguing result of decreasing UCDW temperature in the Australian sector north of the PF and in the Pacific sector in the SAZ and STCZ (where UCDW lies much deeper than considered in the previous studies, Table 6.2). A study by *Johnson and Orsi* (1997) in the Pacific along 170°W for 1968/9-1990 over 20-40°S also shows a similar result of decreasing temperature (-3×10^{-3} °C/year) in UCDW, but it is not directly comparable to either due to its latitudinal range. Other UCDW studies, for example, *Böning et al.* (2008) and *Aoki et al.* (2005), are on isopycnal surfaces and cannot be directly compared with the results of this study, since here UCDW variables are averaged over the full UCDW density range (27.35-27.75 kg m^{-3}) for temperatures over 1.5°C (Section 3.3).

6.4.4 Mixed layer

The small number of studies and the uneven spatial and temporal distribution of observations in the SO introduces considerable uncertainties (*Jacobs*, 2006; *Boyer et al.*, 2005). One long TS is available for temperature and salinity in the northern part of the Australian region at Maria Island (42.6°S, 148.23°E) and this shows positive trends for both variables from 1949-2005 (*Hill et al.*, 2008). These trends are consistent with those found in this study in that zone (Table 6.10). Similar warming down to 800 m in the 40-50°S band in the Indian Ocean for 1960-1999 was found using the Indian Ocean Thermal Archive by *Alory et al.* (2007). ML temperature and SST trends found here in the SAZ and STCZ are consistent with these results, but no conclusions can be drawn for UCDW trends since UCDW lies at depths up to 2300 m in these zones (Table 6.2). Global graphs of SST trends from 1979-2005, contained in the IPCC Fourth Assessment Report (*Trenberth et al.*, 2007), are patchy, with areas where values are missing. Study of these leads to the following rough conclusions for SST for the various sectors: Indian (increasing, for northern latitudes for part of sector; southern latitudes, unclear), Australian (increasing, for northern latitudes; decreasing near continent in east of sector) and Pacific (decreasing mid-to-northern latitudes, especially in DJF; southern latitudes,

unclear). Despite being a shorter time series, this compares quite well with the ML and SS temperature results of this study (Table 6.10): Indian and Australian (increasing all latitudes, except for DJF/MAM in southern latitudes) and Pacific (decreasing or not significant, DJF all latitudes and northern latitudes; increasing or not significant, southern latitudes, all seasons but DJF).

Trends in the literature for SSS are more difficult to find for the Australian sector as conclusions in the IPCC report (*Trenberth et al.*, 2007) come from vertical sections of salinity constructed by *Boyer et al.* (2005) and these are divided only into the Pacific and Indian Oceans and are annual trends only. These two oceans exhibit very different trends for near-surface salinity: increasing over almost all of the Indian Ocean and decreasing in patches in the Pacific Ocean, with the largest decreases south of 70°S. Again this compares well with the salinity trends in Table 6.10: Indian (increasing, except SON 60-65°S) and Pacific (decreasing or not significant, except for DJF 65-70°S). It should be noted that recent studies of changes in surface layer temperature and salinity (*Hosoda et al.*, 2009; *Roemmich and Gilson*, 2009) using Argo float data are not comparable with these results as the time periods and types of comparisons are different.

Trends for other ML variables such as depth and density and other variables such as Ekman variables and stratification (Tables 6.9 and 6.10) are more difficult to verify, due to a lack of comparable observational studies. Some studies suggest decreasing MLD and increasing stratification in certain regions (*Bindoff et al.*, 2007), in contrast to many of the results found here for 1958-2007 (except for MLD in the SZ and SAZ in the Indian sector and stratification in the Pacific sACCZ and Indian STCZ). Whether these results are inconsistent is unclear, as they may be related to limitations associated with the SODA product or they may be differences that are due to regional rather than hemispheric trends.

6.5 Conclusions

This chapter considers the meridional circulation in the SO in three sectors, Indian, Australian and Pacific, using the SODA 2.0.2/2.0.4 reanalysis. Climatologies and annual trends for 1958-2007 are presented for UCDW and ML variables, as well as stratification, wind stress and Ekman variables, and are analysed by frontal zone.

Trends in ML and SS variables are often similar in the Australian and Indian sectors; for example, any trends identified in density, salinity and temperature are positive. Trends in the Pacific sector are often of opposite sign to the other two sectors, in particular trends in salinity. Both ML salinity and

SSS are decreasing in all sectors north of the sACCf in the Pacific sector, in direct contrast to increasing salinity in the same latitudes in the Australian and Indian sectors. These results are consistent with the work of *Boyer et al.* (2005), who plotted vertical sections of salinity trends in the Indian and Pacific Oceans.

ML temperature and SST trends are generally increasing, although it is consistently the case, across all three ocean sectors, that they are not increasing in DJF and MAM in the sACCZ or in DJF in the AZ. The explanation for this in DJF, that was put forward in Chapter 5 for the Australian sector, would seem to hold in all three sectors; that is, that increasing wind stress in DJF mixes cooler remnant winter water into the ML, counteracting the effect of surface warming.

The above differences in upper ocean trends seem to be related, at least in part, to differences in the wind climatologies in the three sectors, including wind strength and position (Figures 6.6 and 6.6). In turn, changes in mean wind strength in each sector can be related to changes in SAM and, in the Pacific and northern latitudes of the Australian sector, to ENSO (Table 6.4).

It would seem that trends in UCDW variables may well be decoupled from surface trends and occur on time-scales that are centennial rather than decadal. This conclusion is based on the small number of significant correlations between mean wind stress and UCDW variables (Table 6.5) and their inconsistent signs, as well as the fact that there are fewer correlations in the sACCZ and AZ, where UCDW is nearer to the surface and more likely to be affected by the winds. However, the fact that there are a greater number of correlations north of the PF, where UCDW is deep, including some higher values, is worthy of consideration, as are trends such as decreasing temperature north of the PF, in both the Australian and Pacific sectors. Since only weak and inconsistently signed correlations were found, up to a 10-year lag, between UCDW variables and mean wind stress, it would seem that either UCDW trends are decoupled from trends in the winds or else the lag is such that it cannot be tested with the data available here.

There are differences in UCDW between the three sectors not just in terms of trends, but also in climatological values. Even though climatological values for UCDW density and salinity are consistent between sectors, differences are found in climatological values for UCDW vertical velocity, top upwelling depth and possibly temperature (Table 6.2). Trends in UCDW variables (Table 6.7) also vary depending on their geographical region. Despite there being many similarities between the Indian and Australian sectors (increasing vertical velocity north of the PF, decreasing density when shoaling, upwelling nearer to the surface), there is a major difference between them in UCDW temperature

trends. UCDW temperature is increasing in all depths in the Indian sector, and in the Australian sector where it is shoaling (sACCZ and AZ), but in the deep in the Australian and Pacific sectors UCDW temperature is decreasing.

It may be that the differing results for the three sectors are somehow related to the fact that UCDW in the Indian and Pacific sectors is comprised mainly of water that recirculates from the ACC into the Indian or Pacific Oceans and then re-enters UCDW (Figure 2.3) in the western Indian Ocean or the south-east Pacific Ocean (*Callahan*, 1972).

There are also differences between the sectors related to UCDW vertical velocity, which is increasing in the Indian (all zones), Australian (all zones, except SZ and AZ) and Pacific (PFZ only) sectors. In addition, it is decreasing in the SZ and STCZ in the Pacific sector. This means that UCDW vertical velocity is increasing in all three sectors in the PFZ, which is the zone where UCDW upwells along steeply tilted isopycnals (Figures 3.3, 6.1 and 6.2). This is an interesting result, which is probably not related to wind stress (Table 6.5) and also does not appear to be related to trends in Ekman pumping rate. However, increasing Ekman pumping rate is found in the sACCZ in summer in all three sectors (Tables A.3, A.6 and A.9). This is not accompanied by an increase in northward Ekman transport, which could mean that nutrients are available for longer in this region.

A study into the number of times UCDW can be detected in the ML, either by upwelling or by upwelling and then moving northward in the ML, shows some interesting results. Firstly, the Pacific sector is unusual in that UCDW can be found in the ML only about half as often as in the other two sectors (Table 6.11 and Figure 6.7) and the main upwelling occurs in autumn/winter/spring, unlike the other two sectors where it occurs in summer/autumn. Secondly, in the Australian sector, there is an increasing trend in the number of times UCDW can be detected in the ML, from the 1960s to the 1990s, consistent with the trends of UCDW upwelling closer to the surface and deepening of the ML in that sector. This is in contrast to a drop in the number of detections in the Indian sector, in the last decade or so. These results have important implications for the delivery of nutrients, especially iron, to the ML for use in primary production, but they must be considered along with trends in other variables, such as MLD, ML temperature and stratification, as well as changes in the light regime, before conclusions can be drawn for a particular sector.

Chapter 7

Interannual variability in phytoplankton biomass and biological productivity in the Australian sector of the Southern Ocean in 1997-2007

This chapter examines climate variability on interannual timescales and its effect on phytoplankton biomass and primary productivity in the Australian sector of the SO, from the Subantarctic zone to the Antarctic continent. Three types of data are utilised: satellite data (for chlorophyll-*a*, PAR and sea-ice concentration), modelled primary productivity data (calculated with the VGPM model of *Behrenfeld and Falkowski* (1997)) and model reanalysis data (SODA for hydrodynamic variables). Seasonal time series (spring and summer only, since the majority of primary production in the SO occurs then), over the study period 1997-2007, are constructed for five-degree latitudinal zones that approximate the SO frontal zones. In order to examine the effect of the various variables on phytoplankton biomass and biological productivity, correlations are computed between the variables and each of chlorophyll-*a* and primary productivity, using detrended time series. The variables considered include a number of climate indices, such as SAM, MEI and PDO, as well as sea-ice concentration, PAR and the SODA-derived variables discussed in Section 3.4.

7.1 Chlorophyll-*a* and Primary Productivity

An example of SeaWiFS chlorophyll-*a* for January 2000 is shown in Figure 7.1, overlaid by an outline of the study region. Mean January (1998-2007) chlorophyll-*a* and primary productivity (VGPM) are shown in Figure 7.2

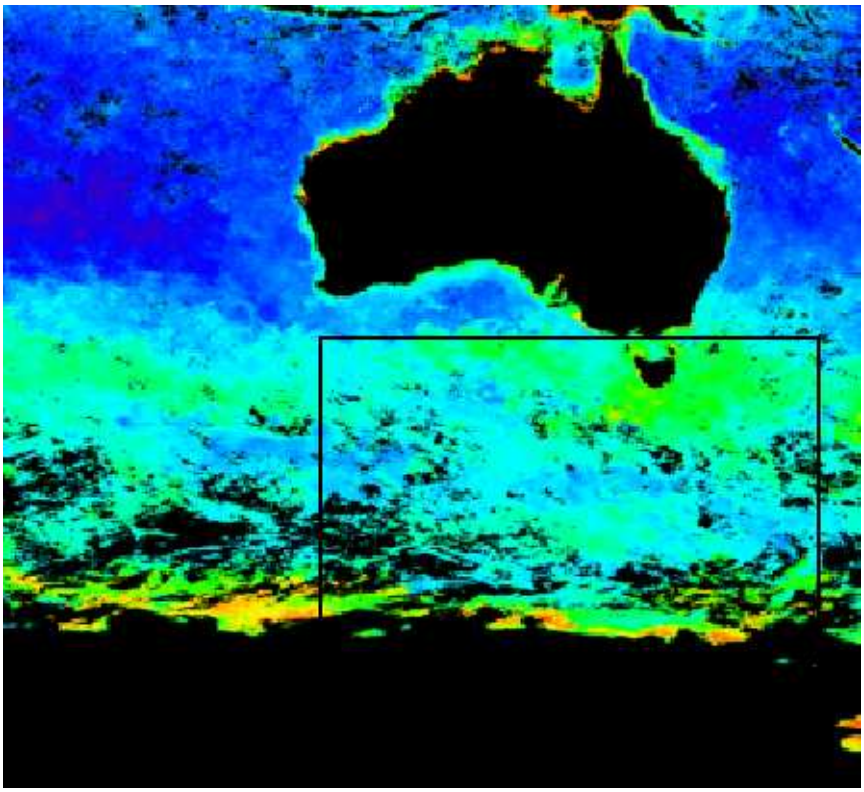

Figure 7.1: SeaWiFS chlorophyll-a for January 2000, including the Australian sector (110-160°E, 40-70°S) considered in this study.

(where slight differences in the Antarctic coastline between the plots are due to the different masks applied). There are high chlorophyll-a values (around 0.5 mg m^{-3}) to the east of Tasmania, with the highest values (some in excess of 1 mg m^{-3}) near the Antarctic continent, consistent with observations (*Wright and van den Enden*, 2000).) The considerable interannual variation in chlorophyll-a is demonstrated in Figure 7.3 for each of the six zones over the period September 1997 to August 2007. In 65-70°S, chlorophyll-a values generally peak around 1 mg m^{-3} or less, although the values for 2000 and 2002 are 2 and 3 times that, respectively. Peak chlorophyll-a values in the 65-70°S zone generally occur in December or January, after the 60-65°S zone where maximum values are usually in November. However in 60-65°S the 2000, 2002 and 2007 peaks are in January, December and December, respectively, corresponding to extreme values of around 0.6 mg m^{-3} in each case, compared with the usual peaks of 0.4 mg m^{-3} or less. During 1997-2007, peak values in the 50-55°S zone were in the range 0.2-0.3 mg m^{-3} and appear to be decreasing with time. Further north, chlorophyll-a values increase again with peaks up to 0.4 and 0.5 mg m^{-3} for 45-50°S and 40-45°S, respectively. These peaks occur anywhere between November and February, illustrating the interannual variability in phenology and magnitude of the bloom.

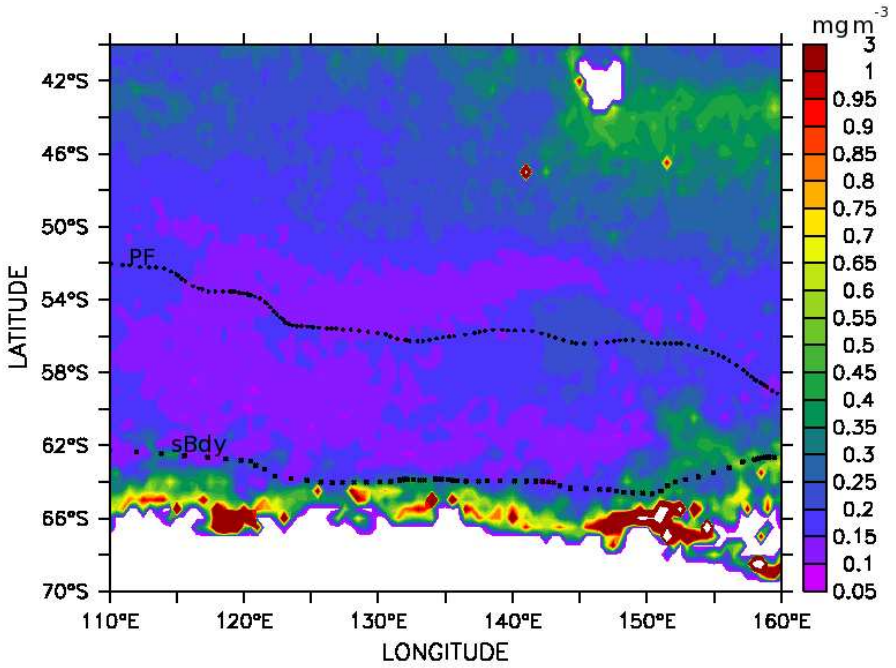

(a)

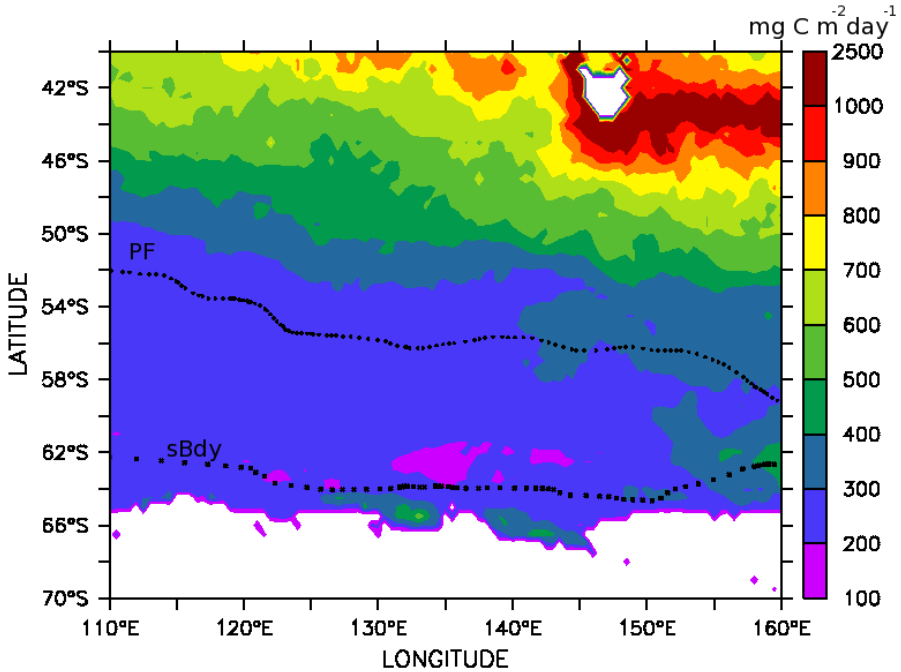

(b)

Figure 7.2: Mean (1998-2007) January values for (a) SeaWiFS chlorophyll-*a* and (b) VGPM primary productivity, overlaid by the PF and sBdy (*Orsi and Ryan*, 2001, updated 2006).

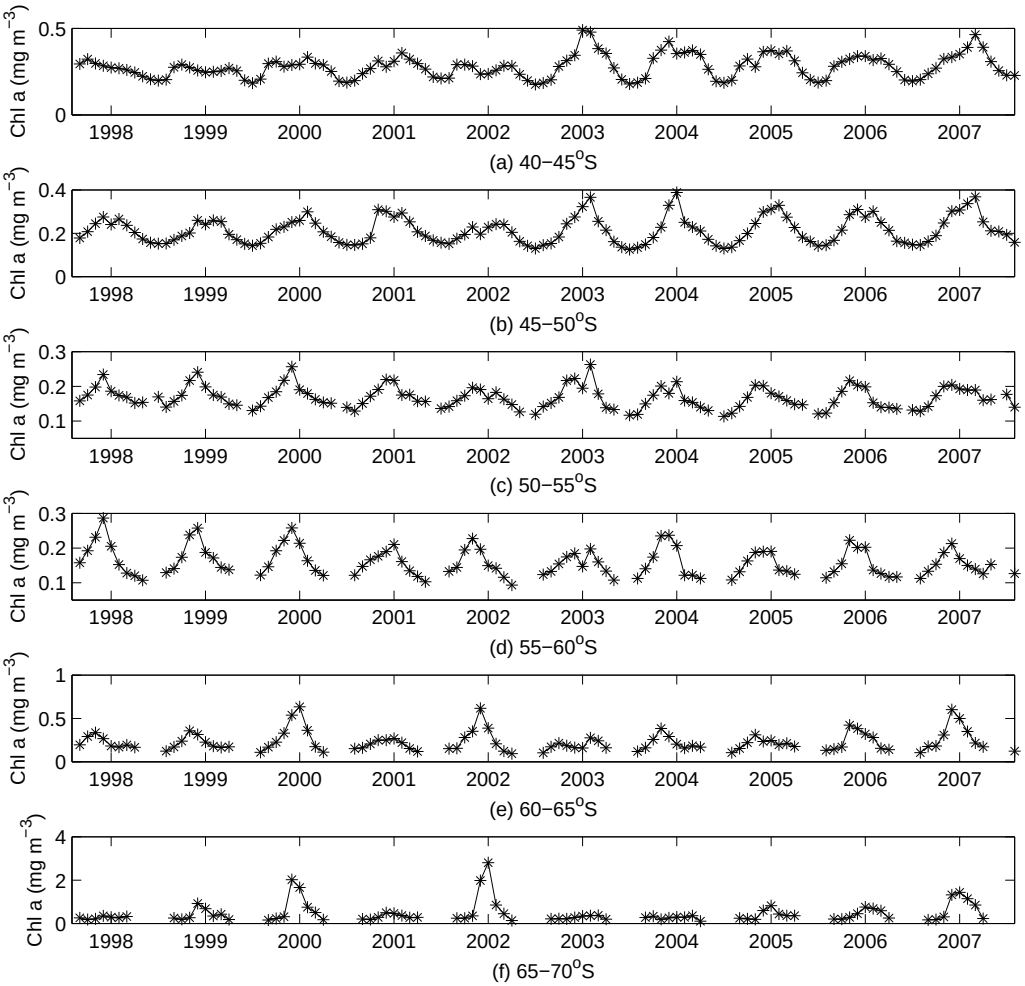

Figure 7.3: SeaWiFS chlorophyll-a time series for September 1997-August 2007 for the (a) 40-45°S, (b) 45-50°S, (c) 50-55°S, (d) 55-60°S, (e) 60-65°S and (f) 65-70°S zones. Winter values are missing, which means that the time series starts again in July for (c), August for (d) and (e) and in September for (f). The tick mark is for January of the year indicated. Note the different vertical scales.

Table 7.1: Climatological values for Austral spring and summer by latitudinal zone (n/a = not applicable).

	65-70°S	60-65°S	55-60°S	50-55°S	45-50°S	40-45°S
Chlorophyll-*a* (mg m^{-3})						
Summer	0.79	0.31	0.19	0.20	0.27	0.36
Spring	0.23	0.24	0.17	0.18	0.20	0.29
Primary Productivity ($mgCm^{-2}day^{-1}$)						
Summer	277.7	250.9	275.5	364.2	592.5	797.0
Spring	72.4	131.5	157.2	246.7	363.6	543.6
Mean Wind Stress (N m^{-2})						
Summer	0.094	0.064	0.12	0.16	0.14	0.089
Spring	0.072	0.078	0.14	0.16	0.15	0.10
Sea-ice Concentration(%)						
Summer	69.8	31.7	n/a	n/a	n/a	n/a
Spring	86.4	59.9	n/a	n/a	n/a	n/a
PAR (Einst. m^{-2} day^{-1})						
Summer	31.4	32.5	36.7	40.0	43.4	48.0
Spring	25.0	21.6	24.5	28.9	32.9	37.7
SST (°C)						
Summer	-0.80	1.15	3.37	6.31	10.32	14.03
Spring	-1.40	-0.71	1.20	4.64	8.73	11.59
MLD (m)						
Summer	86.9	38.7	35.4	48.9	55.4	30.5
Spring	117.4	71.8	88.1	124.0	152.5	112.4
Stratification (s^{-2})						
Summer	2.8×10^{-5}	5.3×10^{-5}	5.3×10^{-5}	5.1×10^{-5}	5.9×10^{-5}	8.2×10^{-5}
Spring	1.7×10^{-5}	3.7×10^{-5}	3.4×10^{-5}	2.4×10^{-5}	2.3×10^{-5}	3.1×10^{-5}
Ekman Transport (Sv)						
Summer	n/a	0.98	2.7	4.5	4.8	3.2
Spring	n/a	1.4	3.0	4.3	4.7	3.8
Ekman Pump Rate (ms^{-1})						
Summer	n/a	1.9×10^{-6}	1.1×10^{-6}	n/a	n/a	n/a
Spring	n/a	1.8×10^{-6}	0.67×10^{-6}	n/a	n/a	n/a
Top UCDW Depth (m)						
Summer	n/a	41.3	52.1	108.8	346.8	1124
Spring	n/a	58.9	70.2	120.9	422.2	1112

Table 7.2: Correlations (significant at the 95% confidence level) between chl a and PP by latitudinal zone.

	65-70°S	60-65°S	55-60°S	50-55°S	45-50°S	40-45°S
Summer	0.89	0.75	0.81	0.86	0.79	0.94
Spring	0.42	0.90	0.92	0.97	0.96	0.77

In contrast to chlorophyll-*a*, primary productivity generally increases to the north (Figure 7.2, Table 7.1). This is evident also in Figure 7.4, which shows a climatology of primary productivity values by latitude. The exception to this is the 65-70°S zone in December, January and February, where primary productivity is higher than in 60-65°S and 55-60°S. This is consistent with high chlorophyll-*a* near the Antarctic shelf, due possibly to nutrients on the shelf but not the upwelling of nutrients, since UCDW is not found south of the Southern Boundary of the ACC ($\sim$ 65°S).

Strong correlations are found between chlorophyll-*a* and primary productivity (0.75-0.97), in both spring and summer in all zones, except for spring in the 65-70°S zone (0.42) (Table 7.2).

7.2 Controls on Chlorophyll-*a* and Primary Productivity

This section will focus on the main factors, found in Tables 7.3 and 7.4, that influence chlorophyll-*a* and primary productivity in the Southern Ocean. It should be noted that no correlations were found between chlorophyll-*a* or primary productivity and the MEI or the southern-most position of UCDW.

7.2.1 Sea-ice concentration

An example of sea-ice concentration is shown in Figure 7.5 for August 2007 and climatological values for sea-ice concentration are given in Table 7.1 and Figure 7.6. Minimum sea-ice concentration occurs in March, with maximum values in June/July. Little or no sea-ice is found north of 60°S and sea-ice concentrations of approximately 86% and 60%, for the 65-70°S and 60-65°S zones in spring, reduce to 70% and 32% in summer. Sea-ice concentration is an important factor in controlling the levels of chlorophyll-*a* (Table 7.3), in agreement with previous studies in this sector (*Sokolov*, 2008), including the inverse nature of the relationship. There are also similar correlations between primary productivity and sea-ice concentration (Table 7.4).

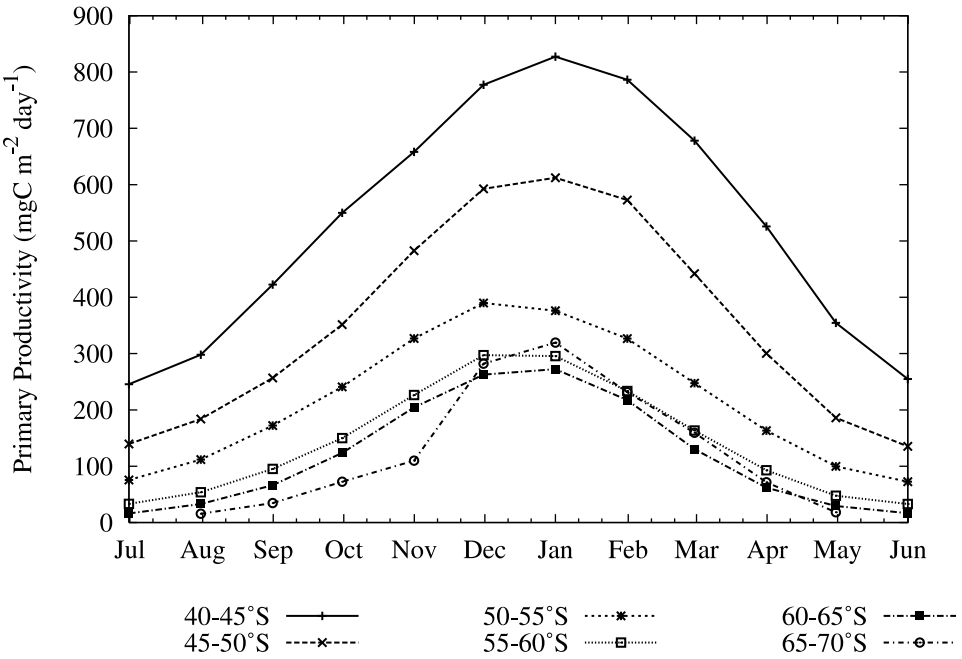

Figure 7.4: Climatological (1997-2007) VGPM primary productivity data by latitudinal zone.

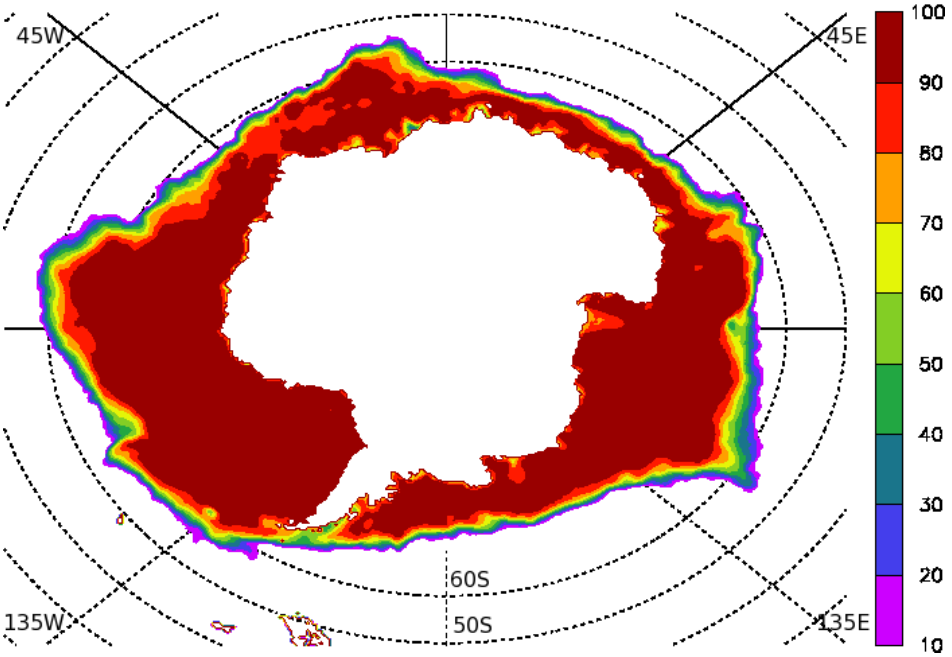

Figure 7.5: Sea-ice concentration (%) for August 2007.

Table 7.3: Correlations (significant at the 95% confidence level) between various variables and chlorophyll-*a*, by latitudinal zone and season, in decreasing order. PAR values for 65-70°S are not available in spring. Abbreviation of variable names is as follows: Sea-ice = Sea-ice concentration, meanWS = Mean wind stress, maxWS = Maximum wind stress, Strat = Stratification, Top UCDW = Top UCDW depth, EkPump = Ekman pumping rate, EkTrans = Ekman transport.

		Summer			
65-70°S	60-65°S	55-60°S	50-55°S	45-50°S	40-45°S
Sea-ice (-0.65)	PDO(-0.67)	PAR(0.70)	PAR(0.44)		PDO(0.47)
PDO(-0.58)	SST(-0.66)	SST(-0.61)	SST(-0.39)		Strat(0.42)
SAM(0.48)	Strat(-0.60)	Strat(-0.47)			
	meanWS(0.55)				
	EkTrans(0.47)				
	Top UCDW(0.39)				
		Spring			
65-70°S	60-65°S	55-60°S	50-55°S	45-50°S	40-45°S
Sea-ice(-0.53)	PAR(0.82)	PAR(0.90)	PAR(0.94)	PAR(0.86)	PAR(0.55)
	Sea-ice(-0.69)	SST(0.59)	MLD(-0.74)	SST(0.82)	MLD(-0.56)
		MLD(-0.58)	SST(0.70)	Strat(0.69)	Strat(0.42)
		EkPump(-0.37)	Strat(0.47)	MLD(-0.68)	SST(0.37)
			meanWS(-0.41)		
			EkTrans(-0.40)		

Table 7.4: Correlations (significant at the 95% confidence level) between various variables and primary productivity, by latitudinal zone and season, in decreasing order. PAR values for 65-70°S are not available in spring. Abbreviation of variable names is as in Table 7.3

.

		Summer			
65-70°S	60-65°S	55-60°S	50-55°S	45-50°S	40-45°S
PDO(-0.57)	SST(-0.52)	PAR(0.82)	PAR(0.70)		Strat(0.45)
SAM(0.48)	PAR(0.50)	MLD(0.39)			
Sea-ice(-0.45)	Top UCDW(0.45)				
	PDO(-0.44)				
		Spring			
65-70°S	60-65°S	55-60°S	50-55°S	45-50°S	40-45°S
Sea-ice(-0.81)	PAR(0.96)	PAR(0.98)	PAR(0.98)	PAR(0.95)	PAR(0.94)
Strat(0.51)	Sea-ice(-0.79)	SST(0.79)	MLD(-0.76)	SST(0.82)	MLD(-0.84)
maxWS(-0.38)	EkPump(-0.47)	MLD(-0.70)	SST(0.73)	MLD(-0.71)	SST(0.77)
	SST(0.38)	maxWS(-0.38)	Strat(0.51)	Strat(0.43)	
	maxWS(-0.37)		maxWS(-0.43)	meanWS(-0.39)	
			meanWS(-0.43)	EkTrans(-0.36)	
			EkTrans(-0.41)		

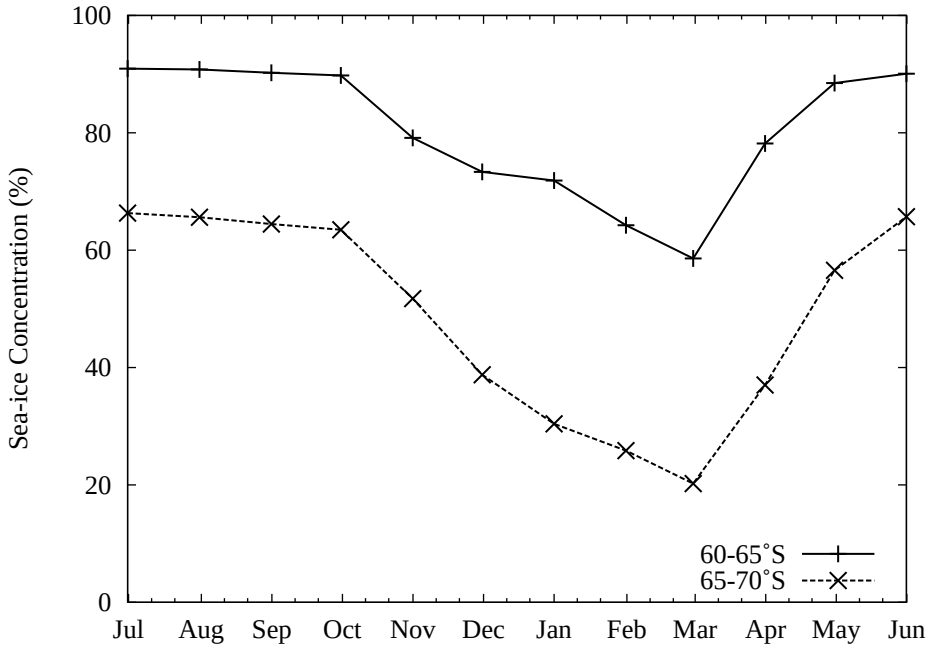

Figure 7.6: Climatological sea-ice concentration (%).

7.2.2 PAR

Climatological values for PAR are given in Table 7.1, where PAR is shown to increase northwards, except in spring in the most southerly zone, where the value of PAR is higher in the 65-70°S zone than in 55-65°, due to decreased cloud cover (*Sokolov*, 2008). Light availability has been suggested as one of the major controls on primary productivity in the Southern Ocean (*Nelson and Smith*, 1991). Here, PAR was found to be highly positively correlated with chlorophyll-*a* in spring (0.82-0.94, except for 0.55 in 40-45°S, Table 7.3) and primary productivity in spring (0.94-0.98, Table 7.4), when the region is light-limited. These correlations are found for all zones except 65-70°S, where values for PAR are generally not available between May and September, so that in this case there is no SON time series. PAR is also positively correlated with chlorophyll-*a* (50-60°S) and primary productivity (50-65°S) in summer.

7.2.3 SST

Climatological values for summer and spring SST (Table 7.1) increase to the north, with spring values lower than summer values. Results of correlations between chlorophyll-*a* or primary productivity and SST, (Tables 7.3 and 7.4, respectively) show that, in summer, there is a negative correlation between SST and both chlorophyll-*a* (50-65°S) and primary productivity (60-65°S), whereas in spring (40-60°S) there is a positive relationship. No significant correlations between SST and chlorophyll-*a* and primary productivity are found in 65-70°S in either season. The difference between the direction of the correlations in

spring and summer may be related to the fact that in spring increasing temperature leads to increasing ice melt, which leads both to increased iron being released as well as to the formation of shallower mixed layers, both of which are related to increases in chlorophyll-a and primary productivity. However, in summer in 50-60°S where chlorophyll-a is low (Table 7.1), increasing SST may not increase chlorophyll-a if nutrients such as iron are limiting (*de Baar et al.*, 2005).

7.2.4 Mixed layer depth and stratification

The depth of the mixed layer (Table 7.1) varies between latitudinal zones and seasons. Deeper mixed layers occur in spring than in summer and the mixed layer generally shallows towards the Antarctic continent, except for the most northerly zone and 65-70°S, which are both exceptions. Negative correlations, between MLD and both chlorophyll-a and primary productivity, are found in spring for all but the two southern-most zones (Tables 7.3 and 7.4). These results are consistent with previous studies (*Mitchell and Holm-Hansen*, 1991; *de Baar et al.*, 2005), indicating that as the mixed layer deepens, chlorophyll-a decreases (due to light limitation). Interestingly, no significant correlations are found in summer between MLD and chlorophyll-a, and only one between MLD and primary productivity. This would seem to indicate that mixed layers are already sufficiently shallow in summer.

Climatological values for stratification in summer, also given in Table 7.1, generally increase to the north. However, in spring, the highest value is in the 60-65°S zone, north of which stratification decreases, except in the most northerly zone. Stratification is higher in summer than in spring in all cases, generally by a factor of 1.5-2.5, due to higher temperatures, sea-ice melt and lower wind stress. Positive correlations are found between stratification and both chlorophyll-a and primary productivity in spring in 40-55°S and summer in 40-45°S (Tables 7.3 and 7.4). The opposite is true for the only other correlation between stratification and chlorophyll-a in summer though, which occurs in 60-65°S, a region of low wind stress in summer (Table 7.1), where decreased stratification (and increased mixing of nutrients) may be related to an increase in chlorophyll-a.

7.2.5 PDO

A number of significant correlations are found between the PDO and both chlorophyll-a and primary productivity (Tables 7.3 and 7.4), but only in summer. The sign of the correlations is negative in 60-70°S and positive in 40-50°S. The fact that there are correlations between chlorophyll-a and PDO is con-

sistent with work by *Martinez et al.* (2009) who have recently shown that multi-decadal changes in global phytoplankton abundance can be related to basin-scale oscillations of the physical ocean (ie. the PDO in this region), which affect SST and hence chlorophyll-*a*.

7.2.6 Comparison of controls on chlorophyll-*a* with controls on primary productivity

As would be expected from the form of Equation (3.1), significant correlations are found between primary productivity and chlorophyll-*a*, PAR, MLD and SST (Tables 7.2 and 7.4). Interestingly, the modelled primary productivity is also correlated with sea-ice concentration, stratification and mean and maximum wind stress, which are not represented explicitly in the model. A comparison of Tables 7.3 and 7.4 shows very similar results for correlations of factors with either chlorophyll-*a* or primary productivity. In the more detailed analysis to follow, the work will focus on correlations with chlorophyll-*a*, given the various caveats associated with the modelling of primary productivity.

7.3 Controls on Chlorophyll-*a* by Zone

7.3.1 Spring

Based on the results from Table 7.3, the important factors that influence chlorophyll-*a* in the Southern Ocean during spring are: sea-ice concentration in 60-70°S (negative correlation); PAR, which is highly positively correlated across all zones, except 65-70°S where September data is missing; SST (positive correlation) and MLD (negative correlation) for 40-60°S and stratification (positive correlation) for 40-55°S. It should be noted, however, that many of these factors covary. Some (lower-valued) correlations are also found in 50-55°S between chlorophyll-*a* and Ekman transport and mean wind stress and in 55-60°S between chlorophyll-*a* and Ekman pumping rate. Interestingly, these correlations are negative in each case, indicating an increase in chlorophyll-*a* associated with a decrease in the other variable. In the case of mean wind stress this may indicate that increased chlorophyll-*a* is related to reduced mixing of phytoplankton away from available light, given the importance of light in spring. A possible explanation for the negative correlation between chlorophyll-*a* and both the Ekman pumping rate and the northward Ekman transport may involve an increased phytoplankton residence time, due partly to an increased residence time for essential nutrients such as iron, which are found in this region in spring (see Figure 5.15) and remain in the region for sufficient time to be utilized by phytoplankton (see Section 2.9.5).

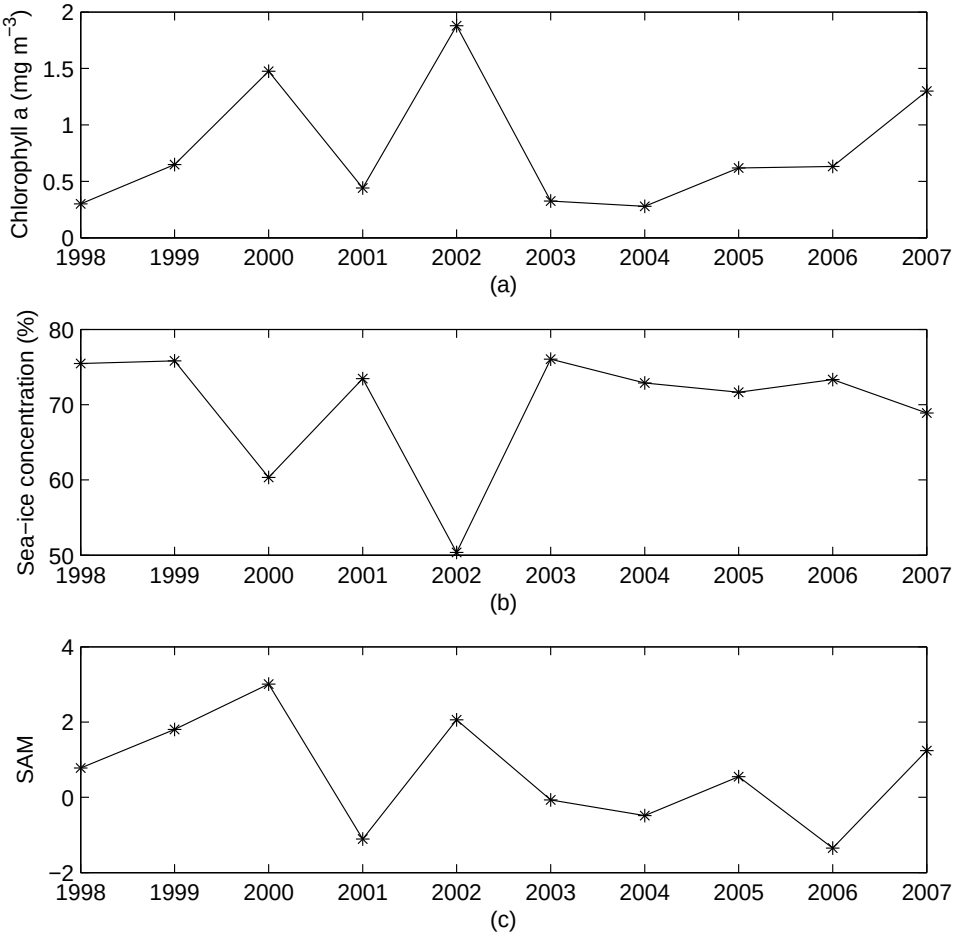

Figure 7.7: Mean summer time series for 1998-2007 in 65-70°S zone for (a) Chlorophyll-*a*, (b) Sea-ice concentration and (c) SAM.

7.3.2 The 65-70°S zone in summer

In the 65-70°S zone, significant correlations exist between chlorophyll-*a* and sea-ice concentration (negative), PDO (negative) and SAM (positive) (Table 7.3). However, since no correlation was found between SAM and sea-ice concentration, in contrast to PDO and sea-ice concentration, which were found to be correlated, this work will concentrate on the former variables. Examination of the time series for chlorophyll-*a*, sea-ice concentration and SAM in Figure 7.7 indicates that the maximum chlorophyll-*a* values in 2000 and 2002 coincide with low sea-ice concentration and high SAM values. Using a multi-variate linear regression model it is found that sea-ice concentration and SAM together can explain 51% of the variance in chlorophyll-*a*, even though the seasonal time series in Figure 7.7 do not all show the same trend over the 10 years.

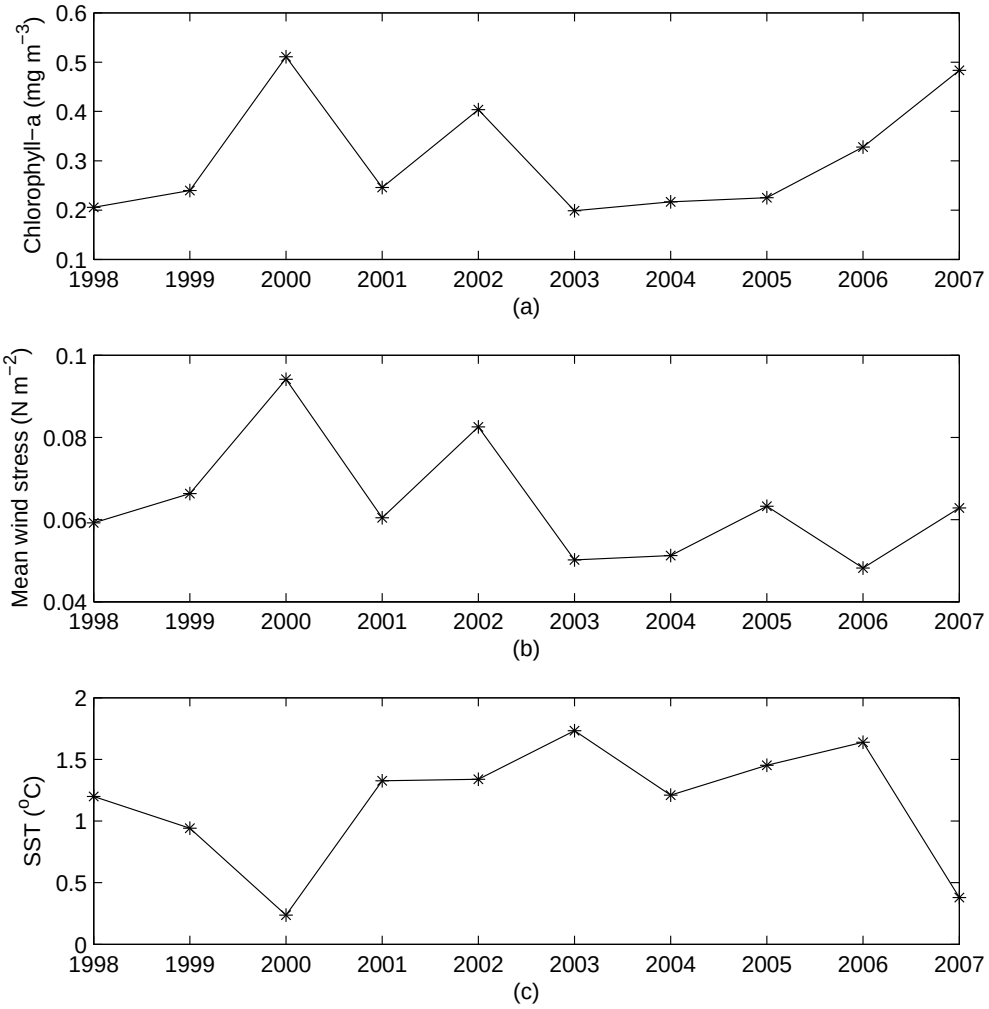

Figure 7.8: Mean summer time series for 1998-2007 in 60-65°S zone for (a) Chlorophyll-*a*, (b) Mean wind stress and (c) SST.

7.3.3 The 60-65°S zone in summer

The largest list of factors affecting chlorophyll-*a* in summer is found for the 60-65°S zone in summer: PDO, SST and stratification (negatively correlated); mean wind stress, northward Ekman transport and UCDW top depth (positively correlated). Since nutrient-rich UCDW upwells between the PF and the sBdy of the ACC and then moves northward under Ekman transport, it seems worthwhile to investigate these connections, despite the fact that the correlations are relatively low. Many of the factors in the list above co-vary (for example, stratification is affected by SST and mean wind stress) and only SST and mean wind stress are found to be uncorrelated. The time series for these two variables, as well that for chlorophyll-*a*, are shown in Figure 7.8, where it can be seen that high chlorophyll-*a*, again in 2000, 2002 and 2007, is related to high mean wind stress occurring at the same time as low SST. In this case, SST and mean wind stress together account for 55% of the variance in chlorophyll-*a* (noting again that the 10-year trends are not the same for each of the variables).

The positive correlation between UCDW top depth and chlorophyll-*a* is interesting, in that it implies that when UCDW is not advected as close to the surface, chlorophyll-*a* increases. A negative correlation is found between UCDW top depth and SST; that is, when UCDW is nearer to the surface, SST increases (and chlorophyll-*a* decreases). In summer in the 60-65°S zone, the climatological value for SST is around 1.2°C (Table 7.1), while the UCDW temperature is around 1.9°C (Table 5.1). This is consistent with UCDW nearing the surface having a warming effect on SST, as indicated above. However, this is clearly not the whole story, firstly, because these two factors do not explain all the variance in chlorophyll-*a* and secondly, because UCDW carries nutrients that are essential for primary production. It is hypothesised that favourable conditions for phytoplankton growth, in summer in the 60-65°S zone, involve high wind stress to mix these nutrients into the mixed layer, combined with low SST (Figure 7.8). Iron sources could include both UCDW (which intrudes into the mixed layer mainly in summer and autumn in this zone), as well as the melting sea-ice, since a significant correlation between sea-ice concentration in the previous spring and chlorophyll-*a* in the following summer is also found (not presented).

7.3.4 The 50-55°S and 55-60°S zones in summer

Both PAR (positive correlation) and SST (negative correlation) are significant factors affecting chlorophyll-*a* in 50-60°S in summer, in addition to stratification in 55-60°S (Table 7.3). Similarly, PAR is positively correlated with

primary productivity in 50-60°S and MLD in 55-60°S (Table 7.4). Again, as in spring, these factors covary.

7.3.5 The 40-45°S and 45-50°S zones in summer

None of the factors considered here was found to be significantly correlated with chlorophyll-*a* in the 45-50°S zone. However, PDO and stratification were both positively correlated with chlorophyll-*a* in the 40-45°S zone (Table 7.3), in contrast to the negative correlations found between these variables and chlorophyll-*a* further south. Both of these regions can be impacted by mineral dust deposition from the Australian continent (*Gabric et al.*, 2010) and this is consistent with the large interannual variability in the phenology and magnitude of the bloom (Figure 7.3).

7.4 Comparison with Previous Studies

In their study of primary production in the SO in 1997-2006, *Arrigo et al.* (2008) found that interannual variability in primary production covaried with sea-ice cover, although changes in SST played a role. This study agrees with those results, finding an inverse relationship between chlorophyll-*a* and sea-ice concentration, as pointed out for this region by *Sokolov* (2008), as well as the same relationship with primary production. Other studies have highlighted the importance of irradiance in the light-limited SO (*Smith and Comiso*, 2008) and this work finds strong correlations between PAR and chlorophyll-*a* in spring and in the 50-60°S zones in summer. However, no correlations between PAR and chlorophyll-*a* are found in summer in the two most southerly zones, which agrees with recent work by *Venables and Moore* (2010), who report that for at least 3 months of the year (summer), light limitation does not significantly constrain chlorophyll-*a* in HNLC regions, such as the region under study here.

The fact that chlorophyll-*a* is likely to be affected by MLD, stratification and SST has been shown in previous studies (*Mitchell and Holm-Hansen*, 1991; *de Baar et al.*, 2005; *Behrenfeld et al.*, 2006; *Arrigo et al.*, 2008) and these were found to be important factors here, bearing in mind that they covary. However, no correlations were found here with MLD in summer, perhaps due to shallowing of the mixed layer in that season. The interesting thing about SST is that its correlation with chlorophyll-*a* is negative in summer, but positive in spring (a pattern that is repeated for stratification, apart from the 40-45°S value). Previous work has already identified an inverse relationship between chlorophyll-*a* and SST at global spatial scales and interannual timescales (*Behrenfeld et al.*, 2006; *Martinez et al.*, 2009). In contrast, a recent study (*Saba et al.*, 2010b) has found a positive relationship between the

two at station HOT (Hawaiian Ocean Time-Series), where the authors found that surface fields, such as SST and chlorophyll-*a*, did not necessarily correlate well with the increase in integrated primary productivity, since the deep layer forcing was driving the increase. Also, *Arrigo et al.* (2008) found a complex relationship between primary production and SST in the SO, with positive correlations in some regions and negative correlations in others. They attribute this to the fact that SST affects primary production both directly (through the relationship between temperature and phytoplankton metabolic rate) and indirectly (through the effect of temperature on stratification and sea-ice). The present study also finds correlations between the PDO and both chlorophyll-*a* and primary productivity in summer: positive in 40-45°S (chlorophyll-*a* only) and negative in both 60-65°S and 65-70°S. This is consistent with work by *Martinez et al.* (2009) who looked at the co-variability of chlorophyll-*a* and SST over decadal timescales and concluded that the spatial pattern of the changes bore the imprint of the PDO.

Perhaps surprisingly, this study finds only one significant correlation between both chlorophyll-*a* and primary productivity and SAM (positive in the 65-70°S zone in summer). This is in contrast to a previous study (*Lovenduski and Gruber*, 2005), which used SeaWiFS 8-day data from 1997-2004 and considered zones based on climatological fronts and thus differed slightly from the present study. The *Lovenduski and Gruber* (2005) study linked SAM to different variations in mid- and high-latitude primary production north and south of the Polar Front and suggested that the positive correlation of chlorophyll-*a* and SAM south of the Polar Front was related to an increased supply of iron during upwelling, while the negative correlation north of the Polar Front was because of stronger light limitation due to deeper mixed layers. However, the SAM-chlorophyll-*a* correlations in the study by *Lovenduski and Gruber* (2005) were actually only significant in the Subantarctic zone south of Australia and elsewhere they were small and often not statistically significant. *Arrigo et al.* (2008) conclude that 31% of the variation in annual production in the Southern Ocean is explained by SAM, but again the result is not statistically significant. The short data record and the seasonal approach may explain the lack of significant correlations in our study also. In fact, our study does find a combination of (non-significant) positive (50-70°S) and negative correlations (40-50°S) between SAM and chlorophyll-*a* in summer, in agreement with *Lovenduski and Gruber* (2005). This includes one in the 60-65°S zone that is significant at the 94% confidence level and is likely to be related to other significant factors found in that zone, such as mean wind stress and northward Ekman transport. Finally, it should be noted that in spring all the SAM-chlorophyll-*a* correlations appear to be positive, indicating that different

processes seem to be dominant in spring compared with summer.

When considering factors which affect chlorophyll-a it is worth noting the comments of *Behrenfeld et al.* (2009), who point out that correlations between SST and chlorophyll-a emerge because SST acts as a surrogate for other environmental factors (such as nutrients, including iron, and mixed layer light levels) that vary with SST and directly impact phytoplankton light levels. They also note that the relative importance of these factors varies over space and time, as has been demonstrated in this study.

7.5 Conclusions

Using a combination of satellite, model and model reanalysis data, the effect of interannual climate variability on phytoplankton biomass and primary productivity in the Australian sector of the SO during the period 1997-2007 has been investigated. In five-degree latitudinal zones that approximate the frontal zones of the ACC, factors that affect chlorophyll-a and primary productivity have been identified and examined and found to be very similar.

Apart from sea-ice concentration near the Antarctic continent, which is negatively correlated with both chlorophyll-a and primary productivity, very different factors are found to influence both chlorophyll-a and primary productivity in spring compared with summer.

In spring, the important factors are PAR, SST, MLD and stratification, bearing in mind that some of these factors co-vary. In the north in the 40-45°S zone, PDO and stratification are positively correlated with chlorophyll-a in summer, in contrast to zones further south. In summer in the zones near to and just north of the PF (50-60°S), PAR and SST are the most important factors, with SST negatively correlated with chlorophyll-a. A number of co-varying factors have been found that influence chlorophyll-a in the zone (60-65°S) south of the PF, where entrainment of UCDW brings nutrient-rich water to the near-surface. However, a multiple linear regression finds that 55% of the variance in chlorophyll-a in summer can be explained by a combination of SST (negative correlation) and mean wind stress (positive), whereas, in the 65-70°S zone in summer, sea-ice concentration (negative correlation) and SAM (positive) explain 51% of the variance in chlorophyll-a.

Considerable variability in both the phenology and magnitude of the bloom is found in the period 10 years from September 1997 to August 2007 studied here. In addition, the factors that influence phytoplankton biomass vary both spatially and temporally, since there is not only a difference in the relative importance of the factors in the various latitudinal zones, but there is also a difference between spring and summer.

Chapter 8

Trends in upper ocean structure and meridional circulation in the Australian sector of the Southern Ocean in 1997-2007 compared with trends in 1958-2007 and their connection with trends in primary productivity

The aim of the present chapter is to identify any trends in primary productivity and phytoplankton biomass over the study period (September 1997-August 2007), as well as trends in hydrodynamic variables, and to attempt to set these trends in the context of a longer time-frame. Non-parametric methods are used to identify trends in the various variables and, in the case of the hydrodynamic variables, the trends are compared with trends over the period 1958-2007, previously analysed in Chapter 5. Finally, the trends in various hydrodynamic variables are plotted as "running" sets of trends, to see if the the present trends are outside the range of earlier variability.

8.1 Trends over the Period 1997-2007

Before studying trends over the period 1997-2007, it is worth noting that the SAM does not display an increasing trend in summer and autumn over this time (*Monaghan et al.*, 2008), in contrast to the trend from the 1970s to the

late 1990s (*Thompson and Solomon*, 2002). The SAM index for summer for 1958-2007 is shown in Figure 5.14. The negative trend for 1997-2007 in summer is found to be significant only at the 90% confidence level and the trend for spring is not statistically significant. No trends were found for the PDO index, while the MEI had a positive trend in spring only.

8.1.1 Trends in satellite and SODA-derived variables

In addition to trends in chlorophyll-*a* and primary productivity, trends in all the variables identified in Chapter 7 as possibly affecting chlorophyll-*a* or primary productivity are presented in Table 8.1 for completeness. Sea-surface salinity (SSS) is also presented, although it was not included in the previous chapter as it is only an indirect control through its effect on stratification. No trends in summer or spring were found for PAR or the southern-most position of UCDW. The work in Chapter 5 analysed trends in hydrodynamic variables similar to those here, in the same region but over the longer time period 1958-2007, and when the trends in hydrodynamic variables from Table 8.1 are compared with those (Appendix A, Tables A.3-A.4), two differences are apparent. One is that the 1997-2007 trends are generally about an order of magnitude larger than the 1958-2007 trends and the second is that the sign of the trends is very often opposite to that for the longer time period.

8.1.2 UCDW intrusions into the mixed layer

The vertical advection of nutrient-rich UCDW into the mixed layer is thought to be critical for primary production (*Martin et al.*, 1990b; *Hoppema et al.*, 2003) and this may occur between the Polar Front and the Southern Boundary of the ACC. Here the frequency with which UCDW is entrained in the mixed layer is examined to see if any change has occurred over the period 1997-2007. Rather than using the SODA monthly datasets, here the SODA 5-day datasets (pentads) are used to analyse the frequency of intrusions on a finer time-scale. UCDW is deemed to have entered the mixed layer if the top position of UCDW (UCDW top depth) is shallower than the MLD at any particular grid-point. Values for UCDW top depth and MLD in summer (Table 7.1) may be misleading in that they imply that UCDW does not upwell high enough to enter the mixed layer, but that is because they are climatological rather than actual values.

The number of times UCDW is entrained in the mixed layer is presented by season and year for each of the five-degree latitudinal zones between 50 and 70°S in Figure 8.1, where the 73 pentads in a year are re-combined to form "seasons", which consist of 18 pentads, except for December which contains an

Table 8.1: Trends (per year) for September 1997 to August 2007 by latitudinal zone for Austral spring and summer. Blanks mean no significant trend was found (n/a=not applicable).No significant trends were found for PAR, SAM, MEI, PDO or southern-most position of UCDW.

	65-70°S	60-65°S	55-60°S	50-55°S	45-50°S	40-45°S
Chlorophyll-*a*						
(mg m^{-3} yr^{-1})						
Summer			-2.7×10^{-3}		7.2×10^{-3}	1.2×10^{-2}
Spring			-2.7×10^{-3}			
Primary Productivity						
(mg C $m^{-2}day^{-1}$ yr^{-1})						
Summer					8.4	14.7
Spring						
Mean wind stress						
(Nm^{-2} yr^{-1})						
Summer			-3.7×10^{-3}	-8.3×10^{-3}	-5.5×10^{-3}	
Spring	-8.7×10^{-3}	-5.7×10^{-3}	-1.4×10^{-2}	-1.4×10^{-2}	-5.8×10^{-3}	-4.6×10^{-3}
Sea-ice concentration						
(% yr^{-1})						
Summer			n/a	n/a	n/a	n/a
Spring	-0.31		n/a	n/a	n/a	n/a
SST						
(°C yr^{-1})						
Summer		4.3×10^{-2}	9.5×10^{-2}	6.7×10^{-2}		-4.5×10^{-2}
Spring	-3.3×10^{-2}	-5.4×10^{-2}	4.9×10^{-2}	5.7×10^{-2}		
SSS						
(yr^{-1})						
Summer		-2.0×10^{-2}		2.5×10^{-2}	4.0×10^{-2}	2.6×10^{-2}
Spring	-8.9×10^{-3}	-2.4×10^{-2}		2.3×10^{-2}	4.1×10^{-2}	2.0×10^{-2}
Mixed layer Depth						
(m yr^{-1})						
Summer		-2.4				
Spring	-7.3					
Stratification						
(s^{-2} yr^{-1})						
Summer				-2.6×10^{-6}	-4.1×10^{-6}	
Spring	9.0×10^{-7}		-3.1×10^{-6}	-2.0×10^{-6}	-1.9×10^{-6}	
Ekman transport						
(Sv yr^{-1})						
Summer	n/a		-7.7×10^{-2}	-2.3×10^{-1}	-1.7×10^{-1}	
Spring	n/a		-3.0×10^{-1}	-3.5×10^{-1}	-1.7×10^{-1}	-1.9×10^{-1}
Ekman Pumping						
($ms^{-1}yr^{-1}$)						
Summer	n/a			n/a	n/a	n/a
Spring	n/a	-1.7×10^{-7}		n/a	n/a	n/a
UCDW top depth						
(m yr^{-1})						
Summer	n/a	6.0	13.4	7.7		
Spring	n/a	5.0	12.0	8.4		

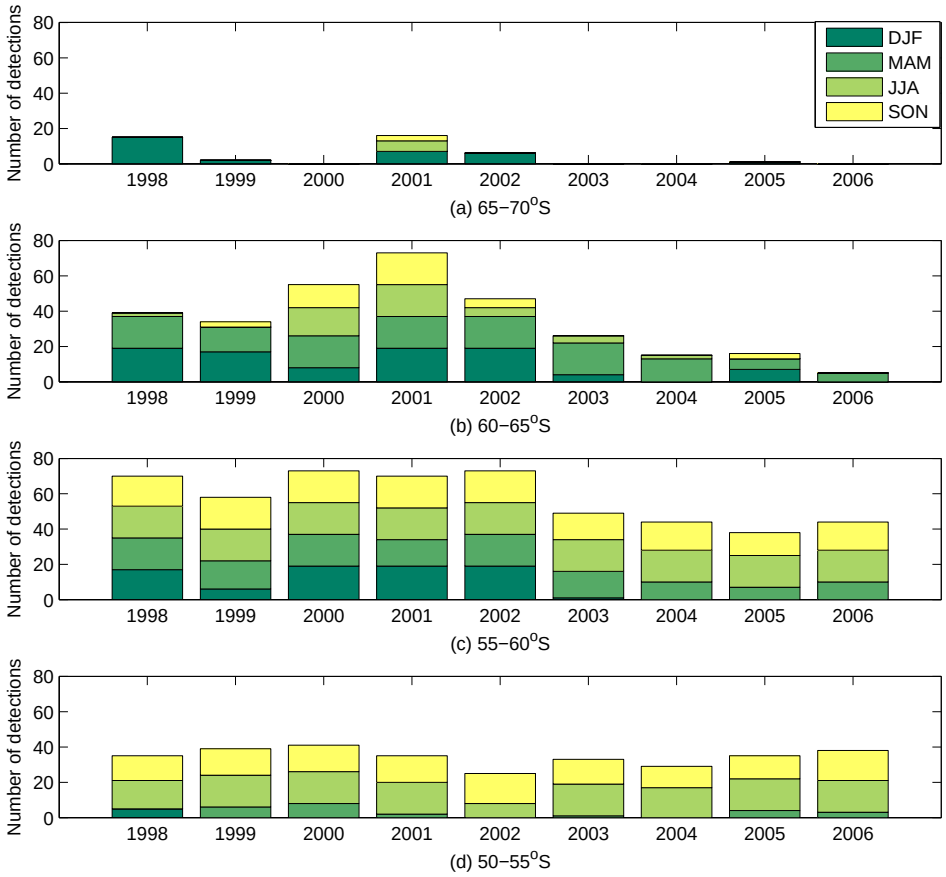

Figure 8.1: Number of times that UCDW is entrained in the mixed layer by season and year in (a) 65-70°S, (b) 60-65°S, (c) 55-60°S and (d) 50-55°S.

extra pentad. Figure 8.1 shows that UCDW reaches the 65-70°S zone only in some years, depending on the position of the Southern Boundary of the ACC, and because of this, neither climatological values (Table 7.1) nor trends (Table 8.1) for UCDW top depth are given in this zone. From Figure 8.1 it can be seen that UCDW is entrained in the 60-70°S zones predominantly in summer and autumn, a situation that was also noted in the previous 1958-2007 work of Chapter 5. In contrast to 60-70°S, in 55-60°S UCDW is found in the mixed layer in all four seasons in 1998-2002 and mainly in autumn and winter in the 50-55°S zone. The overall figure is consistent with the upwelling of UCDW in 60-65°S in summer and autumn, followed by the movement north of this water by Ekman transport, which leads to larger numbers of intrusions in winter and spring in 55-60°S and 50-55°S.

In terms of temporal trends in the number of intrusions of UCDW into the mixed layer in summer and spring, which are the seasons of interest here, a statistically significant decrease in summer is found in the 60-65°S and 55-60°S zones. This does not seem to be the case, however, in spring. These results

are consistent with trends found for UCDW top depth in summer in 60-65°S in Table 8.1 which show that UCDW is found further from the surface and the mixed layer is shallowing. Again, when these results are compared with the analysis for 1958-2007 in Chapter 5, the trend of a decreasing number of intrusions of UCDW in summer into the mixed layer in 1997-2007 is opposite to the trend for the longer time period.

8.1.3 Trends in chlorophyll-*a* and primary productivity

When the summer and spring time series for chlorophyll-*a* are examined for trends, small negative trends in chlorophyll-*a* are found for both seasons in the 55-60°S zone and small positive trends for both chlorophyll-*a* and primary productivity are found in summer in the two most northerly zones (40-50°S) (Table 8.1). These results are presented with the caveat that there is some uncertainty in primary productivity trends that are derived using surface chlorophyll-*a*, given that ocean colour models are more challenged to model short time-period trends (such as those considered here) than longer-period trends (*Saba et al.*, 2010b).

The summer chlorophyll-*a* results are consistent with the work of *Henson et al.* (2010), who produced global maps of the trend in monthly anomalies in SeaWiFS chlorophyll-*a* for September 1997 to December 2007, which show, for the Australian sector, a band of increasing chlorophyll-*a* around 40-45/50°S and a band of decreasing chlorophyll-*a* between about 45/50°S and 60°S, as well as small patches of increasing chlorophyll-*a* near the Antarctic continent. Since the trends in this work are presented by season and those of *Henson et al.* (2010) are annual trends, in order to make the comparison the assumption is made that, where there are opposite trends in summer and spring, the summer trends dominate, due to the larger values for summer both in chlorophyll-*a* and chlorophyll-*a* trends. Trends for primary productivity in summer are also similar to those found, for annual values, by *Henson et al.* (2010), who use primary productivity estimated from three different algorithms, one of which is the VGPM algorithm used here.

Further study is needed into the reasons for the positive trends that are found for chlorophyll-*a* and primary productivity in the two most northerly zones 40-45°S and 45-50°S in summer (Table 8.1), given that the only factors found here that correlate positively with chlorophyll-*a* are PDO and stratification in 40-45°S (Table 7.3) and stratification with primary production (Table 7.4). One factor that needs to be taken into account in these northern latitudes is the effect of mineral deposition of dust from the Australian continent, which can affect both the phenology and the magnitude of the bloom (*Gabric et al.*, 2010). Significant negative trends are also found for chlorophyll-*a* in the

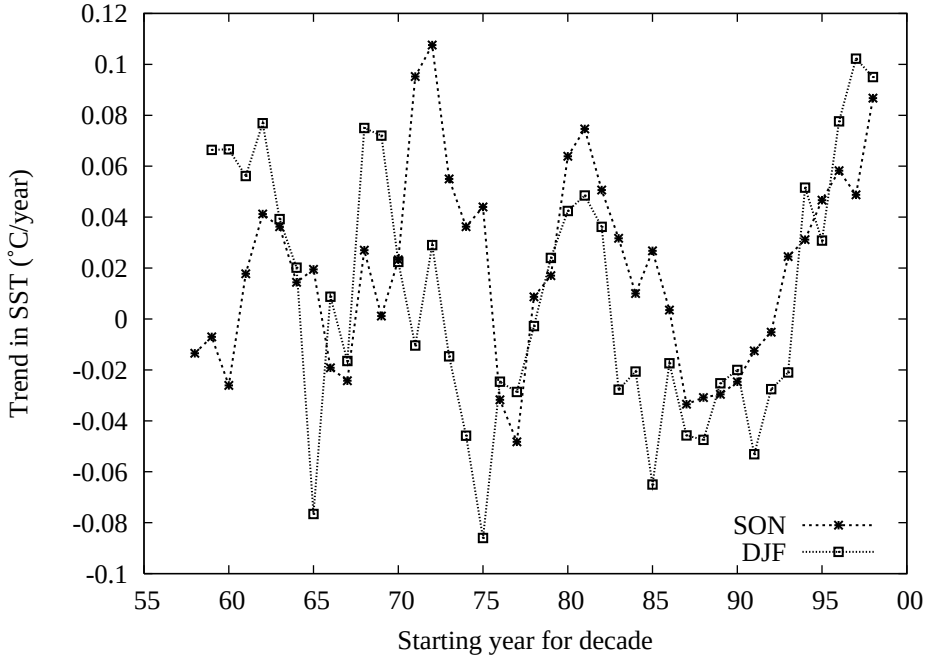

Figure 8.2: Running trends for 10 year sets of SST in 55-60°S, for summer (DJF) and spring (SON), for the decade beginning at the starting year.

55-60°S zone in both summer and spring (Table 8.1). In summer, these trends are consistent with the positive trends found for SST (Table 8.1), in conjunction with the negative correlation between SST and chlorophyll-*a* (Table 7.3) in that zone. The fact that wind stress is also decreasing there, presumably with a concomitant decrease in the mixing of nutrients in the ML, is also consistent with decreasing chlorophyll-*a*. However, SST cannot be the key factor in spring since the positive correlation between SST and chlorophyll-*a* (Table 8.1) then would suggest increasing not decreasing chlorophyll-*a*. In this case, a decrease in wind stress and a decrease in stratification (Table 8.1) may be relevant.

8.2 Comparison of 1997-2007 and 1958-2007 Trends

In order to compare the 1997-2007 trends with previous trends over longer time periods, two types of plots of "running" trends are produced, for each latitudinal zone and season, for the various SODA and SODA-derived variables presented in Table 8.1. The first type involves plotting sets of 10-year (decadal) trends for the decade beginning at the starting year, similar to the plots used by *Henson et al.* (2010) to consider trends in chlorophyll-*a* and primary production. Figure 8.2 shows such a plot for SST in 55-60°S in spring and summer. In this case, the 1998-2007 spring trend (final point on the graph) falls just within the bounds of the previous sets of spring decadal trends. On

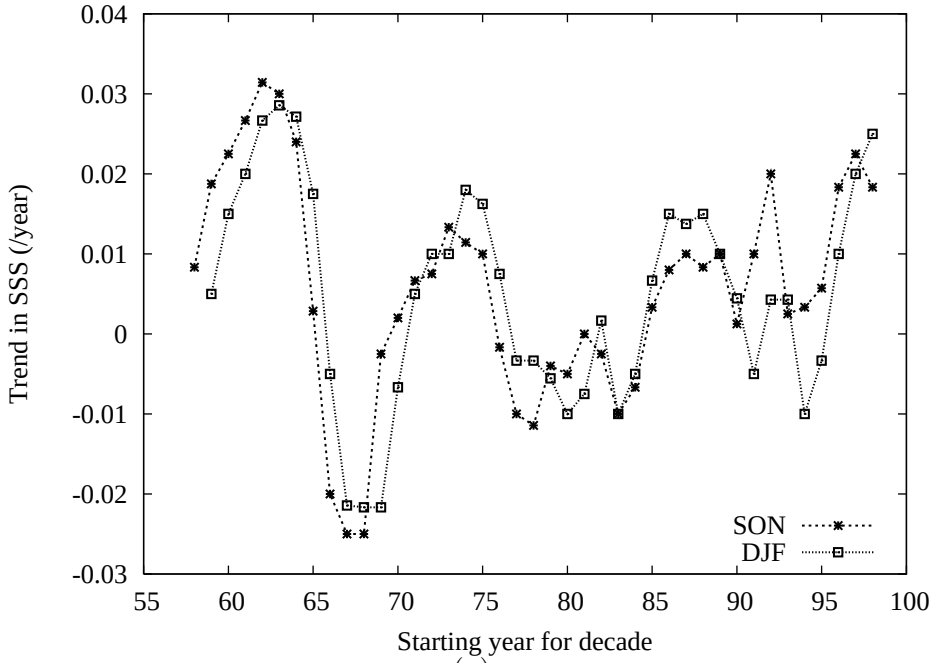

(a)

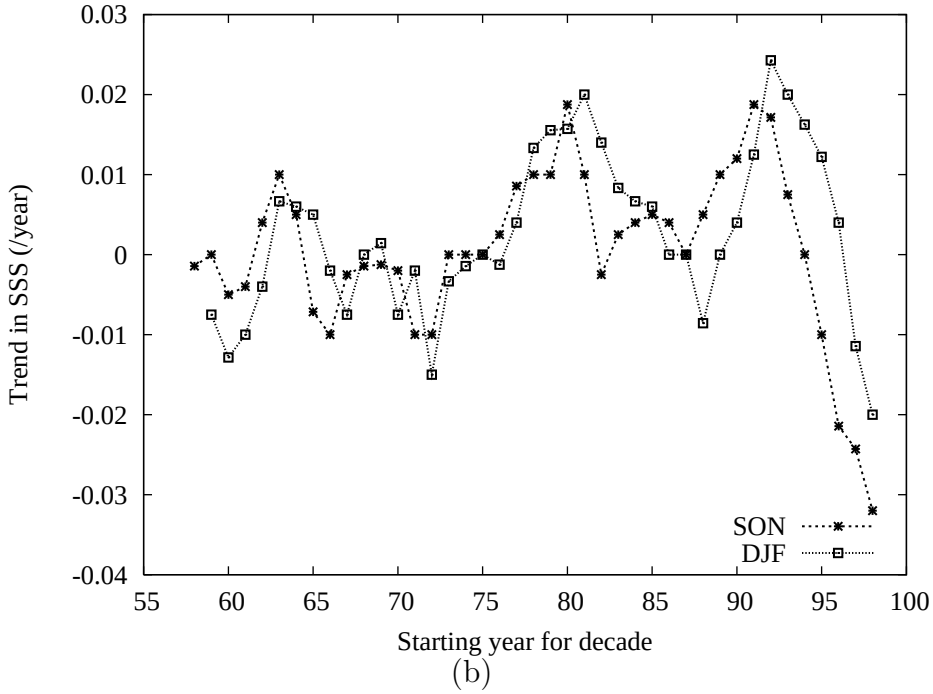

(b)

Figure 8.3: Trends for Sea-surface Salinity for spring (SON) and summer (DJF) in (a) 50-55°S and (b) 60-65°S, for the sets of 10-year time series, which begin at the starting year.

the other hand, the final two points on the graph of summer SST trends (that is the trends for 1997-2006 and 1998-2007) are outside the bounds of any previous summer trends. A similar plot for sea-surface salinity (Figure 8.3) shows that recent sets of 10-year trends for (a) the 50-55°S zone and (b) the 60-65°S zone fall (a) inside and (b) well outside the bounds of previous salinity trends. It is interesting to note that the recent salinity trends in the two zones are in opposite directions.

The second way of considering these trends in a "running" fashion is similar to plots for SAM by *Monaghan et al.* (2008). In this case the trends are calculated from the starting year to 2007, so that in Figures 8.4 and 8.5, the value at 1958 represents the trend in SST or SSS, respectively, from 1958-2007, and the value at 1959 is the trend from 1959-2007, while the final point is the trend for the time series, 1998-2007, considered in this study. The shaded areas show the 95% confidence interval for the trends and this increases as expected for later starting years, where the time series is shorter.

These figures show stable long term trends in SST and SSS, respectively, as well as what appear to be recent changes in the trends. For example, Figure 8.4(d)(blue) shows quite stable near-zero trends, for SST in summer in the 55-60°S zone, until the late 1980s, after which the SST trends become increasingly positive. This is consistent with Figure 8.2, where the last couple of sets of 10-year trends are outside the bounds of previous variability. The difference between SSS trends in different latitudinal zones detected in Figure 8.3 is also illustrated in parts (c) and (e) of Figure 8.5. SSS trends are increasing in the 50-55°S zone and decreasing in the 60-65°S zone for starting years of around 1985. In each of these cases the plots in Figure 8.5 indicate that the trends are becoming increasingly positive (50-55°S) or negative (60-65°S). This is consistent with Figure 8.3(b) but is harder to detect in part (a) of the same figure. When similar analyses are done for the other SODA-derived variables presented in Table 8.1, for each latitudinal zone and season, there appears to have been a detectable change in the trends for many of the variables.

8.3 Discussion

Trends in phytoplankton biomass, various climate indices and hydrodynamic variables have been considered over the period 1997-2007. Trends in hydrodynamic variables over the study period are much larger and often of opposite sign to those previously calculated in Chapter 5 for 1958-2007 and this is illustrated in Figure 8.5, which shows stable long term salinity trends as well as what appear to be recent changes in salinity trends. The other type of plot showing "running" sets of decadal trends, which begins with the 10 year trend

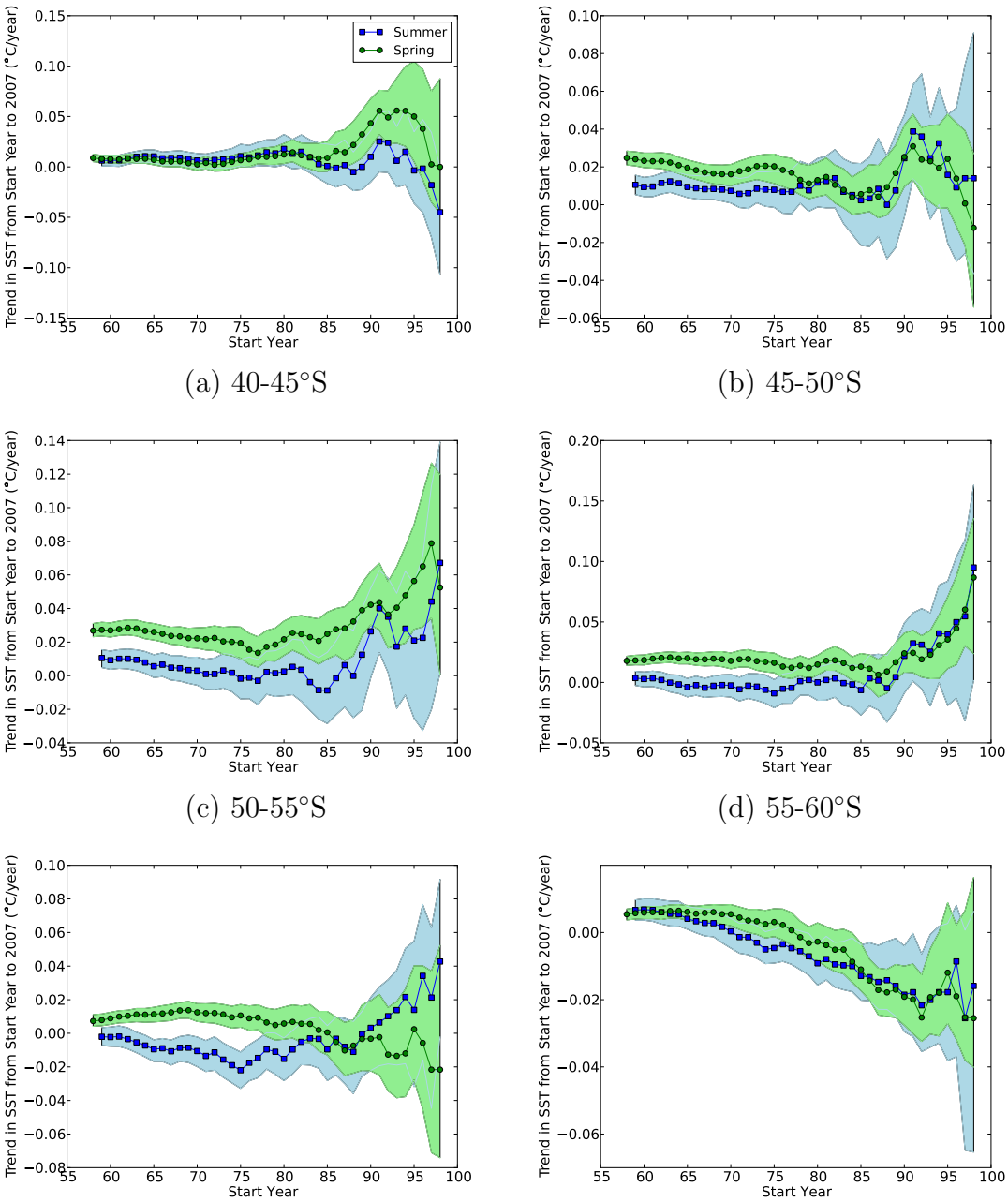

(a) 40-45°S (b) 45-50°S

(c) 50-55°S (d) 55-60°S

(e) 60-65°S (f) 65-70°S

Figure 8.4: Trends for Sea-surface Temperature for summer and spring, for the time series from the starting year to 2007, with the 95% confidence intervals shaded.

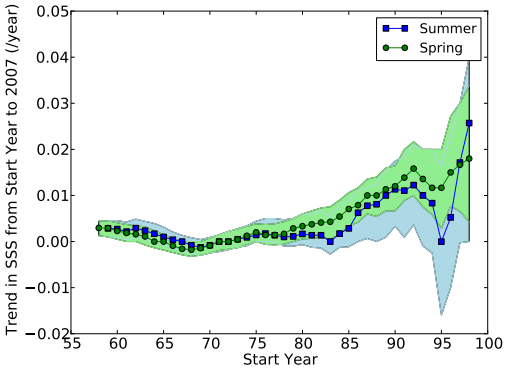

(a) 40-45°S

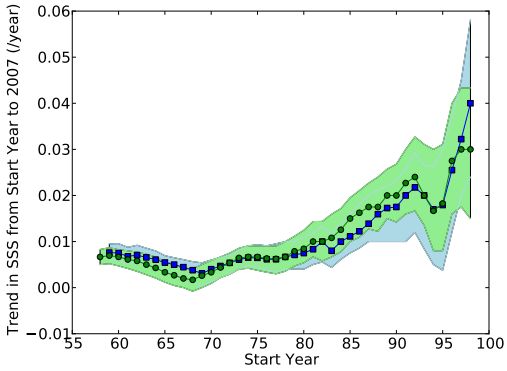

(b) 45-50°S

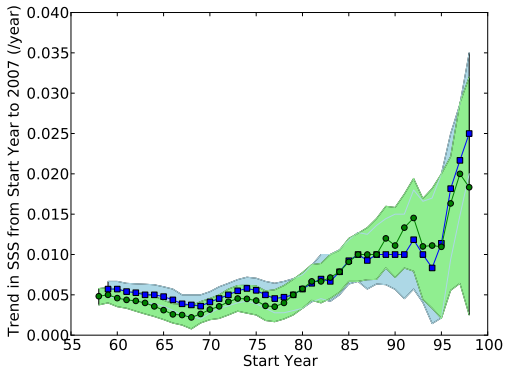

(c) 50-55°S

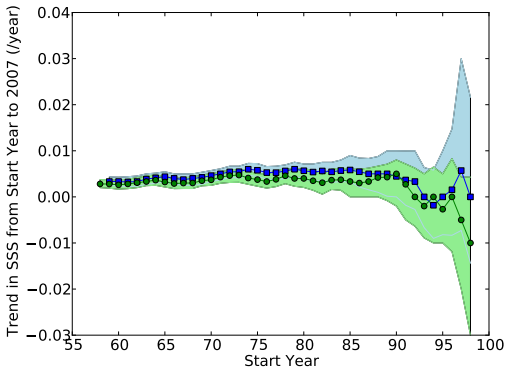

(d) 55-60°S

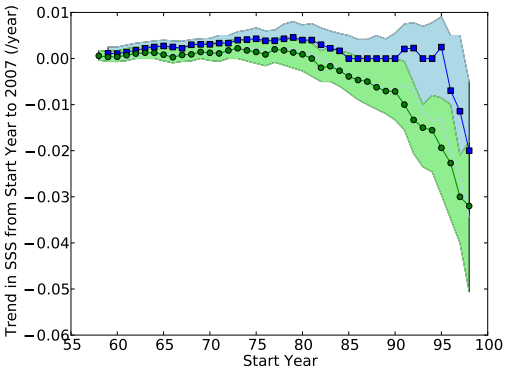

(e) 60-65°S

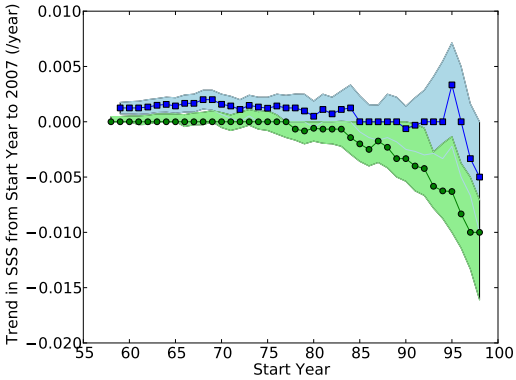

(f) 65-70°S

Figure 8.5: Trends for Sea-surface Salinity for summer and spring, for the time series from the starting year to 2007, with the 95% confidence intervals shaded.

for 1958-1967, then the 1959-1968 trend and so on (Figures 8.2 and 8.3), was produced to match similar plots for chlorophyll-*a* from *Henson et al.* (2010). They found that the 10-year trend in SeaWiFS chlorophyll-*a* was of similar magnitude to trends of previous decades in modelled chlorophyll-*a* and that the same applied to primary production. However, the present study does not find the same result for some of the hydrodynamic trends considered here.

Differences in SST trends, depending on the region and latitudinal zone, have been reported previously (*Trenberth et al.*, 2007). Such differences have also been found in a recent study (*Roemmich and Gilson*, 2009), which compared mean Argo float data (2004-2007) with data from the World Ocean Atlas, 2001 (*Boyer et al.*, 2002). The study found that, in the present study region south of Australia, SST was increasing between about 50 and 60°S and decreasing between about 40 and 50°S (no results were given south of 60°S). This is consistent with the plots from Figure 8.4, including the magnitude of the trends. In addition, the present study also finds possible recent decreases in SST in 60-65°S (spring) and 65-70°S. The recent trends in SSS (Figure 8.5) are also consistent with those found in the study by *Roemmich and Gilson* (2009) and a similar one by *Hosoda et al.* (2009); that is, recent increases in SSS between 40 and 50°S and decreases south of there. These trends are also consistent with decreased precipitation in the northern zones (*Bindoff et al.*, 2010; *Helm et al.*, 2010) and increased precipitation, sea-ice and glacial melt near the Antarctic continent (*Jacobs*, 2006; *Liu and Curry*, 2010).

Since this work is using two different types of "running" plots to examine trends in hydrodynamic variables, it is also worth applying the same approach to examine trends in the SAM. The SAM plots (Figure 8.6(a)) show that in summer SAM has displayed a positive trend until about 1990, after which the trend has become increasingly negative. The situation in spring is a little different in that the SAM trend was near zero until quite recently, after which there are positive and then negative values, which may not be meaningful given the width of the 95% confidence interval there. The plot for SON in part (b) of the figure shows that, while the final value for spring is just outside the bounds of previous variability, that is not the case for the previous points, leading to the speculation that, in spring, SAM is probably not displaying unusual trends in recent years. The plot for SAM in summer in part (b) shows that 10-year trends in recent years are not outside the bounds of earlier variability, although they are the lowest since 1960. In addition, considerable decadal variability can be seen in the 10-year trends in part (b) for both spring and summer. This is consistent with work by *Jones and Widmann* (2004), who have reconstructed the summer (DJ) Antarctic Oscillation (SAM) index over the twentieth century, from sea-level pressure measurements, and have found

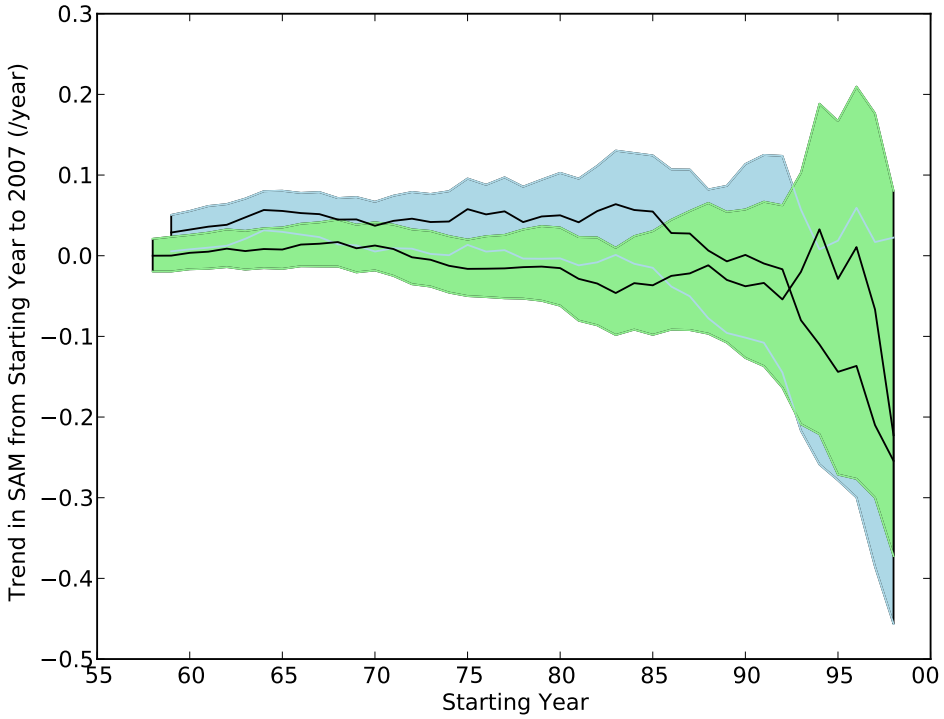

(a)

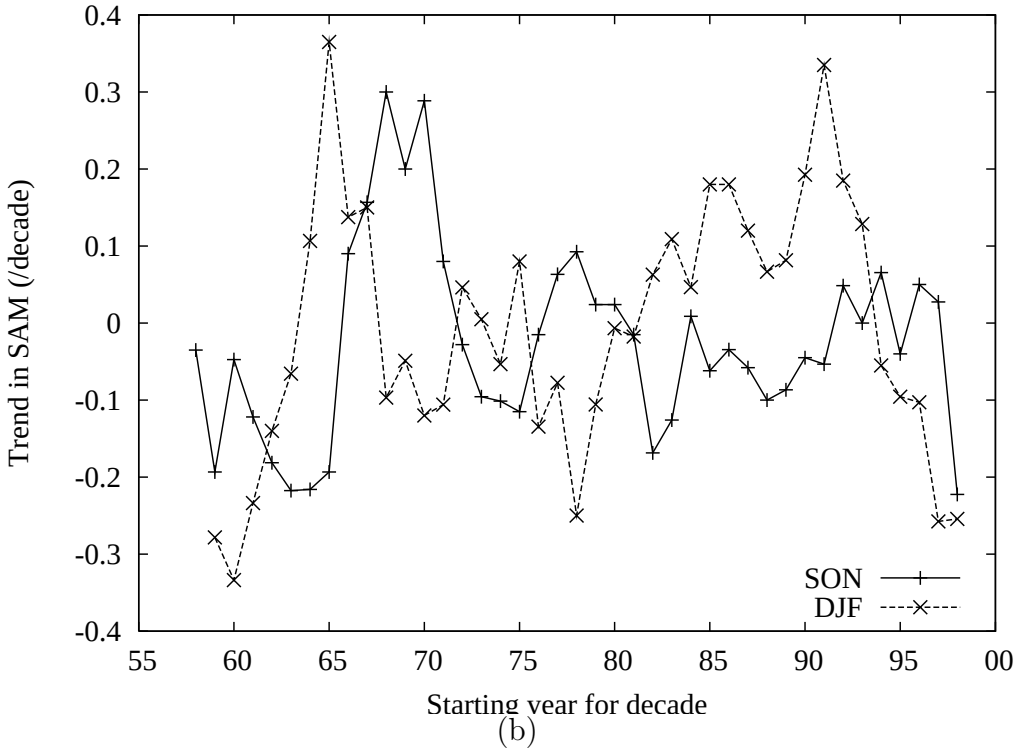

(b)

Figure 8.6: (a) Trends in SAM for summer (blue) and spring (green), for the time series from the starting year to 2007, with the 95% confidence intervals shaded. (b) Trends in SAM for sets of 10-year trends, beginning at the starting year for summer (DJF) and spring (SON).

that recent positive values are not unprecedented.

8.4 Conclusions

This work has studied trends, over the period 1997-2007, in phytoplankton biomass and primary productivity, as well as in hydrodynamic variables and any of the other factors that potentially affect chlorophyll-a and primary productivity (for example, sea-ice concentration, PAR and various climate indices).

Over the period 1997-2007, it is found that chlorophyll-a is decreasing in 55-60°S in both spring and summer, while both chlorophyll-a and primary productivity are increasing in 40-50°S in summer. A decrease in the Ekman transport of nutrients (iron) and an increase in SST, which is negatively correlated with chlorophyll-a, is consistent with the negative trend in chlorophyll-a found in summer in the 55-60°S zone. However, the similar trend in chlorophyll-a found in spring may be related to trends in Ekman transport and stratification rather than SST. The trends in the 40-50°S zone do not appear to be related to trends in the hydrological variables studied here.

Many of the trends for the hydrodynamic variables for 1997-2007 are of opposite sign and up to an order of magnitude larger those found in Chapter 5 for the 1958-2007 time period. For example, an increasingly positive trend in SST is found in 50-60°S in recent years, consistent with a recent study using Argo float data (*Roemmich and Gilson*, 2009). Trends in sea-surface salinity are of opposite sign depending on which latitudinal zone is considered - south of the PF salinity is decreasing and north of the PF it is increasing, again consistent with recent Argo float studies (*Roemmich and Gilson*, 2009; *Hosoda et al.*, 2009) and precipitation studies (*Helm et al.*, 2010; *Bindoff et al.*, 2010).

An investigation into these and other similar trends finds that, in many cases in recent years, there is a discernible change that is outside the bounds of earlier variability. This may indicate that there has been a shift in the last ten to fifteen years in the ocean state of the Southern Ocean.

Chapter 9

Conclusions

Documenting changes in the meridional circulation of UCDW is important for understanding climate change, due to the importance of UCDW in regulating CO_2 in the SO via both the solubility and biological pumps. The variability in the meridional circulation of UCDW in the SO, for the past 50 years, and its connection with variability in phytoplankton biomass and primary production, in the past decade, was examined in this work. The main study region was the Australian region (110-160°E, 40-70°S) of the SO, although comparisons were made with two other sectors: Indian (20-60°E, 40-70°S) and Pacific (130-80°W, 40-75°S). Hydrodynamic data were analysed in five-degree latitudinal zones that were chosen to approximate the SO frontal zones. Given the sparseness and temporal and spatial variability of observational physical data in the SO, the approach taken was to use SODA model reanalysis data, which had the advantage of combining model output with observational data.

Initial work involved establishing that SODA was sufficiently skilled at representing hydrodynamic data in the study region. Then SODA data were used to confirm that there were high dissolved iron concentrations in UCDW and to examine UCDW circulation in the SO using Lagrangian tracking. Various UCDW properties, such as upwelling velocity, the top depth to which UCDW upwells and southern-most position of UCDW, as well as UCDW temperature, density and salinity, were studied. Additional related properties, such as upward Ekman pumping rate and northward Ekman transport, were also studied and trends were calculated for all these UCDW-associated variables for 1958-2007.

Since changes in the meridional circulation of UCDW may be reflected in changes in upper ocean properties, climatological values and trends in ML and SS properties and stratification were also examined. Connections between the global climate indices SAM, MEI and PDO and changes in the SH winds were considered and then the effect of changes in wind stress, on the various UCDW and upper ocean variables, was examined. These analyses were repeated for

the Indian and Pacific sectors and similarities and differences in the three sectors, as well as the robustness of UCDW trends, were studied.

In order to establish connections between hydrodynamic variables and chlorophyll-a or primary production, the above analyses were also repeated for the shorter time period September 1997 - August 2007. This was necessary because satellite data, for chlorophyll-a and other input variables necessary for the primary production model, were not available, in a consistent and uniform manner for the study region, until 1997. Interannual variability in chlorophyll-a, a proxy for phytoplankton biomass, was then studied, as well as factors which influenced chlorophyll-a and primary productivity.

Recent observational studies have suggested that changes are taking place in some SO water mass properties, for example, freshening in AABW (*Rintoul*, 2007). So the (1997-2007) ten-year trends in hydrodynamic variables were compared with the 1958-2007 trends, both in terms of magnitude and direction. In addition, the trends were studied to determine whether the most recent ten-year trends were outside the variability of previous sets of ten-year trends.

The results here show that trends in UCDW upwelling are not related to changes in the SH westerly winds, unless they operate over a longer period than can be detected with the available data. The trends in UCDW properties appear to operate on time-scales that are longer than decadal and this is perhaps not surprising, given that UCDW is part of the global MOC. However, since UCDW upwelling is divergence-driven, it was possible that it could have been affected by changes in wind strength and/or position.

A noteworthy result was that UCDW vertical velocity was increasing (for 1958-2007) in the PFZ in all three ocean sectors studied, as well as in the SAZ and STCZ (except in the Pacific sector). Even though this was generally not the case where UCDW was shoaling (the sACCZ and the AZ) the upward Ekman pumping rate was found to be increasing in summer in the sACCZ, where UCDW is entrained in the ML. This was the case for all three ocean sectors and since this was not accompanied by an increase in northward Ekman transport, an increased amount of nutrients may have been available for a longer period of time in summer for primary production in the zones south of the PF (for example, in the Australian sector in 55-65°S). However, this may or may not translate into an increase in primary production in any of these sectors over the period 1958-2007, given that factors other than nutrient availability also affect primary production.

Differences between the three sectors were found particularly in the number of times that UCDW could be detected in the ML. The number of detections in the Pacific sector was only about half of the number in the other two sectors and the majority of those detections occurred in autumn/winter/spring (as

previously reported), whereas they occurred in summer/autumn in the other two sectors. This result may be significant for the Australian and Indian sectors since it means that nutrients may be available in summer for primary production, when they are most required. An increasing trend was found, from the 1960s to the 1990s, in the number of of detections in the Australian sector. This was consistent with other trends found there, which indicated that UCDW was upwelling closer to the surface and the ML was deepening. This result, in addition to the fact that UCDW was found in the ML most frequently in summer/autumn, may be important for the resupply of nutrients for primary production through the summer.

Unfortunately, it is not possible to assess the importance of increasing UCDW vertical velocity and an increase in the number of detections of UCDW in the ML, in terms of trends in chlorophyll-a, because suitable chlorophyll-a data are available only for the last decade in the study region. These data are too recent to compare with trends over 1958-2007 and the time-series is also too short to allow conclusions to be drawn with any certainty, based on relationships seen in that time period. In addition, the 1997-2007 time period appears to be very different from the 1958-1997 period, possibly due to the change in the SAM from the earlier to the later time period.

This work also found no trends in the southern-most position of UCDW for the Indian and Pacific sectors, with the only trends in the Australian sector being a slight southward movement in autumn and winter. Increasing trends in UCDW temperature (all three sectors) and decreasing trends in UCDW density (Australian and Indian sectors) were found in most seasons in the latitudinal zones where UCDW was shoaling. However, these results did not necessarily apply in the zones where UCDW was found at depths greater than about 1000 m. For example, UCDW temperature, which was increasing in the Indian sector, was decreasing in the Australian and Pacific sectors, north of about the PF. It is suggested that these, and other differences in UCDW between the three ocean sectors, may be explained by the fact that UCDW consists mainly of water that has re-entered the ACC after re-circulating through either the Indian or Pacific Oceans. This allows for variations in its characteristics in the three ocean sectors, since they are partly supplied by water from different sources.

The connection between the three climate indices studied and wind stress varied across the three ocean sectors, although the effect of the SAM (a positive correlation) was felt in the sACCZ, AZ and PFZ in each case. There was also a negative correlation between SAM and mean wind stress in the most northerly and southerly latitudinal zones (STCZ and SZ) in the Australian and Indian sectors, but not in the Pacific sector. Correlations between mean wind stress

and MEI and PDO were similar, with positive correlations in the PFZ, SAZ and STCZ in the Australian sector (and in some cases in the Indian sector) and negative correlations in the Pacific sector. The fact that the winds in the various latitudinal zones are not only correlated with SAM, but also sometimes with MEI and PDO, means that changes in one of these climate indices will not necessarily be associated with uniform changes in the physical ocean state in the various zones, due to the additional effects on the winds. This is true not only when comparing latitudinal zones within an ocean sector, but is also true when one ocean sector is compared with another.

Unlike changes in UCDW, decadal-scale changes in ML and SS variables in all three sectors *were* found to be related to changes in the SH winds, which increased in summer in most of the sACCZ, AZ and PFZ, in line with increases in SAM. Positive correlations between mean wind stress and MLD, ML density, and ML and SS salinity, and negative correlations with ML and SS temperature were found. The relation between mean wind stress and stratification is more complex, since other factors, such as temperature and salinity, determine stratification. Trends in stratification were patchy, with the majority of trends found being negative, although increasing stratification was found in a number of zones in summer.

In the Australian sector, positive trends were found for 1958-2007 in ML density and salinity (north of the sACCf), ML temperature and SST (except in summer in the sACCZ and AZ) and ML depth. The Indian sector results were very similar, except that ML density and MLD trends were patchier and became negative north of the PF. The main differences in the Pacific sector were negative trends in ML density and ML and SS salinity. The temperature results (increasing except in summer in the sACCZ and the AZ) were consistent across all three ocean sectors and the exceptions in summer may have been related to increased winds mixing remnant winter water into the ML and negating the surface warming.

Some of these results appeared initially to be contrary to recent studies, but this was explained when trends for 1997-2007 were compared with those for the longer 1958-2007 time period. In many cases, the 1997-2007 trends were outside the range of variability of previous sets of ten-year trends. In addition, a study of "running" sets of trends from 1958-2007, 1959-2007, ... to 1998-2007, indicated that, in some zones and seasons, the trends have become increasingly positive (for example, SST in 55-60°S or SSS in 50-55°S) or increasingly negative (for example, SSS in 60-65°S). These results were in agreement with recent observational studies. Differences were found between latitudinal zones in recent trends in both SST and SSS. SST was found to increase between about 50° and 60°S and decrease between about 40° and 50°S,

in agreement with previous studies, which reported trends only to 60°S. South of there, SST trends were becoming more negative in 60-65°S, in spring, and 65-70°S. Increasing SSS was found between 40° and 50°S, with decreases south of there, in agreement with Argo float studies and trends in precipitation. In addition, studies of trends in other hydrodynamic variables also indicated that there had been some recent changes in trends. It would seem, therefore, that, in the last decade or two, there may have been a shift in the state of the SO.

The results suggest considerable interannual variability in the magnitude and phenology of the phytoplankton bloom in the study region during 1997-2007, which was affected by different factors, depending on the season and latitudinal zone. Sea-ice concentration was found to be important near the Antarctic continent and irradiance was significant in all zones and seasons, except in summer near the Antarctic continent, in agreement with a previous study. In spring, other important, but co-varying, factors, were SST, MLD and stratification. The factors identified as being significantly correlated with chlorophyll-*a* were almost the same as those that were significantly correlated with primary productivity.

In summer, in the 65-70°S zone, sea-ice concentration together with SAM explained 51% of the variance in chlorophyll-*a*, while in the 60-65°S zone, SST combined with mean wind stress (a combination which is related to UCDW temperature and also nutrient mixing) accounted for 55% of the variance in chlorophyll-*a*. However, in each of these cases there are differences in the 10-year trends of each variable within the set of correlated variables. The small negative trend in chlorophyll-*a* in the 55-60°S zone in summer may be due to decreasing wind stress and consequent decreased mixing of nutrients (iron) into the ML, in combination with an increase in SST, which was negatively correlated with chlorophyll-*a* in that zone in summer.

Lower-valued correlations were found between both chlorophyll-*a* and primary productivity and some of wind stress, Ekman pumping rate and Ekman transport in the sACCZ, AZ and PFZ. These are the zones where UCDW brings nutrient-enriched and, in some of these zones, warmer waters into the ML, either through intrusion or through northward Ekman transport. This highlights the importance of the combination of variability in wind stress and variability in the upwelling of UCDW - not because of the effect of wind stress on the upwelling, but because of the effect that variability in the mixing of nutrients and warmer water into the ML has on primary production.

One important conclusion from the work presented here is related to the importance of the role of SST, when considering variability and trends in chlorophyll-*a* and primary production. This is particularly pertinent in light of the recent changes in trends in SST in spring and summer in the Aus-

tralian sector of the SO (increases in the mid-latitude zones (PFZ and AZ) and decreases nearer to the Antarctic continent). In the present work, SST was found to correlate negatively with chlorophyll-a in summer in all the zones where UCDW was identified in the ML (sACCZ, AZ, PFZ) with a positive correlation in the STCZ. In spring, correlations are positive north of 60°S (AZ, PFZ, SAZ and STCZ), reversing the correlations for the AZ and PFZ.

Previous work has also found differences in the directions of SST- chlorophyll-a correlations, depending on the ocean region being studied (although seasonal differences do not appear to have been considered). The positive correlations here between SST and chlorophyll-a in spring are consistent with physiological factors, such as algal metabolic rate and species composition, as well as the effect of temperature on stratification and sea-ice melt (near the Antarctic continent). The fact that the correlations are reversed in summer may be because these regions become iron-limited in summer, dominating other effects. There is also the connection with the presence of UCDW, which provides a supply of nutrients in summer in these regions, but is also warmer than the surface water in the sACCZ.

The direction of the correlations is of interest with regard to future trends in chlorophyll-a, since recent decreases in SST, in summer in the Australian sector of the SO, near the Antarctic continent (SZ and sACCZ), may imply an increase in chlorophyll-a there, while increases in SST in the mid-latitudes (AZ and PFZ) would suggest the opposite scenario.

Ideally, the next step in this work would be to explore past and future trends in chlorophyll-a and primary productivity, using conclusions drawn from the 1997-2007 study on the importance of the various controls. These trends could include past trends in chlorophyll-a and primary productivity for 1958-2007, based on trends that have been established in hydrodynamic variables over that time period, and also future trends in chlorophyll-a and primary productivity, based on modelling projections of trends in hydrodynamic variables. However, this is problematic with the available datasets, due to the complexity of the situation and the difficulty in identifying all the controls on primary production, as well as the fact that many of the controls co-vary. In addition, it is necessary to be wary of assuming that relationships that hold for the ten year 1997-2007 period can be extrapolated to much longer time-scales. Much longer data sets, than those that exist at present, are necessary to establish trends for chlorophyll-a. These sets would also help to validate the controls on phytoplankton biomass, which would then allow robust conclusions to be drawn about past trends and future trends in chlorophyll-a and primary productivity. Such work should be possible in the future as more satellite data become available.

An important conclusion, suggested by the results here, is that very different controls seem to affect both phytoplankton biomass and primary productivity in spring and summer and, within each of these seasons, in different latitudinal zones. This means that care needs to be taken when inferring trends in chlorophyll-a and primary productivity from model-based predictions of future climate that are not seasonally based, as well as to ensure that the projections apply in the particular latitudinal zone. However, if it is assumed that the 1997-2007 results for controls on chlorophyll-a and primary productivity hold in the future, then this may imply that chlorophyll-a and primary productivity would increase in summer during the 21st century (Tables 7.3 and 7.4) in 65-70°S (SZ). This is because modelling projections of 21st century climate suggest that the positive trend in the SAM will continue (*Miller et al.*, 2006)and that sea-ice concentration will decrease (*Liu and Curry*, 2010). The situation in 60-65°S (sACCZ) seems to be more complex and, while increased wind stress associated with increased SAM would imply increased chlorophyll-a (Table 7.3), the trends also depend on SST and the supply of nutrients (and hence trends in the upwelling of UCDW, which are unclear, since they do not appear to be related to changes in wind stress). Chlorophyll-a in 50-60°S (AZ and PFZ) may decrease in summer due to predicted increases in SST and stratification (*Steinacher et al.*, 2010), but in spring the opposite may occur, since predicted increases in SST and stratification and decreases in MLD (*Boyd et al.*, 2008b), imply increases in both chlorophyll-a and primary productivity (Tables 7.3 and 7.4). These predictions, however, assume that Ekman transport provides a sufficient supply of nutrients, especially iron, from higher latitudes, which may not necessarily be the case. The above results are generally in agreement with results from multi-model mean projections (*Steinacher et al.*, 2010) of changes in primary productivity between 1860-1869 and 2090-2099, which indicate that, for the Australian region of the SO, there will be increases in primary productivity near the Antarctic continent (60-75°S) and decreases in 40-60°S.

Another conclusion from the study of *Steinacher et al.* (2010) was that changes in primary productivity will vary in sign between regions of the SO. This is consistent with the fact that differences were found in this study between hydrodynamic trends in the three sectors of the SO studied, as well as differences in the upwelling of UCDW in those sectors. The techniques used in this study could readily be extended to compare recent trends in hydrodynamic variables in the Indian and Pacific sectors with previous trends for these sectors. Such future work could also include a study of the connections between interannual variability in chlorophyll-a (and primary productivity) and variability in hydrodynamic variables and the upwelling of UCDW in those two

sectors, as well as potentially other sectors in the SO. Such analysis would provide a useful contribution to the important on-going study of CO_2 regulation in the Southern Ocean.

Appendix A

Additional Tables

The Appendix contains tables giving seasonal trends for 1958-2007 by latitudinal zone. There are three sets of tables, one for each of the ocean sectors: Australian (Tables A.2-A.4), Indian (Tables A.5-A.7) and Pacific (Tables A.8-A.10). Each set of tables gives trends, with 95% confidence interval limits, for UCDW variables, other variables (stratification, wind stress and Ekman variables) and ML (and SS) variables.

Table A.1: Trends (per year, with 95% confidence interval limits) for 1958-2007 in global climate indices.

	SAM $\times 10^{-2}$	MEI $\times 10^{-2}$	PDO $\times 10^{-2}$
DJF	2.9±2.2		2.1±1.1
MAM	3.1±2.1	1.3±1.0	2.8±1.2
JJA		1.5±0.9	2.4±1.2
SON	n/s	n/s	n/s

Table A.2: Trends (per year, with 95% confidence interval limits) for 1958-2007 in UCDW variables in the Australian sector. A positive trend in UCDW Top Depth means that UCDW is found closer to the surface. Additional trends are: UCDW Salinity in 60-65°S SON (-3.4±3.4)$\times 10^{-4}$ and UCDW Southern-most Position MAM (-1.1±1.1)$\times 10^{-2}$ and JJA (-1.8±0.6)$\times 10^{-2}$.

UCDW	60-65°S	55-60°S	50-55°S	45-50°S	40-45°S
Vertical velocity $(\mathrm{ms}^{-1}\mathrm{yr}^{-1}) \times 10^{-8}$					
DJF	1.3±1.1		9.4±3.8	5.7±2.5	3.5±0.8
MAM			7.8±4.7	8.8±2.8	3.3±0.7
JJA	1.7±1.4		6.9±3.7	7.4±2.4	3.2±0.8
SON		-7.0±4.7	4.1±4.0	4.5±2.2	3.3±0.8
Temperature $(^{\circ}\mathrm{Cyr}^{-1}) \times 10^{-3}$					
DJF	3.5±0.8		-2.7±0.5	-1.5±0.3	-0.7±0.2
MAM	3.6±0.9		-2.3±0.5	-1.4±0.3	-0.4±0.3
JJA	3.2±0.8		-2.3±0.5	-1.5±0.3	-0.8±0.3
SON	2.9±0.9		-2.4±0.5	-1.7±0.3	-0.8±0.3
Density $(\mathrm{kgm}^{-3}\mathrm{yr}^{-1}) \times 10^{-4}$					
DJF	-4.3±2.0	-2.8±2.8			
MAM	-4.3±1.8				
JJA	-4.2±2.0				
SON	-4.3±1.4				
Top Depth (myr^{-1})					
DJF		0.70±0.70			
MAM		0.32±0.32			
JJA	0.61±0.61	0.52±0.52			
SON	0.68±0.68	0.55±0.55			

Table A.3: Trends (per year, with 95% confidence interval limits) for 1958-2007 in stratification, wind stress and Ekman variables in the Australian sector. No significant trends are found in the position of maximum wind stress.

	Stratification $(s^{-2}yr^{-1}) \times 10^{-7}$	Mean Wind Stress $(Nm^{-2}yr^{-1}) \times 10^{-4}$	Ekman Pumping $(ms^{-1}yr^{-1}) \times 10^{-8}$	Ekman Transport $(Svyr^{-1}) \times 10^{-2}$
65-70°S				
DJF	-1.0±0.7	8.9±3.6		
MAM				
JJA				
SON	-1.0±0.4			
60-65°S				
DJF		3.2±1.7	1.2±0.5	
MAM				
JJA		-3.5±3.0		
SON		-4.2±3.5	-1.3±0.7	-1.0±0.8
55-60°S				
DJF	-1.9±1.8		0.8±0.6	
MAM	-2.2±1.5			
JJA				
SON		-10.5±7.3		-2.4±1.6
50-55°S				
DJF	-4.0±1.4			
MAM	-4.6±1.3			
JJA	-2.5±1.2			
SON		-7.8±5.9		-2.2±1.6
45-50°S				
DJF	-5.5±1.5			
MAM	-5.8±1.6			
JJA	-2.2±1.3			1.7±1.7
SON				
40-45°S				
DJF				
MAM	1.7±1.6	4.0±4.2		
JJA		3.8±3.7		1.6±1.6
SON	-2.0±1.1			

	Max. Wind Stress $(Nm^{-2}yr^{-1}) \times 10^{-4}$
DJF	6.3±4.2
MAM	7.6±5.9
JJA	
SON	-5.9±5.7

Table A.4: Mixed Layer Trends (per year, with 95% confidence interval limits) for 1958-2007 in the Australian sector.

	MLD (myr^{-1})	ML Density ($kgm^{-3}yr^{-1}$) $\times 10^{-3}$	ML Salinity (yr^{-1}) $\times 10^{-3}$	ML Temperature ($°Cyr^{-1}$) $\times 10^{-2}$	SST ($°Cyr^{-1}$) $\times 10^{-2}$	SSS (yr^{-1}) $\times 10^{-3}$
65-70°S						
DJF		0.4±0.5	0.8±0.5	0.6±0.3	0.7±0.3	1.3±0.5
MAM		-0.5±0.5		0.6±0.3	0.8±0.3	
JJA		-0.8±0.5	-0.6±0.6	0.6±0.2	0.8±0.2	
SON		-0.3±0.3		0.5±0.2	0.6±0.2	
60-65°S						
DJF	0.13±0.07		1.0±1.1			1.1±1.4
MAM	0.14±0.09					
JJA	0.17±0.09			1.2±0.3	1.4±0.3	
SON	0.16±0.10			0.6±0.3	0.7±0.4	
55-60°S						
DJF	0.11±0.08	2.4±1.0	3.3±1.0			3.3±1.0
MAM	0.14±0.10	1.3±0.6	2.5±0.7	1.0±0.4	0.9±0.4	2.9±0.7
JJA	0.63±0.16	0.8±0.5	2.2±0.7	1.6±0.4	1.9±0.4	2.8±0.9
SON	0.45±0.17	1.3±0.6	2.7±0.8	1.7±0.4	1.8±0.4	2.8±0.9
50-55°S						
DJF	0.30±0.13	2.9±0.7	5.6±1.1	1.2±0.5	1.1±0.5	5.7±1.0
MAM	0.43±0.15	1.4±0.7	4.7±1.0	1.8±0.4	1.6±0.4	5.5±1.0
JJA	0.79±0.36	0.8±0.7	4.0±1.0	2.2±0.4	2.4±0.4	5.0±0.9
SON	0.70±0.26	1.1±0.7	4.8±1.0	2.6±0.4	2.7±0.4	4.8±1.0
45-50°S						
DJF	0.29±0.14	4.6±1.3	7.6±1.7	1.2±0.5	1.1±0.5	7.6±1.9
MAM	0.45±0.17	2.1±1.0	5.8±1.7	1.8±0.4	1.6±0.4	7.0±1.8
JJA	0.88±0.40		5.8±1.4	2.2±0.3	2.4±0.3	6.2±1.8
SON	1.00±0.40	1.4±1.1	6.4±1.6	2.6±0.3	2.5±0.4	6.7±1.6
40-45°S						
DJF			2.9±1.4	0.7±0.5	0.6±0.5	2.9±1.7
MAM		-2.2±1.2		1.6±0.6	1.5±0.6	
JJA		-1.4±1.4		1.2±0.4	1.2±0.4	2.0±1.5
SON	0.48±0.21		2.1±1.5	1.0±0.3	0.9±0.4	3.0±1.5

Table A.5: Trends (per year, with 95% confidence interval limits) in UCDW variables for 1958-2007 in the Indian sector. A positive trend in UCDW Top Depth means that UCDW is found closer to the surface. No trends were found for UCDW southernmost position.

UCDW	60-65°S	55-60°S	50-55°S	45-50°S	40-45°S
Vertical velocity $(ms^{-1}yr^{-1}) \times 10^{-8}$					
DJF		2.5±1.1	2.9±2.6	2.7±2.7	6.8±4.1
MAM		2.8±1.4	4.0±2.6	7.9±2.3	12.1±5.0
JJA		2.5±1.3	3.0±2.3	7.8±2.1	9.7±5.6
SON		1.7±1.2	3.4±2.2	6.5±2.9	6.9±5.0
Temperature $(°Cyr^{-1}) \times 10^{-3}$					
DJF	2.1±1.8	2.8±1.1	3.3±0.6	0.7±0.3	
MAM		2.4±1.0	3.1±0.6	1.0±0.4	
JJA	1.9±1.3	2.8±0.9	3.3±0.7	1.2±0.4	
SON	1.3±1.1	2.6±0.9	3.1±0.5	0.8±0.3	
Salinity $(yr^{-1}) \times 10^{-4}$					
DJF		-5.3±1.6			
MAM	-3.6±3.6	-3.4±3.4			
JJA		-3.2±3.2			
SON		-3.8±3.8			
Density $(kgm^{-3}yr^{-1}) \times 10^{-4}$					
DJF	-2.8±2.8	-7.1±1.9	-5.3±1.1		
MAM	-5.4±2.8	-5.3±1.7	-4.8±1.4		
JJA	-3.6±3.6	-5.6±1.9	-4.5±1.2		
SON	-3.0±3.0	-5.3±1.8	-4.0±1.1		
Top Depth (myr^{-1})					
DJF		0.8±0.8			
MAM	1.0±1.0	0.7±0.7			
JJA	1.6±1.0	1.1±0.8			
SON		1.1±0.7		0.6±0.6	

Table A.6: Trends (per year, with 95% confidence interval limits) for 1958-2007 in stratification, wind stress and Ekman variables in the Indian sector.

	Stratification $(s^{-2}yr^{-1}) \times 10^{-7}$	Mean Wind Stress $(Nm^{-2}yr^{-1}) \times 10^{-4}$	Ekman Pumping $(ms^{-1}yr^{-1}) \times 10^{-8}$	Ekman Transport $(Svyr^{-1}) \times 10^{-2}$
65-70°S				
DJF	2.2±1.2			
MAM	-1.6±1.0	-4.4±3.6		
JJA	-0.9±0.7	-7.3±3.7		
SON		-6.0±2.9		
60-65°S				
DJF	1.8±1.2	2.2±1.8	1.5±0.6	
MAM	-1.7±1.3			
JJA	-1.2±1.1	-3.1±2.3	-1.5±0.8	
SON			-1.2±0.9	
55-60°S				
DJF		13.7±4.1		2.3±0.8
MAM	-4.5±1.7			
JJA				
SON			-0.8±0.7	
50-55°S				
DJF	-2.0±1.0			
MAM	-3.2±1.7			
JJA	-2.7±1.4			
SON	-2.1±1.2	-7.1±6.2		-1.5±1.5
45-50°S				
DJF	1.3±1.1	-10.2±3.5		-2.9±1.0
MAM				
JJA	-2.0±1.1			
SON	-1.0±0.6	-9.9±4.9		-2.5±1.4
40-45°S				
DJF	4.5±2.2	-13.3±0.4		-4.3±1.1
MAM	3.8±2.3			
JJA				
SON		-6.8±4.0		-2.2±1.3

	Max. Wind Stress $(Nm^{-2}yr^{-1}) \times 10^{-4}$	Position of Max. Wind Stress $(°yr^{-1}) \times 10^{-2}$
DJF	-4.9±4.1	-9.7±3.0
MAM		
JJA		5.6±5.5
SON		

Table A.7: Mixed Layer Trends (per year, with 95% confidence interval limits) for 1958-2007 in the Indian sector.

	MLD (myr^{-1})	ML Density ($kgm^{-3}yr^{-1}$) $\times 10^{-3}$	ML Salinity (yr^{-1}) $\times 10^{-3}$	ML Temperature ($°Cyr^{-1}$) $\times 10^{-2}$	SST ($°Cyr^{-1}$) $\times 10^{-2}$	SSS (yr^{-1}) $\times 10^{-3}$
65-70°S						
DJF	-0.24±0.19			0.9±0.3	0.7±0.4	0.5±0.6
MAM				0.7±0.2	0.4±0.3	0.9±0.7
JJA	-0.41±0.21	-0.8±0.8	-0.8±0.8	0.5±0.2	0.4±0.2	
SON	-0.36±0.21	-0.7±0.7	-0.7±0.7	0.4±0.2	0.3±0.1	
60-65°S						
DJF	0.12±0.08	0.9±0.6				1.3±0.5
MAM		0.7±0.6				2.0±0.6
JJA	0.13±0.09	-0.6±0.6	-0.7±0.7	0.9±0.2	1.1±0.2	1.0±0.7
SON				0.5±0.3	0.5±0.3	
55-60°S						
DJF	0.21±0.09	3.0±0.6	3.7±0.7			3.6±0.9
MAM	0.20±0.10	1.8±0.5	2.8±0.6	0.8±0.4	0.7±0.4	3.6±0.8
JJA	0.56±0.15	1.7±0.3	3.1±0.6	2.1±0.3	2.3±0.3	3.4±0.7
SON	0.42±0.18	1.5±0.4	2.6±0.5			2.7±0.7
50-55°S						
DJF			1.9±0.9	1.3±0.4	1.0±0.5	2.2±0.9
MAM			1.3±0.9	2.1±0.4	2.0±0.4	1.9±1.0
JJA			0.9±0.6	1.9±0.3	2.2±0.3	2.3±0.8
SON	0.65±0.27		1.6±0.7	1.8±0.3	2.0±0.3	2.2±0.7
45-50°S						
DJF	-0.22±0.11		1.7±0.8	2.4±0.5	2.6±0.5	1.5±0.8
MAM	-0.16±0.13	-3.3±0.8	1.2±0.8	3.6±0.5	3.6±0.5	1.4±0.9
JJA		-1.3±0.6	1.4±0.6	2.3±0.4	2.5±0.5	2.5±0.7
SON			2.4±0.7	2.0±0.4	2.1±0.4	2.8±0.5
40-45°S						
DJF	-0.34±0.08	-4.2±0.2	5.0±2.4	4.1±0.7	4.7±0.7	4.8±2.3
MAM	-0.26±0.08	-5.4±0.2	4.3±1.7	5.2±0.7	5.2±0.7	4.6±1.9
JJA		-1.2±1.2	3.2±1.3	2.5±0.6	2.3±0.6	4.0±1.4
SON			4.2±1.5	2.9±0.5	2.7±0.5	4.2±1.6

Table A.8: Trends (per year, with 95% confidence interval limits) in UCDW variables for 1958-2007 in the Pacific sector. No trends were found for UCDW Top Depth or Southern-most position of UCDW. Additional trends are: UCDW Salinity in 65-70°S MAM (-2.2±2.2)$\times 10^{-4}$ and UCDW Density in 60-65°S JJA (-2.6±2.6)$\times 10^{-4}$.

UCDW	65-70°S	60-65°S	55-60°S	50-55°S	45-50°S	40-45°S
Vertical velocity $(ms^{-1}yr^{-1}) \times 10^{-8}$						
DJF	-0.9±0.6					
MAM	-1.0±0.8		3.2±2.5			
JJA	-1.3±0.8		2.1±1.9		-0.7±0.6	
SON	-0.9±0.7		2.1±1.8	-0.9±0.9	-0.7±0.6	-0.6±0.4
Temperature $(°Cyr^{-1}) \times 10^{-3}$						
DJF	0.8±0.8	1.4±0.7				0.3±0.2
MAM	0.9±0.8	1.5±0.8			-0.4±0.3	
JJA		1.4±0.9				
SON	1.0±0.8	1.3±0.8				

Table A.9: Trends (per year, with 95% confidence interval limits) for 1958-2007 in stratification, wind stress and Ekman variables in the Pacific sector.

	Stratification $(s^{-2}yr^{-1}) \times 10^{-7}$	Mean Wind Stress $(Nm^{-2}yr^{-1}) \times 10^{-4}$	Ekman Pumping $(ms^{-1}yr^{-1}) \times 10^{-8}$	Ekman Transport $(Svyr^{-1}) \times 10^{-2}$
70-75°S				
DJF				
MAM				
JJA	-2.1±0.7	-5.0±2.9		
SON	-1.7±0.6			
65-70°S				
DJF		2.1±1.8	0.8±0.6	
MAM				
JJA				
SON			-0.8±0.7	
60-65°S				
DJF	-2.9±1.6	5.7±4.0		1.2±0.8
MAM				
JJA	2.9±1.1			
SON		-7.8±6.5		-1.6±1.2
55-60°S				
DJF	-3.2±1.8	7.1±6.4		1.8±1.3
MAM				
JJA	1.5±1.0			
SON	2.1±1.0	-10.6±8.1		-2.5±1.7
50-55°S				
DJF	-5.4±1.7			
MAM				
JJA				
SON	1.5±1.0	-7.6±5.4		-2.3±1.7
45-50°S				
DJF	-4.4±1.8			
MAM	-2.3±1.8			
JJA				
SON				
40-45°S				
DFJ		-3.6±3.1		
MAM				
JJA		-5.5±4.1		-1.7±1.7
SON				

	Max. Wind Stress $(Nm^{-2}yr^{-1}) \times 10^{-3}$	Position of Max. Wind Stress $(°yr^{-1}) \times 10^{-2}$
DJF		-5.3±5.2
MAM		
JJA		-8.3±8.3
SON	-1.0±0.7	

Table A.10: Mixed Layer Trends (with 95% confidence interval limits) for 1958-2007 in the Pacific sector.

	MLD (myr^{-1})	ML Density ($kgm^{-3}yr^{-1}$) $\times 10^{-3}$	ML Salinity (yr^{-1}) $\times 10^{-3}$	ML Temperature ($°Cyr^{-1}$) $\times 10^{-2}$	SST ($°Cyr^{-1}$) $\times 10^{-2}$	SSS (yr^{-1}) $\times 10^{-3}$
70-75°S						
DJF				0.5±0.3	0.5±0.4	0.6±0.4
MAM		-0.6±0.6		0.6±0.3	0.7±0.3	
JJA	-0.23±0.11			0.4±0.2	0.4±0.2	
SON	-0.25±0.11			0.3±0.2	0.3±0.2	
65-70°S						
DJF	0.16±0.06					0.7±0.5
MAM				0.7±0.5	0.6±0.6	
JJA	-0.19±0.09	-1.0±0.7		1.2±0.3	1.3±0.3	
SON	-0.21±0.10	-0.9±0.6		1.1±0.3	1.2±0.2	
60-65°S						
DJF	0.22±0.10		-0.9±0.9			
MAM			-1.3±0.7			-0.9±0.8
JJA		-2.5±0.5	-1.7±0.6	1.7±0.5	1.9±0.7	-1.3±0.7
SON		-2.9±0.6	-1.5±0.8	2.3±0.6	2.4±0.6	-1.3±0.7
55-60°S						
DJF	0.24±0.12					
MAM		-1.4±0.9		0.7±0.5	0.7±0.5	
JJA	0.45±0.46	-2.9±0.9	-0.9±0.9	1.8±0.5	2.0±0.5	
SON		-2.9±1.0	-1.3±1.1	2.1±0.5	2.3±0.5	-1.5±1.3
50-55°S						
DJF	0.24±0.11			-1.0±0.5	-0.9±0.6	
MAM	0.32±0.16		-1.3±1.3			
JJA	0.52±0.30	-2.5±1.0	-2.1±0.9	0.8±0.3	0.9±0.3	-1.7±1.7
SON		-2.5±1.0	-1.8±1.0	1.0±0.3	1.1±0.4	-1.8±1.3
45-50°S						
DJF	0.07±0.06		-1.7±1.1	-1.3±0.4	-1.2±0.5	-1.6±1.0
MAM	0.08±0.08		-1.5±1.1	-0.6±0.4	-0.7±0.4	-1.5±1.1
JJA	0.35±0.18	-1.1±1.1	-1.6±1.1			-1.3±1.3
SON		-1.5±0.9	-2.0±0.9			-1.7±1.1
40-45°S						
DJF			-1.1±1.1	-0.7±0.5	-0.8±0.5	-1.1±1.1
MAM			-1.3±1.3			-1.3±1.1
JJA	0.16±0.12		-1.3±1.3	-0.8±0.4	-0.9±0.4	-1.2±1.2
SON	0.23±0.12		-2.0±1.2	-0.7±0.4	-0.8±0.4	-1.9±1.2

Bibliography

Adler, R., et al. (2003), The version 2 Global Precipitation Climatology Project (GPCP) monthly precipitation analysis (1979-present), *Journal of Hydrometeorology*, *4*, 1147–1167.

Alderkamp, A.-C., H. J. W. de Baar, R. J. W. Visser, and K. R. Arrigo (2010), Can photoinhibition control phytoplankton abundance in deeply mixed water columns of the Southern Ocean?, *Limnology and Oceanography*, *55*(3), 1248–1264.

Alory, G., S. Wijffels, and G. Meyers (2007), Observed temperature trends in the Indian Ocean over 1960-1999 and associated mechanisms, *Geophysical Research Letters*, *34*(2), L02606.

Aoki, S., M. Yoritaka, and A. Masuyama (2003), Multidecadal warming of subsurface temperature in the Indian sector of the Southern Ocean, *Journal of Geophysical Research*, *108*(C4), 8081.

Aoki, S., N. L. Bindoff, and J. A. Church (2005), Interdecadal water mass changes in the Southern Ocean between 30 degrees E and 160 degrees E, *Geophysical Research Letters*, *32*(7), L07607.

Arblaster, J. M., and G. A. Meehl (2006), Contributions of external forcings to Southern Annular Mode trends, *Journal of Climate*, *19*(12), 2896–2905.

Archer, D. E., and K. Johnson (2000), A model of the iron cycle in the ocean, *Global Biogeochemical Cycles*, *14*(1), 269–279.

Arrigo, K. R., G. L. van Dijken, and S. Bushinsky (2008), Primary production in the Southern Ocean, 1997-2006, *Journal of Geophysical Research-Oceans*, *113*(C8), C08004.

Barbini, R., F. Colao, R. Fantoni, L. Fiorani, I. G. Okladnikova, and A. Palucci (2005), LIDAR calibrated satellite sensed primary production in the Southern Ocean, *Journal of Optoelectronics and Advanced Materials*, *7*(2), 1091–1101.

Behrenfeld, M. J. (2010), Abandoning Sverdrup's critical depth hypothesis on phytoplankton blooms, *Ecology*, *91*(4), 977–989.

Behrenfeld, M. J., and P. G. Falkowski (1997), Photosynthetic rates derived from satellite-based chlorophyll concentration, *Limnology and Oceanography*, *42*, 1–20.

Behrenfeld, M. J., D. A. Siegel, R. T. O'Malley, and S. Maritorena (2009), Global ocean phytoplankton, *Special Supplement to the Bulletin of the American Meteorological Society*, *90*(8), S68–S73.

Behrenfeld, M. J., et al. (2006), Climate-driven trends in contemporary ocean productivity, *Nature*, *444*(7120), 752–755.

Berkman, P. A., D. S. Marks, and G. P. Shreve (1981), Winter sediment resuspension in mcMurdo Sound, Antarctica, and its ecological implications, *Polar Biology*, *6*(1), 1–3.

Biastoch, A., C. Böning, J. Getzlaff, J. Molines, and G. Madec (2008), Causes of interannual-decadal variability in the Meridional Overturning Circulation of the Midlatitude North Atlantic Ocean, *Journal of Climate*, *21*(24), 6599–6615.

Bindoff, N., et al. (2007), *Climate change 2007: The Physical Science basis. Contribution of Working Group I to the Fourth Assessment Report of the Intergovernmental Panel on Climate Changeorking Group I to the Fourth Assessment Report of the Intergovernmental Panel on Climate Change*, Observations: Oceanic Climate Change and Sea Level, Cambridge University Press, Cambridge.

Bindoff, N. L., K. P. Helm, A. Meijers, and S. Downes (2010), The evolving state of Antarctica and Southern Ocean over the last three decades, in *Atmosphere, Ocean, Environment and Society*, Conference Abstracts, p. 9, AMOS.

Blain, S., G. Sarthou, and P. Laan (2008), Distribution of dissolved iron during the natural iron-fertilization experiment KEOPS (Kerguelen Plateau, Southern Ocean), *Deep Sea Research Part II: Topical Studies in Oceanography*, *55*(5-7), 594–605.

Blain, S., et al. (2007), Effect of natural iron fertilization on carbon sequestration in the Southern Ocean, *Nature*, *446*(7139), 1070–U1.

Böning, C. W., A. Dispert, M. Visbeck, S. R. Rintoul, and F. U. Schwarzkopf (2008), The response of the Antarctic Circumpolar Current to recent climate change, *Nature Geoscience*, *1*(12), 864–869.

Borges, A. V., B. Tilbrook, N. Metzl, A. Lenton, and B. Delille (2008), Inter-annual variability of the carbon dioxide oceanic sink south of Tasmania, *Biogeosciences*, *5*(1), 141–155.

Bost, C. A., C. Cotte, F. Bailleul, Y. Cherel, J. B. Charrassin, C. Guinet, D. G. Ainley, and H. Weimerskirch (2009), The importance of oceanographic fronts to marine birds and mammals of the southern oceans, *Journal of Marine Systems*, *78*(3), 363–376.

Bowie, A. R., D. Lannuzel, T. A. Remenyi, T. Wagener, P. J. Lam, P. W. Boyd, C. Guieu, A. T. Townsend, and T. W. Trull (2009), Biogeochemical iron budgets of the Southern Ocean south of Australia: Decoupling of iron and nutrient cycles in the subantarctic zone by the summertime supply, *Global Biogeochemical Cycles*, *23*, GB4034.

Boyce, D. G., M. R. Lewis, and B. Worm (2010), Global phytoplankton decline over the past century, *Nature*, *466*(7306), 591–596.

Boyd, P. W., and D. Mackie (2008), Comment on the Southern Ocean biological response to aeolian iron deposition, *Science*, *319*(5860).

Boyd, P. W., S. C. Doney, R. Strzepek, J. Dusenberry, K. Lindsay, and I. Fung (2008), Climate-mediated changes to mixed-layer properties in the Southern Ocean: assessing the phytoplankton response, *Biogeosciences*, *5*(3), 847–864.

Boyd, P. W., et al. (2000), A mesoscale phytoplankton bloom in the polar Southern Ocean stimulated by iron fertilization, *Nature*, *407*(6805), 695–702.

Boyd, P. W., et al. (2007), Mesoscale iron enrichment experiments 1993-2005: Synthesis and future directions, *Science*, *315*(5812), 612–617.

Boyer, T., J. Antonov, H. Garcia, D. Johnson, R. Locarnini, A. Mishonov, M. Pitcher, O. Baranova, and I. Smolyar (2006), *World Ocean Database 2005*, Chap. 1: Introduction, NOAA Atlas NESDIS 60, U.S. Government Printing Office, Washington, D.C.

Boyer, T. P., S. Levitus, J. I. Antonov, R. Locarnini, and H. E. Garcia (2005), Linear trends in salinity for the World Ocean, 1955-1998, *Geophysical Research Letters*, *32*, L01604.

Boyer, T., Stephens, C., Antonov, J., Corkwright, M. E., Locarnini, R. A., O'Brien, T. D. and Garcia, H. (2002), *World Ocean Atlas 2001* (ed. Levitus, S.) Vol. 2, Salinity, NOAA Atlas NESDIS 50 U.S. Government Printing Office, Washington, D.C.

Breitbarth, E., et al. (2009), Iron biogeochemistry across marine systems at changing times – conclusions from the workshop held in Gothenburg, Sweden (14–16 May 2008), *Biogeosciences Discussions*, *6*(4), 6635–6694.

Broecker, W. S. (1991), The great ocean conveyor, *Oceanography*, *4*, 79–89.

Butler, A. H., D. W. J. Thompson, and K. R. Gurney (2007), Observed relationships between the Southern Annular Mode and atmospheric carbon dioxide, *Global Biogeochemical Cycles*, *21*(4), GB4014.

Callahan, J. E. (1972), The structure and circulation of Deep Water in the Antarctic, *Deep-Sea Research*, *19*, 563–575.

Carr, M. E., et al. (2006), A comparison of global estimates of marine primary production from ocean color, *Deep-Sea Research Part II-Topical Studies in Oceanography*, *53*(5-7), 741–770.

Carton, J. A., and B. S. Giese (2008), A reanalysis of ocean climate using SODA, *Monthly Weather Review*, *136*(8), 2999–3017.

Carton, J. A., and A. Santorelli (2008), Global decadal upper-ocean heat content as viewed in nine analyses, *Journal of Climate*, *21*(22), 6015–6035.

Carton, J. A., G. A. Chepurin, and Y.-S. Chang (), Variability of shallow water masses of the northern and tropical oceans as viewed in nine ocean analyses, *Journal of Climate*, *(submitted)*.

Carton, J. A., G. Chepurin, X. H. Cao, and B. Giese (2000), A Simple Ocean Data Assimilation analysis of the global upper ocean 1950-95. Part I: Methodology, *Journal of Physical Oceanography*, *30*(2), 294–309.

Carton, J. A., B. S. Giese, and S. A. Grodsky (2005), Sea level rise and the warming of the oceans in the Simple Ocean Data Assimilation (SODA) ocean reanalysis, *Journal of Geophysical Research-Oceans*, *110*(C9), C09006.

Cassar, N., M. L. Bender, B. A. Barnett, S. Fan, W. J. Moxim, H. Levy, and B. Tilbrook (2007), The Southern Ocean biological response to aeolian iron deposition, *Science*, *317*(5841), 1067–1070.

Chepurin, G. A., J. A. Carton, and D. Dee (2005), Forecast model bias correction in ocean data assimilation, *Monthly Weather Review*, *133*(5), 1328–1342.

Ciasto, L. M., and D. W. J. Thompson (2008), Observations of large-scale ocean-atmosphere interaction in the Southern Hemisphere, *Journal of Climate*, *21*(6), 1244–1259.

Coale, K. H. (1991), Effects of Iron, Manganese, Copper, and Zinc enrichments on productivity and biomass in the sub-Arctic Pacific, *Limnology and Oceanography*, *36*(8), 1851–1864.

Coale, K. H., X. J. Wang, S. J. Tanner, and K. S. Johnson (2003), Phytoplankton growth and biological response to iron and zinc addition in the Ross Sea and Antarctic Circumpolar Current along 170 degrees W, *Deep-Sea Research Part II-Topical Studies in Oceanography*, *50*(3-4), 635–653.

Coale, K. H., R. M. Gordon, and X. J. Wang (2005), The distribution and behavior of dissolved and particulate iron and zinc in the Ross Sea and Antarctic Circumpolar Current along 170 degrees W, *Deep-Sea Research Part I-Oceanographic Research Papers*, *52*(2), 295–318.

Coale, K. H., et al. (2004), Southern Ocean iron enrichment experiment: Carbon cycling in high- and low-Si waters, *Science*, *304*(5669), 408–414.

Comiso, J. (1999, updated 2008), *Bootstrap sea ice concentrations from NIMBUS-7 and DMSP SSM/I, 1997-2007.*, National Snow and Ice Data Center, Boulder, Colorado, USA.

Comiso, J. C., C. R. McClain, C. W. Sullivan, J. P. Ryan, and C. L. Leonard (1993), Coastal Zone Color Scanner pigment concentrations in the Southern-Ocean and relationships to geophysical surface-features, *Journal of Geophysical Research-Oceans*, *98*(C2), 2419–2451.

Constable, A. J., S. Nicol, and P. G. Strutton (2003), Southern Ocean productivity in relation to spatial and temporal variation in the physical environment, *Journal of Geophysical Research-Oceans*, *108*(C4), 8079.

Croot, P. L., K. Andersson, M. Ozturk, and D. R. Turner (2004), The distribution and specification of iron along 6 degrees E in the Southern Ocean, *Deep-Sea Research Part II-Topical Studies in Oceanography*, *51*(22-24), 2857–2879.

de Baar, H. J. W., et al. (2005), Synthesis of iron fertilization experiments: From the Iron Age in the Age of Enlightenment, *Journal of Geophysical Research-Oceans*, *110*(C9), C09S16.

DeBaar, H. J. W., J. T. M. DeJong, D. C. E. Bakker, B. M. Loscher, C. Veth, U. Bathmann, and V. Smetacek (1995), Importance of iron for plankton blooms and carbon-dioxide drawdown in the Southern-Ocean, *Nature*, *373*(6513), 412–415.

Denman, K., et al. (2007), *Couplings Between Changes in the Climate System and Biogeochemistry. In: Climate Change 2007: The Physical Science Basis. Contribution of Working Group I to the Fourth Assessment Report of the Intergovernmental Panel on Climate Change*, Cambridge University Press, Cambridge, United Kingdom and New York, NY, USA.

Dierssen, H. M., M. Vernet, and R. C. Smith (2000), Optimising models for remotely estimating primary production in Antarctic coastal waters, *Antarctic Science*, *12*, 20–32.

Doney, S. C., B. Tilbrook, S. Roy, N. Metzl, C. Le Quere, M. Hood, R. A. Feely, and D. Bakker (2009), Surface-ocean CO2 variability and vulnerability, *Deep Sea Research Part II: Topical Studies in Oceanography*, *56*(8-10), 504–511.

Drost, F., and M. H. England (2009), Spatial aspects of the Southern Annular Mode, in *Extremes: Climate and Water in the Southern Hemisphere*, Short Abstracts, p. 46, AMS/AMOS.

Ellwood, M. J., P. W. Boyd, and P. Sutton (2008), Winter-time dissolved iron and nutrient distributions in the Subantarctic Zone from 40-52S; 155-160E, *Geophysical Research Letters*, *35*(11), L11604.

Elrod, V. A., W. M. Berelson, K. H. Coale, and K. S. Johnson (2004), The flux of iron from continental shelf sediments: A missing source for global budgets, *Geophysical Research Letters*, *31*.

Feng, Y., et al. (2010), Interactive effects of iron, irradiance and CO2 on Ross Sea phytoplankton, *Deep Sea Research Part I: Oceanographic Research Papers*, *57*(3), 368–383.

Field, C., M. Behrenfeld, J. Randerson, and P. Falkowski (1998), Primary production of the biosphere: Integrating terrestrial and oceanographic components, *Science*, *291*, 237–240.

Fung, I. Y., S. K. Meyn, I. Tegen, S. C. Doney, J. G. John, and J. K. B. Bishop (2000), Iron supply and demand in the upper ocean, *Global Biogeochemical Cycles*, *14*(1), 281–295.

Fyfe, J. C., and O. A. Saenko (2006), Simulated changes in the extratropical Southern Hemisphere winds and currents, *Geophysical Research Letters*, *33*(6), L06701.

Fyfe, J. C., O. A. Saenko, K. Zickfeld, M. Eby, and A. J. Weaver (2007), The role of poleward-intensifying winds on Southern Ocean warming, *Journal of Climate*, *20*(21), 5391–5400.

Gabric, A. J., R. Cropp, G. P. Ayers, G. McTainsh, and R. Braddock (2002), Coupling between cycles of phytoplankton biomass and aerosol optical depth as derived from SeaWiFS time series in the Subantarctic Southern Ocean, *Geophysical Research Letters*, *29*(7), 1112.

Gabric, A. J., R. A. Cropp, G. H. McTainsh, B. M. Johnston, H. Butler, B. Tilbrook, and M. Keywood (2010), Australian dust storms in 2002-2003 and their impact on Southern Ocean biogeochemistry, *Global Biogeochemical Cycles*, *24*, GB2005.

Garabato, A. C. N., D. P. Stevens, A. J. Watson, and W. Roether (2007), Short-circuiting of the overturning circulation in the Antarctic Circumpolar Current, *Nature*, *447*(7141), 194–197.

Garcia, H. E., R. A. Locarnini, T. P. Boyer, and J. I. Antonov (2006), *World Ocean Atlas 2005, Volume 4: Nutrients (phosphate, nitrate, silicate)*, NOAA Atlas NESDIS 64, U.S. Government Printing Office, Washington, D.C.

Gemmell, A., G. C. Smith, K. Haines, and J. D. Blower (2008), Evaluation of water masses in ocean synthesis products, *CLIVAR Exchanges*, *13*(4), 7–9.

Gervais, F., U. Riebesell, and M. Y. Gorbunov (2002), Changes in primary productivity and chlorophyll a in response to iron fertilization in the Southern Polar Frontal Zone, *Limnology and Oceanography*, *47*(5), 1324–1335.

Giese, B. S. (2006), SODA method, *CLIVAR/GODAE report*, Second meeting on Ocean Synthesis Evaluation, Reading, UK.

Gilbert, R. O. (1987), *Statistical methods for environmental pollution monitoring*, Van Nostrand Reinhold Company Inc., New York.

Gille, S. T. (2002), Warming of the Southern Ocean since the 1950s, *Science*, *295*(5558), 1275–1277.

Gille, S. T. (2008), Decadal-scale temperature trends in the Southern Hemisphere Ocean, *Journal of Climate*, *21*(18), 4749–4765.

Gordon, A. L. (1967), *Structure of Antarctic waters between 20W and 170W*, *Antarct. Map Folio Ser.*, vol. 6, Am. Geogr. Soc., New York.

Gordon, A. L., and B. A. Huber (1990), Southern-Ocean winter mixed layer, *Journal of Geophysical Research-Oceans*, *95*(C7), 11,655–11,672.

Gruber, N., et al. (2009), Oceanic sources, sinks, and transport of atmospheric CO2, *Global Biogeochemical Cycles*, *23*, GB1005.

Hall, A., and M. Visbeck (2002), Synchronous variability in the Southern Hemisphere atmosphere, sea ice, and ocean resulting from the Annular Mode, *Journal of Climate*, *15*(21), 3043–3057.

Helm, K. P., Bindoff, N. L. and Church, J. A. (2010), Changes in the global hydrological-cycle inferred from ocean salinity, *Geophysical Research Letters*, *37*(18), L18701.

Henson, S. A., J. L. Sarmiento, J. P. Dunne, L. Bopp, I. Lima, S. C. Doney, J. John, and C. Beaulieu (2010), Detection of anthropogenic climate change in satellite records of ocean chlorophyll and productivity, *Biogeosciences*, *7*(2), 621–640.

Hess, A., H. Iyer, and W. Malm (2001), Linear trend analysis: a comparison of methods, *Atmospheric Environment*, *35*(30), 5211–5222.

Hill, K. L., S. R. Rintoul, R. Coleman, and K. R. Ridgway (2008), Wind forced low frequency variability of the East Australia Current, *Geophysical Research Letters*, *35*(8), L08602.

Hirsch, R. M., J. R. Slack, and R. A. Smith (1982), Techniques of trend analysis for monthly water quality data, *Water Resources Research*, *18*, 107–121.

Hiscock, M. R., J. Marra, W. O. Smith, R. Goericke, C. Measures, S. Vink, R. J. Olson, H. M. Sosik, and R. T. Barber (2003), Primary productivity and its regulation in the Pacific Sector of the Southern Ocean, *Deep-Sea Research Part II-Topical Studies in Oceanography*, *50*(3-4), 533–558.

Hoffmann, L. J., I. Peeken, K. Lochte, P. Assmy, and M. Veldhuis (2006), Different reactions of southern ocean phytoplankton size classes to iron fertilization, *Limnology and Oceanography*, *51*(3), 1217–1229.

Holbrook, N. J., and N. L. Bindoff (1997), Interannual and decadal temperature variability in the southwest Pacific Ocean between 1955 and 1988, *Journal of Climate*, *10*(5), 1035–1049.

Hoppema, M., E. Fahrbach, and H. J. W. De Baar (2000), Surface layer balance of the southern Antarctic Circumpolar Current (prime meridian) used to derive carbon and silicate consumptions and annual air-sea exchange for CO_2 and oxygen, *Journal of Geophysical Research-Oceans*, *105*(C5), 11,359–11,371.

Hoppema, M., H. J. W. de Baar, E. Fahrbach, H. H. Hellmer, and B. Klein (2003), Substantial advective iron loss diminishes phytoplankton production in the Antarctic Zone, *Global Biogeochemical Cycles*, *17*(1), 1025.

Hosoda, S., T. Suga, N. Shikama, and K. Mizuno (2009), Global surface layer salinity change detected by Argo and its implication for hydrological cycle intensification, *Journal of Oceanography*, *65*(4), 579–586.

IHO (1953), Limits of oceans and seas, *Special publication number 23*, International Hydrographic Organization.

Ito, T., M. Woloszyn, and M. Mazloff (2010), Anthropogenic carbon dioxide transport in the Southern Ocean driven by Ekman flow, *Nature*, *463*(7277), 80–83.

Iudicone, D., I. Stendardo, O. Aumont, K. B. Rodgers, G. Madec, L. Bopp, O. Mangoni, and M. Ribera d'Alcala' (2010), Watermasses as a unifying framework for understanding the Southern Ocean carbon cycle, *Biogeosciences Discussions*, *7*(3), 3393–3451.

Jacobs, S. (2006), Observations of change in the Southern Ocean, *Philosophical Transactions of the Royal Society A-Mathematical Physical and Engineering Sciences*, *364*(1844), 1657–1681.

Jacobson, M. C., R. J. Charlson, H. Rodhe, and G. H. Orians (2000), *Earth System Science: From biogeochemical cycles to global change*, *International Geophysics Series*, vol. 72, Academic Press.

Jickells, T. D., et al. (2005), Global Iron connections between desert dust, ocean biogeochemistry, and climate, *Science*, *308*(5718), 67–71.

Johnson, G. C., and A. H. Orsi (1997), Southwest Pacific Ocean water-mass changes between 1968/69 and 1990/91, *Journal of Climate*, *10*(2), 306–316.

Johnson, K. S., F. P. Chavez, and G. E. Friederich (1999), Continental-shelf sediment as a primary source of iron for coastal phytoplankton, *Nature*, *398*(6729), 697–700.

Jones, J. M., and M. Widmann (2004), Atmospheric science: Early peak in Antarctic oscillation index, *Nature*, *432*(7015), 290–291.

Kawabe, M., and S. Fujio (2010), Pacific ocean circulation based on observation, *Journal of Oceanography*, *66*(3), 389–403.

Khatiwala, S., F. Primeau, and T. Hall (2009), Reconstruction of the history of anthropogenic CO2 concentrations in the ocean, *Nature*, *462*(7271), 346–349.

Lalli, C. M., and T. R. Parsons (1997), *Biological Oceanography: An Introduction*, 2nd ed., Elsevier Butterworth-Heinemann.

Lannuzel, D., V. Schoemann, J. de Jong, J. L. Tison, and L. Chou (2007), Distribution and biogeochemical behaviour of iron in the East Antarctic sea ice, *Marine Chemistry*, *106*(1-2), 18–32.

Lannuzel, D., T. Remenyi, P. Lam, A. Townsend, E. Ibisanmi, E. Butler, T. Wagener, V. Schoemann, and A. R. Bowie (2010a), Distributions of dissolved and particulate iron in the sub-Antarctic and Polar Frontal Southern Ocean (Australian sector), *Deep-Sea Research Part II-Topical Studies in Oceanography*, (accepted).

Lannuzel, D., V. Schoemann, J. de Jong, B. Pasquer, P. van der Merwe, F. Masson, J.-L. Tison, and A. Bowie (2010b), Distribution of dissolved iron in Antarctic sea ice: Spatial, seasonal, and inter-annual variability, *Journal of Geophysical Research*, *115*(G3).

Large, W. G., J. C. McWilliams, and S. C. Doney (1994), Oceanic vertical mixing - a review and a model with a nonlocal boundary-layer parameterization, *Reviews of Geophysics*, *32*(4), 363–403.

Le Quere, C., et al. (2007), Saturation of the Southern Ocean CO_2 sink due to recent climate change, *Science*, *316*(5832), 1735–1738.

Lee, T., T. Awaji, M. A. Balmaseda, E. Greiner, and D. Stammer (2009), Ocean state estimation for climate research, *Oceanography*, *22*(3), 160–167.

Lefebvre, W., H. Goosse, R. Timmermann, and T. Fichefet (2004), Influence of the Southern Annular Mode on the sea ice-ocean system, *Journal of Geophysical Research-Oceans*, *109*(C9), C09005.

Lefevre, N., and A. J. Watson (1999), Modeling the geochemical cycle of iron in the oceans and its impact on atmospheric CO2 concentrations, *Global Biogeochemical Cycles*, *13*(3), 727–736.

Lenton, A., and R. J. Matear (2007), Role of the Southern Annular Mode (SAM) in Southern Ocean CO_2 uptake, *Global Biogeochemical Cycles*, *21*(2), GB2016.

Lenton, A., F. Codron, L. Bopp, N. Metzl, P. Cadule, A. Tagliabue, and J. Le Sommer (2009), Stratospheric ozone depletion reduces ocean carbon uptake and enhances ocean acidification, *Geophysical Research Letters*, *36*.

Levitus, S., J. Antonov, and T. Boyer (2005), Warming of the world ocean, 1955-2003, *Geophysical Research Letters*, *32*(2), L02604.

L'Heureux, M. L., and D. W. J. Thompson (2006), Observed relationships between the El Nino-Southern Oscillation and the extratropical zonal-mean circulation, *Journal of Climate*, *19*(2), 276–287.

Liu, J., and J. A. Curry (2010), Accelerated warming of the Southern Ocean and its impacts on the hydrodological cycle and sea ice, *Proceedings of the National Academy of Sciences*, (Early on-line).

Löscher, B. M. (1999), Relationships among Ni, Cu, Zn, and major nutrients in the Southern Ocean, *Marine Chemistry*, *67*(1-2), 67–102.

Löscher, B. M., H. J. W. DeBaar, J. T. M. DeJong, C. Veth, and F. Dehairs (1997), The distribution of Fe in the Antarctic Circumpolar Current, *Deep-Sea Research Part II-Topical Studies in Oceanography*, *44*(1-2), 143–187.

Lovenduski, N. S., and N. Gruber (2005), Impact of the Southern Annular Mode on Southern Ocean circulation and biology, *Geophysical Research Letters*, *32*(11), L11603.

Lovenduski, N. S., N. Gruber, S. C. Doney, and I. D. Lima (2007), Enhanced CO2 outgassing in the Southern Ocean from a positive phase of the Southern Annular Mode, *Global Biogeochemical Cycles*, *21*(2), GB2026.

Lovenduski, N. S., N. Gruber, and S. C. Doney (2008), Toward a mechanistic understanding of the decadal trends in the Southern Ocean carbon sink, *Global Biogeochemical Cycles*, *22*(3), GB3016.

Lozier, M. S. (2010), Deconstructing the Conveyor Belt, *Science*, *328*(5985), 1507–1511.

Lumpkin, R., and K. Speer (2007), Global ocean meridional overturning, *Journal of Physical Oceanography*, *37*(10), 2550–2562.

Mantua, N. J., and S. R. Hare (2002), The Pacific decadal oscillation, *Journal of Oceanography*, *58*(1), 35–44.

Marinov, I., A. Gnanadesikan, J. R. Toggweiler, and J. L. Sarmiento (2006), The Southern Ocean biogeochemical divide, *Nature*, *441*(7096), 964–967.

Marinov, I., S. C. Doney, and I. D. Lima (2010), Response of ocean phytoplankton community structure to climate change over the 21st century: partitioning the effects of nutrients, temperature and light, *Biogeosciences Discussions*, *7*, 4565–4606.

Marshall, G. J. (2003), Trends in the Southern Annular Mode from observations and reanalyses, *Journal of Climate*, *16*(24), 4134–4143.

Marshall, G. J. (2007), Half-century seasonal relationships between the Southern Annular Mode and Antarctic temperatures, *International Journal of Climatology*, *27*(3), 373–383.

Martin, J. (1990), Glacial-interglacial CO2 change: The iron hypothesis, *Paleoceanography*, *5*(1), 1–13.

Martin, J. H., S. E. Fitzwater, and R. M. Gordon (1990a), Iron deficiency limits phytoplankton growth in Antarctic waters, *Global Biogeochemical Cycles*, *4*, 5–12.

Martin, J. H., R. M. Gordon, and S. E. Fitzwater (1990b), Iron in Antarctic waters, *Nature*, *345*(6271), 156–158.

Martinez, E., D. Antoine, F. D'Ortenzio, and B. Gentili (2009), Climate-driven basin-scale decadal oscillations of oceanic phytoplankton, *Science*, *326*(5957), 1253–1256.

Martinson, D. G., S. E. Stammerjohn, R. A. Iannuzzi, R. C. Smith, and M. Vernet (2008), Western Antarctic Peninsula physical oceanography and spatio-temporal variability, *Deep Sea Research Part II: Topical Studies in Oceanography*, *55*(18-19), 1964–1987.

McClain, C. R., G. C. Feldman, and S. B. Hooker (2004), An overview of the SeaWiFS project and strategies for producing a climate research quality global ocean bio-optical time series, *Deep-Sea Research Part II-Topical Studies in Oceanography*, *51*(1-3), 5–42.

McNeil, B. I., N. Metzl, R. M. Key, R. J. Matear, and A. Corbiere (2007), An empirical estimate of the Southern Ocean air-sea CO2 flux, *Global Biogeochemical Cycles*, *21*(3), GB3011.

Measures, C. I., and S. Vink (2001), Dissolved Fe in the upper waters of the Pacific sector of the Southern Ocean, *Deep-Sea Research Part II-Topical Studies in Oceanography*, *48*(19-20), 3913–3941.

Meskhidze, N., A. Nenes, W. L. Chameides, C. Luo, and N. Mahowald (2007), Atlantic Southern Ocean productivity: Fertilization from above or below?, *Global Biogeochemical Cycles*, *21*(2), GB2006.

Metzl, N. (2009), Decadal increase of oceanic carbon dioxide in Southern Indian Ocean surface waters (1991-2007), *Deep Sea Research Part II: Topical Studies in Oceanography*, *56*(8-10), 607–619.

Metzl, N., C. Brunet, A. Jabaud-Jan, A. Poisson, and B. Schauer (2006), Summer and winter air-sea CO2 fluxes in the Southern Ocean, *Deep Sea Research Part I: Oceanographic Research Papers*, *53*(9), 1548–1563.

Metzl, N., A. Lenton, T. Takahashi, and B. Tilbrook (2009), Decadal variability of oceanic pCO2 observed in the Southern Ocean: contrasting trends before and after 2000, *Geophysical Research Abstracts*, *11*, EGU2009–5519.

Mikaloff Fletcher, S. E., et al. (2006), Inverse estimates of anthropogenic CO2 uptake, transport, and storage by the ocean, *Global Biogeochemical Cycles*, *20*(2), GB2002.

Mikaloff Fletcher, S. E., et al. (2007), Inverse estimates of the oceanic sources and sinks of natural CO2 and the implied oceanic carbon transport, *Global Biogeochemical Cycles*, *21*.

Miller, R. L., G. A. Schmidt, and D. T. Shindell (2006), Forced annular variations in the 20th century Intergovernmental Panel on Climate Change Fourth Assessment Report models, *Journal of Geophysical Research*, *111*.

Milliff, R. F., J. Morzel, D. B. Chelton, and M. H. Freilich (2004), Wind stress curl and wind stress divergence biases from rain effects on QSCAT surface wind retrievals, *Journal of Atmospheric and Oceanic Technology*, *21*(8), 1216–1231.

Mitchell, B. G., and O. Holm-Hansen (1991), Observations and modeling of the Antarctic phytoplankton crop in relation to mixing depth, *Deep-Sea Research Part A-Oceanographic Research Papers*, *38*(8-9), 981–1007.

Moffat, C., B. Owens, and R. C. Beardsley (2009), On the characteristics of Circumpolar Deep Water intrusions to the west Antarctic Peninsula Continental Shelf, *Journal of Geophysical Research*, *114*.

Monaghan, A. J., D. H. Bromwich, W. Chapman, and J. C. Comiso (2008), Recent variability and trends of Antarctic near-surface temperature, *Journal of Geophysical Research-Atmospheres*, *113*(D4), D04105.

Montegut, C. D., G. Madec, A. S. Fischer, A. Lazar, and D. Iudicone (2004), Mixed layer depth over the global ocean: An examination of profile data and a profile-based climatology, *Journal of Geophysical Research-Oceans*, *109*(C12), C12003.

Monterey, G., and S. Levitus (1997), *NOAA Atlas NESDIS 14*, chap. Seasonal Variability of Mixed Layer Depth for the World Ocean, p. 96, U.S. Government Printing Office.

Moore, J. K., and M. R. Abbott (2000), Phytoplankton chlorophyll distributions and primary production in the Southern Ocean, *Journal of Geophysical Research-Oceans*, *105*(C12), 28,709–28,722.

Moore, J. K., and M. R. Abbott (2002), Surface chlorophyll concentrations in relation to the Antarctic Polar Front: seasonal and spatial patterns from satellite observations, *Journal of Marine Systems*, *37*(1-3), 69–86.

Moore, J. K., and S. C. Doney (2006), Remote sensing observations of ocean physical and biological properties in the region of the Southern Ocean Iron Experiment (SOFeX), *Journal of Geophysical Research-Oceans*, *111*(C6), C06026.

Moore, J. K., M. R. Abbott, J. G. Richman, W. O. Smith, T. J. Cowles, K. H. Coale, W. D. Gardner, and R. T. Barber (1999), SeaWiFS satellite ocean color data from the Southern Ocean, *Geophysical Research Letters*, *26*(10), 1465–1468.

Moore, J. K., S. C. Doney, D. M. Glover, and I. Y. Fung (2002), Iron cycling and nutrient-limitation patterns in surface waters of the World Ocean, *Deep-Sea Research Part II-Topical Studies in Oceanography*, *49*(1-3), 463–507.

Morel, A., and J.-F. Berthon (1989), Surface pigments, algal biomass profiles, and potential production of the euphotic layer: Relationships reinvestigated in view of remote-sensing applications, *Limnology and Oceanography*, *34*(8), 1545–1562.

Morel, F. M. M., and N. M. Price (2003), The biogeochemical cycles of trace metals in the oceans, *Science*, *300*(5621), 944–947.

Morrow, R., G. Valladeau, and J. B. Sallee (2008), Observed subsurface signature of Southern Ocean sea level rise, *Progress in Oceanography*, *77*, 351–366.

Nelson, D. M., and W. O. Smith, Jr. (1991), Sverdrup revisited: critical depths, maximum chlorophyll levels, and the control of southern ocean productivity by the irradiance mixing regime, Limnology and Oceanography, *36*, 1650–1661.

Nicol, S., T. Pauly, N. L. Bindoff, S. Wright, D. Thiele, G. W. Hosie, P. G. Strutton, and E. Woehler (2000), Ocean circulation off east Antarctica affects ecosystem structure and sea-ice extent, *Nature*, *406*(6795), 504–507.

Nishikawa, J., S. Toczko, and G. W. Hosie (2010), Distribution and community structure of euphausiids in the Southern Ocean along the 140E meridian during the austral summer 2001/2002, *Deep Sea Research Part II: Topical Studies in Oceanography*, *57*(7-8), 559–564.

Olbers, D., D. Borowski, C. Volker, and J. O. Wolff (2004), The dynamical balance, transport and circulation of the Antarctic Circumpolar Current, *Antarctic Science*, *16*(4), 439–470.

O'Reilly, J. E., S. Maritorena, B. G. Mitchell, D. A. Siegel, K. L. Carder, S. A. Garver, M. Kahru, and C. McClain (1998), Ocean color chlorophyll algorithms for SeaWiFS, *Journal of Geophysical Research*, *103*.

Orr, J. C., et al. (2001), Estimates of anthropogenic carbon uptake from four three-dimensional global ocean models, *Global Biogeochemical Cycles*, *15*(1), 43–60.

Orsi, A., and U. Ryan (2001, updated 2006), Locations of the various fronts in the Southern Ocean, Australian Antarctic Data Centre - CAASM Metadata (http://data.aad.gov.au/aadc/metadata/).

Orsi, A. H., T. Whitworth, and W. D. Nowlin (1995), On the meridional extent and fronts of the Antarctic Circumpolar Current, *Deep-Sea Research Part I-Oceanographic Research Papers*, *42*(5), 641–673.

Palter, J. B., J. L. Sarmiento, A. Gnanadesikan, J. Simeon, and D. Slater (2010), Fueling primary productivity: nutrient return pathways from the deep ocean and their dependence on the Meridional Overturning Circulation, *Biogeosciences Discussions*, *7*(3), 4045–4088.

Park, Y.-H., L. Gamberoni, and E. Charriaud (1993), Frontal structure, water masses, and circulation in the Crozet Basin, *Journal of Geophysical Research*, *98*(C7), 12,361–12,385.

Patterson, S. L., and T. Whitworth (1990), *Antarctic Sector of the Pacific*, chap. Physical Oceanography, pp. 55–93, Elsevier, New York.

Peloquin, J. A., and W. O. Smith (2007), Phytoplankton blooms in the Ross Sea, Antarctica: Interannual variability in magnitude, temporal patterns, and composition, *Journal of Geophysical Research-Oceans*, *112*(C8), C08013.

Pollard, R., P. Treguer, and J. Read (2006), Quantifying nutrient supply to the Southern Ocean, *Journal of Geophysical Research-Oceans*, *111*(C5), C05011.

Pollard, R. T., J. F. Read, J. T. Allen, G. Griffiths, and A. I. Morrison (1995), On the physical structure of a front in the Bellingshausen Sea, *Deep-Sea Research Part II-Topical Studies in Oceanography*, *42*(4-5), 955–982.

Pollard, R. T., M. I. Lucas, and J. F. Read (2002), Physical controls on biogeochemical zonation in the Southern Ocean, *Deep-Sea Research Part II-Topical Studies in Oceanography*, *49*(16), 3289–3305.

Pollard, R. T., et al. (2009), Southern Ocean deep-water carbon export enhanced by natural iron fertilization, *Nature*, *457*(7229), 577–U81.

Prezelin, B. B., E. E. Hofmann, C. Mengelt, and J. M. Klinck (2000), The linkage between Upper Circumpolar Deep Water (UCDW) and phytoplankton assemblages on the west Antarctic Peninsula continental shelf, *Journal of Marine Research*, *58*(2), 165–202.

Prezelin, B. B., E. E. Hofmann, M. Moline, and J. M. Klinck (2004), Physical forcing of phytoplankton community structure and primary production in continental shelf waters of the Western Antarctic Peninsula, *Journal of Marine Research*, *62*(3), 419–460.

Rahmstorf, S. (2006), *Encyclopedia of Quaternary Sciences*, Elsevier.

Reid, J. L. (1981), *Evolution of Physical Oceanography*, chap. On the mid-depth circulation of the world ocean, pp. 70–111, MIT Press, Cambridge, MA.

Reid, J. L., J. W. D. Nowlin, and W. C. Patzert (1977), On the characteristics and circulation of the Southwestern Atlantic Ocean, *Journal of Physical Oceanography*, *7*, 62–91.

Reiss, C. S., C. D. Hewes, and O. Holm-Hansen (2009), Influence of atmospheric teleconnections and Upper Circumpolar Deep Water on phytoplankton biomass around Elephant Island, Antarctica, *Marine Ecology Progress Series*, *377*, 51–62.

Rintoul, S. R. (2007), Rapid freshening of Antarctic Bottom Water formed in the Indian and Pacific oceans, *Geophysical Research Letters*, *34*(6), L06606.

Rintoul, S. R., and S. Sokolov (2001), Baroclinic transport variability of the Antarctic Circumpolar Current south of Australia (WOCE repeat section SR3), *Journal of Geophysical Research-Oceans*, *106*(C2), 2815–2832.

Rintoul, S. R., and T. W. Trull (2001), Seasonal evolution of the mixed layer in the Subantarctic Zone south of Australia, *Journal of Geophysical Research-Oceans*, *106*(C12), 31,447–31,462.

Roemmich, D., and J. Gilson (2009), The 2004-2008 mean and annual cycle of temperature, salinity, and steric height in the global ocean from the Argo Program, *Progress In Oceanography*, *82*(2), 81–100.

Rose, J. M., et al. (2009), Synergistic effects of iron and temperature on Antarctic phytoplankton and microzooplankton assemblages, *Biogeosciences*, *6*(12), 3131–3147.

Russell, J. L., K. W. Dixon, A. Gnanadesikan, R. J. Stouffer, and J. R. Toggweiler (2006), The Southern Hemisphere westerlies in a warming world: Propping open the door to the deep ocean, *Journal of Climate*, *19*(24), 6382–6390.

Saba, V. S., et al. (2010a), An evaluation of ocean color model estimates of marine primary productivity in coastal and pelagic regions across the globe, *Biogeosciences Discussions*, *7*(5), 6749–6788.

Saba, V. S., et al. (2010b), Challenges of modeling depth-integrated marine primary productivity over multiple decades: A case study at BATS and HOT, *Global Biogeochemical Cycles*, *24*(3), GB3020.

Sabine, C. L., et al. (2004), The oceanic sink for anthropogenic CO2, *Science*, *305*(5682), 367–371.

Saenko, O. A., J. C. Fyfe, and M. H. England (2005), On the response of the oceanic wind-driven circulation to atmospheric CO2 increase, *Climate Dynamics*, *25*(4), 415–426.

Sallee, J. B., K. Speer, and R. Morrow (2008), Response of the Antarctic Circumpolar Current to atmospheric variability, *Journal of Climate*, *21*(12), 3020–3039.

Sallee, J. B., K. G. Speer, and S. R. Rintoul (2010), Zonally asymmetric response of the Southern Ocean mixed-layer depth to the Southern Annular Mode, *Nature Geoscience*, *3*, 273–279.

Santoso, A., M. H. England, and A. C. Hirst (2006), Circumpolar Deep Water circulation and variability in a coupled climate model, *Journal of Physical Oceanography*, *36*(8), 1523–1552.

Sarmiento, J. L., N. Gruber, M. A. Brzezinski, and J. P. Dunne (2004), High-latitude controls of thermocline nutrients and low latitude biological productivity, *Nature*, *427*(6969), 56–60.

Scharek, R., M. A. VanLeeuwe, and H. J. W. DeBaar (1997), Responses of Southern Ocean phytoplankton to the addition of trace metals, *Deep-Sea Research Part II-Topical Studies in Oceanography*, *44*(1-2), 209–227.

Schlitzer, R., P. Monfray, and N. Hoepffner (2003), Global ocean productivity and the fluxes of carbon and nutrients: combining observations and models,

JGOFS (Joint Global Ocean Flux Study) Report 38, Report of a Workshop held at the Institute for Environment and Sustainability, EC Joint Research Centre, Ispra, Italy.

Schmitz, W. J. (1996), On the World Ocean Circulation: Volume II. The Pacific and Indian Oceans/A global update, *Tech. Rep. WHOI-96-08*, Woods Hole Oceanographic Institution, Woods Hole, Massachusetts, 02543.

Schott, F. A., L. Stramma, W. Wang, B. S. Giese, and R. Zantopp (2008), Pacific subtropical cell variability in the SODA 2.0.2/3 assimilation, *Geophysical Research Letters*, *35*, L10607.

Schott, F. A., L. Stramma, B. S. Giese, and R. Zantopp (2009), Labrador Sea convection and subpolar North Atlantic Deep Water export in the SODA assimilation model, *Deep Sea Research Part I: Oceanographic Research Papers*, *56*(6), 926–938.

Sedwick, P. N., and G. R. DiTullio (1997), Regulation of algal blooms in Antarctic shelf waters by the release of iron from melting sea ice, *Geophysical Research Letters*, *24*(20), 2515–2518.

Sedwick, P. N., P. R. Edwards, D. J. Mackey, F. B. Griffiths, and J. S. Parslow (1997), Iron and manganese in surface waters of the Australian Subantarctic region, *Deep-Sea Research Part I-Oceanographic Research Papers*, *44*(7), 1239–1253.

Sedwick, P. N., G. R. DiTullio, and D. J. Mackey (2000), Iron and manganese in the Ross Sea, Antarctica: Seasonal iron limitation in Antarctic shelf waters, *Journal of Geophysical Research-Oceans*, *105*(C5), 11,321–11,336.

Sedwick, P. N., A. R. Bowie, and T. W. Trull (2008), Dissolved iron in the Australian sector of the Southern Ocean (CLIVAR SR3 section): Meridional and seasonal trends, *Deep-Sea Research Part I-Oceanographic Research Papers*, *55*(8), 911–925.

Sen Gupta, A., and M. H. England (2006), Coupled ocean-atmosphere-ice response to variations in the Southern Annular Mode, *Journal of Climate*, *19*(18), 4457–4486.

Sievers, H. A., and W. D. Nowlin (1984), The stratification and water masses at Drake Passage, *Journal of Geophysical Research-Oceans*, *89*(NC6), 489–514.

Simmonds, I., and D. A. Jones (1998), The mean structure and temporal variability of the semiannual oscillation in the southern extratropics, *International Journal of Climatology*, *18*, 473–504.

Sloyan, B. M., and S. R. Rintoul (2001), The Southern Ocean limb of the global deep overturning circulation, *Journal of Physical Oceanography*, *31*(1), 143–173.

Smith, R. D., J. K. Dukowicz, and R. C. Malone (1992), Parallel ocean general circulation modeling, *Physica D*, *60*, 38–61.

Smith, W. O., and J. C. Comiso (2008), Influence of sea ice on primary production in the Southern Ocean: A satellite perspective, *Journal of Geophysical Research-Oceans*, *113*(C5), C05S93.

Smith, W. O., and D. M. Nelson (1985), Phytoplankton bloom produced by a receding ice edge in the Ross Sea - Spatial coherence with the density field, *Science*, *227*(4683), 163–166.

Smith, W. O., J. Marra, M. R. Hiscock, and R. T. Barber (2000), The seasonal cycle of phytoplankton biomass and primary productivity in the Ross Sea, Antarctica, *Deep-Sea Research Part II-Topical Studies in Oceanography*, *47*(15-16), 3119–3140.

Sohrin, Y., S. Iwamoto, M. Matsui, H. Obata, E. Nakayama, K. Suzuki, N. Handa, and M. Ishii (2000), The distribution of Fe in the Australian sector of the Southern Ocean, *Deep-Sea Research Part I-Oceanographic Research Papers*, *47*(1), 55–84.

Sokolov, S. (2008), Chlorophyll blooms in the Antarctic Zone south of Australia and New Zealand in reference to the Antarctic Circumpolar Current fronts and sea ice forcing, *Journal of Geophysical Research-Oceans*, *113*, C03022.

Sokolov, S., and S. R. Rintoul (2002), Structure of Southern Ocean fronts at 140 degrees E, *Journal of Marine Systems*, *37*(1-3), 151–184.

Sokolov, S., and S. R. Rintoul (2007), On the relationship between fronts of the Antarctic Circumpolar Current and surface chlorophyll concentrations in the Southern Ocean, *Journal of Geophysical Research-Oceans*, *112*(C7), C07030.

Speer, K., S. R. Rintoul, and B. Sloyan (2000), The diabatic Deacon cell, *Journal of Physical Oceanography*, *30*(12), 3212–3222.

Stammerjohn, S. E., D. G. Martinson, R. C. Smith, X. Yuan, and D. Rind (2008), Trends in antarctic annual sea ice retreat and advance and their relation to El Nino-Southern Oscillation and Southern Annular Mode variability, *Journal of Geophysical Research-Oceans*, *113*(C3), C03S90.

Steinacher, M., F. Joos, T. L. Frölicher, L. Bopp, P. Cadule, S. C. Doney, M. Gehlen, B. Schneider, and J. Segschneider (2010), Projected 21st century decrease in marine productivity: a multi-model analysis, *Biogeosciences*, *7*, 979–1005.

Stockdale, T., A. Busalacchi, D. Harrison, and R. Seager (1998), Ocean modeling for ENSO, *Journal of Geophysical Research*, *103*(14), 14,325–14,355.

Tagliabue, A., L. Bopp, O. Aumont, and K. R. Arrigo (2009), Influence of light and temperature on the marine iron cycle: From theoretical to global modeling, *Global Biogeochemical Cycles Cycles*, *23*.

Takahashi, T., et al. (2002), Global sea-air CO2 flux based on climatological surface ocean pCO2, and seasonal biological and temperature effects, *Deep Sea Research Part II: Topical Studies in Oceanography*, *49*(9-10), 1601–1622.

Takahashi, T., et al. (2009), Climatological mean and decadal change in surface ocean pCO2, and net sea-air CO2 flux over the global oceans, *Deep Sea Research Part II: Topical Studies in Oceanography*, *56*(8-10), 554–577.

Thompson, D. W. J., and S. Solomon (2002), Interpretation of recent Southern Hemisphere climate change, *Science*, *296*(5569), 895–899.

Thompson, D. W. J., J. M. Wallace, and G. C. Hegerl (2000), Annular modes in the extratropical circulation. Part II: Trends, *Journal of Climate*, *13*(5), 1018–1036.

Thorne, P. W., and R. S. Vose (2010), Reanalyses suitable for characterizing long-term trends, *Bulletin of the American Meteorological Society*, *91*(3), 353–360.

Tjiputra, J. F., K. Assmann, and C. Heinze (2010), Anthropogenic carbon dynamics in the changing ocean, *Ocean Science*, *6*(3), 605–614.

Toggweiler, J. R., and J. Russell (2008), Ocean circulation in a warming climate, *Nature*, *451*(7176), 286–288.

Tomczak, M., and J. S. Godfrey (1994), *Regional Oceanography: An Introduction*, 1st ed., Pergamon Press.

Tortell, P. D., et al. (2008), CO2 sensitivity of Southern Ocean phytoplankton, *Geophysical Research Letters*, *35*, L04605.

Trenberth, K., et al. (2007), *Climate change 2007: The Physical Science basis. Contribution of Working Group I to the Fourth Assessment Report of the Intergovernmental Panel on Climate Change*, Observations: Surface and Atmospheric Climate Change, Cambridge University Press, Cambridge.

Trenberth, K. E., and J. M. Caron (2000), The Southern Oscillation revisited: Sea level pressures, surface temperatures, and precipitation, *Journal of Climate*, *13*(24), 4358–4365.

Trenberth, K. E., W. G. Large, and J. G. Olson (1990), The mean annual cycle in global ocean wind stress, *Journal of Physical Oceanography*, *20*(11), 1742–1760.

Trenberth, K. E., D. P. Stepaniak, and L. Smith (2005), Interannual variability of patterns of atmospheric mass distribution, *Journal of Climate*, *18*(15), 2812–2825.

Tynan, C. T. (1998), Ecological importance of the Southern Boundary of the Antarctic Circumpolar Current, *Nature*, *392*(6677), 708–710.

Uppala, S., et al. (2005), The ERA-40 re-analysis, *Quarterly Journal of the Royal Meteorological Society*, *131*, 2961–3012.

van Aken, H. M. (2007), *The oceanic themohaline circulation: An introduction*, 1st ed., Springer, New York.

van Loon, H. (1967), The half-yearly oscillations in the middle and high southern latitudes and the coreless winter, *Journal of Atmospheric Science*, *24*, 472–486.

Venables, H., and C. M. Moore (2010), Phytoplankton and light limitation in the Southern Ocean: Learning from high-nutrient, high-chlorophyll areas, *Journal of Geophysical Research*, *115*, C02015.

Verdy, A., J. Marshall, and A. Czaja (2006), Sea surface temperature variability along the path of the Antarctic Circumpolar Current, *Journal of Physical Oceanography*, *36*(7), 1317–1331.

Verdy, A., S. Dutkiewicz, M. J. Follows, J. Marshall, and A. Czaja (2007), Carbon dioxide and oxygen fluxes in the Southern Ocean: Mechanisms of interannual variability, *Global Biogeochemical Cycles*, *21*(2), GB2020.

Visbeck, M. (2007), Oceanography - power of pull, *Nature*, *447*(7143), 383–383.

Visbeck, M. (2009), A station based Southern Annular Mode index from 1884-2005, *Journal of Climate*, *22*(4), 940–950.

Wagener, T., C. Guieu, R. Losno, S. Bonnet, and N. Mahowald (2008), Revisiting atmospheric dust export to the Southern Hemisphere ocean: Biogeochemical implications, *Global Biogeochemical Cycles*, *22*(2), GB2006.

Watson, A. J., D. C. E. Bakker, A. J. Ridgwell, P. W. Boyd, and C. S. Law (2000), Effect of iron supply on Southern Ocean CO2 uptake and implications for glacial atmospheric CO2, *Nature*, *407*(6805), 730–733.

Watson, R. T., M. C. Zinyowera, and R. H. Moss (Eds.) (1996), *Climate change 1995, Impacts, adaptions and mitigation of climate change: scientific-technical analysies*, Contribution of Working Group 2 to the Second Assessment Report of the Intergovernmental Panel on Climate Change, Cambridge University Press, UK.

Westwood, K. J., F. Brian Griffiths, K. M. Meiners, and G. D. Williams (2010), Primary productivity off the Antarctic coast from 30-80e; BROKE-West survey, 2006, *Deep Sea Research Part II: Topical Studies in Oceanography*, *57*(9-10), 794–814.

Whitehouse, M. J., R. E. Korb, A. Atkinson, S. E. Thorpe, and M. Gordon (2008a), Formation, transport and decay of an intense phytoplankton bloom within the High-Nutrient Low-Chlorophyll belt of the Southern Ocean, *Journal of Marine Systems*, *70*, 150–167.

Whitehouse, M. J., M. P. Meredith, P. Rothery, A. Atkinson, P. Ward, and R. E. Korb (2008b), Rapid warming of the ocean around South Georgia, Southern Ocean, during the 20th century: Forcings, characteristics and implications for lower trophic levels, *Deep-Sea Research Part I-Oceanographic Research Papers*, *55*(10), 1218–1228.

Whitworth, T., and W. D. Nowlin (1987), Water masses and currents of the Southern-Ocean at the Greenwich Meridian, *Journal of Geophysical Research-Oceans*, *92*(C6), 6462–6476.

Whitworth, T., W. D. Nowlin, and S. J. Worley (1982), The net transport of the Antarctic Circumpolar Current through Drake Passage, *Journal of Physical Oceanography*, *12*(9), 960–971.

Williams, G. D., S. Nicol, S. Aoki, A. J. S. Meijers, N. L. Bindoff, Y. Iijima, S. J. Marsland, and A. Klocker (2010), Surface oceanography of BROKE-West, along the Antarctic margin of the south-west Indian Ocean (30-80E), *Deep Sea Research Part II: Topical Studies in Oceanography*, *57*(9-10), 738–757.

Wolter, K. (1987), The Southern Oscillation in surface circulation and climate over the tropical Atlantic, Eastern Pacific, and Indian Oceans as captured by cluster analysis, *Journal of Climate and Applied Meteorology*, *26*(4), 540–558.

Wolter, K., and M. S. Timlin (1993), Monitoring ENSO in COADS with a seasonally adjusted principal component index, in *Proceedings of the 17th Climate Diagnostics Workshop*, Oklahoma Climate Survey, pp. 52–57, NOAA/N MC/CAC, CIMMS and the School of Meteorology, University of Oklahoma.

Wright, S. W., and R. L. van den Enden (2000), Phytoplankton community structure and stocks in the East Antarctic marginal ice zone (BROKE survey, January – March 1996) determined by CHEMTAX analysis of HPLC pigment signatures, *Deep Sea Research Part II: Topical Studies in Oceanography*, *47*(12), 2363–2400.

Yang, X.-Y., D. Dongxiao, J. Wang, and R. X. Huang (2007a), Connection between the decadal variabitity in the Southern Ocean circulation and the Southern Annular Mode, *Geophysical Research Letters*, *34*, L16604.

Yang, X. Y., R. X. Huang, and D. X. Wang (2007b), Decadal changes of wind stress over the Southern Ocean associated with antarctic ozone depletion, *Journal of Climate*, *20*(14), 3395–3410.

Zhang, J. (2007), Increasing Antarctic sea ice under warming atmospheric and oceanic conditions, *Journal of Climate*, *20*(11), 2515–2529.

Zheng, Y., and B. S. Giese (2009), Ocean heat transport in Simple Ocean Data Assimilation: Structure and mechanisms, *Journal of Geophysical Research*, *114*.

Zickfeld, K., J. C. Fyfe, M. Eby, and A. J. Weaver (2008), Comment on 'Saturation of the Southern Ocean CO2 sink due to recent climate change', *Science*, *319*(5863).